Beurteilung metallischer Implantatmaterialien hinsichtlich ihrer Biokompatibilität und Beteiligung an der aseptischen Implantatlockerung

Kumulative Dissertation

zur Erlangung des akademischen Grades

Doctor rerum humanarum (Dr. rer. hum.)

an der Medizinischen Fakultät der Universität Rostock

Rostock, August 2017

vorgelegt von:

Dipl.-Biol. Jana Markhoff

aus Rostock

geb. am 10.11.1986 in Luckau

urn:nbn:de:gbv:28-diss2018-0077-6

Gutachter:

1. Gutachter:
   Prof. Dr. med. habil. Dipl.-Ing. Rainer Bader
   Forschungslabor für Biomechanik und Implantattechnologie
   Orthopädische Klinik und Poliklinik, Universitätsmedizin Rostock

2. Gutachter:
   Prof. Dr. Barbara Nebe
   Arbeitsbereich Zellbiologie
   Zentrum für Medizinische Forschung, Universitätsmedizin Rostock

3. Gutachter:
   PD Dr. Elmar Willbold
   NIFE - Niedersächsisches Zentrum für Biomedizintechnik, Implantatforschung und Entwicklung, Labor für Biomechanik und Biomaterialien
   Orthopädische Klinik im Annastift, Medizinische Hochschule Hannover

Datum der Einreichung: 30. August 2017

Datum der Verteidigung: 24. April 2018

Inhaltsverzeichnis

1 Einleitung

Der Bedarf und die Ansprüche an Implantate für den Einsatz bei Knochenfrakturen, Metastasen sowie Infektionen, Osteoporose, Arthrose und anderen Erkrankungen des Knochengewebes und des muskuloskelettalen Apparates sind deutlich gestiegen[1,2]. Mitunter kommt es aufgrund fehlender Stabilität, Inflammation sowie Osteolysen, bedingt durch Abriebpartikel, zum Versagen derartiger Implantate[1]. Für eine optimale, langhaltende Integration ist somit die Entwicklung neuer Implantatdesigns, Oberflächenmodifikationen und Materialien anzustreben.

1.1. Bone Remodeling

Im gesunden Knochen wird der aufeinander abgestimmte, kontinuierliche Prozess des Bone Remodelings (Tab. 1), unterteilt in vier Phasen unterschiedlicher Länge (Abb. 1), durch verschiedene Faktoren (Entzündungen, Hormonspiegel, mechanische Stimulation) initiiert, moduliert und reguliert[3,4]. Generell erfolgt die Entfernung des mineralisierten Knochens durch Osteoklasten (OK), gefolgt von einer Neuformation und Mineralisierung der Knochenmatrix durch Osteoblasten (OB) (Abb. 1)[3]. In einer temporären Struktur (Basic multicellular unit BMU) interagieren dabei OK mit OB, knochensäumenden Zellen (Bone lining cells) und Osteozyten[4,5].

Tab. 1: Statistik des Bone remodelings im gesunden Erwachsenen, modifiziert[5].

- Lebenserwartung einer BMU ~ 6 - 9 Monate (aufeinanderfolgende Remodelings am selben Ort alle ~ 2 - 5 Jahre)
- Größe einer BMU ~ 1 – 2 mm lang/ ~ 0,2 – 0,4 mm breit
- Lebenserwartung Osteoklasten ~2 Wochen | Lebenserwartung aktiver Osteoblasten ~3 Monate
- Umsatzrate ~ 25 µm/Tag (Umgesetztes Knochenvolumen pro BMU ~0,025 mm³)
- Umsatzrate des ganzen Skeletts ~ 10 % pro Jahr (Kompletterneuerung 10 Jahre)

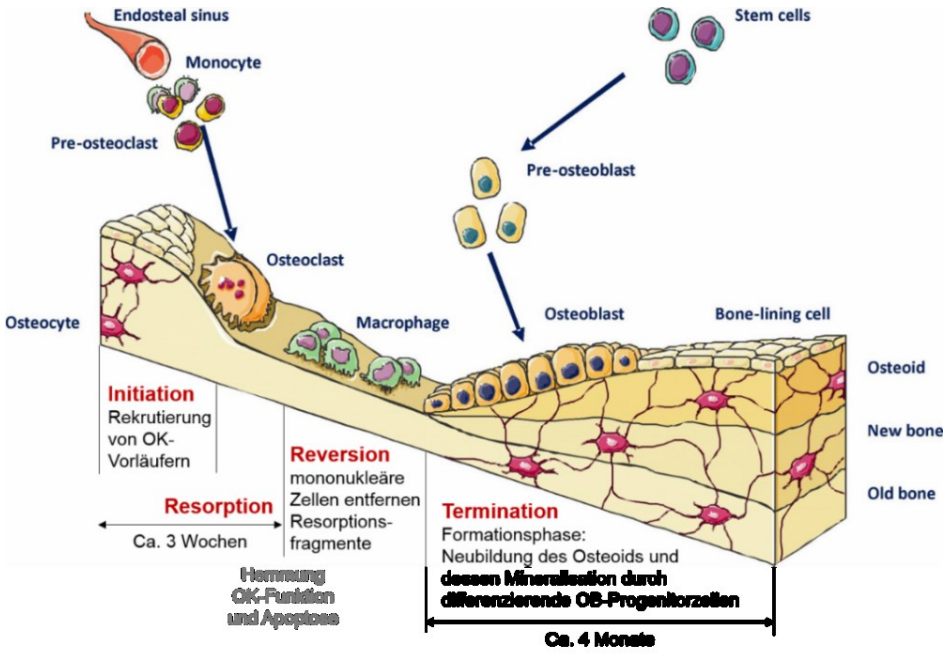

Abb. 1: Prozess des Bone Remodelings (modifiziert nach[6–12]).

1.2. Endoprothetische Implantate

Eingeschränkte Körperfunktionen können u. a. mit metallischen, keramischen sowie polymerischen und Verbundmaterialien versorgt werden[13]. In Bereichen hoher mechanischer Belastung (z. B. Femur, Tibia), kommt es v. a. zum Einsatz metallischer Implantate aus Edelstahl, CoCrMo- oder Titanlegierungen[1]. Aufgrund ihrer mechanischen Eigenschaften (Elastizitätsmodul, hohe Bruchfestigkeit, Zähigkeit) sowie der Ausbildung einer stabilen Titanoxidschicht und der damit einhergehenden Korrosionsbeständigkeit und Biokompatibilität machen Titanlegierungen wie Ti6Al4V einen Anteil von 70-80 % aller metallischen Biomaterialien aus[1,13,14]. Der Ersatz geschädigter, funktionsgehemmter Gelenke durch künstliche Gelenke gehört indes zu den am häufigsten durchgeführten chirurgischen Operationen und blickt auf eine lange Historie zurück[2]. Das Problem der aseptischen Implantatlockerung wurde bereits in den frühen 1960ern beobachtet. Die verschiedenen Materialien lassen sich in hard-on-hard Paarungen (Keramik-Metall-Paarungen) und hard-on-soft Paarungen mit Polyethylen (PE) unterscheiden[15–17]. Für die dauerhafte Beständigkeit und Funktion einer Endoprothese sind neben Patientenfaktoren (Body-Mass-Index, Aktivität, Genetik, Alter, Geschlecht) und chirurgischen Faktoren (Erfahrung, Zementierung, Stabilität), Implantat-assoziierte Faktoren wie Design, Herstellung sowie Gleitpaarung und Materialeigenschaften entscheidend[13,18,19].

Aufbau von Hüft- und Knieendoprothesen

Der Einsatz eines künstlichen Hüftgelenkes ist eine der meist durchgeführten Operationen in Deutschland[20] und wird sogar als Operation des Jahrhunderts bezeichnet[21]. Zwei miteinander artikulierende Komponenten (Pfannen-/Femurelement) machen eine Hüftendoprothese aus (Abb. 2A)[13]. CoCrMo, Ti6Al4V sowie Oxidkeramiken werden als Materialien für Hüftpfannen, -stiele sowie -köpfe genutzt, Keramiken und ultrahochmolekulargewichtiges Polyethylen (UHMWPE) für Pfanneneinsätze[13].

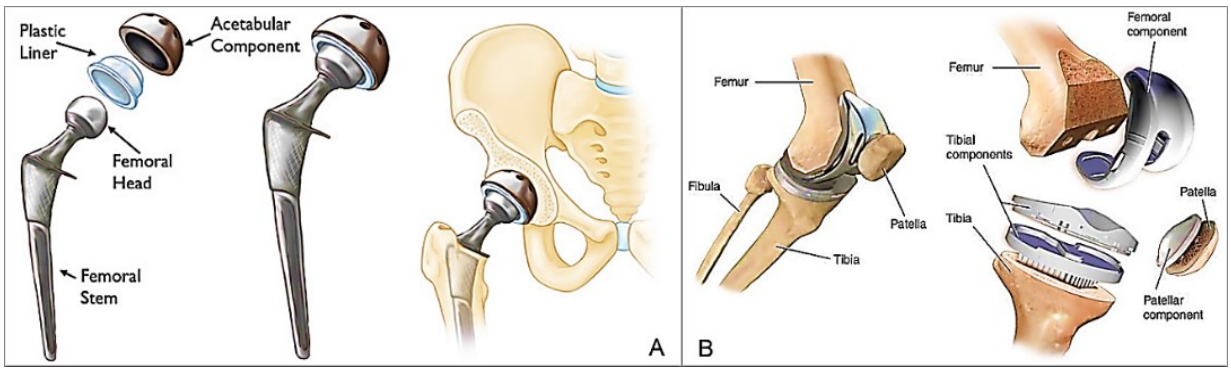

A - www.orthoinfo.aaos.org/topic.cfm?topic=a00377 | B - www.summitmedicalgroup.com/library/adult_health/aha_total_knee_replacement, letzte Besuche 14.06.17

Abb. 2: Komponenten und Position einer Hüfttotal- (A) und einer Knieendoprothese (B).

In der Knieendoprothetik komplettiert neben der femoralen und tibialen Komponente (Plateau, Insert), die Patella-Komponente das Implantatspektrum (Abb. 2B)[22]. Die meist zementierten

Femur- und Tibiaplateau-Elemente bestehen dabei aus metallischen Materialien wie Titanlegierungen, CoCrMo oder rostfreiem Stahl, seltener aus Oxidkeramiken[22]. PE wird für Inserts und Patella-Rückflächenersatz eingesetzt.

1.3. Biokompatibilität und Osseointegration

Biomaterialien, eingesetzt zur Behandlung, Unterstützung bzw. Übernahme der lokalen Körperfunktionen, interagieren mit Geweben und Körperflüssigkeiten und sind somit vielerlei Einflüssen ausgesetzt[20,23]. Die Biokompatibilität des eingesetzten Materials wird u. a. durch dessen Oberflächeneigenschaften (Chemie, Rauheit, Topografie, Porosität, Beschichtung), Korrosions- und Abriebbeständigkeit bestimmt[1,13,24]. Biokompatibilität beschreibt dabei die Fähigkeit eines Materials, die nicht-fibrotische Wundheilung, Rekonstruktion und Gewebeintegration im Rahmen seiner spezifischen Anwendung ohne unerwünschte lokale oder systemische Effekte und entsprechende Gewebeantwort auszulösen und zu lenken[25,26]. Dabei wird ein langfristiger Verbleib des Materials mit nur geringer inflammatorischer Reaktion („Biotoleranz“) angestrebt[25]. Auch dessen Zyto- und Genotoxizität, Mutagenität sowie Karzinogenität sind entscheidend[27]. Die biologische Beurteilung von Medizinprodukten erfolgt anhand der ISO 10993. Maßgeblich durch Brånemark erforscht[28], stellt die Osseointegration eine „strukturelle und funktionelle Koexistenz zwischen differenzierten, […] biologischen Geweben und strikt definierten, kontrollierten synthetischen Komponenten zur fortwährenden Unterstützung spezifischer klinischer Funktionen ohne Initiierung eines Abstoßungsmechanismus“ dar[23]. Dieser komplexe Prozess erfolgt anhand chemischer, mechanischer sowie biologischer Integration[24]. Das dynamische, interaktive Gewebe-Implantat-Interface ist Makro- und Mikrobewegungen ausgesetzt, die entscheidend zur Verbindung beider Komponenten beitragen[24].

1.1.1 Zelltypen im Implantat-Knochen-Interface

Osteoblasten: Knochenaufbauende OB (Größe 15-30 µm, 4-6 % Anteil im Knochen) entstammen multipotenten mesenchymalen Stammzellen (MSCs), aus denen auch Adipozyten, Myoblasten und Chondrozyten hervorgehen[9,29–32]. Ihr mehrstufiger Differenzierungsprozess (Abb. 3) erfordert die Expression spezifischer Gene (z. B. bone morphogenetic proteins) und unterliegt pro-osteogenen Signalwegen[30]. Im Laufe der OB-Entwicklung ist eine Verifizierung anhand zellspezifischer Transkriptionsfaktoren wie Runt-related transcription factor 2, Osterix und alkalischer Phosphatase möglich[4]. Reife OB exprimieren aktiv nicht-kollagene Matrixproteine (Osteocalcin, Proteoglykane, Typ 1-Kollagen)[30]. Auf die Ablagerung der organischen Matrix (Osteoid) durch den polarisierten OB folgt deren Mineralisierung mit Hydroxylapatit-Kristallen[30,33]. Nach der Ausbildung neuen Knochengewebes gehen OB in Apoptose, entwickeln sich zu ruhenden knochensäumenden Zellen (Bone lining cells) oder eingebetteten dendritischen, mechanosensitiven Osteozyten (Abb. 3)[12,29,34]. Kollagenproduzierende, vielgestaltige

Fibroblasten (FB) machen das Stroma nahezu aller Gewebe aus[35] und entstehen wahrscheinlich gewebespezifisch aus endo- und epithelialen Zellen, Knochenmark oder Bindegewebe[35].

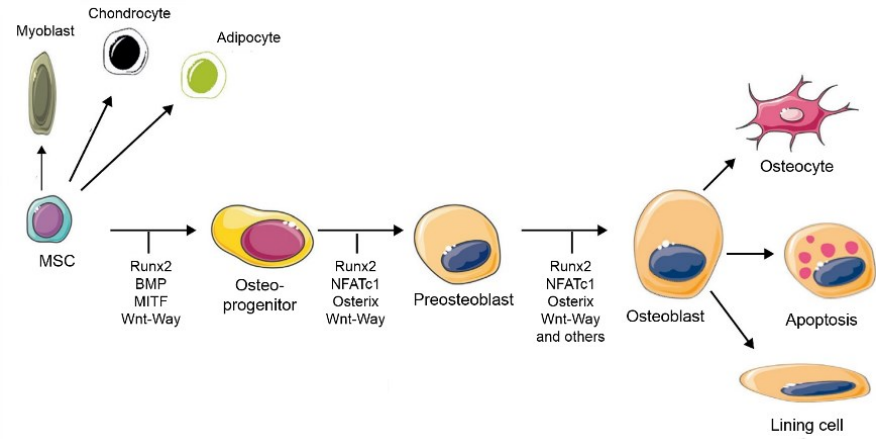

Abb. 3: Entwicklungslinie und Schicksale von OB aus MCSs; modifiziert nach[11].

Osteoklasten: Knochenresorbierende, mehrkernige OK (Größe 50-100 µm, 1-2 % Anteil im Knochen) entspringen, wie phagozytotische Makrophagen (MP) (Abb. 5), myeloiden Vorläuferzellen hämatopoetischer Abstammung, wobei ihre zytokingesteuerte Differenzierung und Proliferation v. a. von Zellen der OB-Linie bestimmt wird (Abb. 4)[5,11,29,36–38].

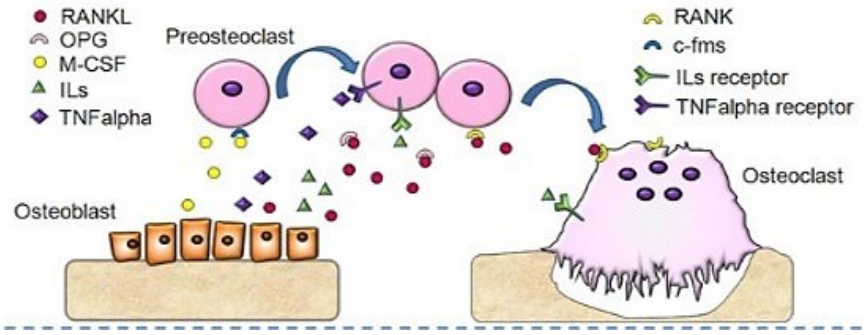

Abb. 4: Zusammenspiel von OK und OB über die RANKL/RANK/ OPG-Achse[41].

Der transmembrane Macrophage colony-stimulating factor (M-CSF) sowie RANKL (Receptor Activator of NF-κB Ligand) sind die für die Differenzierung zu OK erforderlichen Zytokine und werden vorrangig von Knochenmarksstammzellen und OB produziert[36]. Der myeloidspezifische, frühe Transkriptionsfaktor PU.1 reguliert die initialen Stadien der Myeloid-Differenzierung[12,39] und veranlasst zusammen mit dem Microphthalmia-associated transcription factor (MITF) die Rekrutierung des Nuclear factor of activated T-cells cytoplasmic 1 (NFATc1). Transkriptionsfaktor cFos und NFATc1 sind ausschlaggebende Faktoren für die terminale Differenzierung und Aktivierung der OK[40]. M-CSF induziert durch die Interaktion mit seinem Rezeptor c-Fms an frühen OK-Vorläufern deren Proliferation, Differenzierung und Fusion[4,30]. RANKL bindet an seinen, auf dendritischen Zellen, OK und deren Vorläufern lokalisierten, transmembranen Receptor Activator of NF-κB (RANK), woraus die Differenzierung von Vorläufer-

zellen in reife OK resultiert[30]. Auch die Aktivierung reifer OK und somit die Stimulation zur Resorption des Knochens ist möglich[36]. Die RANKL-RANK-Wechselwirkung resultiert in der Expression weiterer osteoklastogener Faktoren, was kaskadenartig zur Fusion der OK-Vorläufer und der Regulation von tartrate resistant acid phosphatase (TRAcP) sowie Cathepsin K, wichtigen OK-spezifischen Genen für die Resorption der Knochenmatrix, beiträgt[4,39]. Die Bindung von RANKL an seinen löslichen Fangrezeptor OPG, produziert von zahlreichen Zellen wie OB und FB, ist ebenfalls möglich, verhindert dadurch aber die Bindung an den eigentlichen Rezeptor und somit den Vorgang der Osteoklastogenese[4,36,39]. Der Vorgang der Osteoklastogenese ist in Abb. 5 dargestellt.

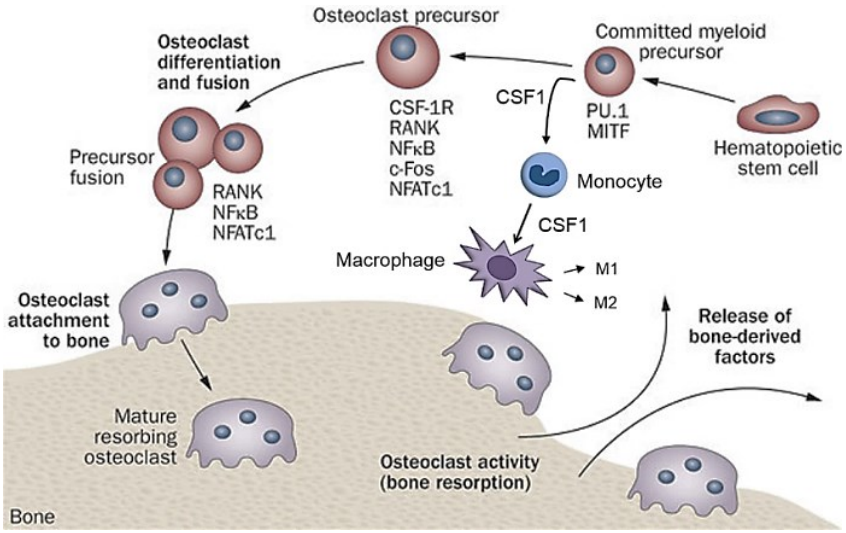

Abb. 5: Differenzierung hämatopoetischer Stammzellen zu Makrophagen (M1-/M2-Makrophagen) und reifen, knochenresorbierenden OK; modifiziert nach[38,42].

1.1.2 Knochenresorption

Die Polarisierung der mobilen OK (Abb. 6) ausschlaggebend für den Resorptionsprozess, erfordert die Neuanordnung des Aktin-Zytoskeletts und erfolgt erst nach Knochenkontakt[4,10,12,39]. Die Migration der Vorläuferzellen wird neben Monocyte chemoattractant protein 1 (MCP-1) u. a. durch Matrix Metalloproteinasen (MMPs) vermittelt[10,12,43]. Die Ausbildung eines F-Aktin-Ringes mit einer dichten, zusammenhängenden Zone hochaktiver Podosomen bildet die „sealing zone“ und resultiert in einer abgegrenzten Membran, die sich zur „ruffled border“, bestehend aus einer Vielzahl von Mikrovilli, entwickelt[4,44]. Die Kontaktaufnahme zur Knochenoberfläche erfolgt dabei u. a. über das Integrin $\alpha_V\beta_3$, den Rezeptor für Vitronectin (VNR), und induziert so die resorptive Zellaktivität[43]. Die „ruffled border“ beherbergt auf ihrer vergrößerten Oberfläche einzigartige vakuoläre H^+-ATPasen (V-ATPasen)[45,46]. Eine Carbonic Anhydrase II produziert aus Carbonsäure die darüber transportierten H^+-Ionen sowie Bicarbonat[11,39,47]. Mittels eines Bicarbonat/Chlorid-Austauschers gelangt dieses aus der Zelle und einströmende Chloridionen gelangen über entsprechende Kanäle ebenfalls in die Resorptionslakune (Howship-Lakune)[46,47]. Die resultierende Ansäuerung auf pH 3-4 ermöglicht die Auflösung der Hydroxylapatit-Kristalle[4].

Protonen und lysosomale Enzyme, wie TRAcP, die Gelatinase MMP-9 und die Proteinase Cathepsin K (CTSK) gelangen in die Lakune und beteiligen sich am Prozess der Knochenresorption[4,29,39,48,49]. Der Abtransport der Degradationsprodukte, welche die Zelle über Exozytose an der sekretorischen Domäne verlassen, erfolgt durch Endozytose über die „ruffled border“[4,11,43]. Auch während der Zellmigration ist die Knochenresorption möglich[44]. Die wichtigsten Differenzierungsmarker (RANKL, M-CSF) und die biochemischen Vorgänge der Resorption durch einen polarisierten, adhärenten OK sind in Abb. 6 dargestellt.

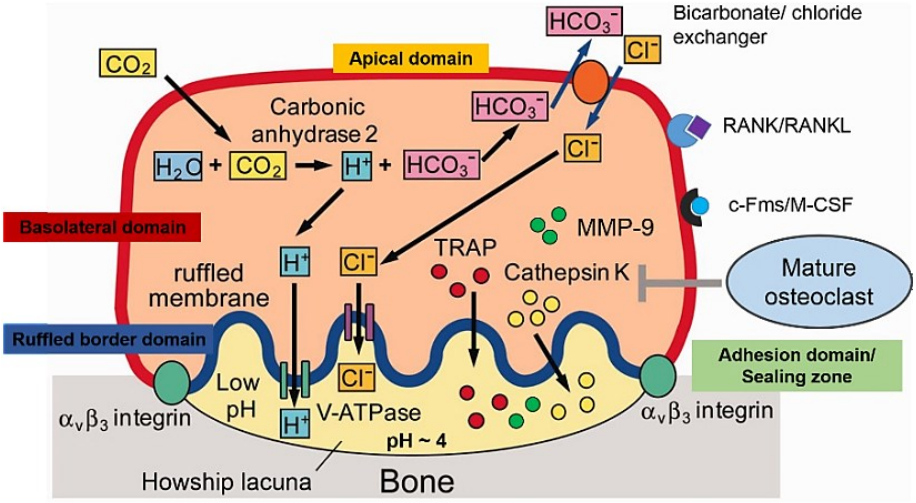

Abb. 6: Resorption der Knochenmatrix durch einen polarisierten Osteoklasten - modifiziert nach[39,41,47].

1.4. Aseptische Lockerung durch Partikelabrieb

Mittel- bis langfristig gesehen, ist die aseptische Lockerung als Folge übermäßigen Materialabriebs der Hauptgrund (75 %) für das Versagen von Endoprothesen[15,50]. Durch die Relativbewegungen artikulierender Implantatkomponenten miteinander oder dem umliegenden Knochengewebe und mechanische Belastungen kommt es zur Entstehung von Abriebpartikeln[22], deren Anreicherung im Gelenkspalt und im periprothetischen Raum[51], aber auch zur Verteilung (Fluiddruck) in entlegenere Gebiete[51]. Das periprothetische Gewebe besteht aus einer Vielzahl verschiedener Zelltypen (OB, OK, FB, Osteoprogenitorzellen), wobei Zellen der phagozytotischen Monozyten/MP-Linie als eine der ersten auf Partikel reagieren[15]. Partikelkontakt, die Phagozytose oder Pinozytose von Partikeln (Größe 150 nm - 10 µm) durch MP, OB oder OK resultieren in der Ausschüttung einer Vielzahl von Mediatoren (z. B. Interleukine, Tumornekrosefaktoren TNF, MCP-1) (Abb. 7)[15,52]. Partikel von 0,24 - 7,2 µm Größe gelten als besonders reaktiv und inflammatorisch[15]. MCP-1 als wichtiges chemotaktisches Zytokin rekrutiert v. a. Monozyten und OK; matrixabbauende MMPs werden freigesetzt[15]. Verschiedene Partikeltypen wirken unterschiedlich auf osteogene Zellen[15]. Durch die Produktion von RANKL, M-CSF und allerlei Zytokinen haben OB großen Anteil an der Differenzierung, Reifung und Formation resorbierender OK[15]. Makrophagen stellen im periprothetischen Gewebe multi-

taskingfähige Zellen dar. Neben der Ausschüttung OK-aktivierender Zytokine und der Stimulation der Knochenlyse besitzen sie Mikrostrukturen, um sich aktiv an der Knochenresorption zu beteiligen[15]. Die abriebinduzierte osteolytische Kaskade resultiert so in verstärkter OK-Aktivität und der Inhibition von OB-Differenzierung, -Funktionalität und deren Apoptose[15].

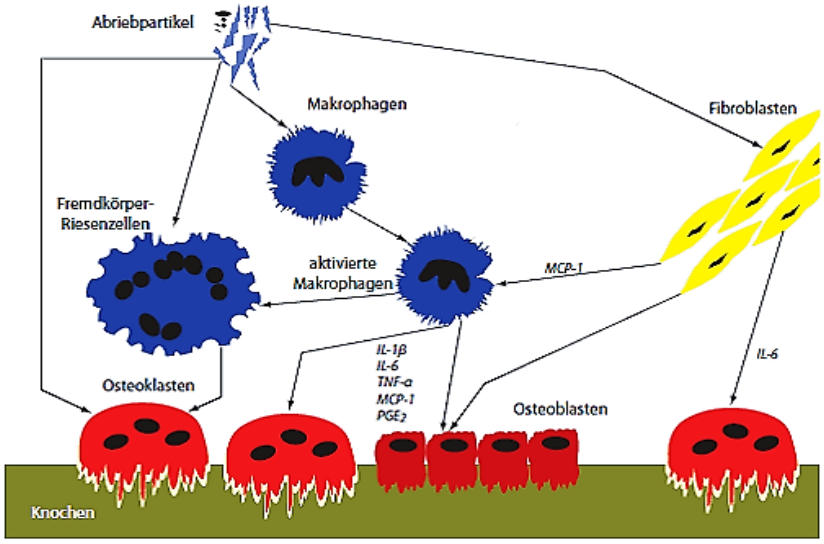

Abb. 7: Einflusswege von Abriebpartikeln im Zuge der aseptischen Implantatlockerung[53].

1.5. Stand der Forschung

Der Einfluss der Oberflächeneigenschaften auf die Zell-Material-Interaktion ist umfassend untersucht[26]. Gegenüber reinem Titan und CoCr-Legierungen konnten für Ti6Al4V-Oberflächen verbesserte mechanische Eigenschaften und eine erhöhte OB-Adhäsion und -proliferation in vitro nachgewiesen werden[26,54]. Die biochemische Modifizierung oder Funktionalisierung metallischer Oberflächen kann zur verbesserten Verankerung im Knochen beitragen, da sie die Proteinadsorption und somit die Zelladhäsion entscheidend beeinflusst[26]. Auch die Oberflächenenergie und Hydrophilie wirken sich darauf aus[26]. Die Topographie, definiert durch Rauheit und Orientierung, stellt einen wichtigen Faktor für eine erfolgreiche Osseointegration dar. So ist die Adhäsion, Proliferation sowie Differenzierung der OB signifikant durch diese beeinflusst[26]. Zudem ist es möglich, die zellspezifische Differenzierung mittels Oberflächentopographie zu stimulieren[26]; OB zeigen eine Präferenz für raue, FB für glatte Oberflächen[55]. Je nach Rauheitswert (Makro- bis Nanorauheit) wird die Knochenantwort sowohl in vitro als auch in vivo beeinflusst[26]. Bei großen Implantaten, die ein Einwachsen des Knochens und die Vaskularisierung des Gewebes erfordern, sind die Porosität, Porengröße und Interkonnektivität weitere wichtige Faktoren, um die Differenzierung, Proliferation und Migration osteogener Zellen zu ermöglichen[26,54]. Sie haben dabei einen entscheidenden Einfluss auf die mechanischen Eigenschaften des eingesetzten Materials, welche ihrerseits zur Formation oder Reduktion des Knochens beitragen können (Shear stress, physikalische Belastung, Mechanosensitivität)[56]. Aufgrund der größeren Oberfläche für die initiale Zelladhäsion ermöglichen hohe

Porositäten eine verbesserte Zellproliferation und -migration[57–60]. Bei Porengrößen von 450 - 500 µm ist bereits eine Verstopfung der Poren möglich, was zum Nähr- und Sauerstoffmangel in tieferen Ebenen poröser Scaffolds und somit zur Ansäuerung führen kann[61]. Aber auch zu große Poren wirken sich negativ auf das Einwachsverhalten aus. Für eine ausreichende Durchlässigkeit und mechanische Eigenschaften ähnlich des spongiösen Knochens sind Porositäten bis zu 75 % notwendig[54,62,63], was eine verbesserte Zellmigration, v. a. bei dynamischer Kultivierung, ermöglicht[64,65]. Dabei spielen Flussrate und -frequenz des Kulturmediums eine große Rolle für die Zellanhaftung und Nekrose[66]. Gerade bei größeren porösen Strukturen variieren Fließgeschwindigkeit und Scherkräfte in den verschiedenen Zonen des Scaffolds. Mechanosensitive OB sind gegenüber oszillatorischen und pulsierenden Perfusionssystemen reaktiver als in gleichmäßig fließenden[67,68]. Materialien wie die Formgedächtnislegierung Nitinol mit seinen speziellen superelastischen Eigenschaften eröffnen neue Möglichkeiten für die Herstellung medizinischer Implantate besonders in lasttragenden Bereichen[54]. In vitro konnte bereits eine gute Zytokompatibilität nachgewiesen werden, dennoch bestehen Bedenken aufgrund des hohen Nickelanteils und dem Austritt toxischer Nickel-Ionen[54,69,70]. Verschiedene Oberflächenmodifikationen (elektro-/chemische, Hitzebehandlung, Beschichtungen) könnten dies durch Ausbildung einer Diffusionsbarriere verhindern[71,72]. Nicht-toxisches und nicht-allergenes Niob als vielversprechendes neues Implantatmaterial ist durch die Ausbildung einer selbst-passivierenden inerten Oxidschicht korrosionsbeständig[73] und mindert zudem den Elastizitätsmodul von Titanlegierungen bei gleichzeitig verbesserter Materialstärke[26]. Der Elastizitätsmodul beschreibt dabei bei festen Körpern den Zusammenhang von Dehnung und Spannung bei deren Verformung. Niob und seine Legierungen zeigten in vitro ähnliche oder sogar bessere Biokompatibilität als reines Titan und Ti6Al4V[74,75]. Während der Einfluss der Partikel auf OB und MP hinreichend untersucht ist, ist die Anzahl wissenschaftlicher Studien zu OK unter partikulärem Einfluss gering. Als Antwort auf metallische Partikel schütten FB osteolytische Enzyme aus[15]. Nach dem Versagen von Prothesen konnten in deren umliegendem Gewebe hohe Konzentrationen der Kollagenase Cathepsin K und ein saures Milieu bestimmt werden, was auf eine hohe OK-Aktivität hinweist[50]. Die Eigenschaften der jeweiligen Partikel wie Größe, Morphologie, Konzentration, Volumen als auch Oberflächenrauheit, -ladung und chemische Zusammensetzung spielen eine wichtige Rolle bei der Ausbildung der zellulären Antwort[15,51]. Bei hard-on-soft-Paarungen kommt es zur Ausbildung vergleichsweise großer Partikel[15]. Kleinere Partikel und größere Konzentrationen haben einen stärkeren Einfluss auf die anwesenden Zellen im Knochen-Implantat-Interface, ebenso wie längliche und kantige Partikel gegenüber runden[15]. Dies zeigt sich durch eine verstärkte Immunantwort sowie die vermehrte Ausschüttung matrixabbauender und inflammatorischer Marker, aber auch durch die spezifische Hemmung oder Aktivierung von osteolyserelevanten Zellen. Titanpartikel zeigen bei gleicher Größe ein höheres inflammatorisches Potential als solche aus PE[15]. Prinzipiell kann

jeder Partikeltyp eine spezifische Reaktion auf Zellebene auslösen, wobei PE-Partikel ca. 70-90 % der Abriebpartikel ausmachen[15]. Dabei kann der Abrieb neben der unlöslichen Partikelform auch als lösliche Ionen auftreten, welche ebenfalls Osteolysen verursachen können[15].

2 Zielsetzung und Fragestellung

Gerade in lasttragenden Bereichen (Femur, Tibia) spielen neben der erforderlichen Biokompatibilität auch mechanische Eigenschaften der eingesetzten Biomaterialien eine große Rolle. Daher kommen hier vorrangig metallische Materialien zur Anwendung. So kann z. B. Ti6Al4V für die Entwicklung poröser Scaffolds zur Behandlung großer Knochendefekte verwendet werden (Studie I), da es aufgrund seiner mechanischen Eigenschaften die Herstellung solcher Scaffolds und die Variation hinsichtlich Porendesign, Porosität, Porengröße sowie Interkonnektivität ermöglicht. Vier Konfigurationen von Ti6Al4V-Scaffolds wurden bezüglich ihrer Besiedlung mit humanen OB (hOB) bei statischer als auch dynamischer Kultivierung im Bioreaktor beurteilt, um die optimale Struktur und Kulturbedingung zu ermitteln. Für neuartige medizinische Anwendungen stellen Formgedächtnislegierungen eine vielversprechende Option dar. Im Rahmen eines Projektes zur Entwicklung adaptiver Prothesensysteme erfolgte daher die zell- und molekularbiologische Beurteilung von Nitinoloberflächen als potentielles Material mit „shape memory effect“ im Vergleich zum gängigen Ti6Al4V (Studie II). β-Stabilisatoren, wie z. B. Niob, verbessern die Materialeigenschaften von Titanlegierungen zusätzlich. Daher stellen auch Niob und seine Legierungen (v. a. Ti-42Nb) attraktive neue Biomaterialien dar. Vier Oberflächen und vor dem Hintergrund der aseptischen Implantatlockerung erstmals entsprechende Partikel dieser Materialien wurden daher auf ihre Wirkung auf humane Zellen untersucht (Studie III). Um das Problem der aseptischen Lockerung erneut aufzugreifen, wurden reife, humane OK (hOK) mit Titan- und Zirkoniumoxidpartikeln kultiviert und bezüglich eines dosis-, partikel- und zeitabhängigen Einflusses ausgewertet (Studie IV).

Daher ergeben sich folgende Fragstellungen für die vorliegende Arbeit:

1. Inwieweit beeinflussen die Konfiguration poröser Ti6Al4V-Scaffolds und die Kultivierungsmethode die Migration und Proliferation humaner Osteoblasten?
2. Wie verhält sich die Biokompatibilität der Formgedächtnislegierung Nitinol zu humanen Osteoblasten, Fibroblasten und Makrophagen?
3. Welchen Einfluss haben Oberflächen aus Niob und Nioblegierungen auf humane Osteoblasten und Fibroblasten? Wie wirken verschiedene Konzentrationen von Pulvern aus Niob und Nioblegierungen auf humane Osteoblasten?
4. Wirken Abriebpartikel zeit-, dosis- und partikelabhängig auf reife humane Osteoklasten?

3 Material & Methoden

Alle Arbeiten zur Zellisolierung und Versuchsdurchführung wurden unter der Sterilbank durchgeführt. Die Kultivierung erfolgte im Brutschrank (37 °C, 5% CO_2) in zellspezifischen Medien mit Zugabe fötalen Kälberserums, Antibiotika und Wachstumsfaktoren. Je nach Versuchsdauer erfolgte ein regelmäßiger Mediumaustausch. Die Herkunft der verwendeten Materialien und Chemikalien ist in den jeweiligen Studien wiedergegeben. Die Darstellung der Oberflächen und Pulver erfolgte mittels Feldemissions- bzw. Rasterelektronenmikroskopie (Studie I-III). Rauheiten wurden mit einer taktilen Messmethode ermittelt (Studie II, III).

3.1. Zellisolierung

In den Studien I-IV wurden neben Zelllinien vorrangig humane Primärzellen verwendet. Eine Patienteneinwilligung sowie die Genehmigung der Ethikkommission der Universität Rostock für die Verwendung der jeweiligen Humanzellen lagen vor. Die Kultivierung der Osteosarkom-Zelllinie MG-63 ist in Studie II dargestellt. Für die zellbiologischen Untersuchungen wurden vorrangig humane Osteoblasten verwendet, welche nach dem Einsetzen einer Hüftendoprothese mechanisch und enzymatisch aus der Knochenspongiosa des Hüftkopfes isoliert wurden (Ethikvotum: A 2010-10)[76]. Die mechanische Isolierung humaner FB (hFB) wurde an Hautbiopsien (Brust, Augenlid) vorgenommen (Ethikvotum: A 2013-0092). Zur Gewinnung und Differenzierung von MP sowie OK wurden mononukleäre Zellen aus Buffy Coats isoliert, erhalten vom Institut für Transfusionsmedizin der Universitätsmedizin Rostock (Ethikvotum: A 2011-140). Die Isolierung, Kultivierung und Differenzierung der Humanzellen sind in Studie II und IV ausführlich dargestellt. Vor der Besiedlung der Pellets bzw. Scaffolds erfolgte die Sterilisation im Ultraschallbad sowie mittels Autoklav oder Wärmeschrank. Probekörper mit hoher Oberflächenporosität bzw. Mikrostrukturierung wurden vor der Besiedlung mit Kulturmedium gesättigt, um Luftblasen zu vermeiden. Für Expositionsversuche mit Abriebpartikeln (Studie IV) bzw. Pulvern (Studie III) wurden diese portioniert (5 mg) und bei 25 kGy gammasterilisiert. Eine Stocklösung wurde durch Zugabe von 500 µl PBS hergestellt und basierend auf Vorarbeiten der Arbeitsgruppe für den Einsatz im Zellversuch entsprechend verdünnt. Zur Untersuchung der Biokompatibilität der jeweiligen Materialien erfolgte die direkte Kultivierung der spezifischen Zellen auf den Probekörpern (Abb. 8b) bzw. mit Partikeln oder Pulvern (Abb. 8c), aber auch mit Überständen inkubierter Proben (Studie II) (Abb. 8a). Als Wachstumskontrolle diente gängige Zellkulturplastik (Studie II, III, IV). Soweit nicht anders angegeben, erfolgte die Kultivierung im statischen System. Für die dynamische Kultivierung strukturierter Ti6Al4V-Scaffolds (Studie I) wurden diese nach 24 h statischer Vor-Kultivierung mit OB mittels eines Halterungssystems in einen Bioreaktor (Minucells and Minutissue GmbH) eingesetzt (Abb. 9). Über gaspermeable

Silikonschläuche, Luer-Lock-Anschlüsse und eine peristaltische Pumpe wurde ein konstant aufwärts gerichteter Mediumfluss (50 µl/min) aus einem Frisch-mediumreservoir ermöglicht.

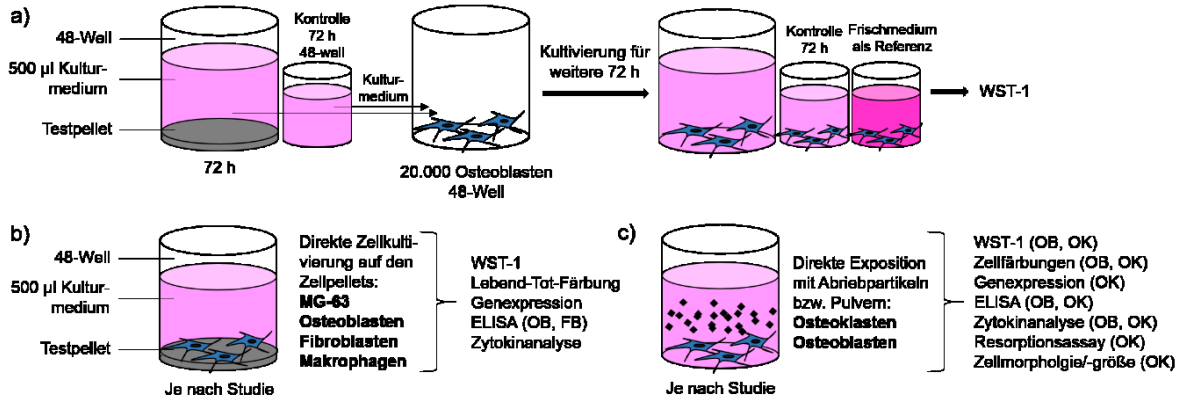

Abb. 8: Angewandte Test-Setups zur Exposition von Zellen mit Biomaterialien. a) Kultivierung von OB mit probenexponiertem Kulturmedium, b) Direkte Zellkultivierung verschiedener Zelltypen auf Testpellets; c) Direkte Exposition von OB und OK mit absinkenden Partikeln bzw. Pulvern.

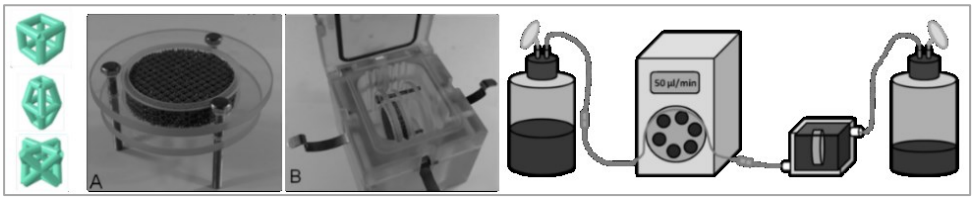

Abb. 9: links: Porendesigns der Ti6Al4V-Scaffolds; Einbringen der entsprechenden Scaffolds mittels Ringhalterung (A) in den Bioreaktor (B) und Versorgungsschema der dynamischen Kultivierung (rechts).

3.2. Zellbiologische Untersuchungen

Metabolische Aktivität und Zellfärbungen: Anhand eines kolorimetrischen Stoffwechsel-aktivitätstests (WST-1 Test), beschrieben in Studie III, wurde die Zellvitalität beurteilt. Die angewandte Lebend-Tot-Färbung beruht auf einer Zwei-Farb-Fluoreszenz-Messung, die eine simultane Darstellung lebender und toter Zellen ermöglicht (s. Studie III). Die Charakterisierung des osteoklastischen Zelltyps erfolgte mittels Färbung der TRAcP (s. Studie IV); Zellen mit mehr als drei Zellkernen wurden als OK verifiziert. Zur quantitativen Analyse der Zellgrößen wurden mikroskopische Aufnahmen hinsichtlich minimaler, maximaler und durchschnittlicher Zellgröße ausgewertet (s. Studie IV).

Knochenresorptionsassay: Nach 7 d Differenzierung erfolgte die Aussaat und Kultivierung von OK in OsteoLyse™ Zellkultur-Stripes. Die Fluoreszenz gesammelter Überstände wurde mit einem speziellen Fluorophore Releasing Reagent in einer schwarzen 96-Well Assayplatte nach ausreichender Vermischung mittels Tecan Reader gemessen (s. Studie IV).

Genexpressionsanalysen: Um die Expression verschiedener Gene in den jeweiligen Studien bestimmen zu können, wurde zunächst mittels TRIzol Reagenz und Direct-zol RNA Kit die RNA aus den Zellen isoliert und im Tecan-Reader gemessen. Mittels Reverser Transkription wurde

die RNA anschließend in cDNA umgeschrieben. Die Durchführung der quantitativen Real time-PCR (qRT-PCR) sowie die verwendeten Primer und deren Sequenzen sind in den Studien II und IV dargestellt.

Proteinsynthese mittels ELISA: Mittels Enzym-linked immunosorbent assays (ELISA) wurden matrixspezifische Proteine im Zellkulturüberstand bestimmt (Abb. 10). Typ 1-Kollagen wird als Pro-Kollagen synthetisiert und durch enzymatische Abspaltung des carboxyterminalen Propeptids (C1CP) als biochemischem Marker aktiviert. MMPs, Endopeptidasen v. a. für Typ 1-Kollagen, werden als inaktive Vorstufe synthetisiert und nach Abtrennung einer Pro-Domäne aktiviert. Der Tissue inhibitor of MMP-1 (TIMP-1) spielt eine Rolle im Matrix-Remodeling, indem er die MMP-1-Aktivität reguliert. Die Proteinkonzentrationen wurden anhand von Standardkurven bestimmt.

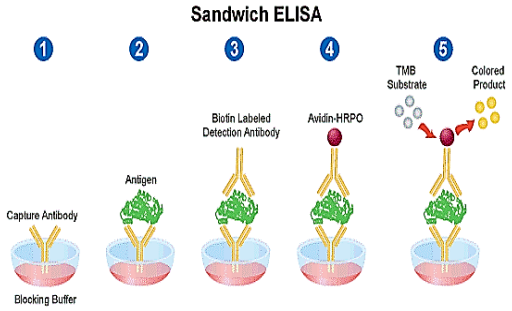

1) Antikörper (AK)-beschichtete Platte, spezifisch für AG
2) Probenzugabe; Bindung der entsprechenden Antigene (AG)
3) Zugabe eines Biotin-gelabelten Antikörpers, Bindung an AK aus 2)
4) Zugabe eines Enzymkonjugates
5) Zugabe einer Substratlösung; umgesetzt durch 4)

Antigen	Gelabelter AK	Enzymkonjugat	Substrat	Wellenlänge
C1CP	polyklonale Anti-C1CP-AK	alkalisch	p-Nitrophenyl-Phosphat	405 nm
MMP-1	biotinylierter Anti-Human MMP-1-AK	Meerrettich-Peroxidase (HRP)-konjugiertes Streptavidin	Tetramethylbenzidin	450 nm
TIMP-1	biotinylierter Anti-Human TIMP-1-AK	HRP-konjugiertes Streptavidin	Tetramethylbenzidin	450 nm

Abb. 10: Prinzip eines Sandwich-ELISAs (www.leinco.com/sandwich_elisa, letzter Besuch 28.06.17)

Zytokin-Multiplex: Zur Quantifizierung der Zytokine wurde ein Multiplex Cytokine Assay verwendet, welcher auf der simultanen Multi-Zytokin-Detektion mit Hilfe von Microsphere Beads (Polystyrenperlen ø 5,5 µm), monoklonalen Antikörpern und spezifischen Fluoreszenzfarbstoffen basiert und nach dem Prinzip eines Sandwich-ELISAs (Abb. 10) funktioniert. Eine Beschreibung erfolgt in den Studien II und III.

3.3. Statistische Analyse

Die statistische Signifikanz wurde mittels IBM® SPSS® Statistics Version 20 (IBM Corp., NY, USA) ermittelt. Die Signifikanzgrenze lag bei $*p < 0{,}05$; die Signifikanzstufen bei $*p < 0{,}05$; $**p < 0{,}01$ und $***p \leq 0{,}001$. Die ermittelten Daten wurden je nach Studie als Mittelwerte ± Standardabweichung (Studie I, IV) bzw. ± Standardfehler (standard error of the mean, SEM) (Studie II, III) sowie als Boxplotdiagramme dargestellt (Studie II, III, IV). Die Boxen geben dabei den Interquartilsabstand an, davon ausgehende Linien (sog. „Whiskers“) markieren den Minimal- und Maximalwert. Horizontale Linien innerhalb der Boxen kennzeichnen den Median.

Die statistische Signifikanz zwischen den porösen Ti6Al4V-Scaffolds (Studie I) als auch die multiplen Vergleiche der Nitinol-Studie (II) wurden mittels ANOVA Post-Hoc LSD ermittelt. Der nicht-parametrische zweiseitige Mann-Whitney U-Test kam für die statistischen Vergleiche der Niob-Oberflächen und -Pulver (Studie III) sowie die Partikelstudie (IV) zur Anwendung.

4 Ergebnisse

4.1. Studie I: Ti6Al4V-Scaffolds unter statischer und dynamischer Kultivierung

Zur Überbrückung großer Knochendefekte in lasttragenden Bereichen dienen mikrostrukturierte dreidimensionale Materialien als Leitstruktur für die Ausbildung neuen Knochengewebes. In Studie I wurden vier verschiedene (Porendesign: kubisch, diagonal, pyramidal; Porengröße, Porosität), mit unterschiedlichen Fertigunggsverfahren (kubische Struktur: Selektives Laserstrahlschmelzen SLM, Elektronenstrahlschmelzen EBM) hergestellte Ti6Al4V-Scaffolds hinsichtlich ihrer Besiedlung mit hOB bei statischer (1 d/ 4 d/ 8 d) als auch dynamischer Kultivierung (4 d) im Bioreaktor untersucht. Im Gesamtprojekt erfolgte zudem auch die mechanische sowie in vivo-Charakterisierung. Die kubischen Mikrostrukturen (Porengröße 700 µm, Porosität ca. 51%) zeigten bei statischer Kultivierung einen signifikanten Anstieg der metabolischen Zellaktivität über den gesamten Zeitraum, jedoch keine signifikanten Unterschiede zwischen den Fertigungsverfahren, wenn auch mit leichter Tendenz zu den SLM-Scaffolds. Es zeigte sich eine deutliche Zunahme der Zelldichte, besonders im Bereich der Stege des Scaffolds sowie auch in tieferen Ebenen, v. a. in den diagonalen und pyramidalen Strukturen. Jedoch kam es auch zum vermehrten Auftreten toter Zellen, vorrangig in den oberen Ebenen. Sowohl die SLM- als auch die EBM-Scaffolds wiesen nach 24 h-Besiedlung deutlich erkennbar lebende Zellen in tieferen Ebenden auf, welche aber im zeitlichen Verlauf, vermutlich durch Mangelversorgung, eingingen. Dennoch traten nach 8 d Kultur bei beiden Strukturen lebende Zellen an der Scaffoldunterseite auf, was auf eine erfolgreiche Zellmigration hinweist. Aufgrund des Bioreaktordesigns gelang die Messung der Kollagensynthese lediglich nach statischer Kultivierung. Über die Zeit war eine signifikante Zunahme der Pro-Kollagen Typ I-Produktion bei beiden kubischen Strukturen erkennbar. Um eine mögliche Divergenz zwischen statischer und dynamischer Kultivierung auszumachen, wurden Scaffolds mit kubischer Struktur (SLM, EBM) für 24 h statisch vorkultiviert, um eine initiale Zelladhäsion zu erreichen und anschließend in das dargestellte System (Abb. 9) überführt und weitere 72 h unter dynamischen Bedingungen kultiviert. Dabei erzielte keine Kultivierungsmethode eine signifikante Zunahme der metabolischen Aktivität. Im direkten Vergleich der SLM- und EBM-Scaffolds bei dynamischer Kultur zeigte sich eine leicht erhöhte Zellaktivität beim kubischen EBM-Scaffold, was zudem eine dichtere Zellbesiedlung aufwies. Die weiteren Strukturen (diagonal, pyramidal) wurden kosten- und fertigungsbedingt mittels SLM hergestellt. Bei statischer Kultivierung mit hOB war die

metabolische Aktivität auf den Scaffolds mit pyramidalem Porendesign im zeitlichen Verlauf signifikant höher als bei der kubischen und diagonalen Struktur, welche die niedrigsten Aktivitätswerte zeigte. Dennoch kam es im Laufe der Kultivierung bei allen Strukturen zur signifikanten Aktivitätssteigerung. Es ergab sich ebenfalls eine deutliche Zunahme der Zelldichte bei allen Strukturen auch in der tieferliegenden Ebene v. a. bei diagonaler und pyramidaler Struktur sowie hohen Anteilen toter Zellen in der kubischen. Im untersuchten Zeitraum ergab sich für alle Strukturen ein signifikanter Anstieg der Pro-Kollagen Typ I-Produktion, mit signifikant geringster Synthese beim Scaffold mit diagonalem Porendesign. Auch hier wurde zu Vergleichszwecken die dynamische Kultivierung, wie beschrieben, durchgeführt. Es konnten bei keiner der Strukturen signifikante Unterschiede der Zellaktivität zwischen beiden Verfahren nachgewiesen werden, was vermutlich auf das Bioreaktordesign und auf die Fließgeschwindigkeit zurückzuführen sein könnte. Allerdings resultierte die pyramidale Struktur in beiden Kultivierungssystemen in einer deutlich höheren (statisch) bzw. signifikant höheren Zellaktivität gegenüber kubischer und diagonaler Struktur. Sie wies zudem als einzige lebende Zellen im Bereich der Scaffoldunterseite sowie in darüber liegenden Ebenen auf; ein möglicher Hinweis auf eine erfolgreiche Zellmigration. Insgesamt zeigte das Ti6Al4V-Scaffold mit pyramidalem Porendesign, kleinster Porengröße und größter Porosität signifikant bessere Ergebnisse hinsichtlich metabolischer Aktivität, Kollagensynthese und Zellmigration. Aufgrund des gewählten Bioreaktorsystems kann keine eindeutige Aussage über einen signifikanten Vorteil der dynamischen Kultivierung getroffen werden; dennoch zeigte sich partiell ein leicht positiver Einfluss.

4.2. Studie II: Wachstum humaner Zellen auf Titanlegierungen und Nitinol

Als Alternative für Anwendungen in der Orthopädischen Chirurgie mit speziellen Anforderungen wurden Formgedächtnislegierungen aus Nitinol (NiTi), unbeschichtet als auch mit DLC (diamond-like carbon)-Beschichtung, hinsichtlich ihrer Biokompatibilität untersucht und Grade 5 Ti6Al4V sowie SLM-gefertigtem Ti6Al4V gegenüber gestellt (Studie II). Die durchgeführten Rauheitsmessungen ergaben deutliche Abweichungen zwischen den verschiedenen Oberflächen. Während Grade 5 Ti6Al4V bei einer durchschnittlichen Oberflächenrauheit (Rz) von ca. 15 µm und SLM-Ti6Al4V bei ca. 70 µm lagen, wiesen die Nitinol-Proben lediglich Werte um 1 µm auf. Neben der OB-Zelllinie MG-63 wurden drei humane Zelltypen (hOB, hFB, hMP) verwendet. Humane OB wurden vorab mit den verschiedenen probenexponierten Kulturmedien kultiviert, wobei ein möglicher negativer Einfluss durch Nickel-Ionen ausgeschlossen werden konnte. Dennoch zeigten alle Konfigurationen sowie eine parallel mitgeführte Mediumkontrolle eine nahezu 40 %ige signifikante Verminderung der Zellaktivität gegenüber einer Frischmediumkontrolle, was vermutlich auf einen erhöhten Nährstoffverbrauch zurückzuführen ist. Bei direkter Besiedlung der Testpellets ergab sich für alle Humanzellen ein ähnliches oberflächenspezifisches Bild hinsichtlich der metabolischen Aktivität, mit Vorteilen bei SLM-Ti6Al4V und

unbeschichtetem NiTi. Bei hOB und hFB lag die Aktivität bei allen Oberflächen jedoch signifikant unter der Wachstumskontrolle. Die höchsten OB-Aktivitäten konnten nach Kultivierung auf SLM-Ti6Al4V und NiTi nachgewiesen werden, gefolgt von NiTi + DLC und Grade 5 Ti6Al4V. Sowohl Grade 5 Ti6Al4V als auch NiTi + DLC resultierten bei hFB gegenüber SLM-Ti6Al4V und NiTi in signifikant niedrigerer Aktivität. Humane MP wiesen im Vergleich insgesamt eine höhere Zellaktivität für alle Gruppen auf. Lediglich auf Grade 5 Ti6Al4V und auf NiTi + DLC zeigten die Zellen eine signifikant verminderte Aktivität verglichen zur Wachstumskontrolle. Bei der Besiedlung der Pellets mit der Zelllinie MG-63 ergaben sich keine deutlichen Unterschiede zwischen den einzelnen Oberflächen; die Aktivität lag insgesamt durchschnittlich bei 50 % der Wachstumskontrolle. Die Lebend-Tot-Färbung lies für nahezu alle Materialien eine dichte Besiedlung mit lebenden Zellen erkennen. Die Genexpressionsanalysen erfolgten für Pro-Kollagen Typ I und MMP-1 sowie verschiedene Zytokine (IL-6, IL-8, MCP-1, TNF-α) (Tab. **2**). Eine zur Kontrolle signifikant verminderte C1CP-Expression auf allen Oberflächen und eine deutlich erhöhte MMP-1-Expression auf Grade 5 Ti6Al4V und den NiTi-Oberflächen konnte für hOB nachgewiesen werden. Ein ähnliches Bild zeigte sich bei hFB oberflächenabhängig für die matrixrelevanten Marker, jedoch mit insgesamt höherer Expression. Die Expression immunrelevanter Marker wies deutliche Unterschiede zwischen den Oberflächen und Zelltypen auf (Tab. 2).

Tab. 2: Genexpression der untersuchten humanen Zellen auf verschiedenen metallischen Oberflächen. Signifikante Abweichungen gegenüber der Wachstumskontrolle (100%): p* < 0,05; p** < 0,01.

	Osteoblasten					Fibroblasten					Makrophagen			
[%]	C1CP	MMP-1	IL-6	IL-8	MCP-1	Col-1	MMP-1	IL-6	IL-8	MCP-1	IL-6	IL-8	MCP-1	TNF-a
Titan Grade 5	57*	266	132	256**	190	78	1016	96	262	137	131	172	99	78
Ti6Al4V SLM	44**	82	45	111	255**	60	63	40*	76	158	30*	51	55	35
Nitinol	42**	194	99	155	125	66	654	72	348	385	61	29	51	70
Nitinol + DLC	65*	141	98	57	75	58	734	26**	55	69	72	10*	25*	85

Die Proteinsynthese bei hOB und hFB zeigte ähnliche oberflächenspezifische Ergebnisse. Auf nahezu allen Oberflächen (v. a. Grade 5 Ti6Al4V, NiTi, NiTi + DLC) war eine deutlich erhöhte Kollagensynthese auszumachen. Ein ähnliches Bild ergab sich für die MMP-1-Synthese von hOB. Demgegenüber war diese bei hFB auf Grade 5 Ti6Al4V zur Kontrolle und den weiteren Proben signifikant erhöht. Auf allen Oberflächen, v. a. auf SLM-Ti6Al4V und NiTi+DLC, zeigten hOB erhöhte Interleukinlevel. Die Synthese von MCP-1 und Vascular Endothelial Growth Factor (VEGF) lag auf allen Oberflächen außer Grade 5 Ti6Al4V deutlich über der Kontrolle. Auch hier reagierten die hFB ähnlich. Eine sehr geringe oder verminderte Zytokinsynthese konnte für hMP auf den Ti6Al4V-Oberflächen nachgewiesen werden, wogegen es auf NiTi und NiTi + DLC zur deutlichen, teils signifikanten Immunreaktion kam. Insgesamt konnte ein zellspezifischer Einfluss der untersuchten Oberflächen nachgewiesen werden. Basierend auf den gewonnenen Ergebnissen kann NiTi eine geeignete Alternative zum gängigen Ti6Al4V darstellen. Die gewählten Oberflächenmodifikationen haben dabei jedoch Einfluss auf die zelluläre Antwort.

4.3. Studie III: Einfluss von Nioboberflächen und -pulvern auf humane Zellen

Durch die Zugabe von β-Stabilisatoren, wie z. B. Niob (Nb), lassen sich die mechanischen Eigenschaften von Titanlegierungen zusätzlich verbessern. Das Ziel der Studie III war es daher, neuartige Niob- (Amperit, Ampertec gesintert, Blech) und Ti-42Nb- (SLM, gesintert) Oberflächen hinsichtlich ihrer Biokompatibilität mit Humanzellen (hOB, hFB) zu beurteilen und dem gängigen Ti6Al4V gegenüber zu stellen. Zwischen den Materialien ergaben sich deutliche Unterschiede hinsichtlich der Oberflächenrauheit. Grade 5 Ti6Al4V sowie Nb Ampertec und das Niobblech wiesen ca. 15-18 µm (Rz) auf, während Nb Amperit um die 7 µm und die Ti-42Nb-Proben bei 40-50 µm lagen. Nahezu alle Oberflächen führten bei hOB zu einer deutlich bis signifikant verminderten Zellaktivität mit signifikanten Unterschieden zwischen den Oberflächen. Lediglich das gesinterte Ti-42Nb führte gegenüber der Kontrolle zu einer signifikant höheren Aktivität. Ein ähnliches Bild ergab sich für die Kultivierung von hFB. Die Lebend-Tot-Färbung stützt diese Ergebnisse, wobei v. a. hOB einen dichten Zellrasen auf den Nb Ampertec und Ti-42Nb-Oberflächen aufwiesen. Bei hOB war die C1CP-Synthese auf allen Oberflächen gegenüber der Kontrolle signifikant vermindert. Dabei führten Nb Amperit, Nb-Blech und sogar Ti6Al4V zu den niedrigsten Syntheseraten. Die C1CP-Synthese der hFB war dagegen lediglich auf Nb Amperit und dem Nb-Blech vermindert. Zu einer deutlichen Zunahme der Syntheserate kam es auf den neuartigen Oberflächen Nb Ampertec und Ti-42Nb/gesintert. Erstmals wurden auch Untersuchungen mit verschiedenen Nb- sowie Ti-42Nb-Pulvern vor dem Hintergrund der aseptischen Endoprothesenlockerung durchgeführt. Nach der Exposition mit vier verschiedenen Pulvern in drei Konzentrationen über zwei Messpunkte zeigte sich ein dosis-, zeit- sowie pulverabhängiger Einfluss auf die metabolische Aktivität sowie bei der Lebend-Tot-Färbung der hOB (Studie III, Abb. 6/8). Auch die Pro-Kollagen Typ I-Produktion war konzentrations- und zeitabhängig beeinflusst (alle: 7 d > 4 d). Nb Amperit führte zu einem Anstieg der Syntheserate proportional zur eingesetzten Konzentration; gegenüber der pulverfreien Wachstumskontrolle durchweg signifikant erhöht. Nb Ampertec und kleinkörniges Ti-42Nb resultierten bei steigender Konzentration in einem signifikanten Abfall der Kollagenproduktion. Die Synthese von IL-6 und IL-8 war bei allen Pulvern nur leicht erhöht. Insgesamt konnten sehr gute Ergebnisse mit den neuartigen Niobmaterialien hinsichtlich ihrer Kultivierung mit Humanzellen gewonnen werden. Dabei traten Abhängigkeiten und Unterschiede zwischen den jeweiligen Pellets und deren Pulverformen auf. Besonders Ti-42Nb zeigte sowohl als Vollmaterial als auch als großkörniges Pulver positive Ergebnisse hinsichtlich Zellaktivität, Kollagensynthese und Inflammation.

4.4. Studie IV: Dosis- und zeitabhängiger Einfluss von Partikeln auf humane OK

Vor dem Hintergrund der aseptischen Lockerung wurde der zeit- und dosisabhängige Einfluss verschiedener Abriebpartikel auf hOK während und nach der Differenzierung untersucht. In der

vorliegenden Studie IV wird der dosisabhängige Effekt von Partikeln (cpTi, ZrO_2) nach je 3 d und 7 d auf reife OK dargestellt. Die initiale zelluläre Partikelaufnahme kann anhand der erstellten lichtmikroskopischen Bilder vermutet werden. Die Ausbildung des osteoklastischen Phänotyps wurde durch die Färbung der TRAcP sowie das Vorkommen von mehr als drei Zellkernen pro Zelle nachgewiesen. Es wird deutlich, dass es über den untersuchten Zeitraum zu einer deutlichen Zunahme der durchschnittlichen Zellgröße ohne eindeutige Abhängigkeiten von Partikeltyp und -dosis kommt. Nach Exposition mit cpTi-Partikeln über 3 d zeigte sich eine dosisabhängig signifikant verminderte metabolische Aktivität der OK gegenüber der partikelfreien Kontrolle. Drei Tage ZrO_2-Einfluss führten zu einer kaum veränderten Aktivität, aber einem signifikanten Abfall nach 7 d bei höchster Konzentration. Die Expression des Adhäsionsmarkers VNR zeigte sich nach 3 d Partikelexposition (cpTi, ZrO_2) dosisunabhängig signifikant erhöht. RANK sowie TRAcP stellen wichtige Faktoren für Osteoklastogenese, Migration und (Resorptions)Aktivität dar. Die Zellen zeigten nach 7 d Partikelexposition eine dosisabhängige Erhöhung der TRAcP-Expression. ZrO_2-Partikel führten über den gesamten Zeitraum zu signifikant höheren Werten als die Kontrolle. Die RANK-Expression war v. a. nach Exposition mit ZrO_2-Partikeln signifikant gesteigert. Die Bestimmung der TRAcP-Proteinsynthese ergab eine erhöhte zeitabhängige Produktion. Alle Partikelkonfigurationen führten in den Zellen nach 3 d zu einer signifikant höheren CTSK-Expression gegenüber der partikelfreien Kontrolle. Weiterhin wurde die Expression und Synthese matrixrelevanter Marker (MMP-1, TIMP-1) bestimmt. Während zunächst eine dosis- und partikelunabhängig erhöhte MMP-1-Expression nachgewiesen werden konnte, fiel diese nach 7 d dosisabhängig deutlich unter die Kontrolle. Die TIMP-1-Expression verhielt sich ähnlich. Diese war zeitabhängig vermindert und zeigte v. a. für 0,1 mg/ml cpTi einen deutlichen Abfall zur Kontrolle. Die MMP-1-Synthese der OK war über den gesamten Zeitraum ähnlich der Kontrolle. TIMP-1 war hingegen besonders nach ZrO_2-Exposition zeit- und dosisabhängig vermindert. Die Resorptionsaktivität der OK war in allen Gruppen besonders nach 7 d deutlich erhöht. Gegenüber der Kontrolle konnte aber kein signifikanter Unterschied nach Partikelexposition ermittelt werden. Anhand der gewonnenen Ergebnisse kann angenommen werden, dass reife Osteoklasten aktiv am Prozess der Osteolyse als Ursache der aseptischen Implantatlockerung beteiligt sind und dabei dosis-, zeit- und typabhängig auf die jeweils eingesetzten Abriebpartikel reagieren.

5 Diskussion

Die vielfältigen Einsatzmöglichkeiten metallischer Biomaterialien (Osteosynthese, künstliche Gelenke, Dentalimplantate) erfordern eine entsprechende Breite an Biokompatibilitätsuntersuchungen. Neben der Beurteilung der Materialien hinsichtlich ihrer Oberflächenbesiedlung (Studie II, III), erfolgte in der vorliegenden Arbeit zudem die Kultivierung auf 3D-Scaffolds im statischen und dynamischen System (Studie I), als auch die Exposition mit Abriebpartikeln und

Pulvern im Hinblick auf Initiierung einer aseptischen Implantatlockerung (Studie III, IV). Aufgrund der mechanischen Eigenschaften, besserer Korrosionsbeständigkeit und Biokompatibilität sind Titan und seine Legierungen rostfreiem Stahl und CoCr-Legierungen, welche mit verzögerter Knochenanhaftung und somit geringerem Osseointegrationspotential assoziiert sind[21], überlegen[77]. Abhängig von ihrer Mikrostruktur bei Raumtemperatur lassen sich Titanlegierungen in α- (cpTi), α + β- (Ti6Al4V) sowie β-Legierungen (NiTi, Ti-42Nb) einteilen. Durch Zugabe entsprechender Elemente (α-, β-Stabilisatoren) kommt es zur Änderung der mechanischen Eigenschaften (Korrosionsbeständigkeit, Festigkeit, Elastizität), welche v. a. in lasttragenden Bereichen von entscheidender Bedeutung sind[77,78]. Commercial pure Titanium (cpTi) und Ti6Al4V zeigen dabei eine ähnliche Morphologie, Topographie sowie Phasenzusammensetzung und Chemie[79]. In vitro wurde für Ti6Al4V-Oberflächen eine bessere OB-Adhäsion gegenüber Titan und CoCr-Legierungen nachgewiesen[26]. Titanoberflächen sind für die spontane Ausbildung eines natürlichen Oxidfilms (Dicke ca. ~2 - 7 nm) bekannt, welcher deren gute chemische Eigenschaften und Biokompatibilität bedingt[77]. Die Modifikation der Oberfläche kann zudem über physikalische (Plasmaspray), chemische (Ätzen) und mechanische Verfahren (Strahlen, Schleifen) erreicht werden[80]. Dies führt zu veränderten Oberflächenparametern und folglich zur veränderten Zellantwort wie verbesserter Zellanheftung[81].

5.1. Studie I: Ti6Al4V-Scaffolds und der Einfluss der Kultivierungsbedingungen

Der Elastizitätsmodul von Titan (114 GPa) weicht deutlich von dem des spongiösen und kortikalen Knochens (0,5 GPa – 20 GPa) ab. Die Steifigkeit poröser Implantate kann durch die Porenstruktur modifiziert und mit zunehmender Porengröße vermindert werden[82]. Da die statische Kultivierung dreidimensionaler Strukturen durch mangelnde Diffusion begrenzt ist (200 - 800 mm), ist die dynamische in einem Bioreaktor von Vorteil[32]. Die Anforderungen an solche Strukturen schließen die Biokompatibilität des verwendeten Materials, eine geeignete Oberfläche zur Anheftung und Besiedlung sowie eine passende Porengröße, hohe Porosität und Interkonnektivität für das Einwachsen der Zellen, eine ausreichende Nährstoffversorgung als auch adäquate mechanische Eigenschaften ein[80]. Besonders additive Fertigungsverfahren (EBM, SLM) können für metallische Materialien zur Herstellung jeglicher poröser Strukturen verwendet werden[83]. Sowohl auf EBM- als auch SLM-Scaffolds aus Ti6Al4V konnte bereits eine gute Zellanhaftung, Proliferation und Differenzierung, abhängig von Design, Porosität und Rauheit, nachgewiesen werden[82,84-86], was sich mit den Ergebnissen der Studie I deckt. Dabei zeigten sich keine signifikanten Unterschiede zwischen beiden Verfahren[87], welche unter dem Rasterelektronenmikroskop unterschiedliche Rauheiten aufwiesen. Die statische Kultivierung der untersuchten SLM-Designs (kubisch, pyramidal, diagonal) resultierte initial nicht in signifikanten Unterschieden der OB-Aktivität; im Laufe der Kultivierung nahm diese jedoch auf der pyramidalen Struktur bis zu Tag 8 signifikant zu. Eine vermehrte Zellausbreitung und -prolife-

ration über ähnliche Zeiträume ist bereits bewiesen[57,88]. In dieser Studie führten die größte Porosität (76 %) und die kleinste Porengröße (400 - 620 µm) zur höchsten Zellaktivität und gutem Einwachsen der hOB. Größere Porosität ist mit verbessertem Knocheneinwachsen assoziiert; als optimale Porengröße werden 100 - 400 µm angegeben; Variationen treten von 20 - 1500 µm auf[80]. Eine vergrößerte Oberfläche, bedingt durch kleinere Poren, ist für die initiale Zelladhäsion und die Überbrückung der Poren vorteilhaft [57]. Verschiedene Porengrößen (µm - nm) sind für die Vaskularisierung des Scaffolds und das Eindringen biologisch aktiver Moleküle notwendig[89]. Ein positiver Einfluss poröser Ti6Al4V-Strukturen auf Zell- und Knochenwachstum konnte sowohl in vitro und in vivo gezeigt werden[80,83]. Auch das verstärkte Zellwachstum auf den Scaffoldstegen bei größeren Poren ist bereits belegt[61]. Die gewählte hohe Porosität der pyramidalen und diagonalen Strukturen (~75 %) ist aus mechanischer Sicht und für eine ausreichende Versorgung optimal[62]. Die Steifheit nimmt dabei aufgrund der zellulären Mechanosensitivität Einfluss auf OB-Wachstum und Matrixsynthese[58]. Wohl unabhängig von der Porengröße[90] ergab die Bestimmung der Kollagensynthese keine signifikanten Unterschiede zwischen den einzelnen Strukturen. Die geringe Zellmigration und das vermehrte Vorkommen toter Zellen in tieferen Ebenen ist womöglich auf die statische Kultivierung und das Verstopfen der Poren zurückzuführen[91]. Das Fehlen eines kontinuierlichen Mediumflusses resultiert in einer Mangelversorgung mit Nähr- und Sauerstoff und einer damit verbundenen Ansäuerung des Mediums[63]. Die dynamische Kultivierung der in Studie I verwendeten Scaffolds mit einer kontinuierlichen Frischmediumzufuhr von 50 µl resultierte gegenüber der statischen Kultivierung lediglich in einer leichten Zunahme der Zellaktivität bei der pyramidalen Struktur; diese war jedoch signifikant höher als auf den weiteren Strukturen. Dies ist zurückzuführen auf die Kombination von optimaler Porosität, Porengröße, Porendesign und Interkonnektivität[62], ähnlich den Parametern von Haslauer et al.[84]. Die weiteren Scaffolds wiesen, im Gegensatz zu anderen Studien[63,66,92], keine deutliche Steigerung der Zellaktivität nach dynamischer Kultivierung auf. In der pyramidalen Struktur zeigte sich eine verbesserte Zellmigration bis an die Scaffoldunterseite, bedingt durch die vorherrschenden Strömungsbedingungen[65]. Abhängig von der verwendeten Struktur konnte demnach ein positiver Einfluss des verwendeten Bioreaktors nachgewiesen werden. Im Vergleich zu anderen Studien ist die gewählte Fließrate gegebenenfalls zu niedrig; diese variieren zwischen 0,01 ml/min bis meist über 0,1 ml/min und sogar 10 ml/ml[66,67,93–96]. Die Fließrate und -frequenz (oszillatorisch, kontinuierlich, pulsierend) haben Einfluss auf die Adhäsion, Proliferation und Nekrose mechanosensitiver OB[66–68] und variieren in den verschiedenen Zonen des Scaffolds, was zusätzlich durch dessen Abmessungen beeinflusst wird[63]. Aufgrund des verwendeten Bioreaktordesigns erfolgt zudem ein Umfließen des Scaffolds, wodurch Fließkraft im Bereich des Scaffolds verloren geht[63]. Generell war es durch die Anwendung des gewählten dynamischen Systems nicht möglich, die Veränderung der Kollagensynthese zu bestimmen.

5.2. Studie II: Biokompatibilität von Nitinol-Oberflächen

Die Elemente Vanadium und Aluminium, aber auch Cobalt und Chrom sind mit der spezifischen Ausbildung systemischer Effekte wie Neuro-, Hepato- und Nephrotoxizität und sogar verminderter Fruchtbarkeit und Embryotoxizität assoziiert[26,97,98]. Zudem kommt es häufig zum Auftreten von Hypersensitivitäten gegen metallische Materialien, v. a. Nickel und seine Ionen[98]. Formgedächtnislegierungen wie Nitinol bestehen zu 55 wt% aus Nickel (Ni) und zu 45 wt% aus Titan (Ti) (NOL für Naval Ordinance Laboratory)[77] und können neue Möglichkeiten für expandierende, komprimierende oder andere funktionelle Implantate eröffnen, da sie sich mit einer reversiblen Verformbarkeit von bis zu 8 % an das mechanische Deformationsverhalten des Knochens anpassen können[99]. Die in Studie II verwendeten Titanlegierungen (Ti6Al4V, SLM-Ti6Al4V, NiTi, NiTi + DLC) wurden hinsichtlich ihrer Besiedlung mit MG-63-Zellen sowie drei humanen Zelltypen (hOB, hFB, hMP) beurteilt. Zunächst wurden alle Proben mit Kulturmedium inkubiert, um einen möglichen negativen Einfluss abgegebener Ionen auf darin kultivierte Zellen auszumachen; dieser konnte jedoch nicht festgestellt werden. Die Probenüberstände wurden nach 72 h stichprobenartig mittels optischer Emissionsspektrometrie mit induktiv gekoppeltem Plasma (ICP-OES) untersucht. Die ermittelten Werte lagen jedoch unter der Messgrenze, bedingt durch die hohe Verdünnung der Proben, welche aufgrund technischer Gegebenheiten notwendig war. Auch Cortoizo et al. konnten nach 48 h keine Ionenfreisetzung feststellen[100]. Nickelionen werden nach Kontakt mit Körperflüssigkeiten oder Kulturmedium abgegeben[70,101,102], dennoch zeigen NiTi-Implantate eine gute Biokompatibilität, welche vom Korrosionsverhalten im Körper abhängig ist[103-106]. Dabei haben pH-Wert, Temperatur und chemische Eigenschaften des jeweiligen Mediums als auch die Rauheit der Oberfläche einen entscheidenden Einfluss auf die Menge und Rate der abgeschiedenen Ionen[100,107]. Der Prozess der Zelladhäsion als auch das Wachstum werden durch die abgeschiedenen Ionen nicht beeinflusst, welche möglicherweise als Co-Faktoren oder Inhibitoren enzymatischer Prozesse fungieren können[103]. Um das Problem der Nickelionenabscheidung zu vermeiden bzw. zu vermindern, kann eine verbesserte Korrosions- und Abriebbeständigkeit z. B. durch eine DLC-Beschichtung erreicht werden[108]. Die Adhäsion, Vitalität als auch Proliferation von Zellen können durch die Verwendung diamantbeschichteter Oberflächen unterstützt werden[17,109]. Diese sind einerseits mit verbesserter OB-Proliferation und hoher Biokompatibilität ohne inflammatorische Reaktionen in vitro und in vivo assoziiert[69,110,111], andererseits sollen unbehandelte Oberflächen vorteilhafter sein[112]. In Studie II zeigte sich die niedrigste metabolische Aktivität von hFB und hMP auf NiTi + DLC, während die Pro-Kollagen 1-Synthese bei hOB und hFB erhöht war. Die MMP-1-Synthese war bei hFB auf nahezu allen Oberflächen gegenüber dessen Substrat CICP vermindert. Die Genexpressionsanalysen zeigten bei keiner der Oberflächen eine deutliche inflammatorische Antwort, während die Konzentrationen an Zytokinen

und Chemokinen im Überstand aller Zelltypen leicht erhöht waren. Eine leichte Zytotoxizität von NiTi-Materialien bei hFB ist bereits bekannt[113]. Zwar kam es auf der DLC-beschichteten NiTi-Oberfläche zu einer verminderten Zelldichte bei MG-63 und hMP, dennoch zeigte sich diese Oberfläche biokompatibel, wenn auch mit geringen inflammatorischen Reaktionen. Die Ergebnisse weisen auf eine vielversprechende Biokompatibilität bei SLM-Ti6Al4V und unbeschichtetem NiTi hin, begründet durch eine hohe metabolische Aktivität aller Humanzellen mit lediglich leichter Inflammation und ohne negativen Einfluss auf die Matrixproduktion. Die gute Biokompatibilität von NiTi wurde für MG-63-Zellen sowie OB und FB bereits bestätigt[112,114]; ebenso für beschichtetes Ti6Al4V und Titan-Nitrit-Beschichtungen[115]. Durch Titanmaterialien werden MP zur Sekretion inflammatorischer Zytokine angeregt[116]. Generell ist die Biokompatibilität und Zellantwort vom Nickelgehalt des Materials abhängig[117] und auch in der gebildeten Oxidschicht begründet[113]. Es ist belegt, dass Nitinol ähnlich biokompatibel wie reines Titan ist[69,102,113,118,119].

5.3. Studie III: Biokompatibilität neuartiger Nioboberflächen

Niob wird als β-Stabilisator eingesetzt, um die mechanischen Eigenschaften von Titanlegierungen zu verbessern, indem es das Elastizitätsmodul (60 - 80 GPa; Knochen ~40 GPa) vermindert, welches bei kompakten Titanimplantaten bei 80 - 130 GPa liegt[120,121]. Studie III stellt verschiedene niobbasierte Oberflächen (Nb Amperit, Nb Ampertec, Nb-Blech, Ti-42Nb gesintert, SLM-Ti-42Nb) hinsichtlich der Besiedlung mit hOB und hFB dem gängigen Ti6Al4V gegenüber. Ähnlich wie bei Nitinol konnten auch für Ti-Nb-Legierungen Superelastizität und ein Formgedächtniseffekt nachgewiesen werden[122,123]. Versuche mit Zelllinien[124] als auch hOB[125] haben gezeigt, dass Niob gegenüber Titan zu einer verbesserten Proliferation, metabolischen Aktivität und Genexpression führt. Die Kultivierung von OB-Zelllinien auf Metallscheiben verschiedener Reinelemente zeigte eine ähnliche initiale Zelladhäsion und eine hohe Proliferation für Titan und Niob[97]. Gesintertes Ti-42Nb, wie in Studie III genutzt, resultierte in besserer Biokompatibilität und Mechanik als Ti6Al4V, auch beschichtete Ti-Nb-Legierungen waren reinem Titan überlegen[74,122]. FB-Zelllinien und (h)OB wiesen auf reinem Niob und Ti-Nb-Legierungen (Ti-10Nb, Ti-35Nb, Ti-45Nb) eine höhere oder ähnliche Zelladhäsion, -vitalität sowie Differenzierung, Proliferation als auch Matrixsynthese gegenüber Titan auf[73,126–129]. Auch für eine Vielzahl weiterer Titanlegierungen mit unterschiedlichen Niobanteilen (Ti-50Nb, Ti-30Nb, Ti-26Nb, Ti-15Nb, Ti-5Nb) ist die Biokompatibilität für Zelllinien von FB und OB bestätigt[118,121,130–132], auch nach Zugabe weiterer Elemente wie Aluminium oder Tantal[133,134]. Hier ergaben stichprobenartige Messungen der Probenüberstände mittels Emissionsspektroskopie ebenfalls keine verwertbaren Ergebnisse. Dennoch ist der konzentrationsabhängige Einfluss von Niobionen auf die Adhäsion, Differenzierung und Proliferation osteogener Zellen bereits belegt[135]; generell sind Nioboberflächen für eine gute Korrosionsresistenz bekannt[136].

5.4. Einfluss der Oberflächeneigenschaften eines Materials (Studie II, III)

In der vorliegenden Studie II zeigten die Oberflächen mit der größten Abweichung im Rauheitswert Rz (SLM-Ti6Al4V Rz ~70 µm; NiTi Rz ~1 µm) eine ähnliche Zellaktivität. Matrixproduktion und Inflammationspotential schienen von der Oberflächenrauheit unbeeinflusst, ebenso die Adhäsion von MG-63-Zellen[114], was sich an der ähnlichen Zellaktivität auf allen Proben der Studie II erkennen lässt. Jedoch ist eine gehemmte MG-63-Proliferation sowie eine vermehrte osteogene Differenzierung bei sehr rauen Titanoberflächen nachgewiesen worden[137]. Die Ergebnisse der Studie III (Niob) belegen, dass OB raue Oberflächen bevorzugen, da die Nb Ampertec- und Ti-42Nb-Oberflächen mit den größten Rauheiten hinsichtlich metabolischer Aktivität und Kollagensynthese die besten Ergebnisse lieferten. Insgesamt traten zwischen den Proben starke Unterschiede bezüglich des Rauheitswertes Rz auf. Demnach scheint neben der oberflächlichen Rauheit auch das Material selbst eine Rolle zu spielen. Bei ähnlicher Rauheit erzielten Nb Ampertec und das Niobblech sowohl für hOB als auch hFB konträre Ergebnisse. Trotz umfangreicher Reinigung und Sterilisation könnte dies durch mögliche fertigungsbedingte Rückstände auf dem Niobblech bedingt sein. Besonders die Oberflächenrauheit, -topografie und -chemie sind entscheidend für die zellspezifische Antwort[101,129,138]; dabei vorrangig die äußerste Schicht (ca. 100 nm)[26]. So ist die osteogene Adhäsion und Proliferation rauheitsabhängig[129,139–141]; die topografischen Eigenschaften eines Materials beeinflussen die Stimulation der entwicklungsspezifischen Zelldifferenzierung[26]. Raue, hydrophile Titanoberflächen können die OB-Differenzierung und -proliferation auslösen[26]. Eine Modifikation der Oberflächeneigenschaften resultiert ebenfalls in einer veränderten Zellantwort[78]. Die Struktur, Rauheit und Orientierung machen eine Implantat-oberfläche aus, wobei eine Unterteilung (Ra) in minimale Rauheit (0,5 – 1 µm), mittlere Rauheit (1 – 2 µm) und rau (2 – 3 µm) erfolgen kann[78]. Eine mittelmäßige Rauheit (Rz ~5 – 16 µm; Ra ~ 1,25 µm) ermöglicht eine optimale Zellanhaftung sowie eine stärkere Zellantwort in vitro und in vivo, während Mikro- und Ultratopografien die Osteogenese beeinflussen[26]. Weiterhin werden Zellmorphologie und die Synthese zellspezifischer Marker verändert[26]. Jedoch führen Rauheiten von über Rz 16 µm (Ra > 4 µm) in vitro zu einer Hemmung der Zelldifferenzierung[142]; Goriainov et al. erkannten ab ca. Rz 10 µm (Ra > 2,5 µm) eine verminderte OB-Proliferation bei induzierter Differenzierung[26]. Eine verbesserte OB-Adhäsion und Osseointegration konnten für nanostrukturierte Titanbeschichtungen nachgewiesen werden, wobei raue Strukturen zu einer verstärkten OB-Differenzierung und schnelleren Zellausbreitung führten[81]. Dennoch bestehen über die bevorzugte Rauheit von OB kontroverse Studien[55,137,143–145], auch ihr Reifungsstatus beeinflusst die zelluläre Antwort[142]. Die Vorliebe von FB für glatte Oberflächen ist umfassend bestätigt[137,143,146]. Dies kann in dieser Studie nicht belegt werden, da auch hFB die höchsten Werte auf den sehr rauen Proben zeigten. Die Aktivierung und Polarisierung von Monozyten und MP wird dagegen durch raue Oberflächen ausgelöst

und durch Porosität beeinflusst[147-149]. Dabei scheint das Oberflächenmaterial den Einfluss der Topografie weniger zu tangieren[26]. Das orthopädische Element ist nach seiner Implantation biologischen Flüssigkeiten ausgesetzt, was in der Modifikation der Oberfläche durch Wirtsionen und -zellen resultiert. Der eigentliche Prozess der Oberflächenbesiedlung mit rekrutierten Zellen scheint dabei relativ unspezifisch zu sein[26].

5.5. Zelluläre Reaktionen auf Fremdkörper im Knochen-Implantat-Interface

Unabhängig von ihrer Zusammensetzung führen nahezu alle Materialien zu einer Fremdkörperreaktion, vorrangig vermittelt durch MP, welche sich in einer einzigartigen inflammatorischen Antwort widerspiegelt[149]. Nach dem Eindringen eines Fremdkörpers unterscheiden sie zunächst zwischen fremd und nicht fremd und binden über integrinvermittelte adhäsive Interaktionen an erkannte Fremdkörper, was u. a. zur Neuanordnung ihres Aktinzytoskeletts, Zellwanderung, der Aktivierung spezifischer Zellfunktionen sowie Zelldifferenzierung und -proliferation führt[32,150]. Die Erkennung synthetischer, künstlicher Biomaterialien durch MP stellt eine neue Herausforderung für die Zelle dar und wird durch die Oberflächenchemie des Substrates, die präadhäsive Proteinadsorption und die individuelle Reaktion des Implantatempfängers bestimmt[150]. Makrophagen als spezialisierte, „professionelle“ Phagozyten im Wirtsimmunsystem sind verantwortlich für den Schutz bzw. die Abwehrreaktion bei Infektionen, Transplantationen sowie bei der Implantation von Biomaterialien und der Beseitigung von Mikroorganismen, geschwächter oder apoptotischer Zellen[150]. In vivo reagieren sie in Hart- und Weichgeweben aktiv auf nahezu alle Biomaterialien, deren Eigenschaften und Größe bestimmen die Art und Weise der MP-Antwort. Dabei werden Abriebpartikel, die kleiner sind als einkernige MP (~10 µm), phagozytiert; bei größeren Partikeln (10 – 100 µm) und Vollmaterialien (Platten, Schrauben, Implantate) kommt es durch Zellfusion zur Ausbildung osteoklastenähnlicher, aber resorptionsträger Fremdkörperriesenzellen (FBGCs)[150]. Die Phagozytose von Abriebpartikeln ist ein wesentlicher Schritt bei der Ausbildung einer Osteolyse und der aseptischen Lockerung. Makrophagen als auch FBGCs sind mit chronischen Entzündungen, osteolytischen Effekten und gestörter Knochenformation assoziiert; MP zudem in die Degradation von Biomaterialien involviert[150]. Kann die akute Entzündungsantwort nicht aufgelöst werden, entwickelt sich eine chronische Entzündung mit einer fibrösen Einkapselung des eingesetzten Materials[149]. Vollmaterialien und metallische Partikel lösen unterschiedliche biologische Antworten aus[151]. Obwohl die Antwort auf Abriebpartikel hauptsächlich durch MP vermittelt wird, sind etliche andere Zelltypen beteiligt[149]. Inflammation und Knochenresorption sind die Folge von partikulärem cpTi und Ti6Al4V[151]. Nach Exposition mit cpTi-Partikeln schütten OB vermehrt IL-6 aus und zeigen eine erhöhte Kollagenexpression, während FB zeit- und dosisabhängig verstärkt MCP-1, MMPs und IL-6 produzieren[151]. Titanpartikel sind mit der Produktion proinflammatorischer Zytokine (IL-6, MCP-1, TNF-α) und der Ausbildung einer leichten Entzündungsreaktion assoziiert[151].

5.6. Studie III: Niobpulver im Kontext der aseptischen Implantatlockerung

Vor dem Hintergrund der aseptischen Implantatlockerung wurden erstmals Expositionsversuche mit Niobpulvern (Nb Amperit, Nb Ampertec, sphärisches Ti-42Nb in zwei Partikelgrößen) durchgeführt. Der dosis-, pulver- und zeitabhängige Einfluss auf hOB wurde untersucht. Nb Ampertec als auch Ti-42Nb (63 µm < x) resultierten mit zunehmender Konzentration und Kultivierungsdauer in verminderter Zelldichte und -aktivität sowie vermehrtem Zellsterben. Großkörniges Ti-42Nb führte, proportional zu Zeit und Konzentration, zu einem Anstieg der Zellaktivität, jedoch wie Nb Amperit mit leicht reduzierter Zelldichte. Bei der Einordnung der Ergebnisse der Expositionsversuche aus Studie III sind verschiedene Faktoren zu beachten. Die verwendeten Pulver zeichnen sich durch eine unterschiedliche chemische Zusammensetzung und Form aus. Reine Pulver (Nb Ampertec, Nb Amperit) mit unregelmäßiger, kantiger Morphologie stehen gleichmäßig runden Pulverpartikeln aus Ti-42Nb-Legierungen gegenüber. Dies resultiert in vier verschiedenen Partikelgrößen zwischen 15 - 350 µm. Womöglich ist die am stärksten verminderte hOB-Aktivität und Kollagensynthese durch das Nb Ampertec-Pulver, welches als Vollmaterial sehr positive Ergebnisse lieferte, in seiner groben Morphologie und der größeren Pulvergröße gegenüber dem weiteren Reinpulver Nb Amperit begründet. Die Ti-42Nb-Pulver zeigten bezüglich der Partikelgröße ein entgegengesetztes Bild, weshalb der Einfluss auf die Zellaktivität und Kollagenproduktion auf die chemische Partikelzusammensetzung und weniger die Partikelgröße zurückzuführen sein könnte. Zumindest für PE-Partikel ist die Abhängigkeit der zellulären Antwort von der Partikelform belegt. Sphärische, gleichmäßige Partikel sind weniger aggressiv als andere Morphologien wie Fibrillen oder kantige Partikel[152,153]. Frühere in vitro-Arbeiten zum Einfluss von Niob- oder niobhaltigen Partikeln sind rar, weshalb ein Vergleich der eigenen Ergebnisse erschwert ist. Partikel von Niob-Legierungen (z. B. Ti-6Al-7Nb) verursachen in Monozyten eine geringere Entzündungsantwort als gängiges Ti6Al4V[75]. OB-Zelllinien unter dem mehrtägigen Einfluss von Nb- und Ti-Abrieb in unterschiedlichen Konzentrationen zeigten eine dosisabhängig verminderte Zellvitalität; stärker reduziert mit Titanpartikeln[154,155]. Auch Ti6Al4V-Partikel werden in vitro mit zytotoxischen Effekten in Verbindung gebracht[26]; Metallpulver aus Titan und Niob zeigen gegenüber den biokompatiblen Vollmaterialien zytotoxische Auswirkungen[121]. Die verwendeten Pulver führten lediglich zu einem sehr geringen Anstieg von IL-6 und IL-8, ohne eindeutige Abhängigkeit von Konzentration und Pulvertyp. Vergleichbare Studien zur Untersuchung von Zellaktivität, Kollagensynthese und Inflammationspotential hOB unter dem Einfluss von Niobpulvern liegen bis dato nicht vor.

5.7. Studie IV: Beteiligung knochenresorbierender OK an der Osteolyse

Die zellulären Antworten von OB und MP unter Partikeleinfluss sind bereits umfassend untersucht. In vitro reagieren MP auf Metallpartikel mit der Produktion von Cathepsin K[156]; kerami-

sche Partikel lösen in MP die Produktion osteolytischer Zytokine aus[157]. Osteoblasten sezernieren vermehrt Zytokine und führen so indirekt zu verminderter Knochenformation, welche zudem durch eine erhöhte OK-Aktivität unterstützt wird[157]. Auch weisen OB eine ähnliche inflammatorische Signalantwort wie MP auf und reagieren auf metallischen und PE-Abrieb mit verminderter Kollagenexpression; demgegenüber zeigen MP nach Partikelexposition in vitro eine gehemmte MMP-Produktion[157]. Aufgrund der überschaubaren Anzahl entsprechender Arbeiten wurde der Einfluss von cpTi- und ZrO_2-Partikeln auf die Morphologie und Funktionalität reifer OK untersucht (Studie IV). Die Ergebnisse zum Einfluss auf reifende Prä-OK befinden sich derzeit im Review-Prozess. Differenzierte Monozyten wurden mit Partikeln (je 0,01/ 0,1 mg/ml) inkubiert (3 d, 7 d). Wie bereits anderweitig belegt[158,159], konnte die Partikelaufnahme durch die OK gezeigt werden, sodass ein direkter Einfluss auf die OK-Differenzierung und -Resorption erfolgt[159–161]. Eine leichte, initiale Zunahme der Zellgröße als Folge vermehrter Zellfusion konnte nach Partikelexposition festgestellt werden; jedoch kein deutlicher Effekt auf eine erhöhte Zellkernanzahl (Studie IV), welche in direkter Verbindung mit der Resorptionsaktivität steht[162]. Ein stimulierender Effekt metallischer Partikel auf die Größe und Anzahl sich entwickelnder OK wurde bereits gezeigt[163]; auch eine erhöhte Zellzahl in vivo[160]. Partikel scheinen einen größeren Einfluss auf OK-Rekrutierung und -Differenzierung als auf deren Aktivierung und Überleben zu haben[160]. In Studie IV kam es zu keinem Zeitpunkt zu deutlichen Abweichungen der Stoffwechselaktivität nach Exposition mit Metall- und Keramikpartikeln in unterschiedlichen Konzentrationen, vermutlich begründet in einer verminderten mitochondrialen Dynamik aufgrund der Partikelaufnahme[164]. Ein partikulärer Einfluss auf die OK-Proliferation ist ebenfalls anzunehmen[163]. Verschiedene Partikelcharakteristiken beeinflussen die OK-Formation unsignifikant[17]. Die signifikanten Unterschiede OK-spezifischer und matrixrelevanter Gene zwischen partikelfreier Kontrolle und den exponierten Gruppen weisen auf eine direkte Beteiligung reifer OK an der verstärkten Resorption des Knochens und der daraus resultierenden Osteolyse hin. Der Adhäsionsmarker VNR wies nach Partikelexposition, insbesondere mit ZrO_2, erhöhte Expressionslevel auf. TRAcP sowie RANK als Regulatoren der Differenzierung und Aktivität wurden ebenfalls verstärkt exprimiert; v. a. durch den Einfluss der ZrO_2-Partikel. Die anfänglich signifikant erhöhte CTSK-Expression, als Marker der OK-Resorption, fiel im zeitlichen Verlauf der OK-Kultivierung unter den Kontroll-wert. Insgesamt zeigte sich eine partikelinduzierte Zunahme relevanter Gene und OK-Aktivität, ebenfalls belegt durch Zhang et al.[159]. Entgegen anderer Arbeiten mit Zementpartikeln konnte keine signifikant vermehrte Resorption auf Proteinlevel nachgewiesen werden[159,165]. In der initialen Kultivierungsphase konnte allerdings eine signifikant erhöhte MMP-1-Expression ermittelt werden. Dessen Produktion wird beeinflusst durch das resorptionsfördernde IL-1[166]. In vivo besteht ein signifikanter und direkter Zusammenhang zwischen MMP-Expression, erhöhter OK-Anzahl und Knochenresorption[167]. In Studie IV zeigte sich im zeitlichen Verlauf nach Partikelexposition eine

abnehmende TIMP-1-Expression und -Synthese. Insbesondere die ZrO_2-Partikel beeinträchtigten dabei die TIMP-1-Synthese der OK. Dessen Überexpression in OB kann in vitro sowie in vivo zu einer Hemmung der OK-Resorption führen[168,169].

5.8. Einfluss der Partikeleigenschaften auf die Osteolyse (Studie III, IV)

Einflussfaktoren bei der zellulären Reaktion (Proliferation, Differenzierung, Ausschüttung inflammatorischer Mediatoren) auf Partikelabrieb sind v. a. die Partikelgröße und -konzentration, aber auch deren Zusammensetzung sowie mögliche Ionen[17,101,102]. Abriebpartikel initiieren die systemische Migration von MZ/MP zum Ort ihrer Entstehung[156]. Makrophagen kommt eine entscheidende Rolle bei der Erkennung von Abriebpartikeln zu; dies schließt das Abtasten, Chemotaxis sowie Phagozytose ein[156]. An der durch partikulären Abrieb ausgelösten chronisch entzündlichen Antwort und Osteolyse im Knochen-Implantat-Interface sind neben MP/FBGCs, FB und OB auch OK beteiligt[17]. Nach der Aufnahme der Partikel kommt es zu deren Akkumulation, was schließlich zum Aufreißen der endosomalen Membran und zur Ausschüttung von Cathepsinen in das Cytosol führt[156]. Objekte, welche für die Phagozytose zu groß sind, werden von OK durch Abgabe entsprechender Säuren und Enzyme extern abgebaut[170]. Nicht nur die Phagozytose, auch die oberflächliche Strukturerkennung über entsprechende Rezeptoren vermittelt die Antwort auf Partikel[155,156]. Dabei spielt womöglich auch die hohe Affinität von Lipopolysaccharidproteinen (LPS) zu Partikeloberflächen und deren leichte Anhaftung eine Rolle, da LPS-freie Titanpartikel eine geringere Expression inflammatorischer Zytokine hervorrufen[156]. Abriebpartikel aus dem Simulator und periprothetischem Gewebe variieren in ihren Morphologien und treten in Größen unter 1 µm auf[17]. Hüftprothesen produzieren gegenüber Knieprothesen zumindest kleinere PE-Partikel, jedoch ohne signifikante Abweichungen der Abriebrate[17]. Mögliche Einflussfaktoren auf Größe, Form und Anzahl von Partikelabrieb wurden diskutiert[171]. Aus Geweben isolierte Metallpartikel von MoP-Gelenken weisen geringere Partikelgrößen auf als entsprechender PE-Abrieb[17]. Gelenktyp, Gleitpaarung als auch Material und Faktoren wie Fluide und Belastung beeinflussen die entstehenden Partikelmorphologien[17]. Zudem führt offensichtlich eine positive Oberflächenladung zu einer verstärkten Partikelaufnahme[172]. Versuche mit Nanopartikeln ergaben, dass nicht-phagozytotische Zellen bevorzugt kationische Partikel und phagozytotische Zellen eher anionische Partikel aufnehmen[173]. Gleitpaarungen mit PE-Komponente produzieren größere Partikel als MoM- und CoC-Prothesen[17,157]. Zudem ist das Volumen der Partikel aus MoM-Paarungen am größten, welche zudem eine sehr starke Immunantwort hervorrufen. CoC-Paarungen zeigen eine 10x geringere Partikelformation und weisen eine geringe Entzündungsantwort auf[157]. Unabhängig von Endoprothesendesign oder Materialeigenschaften produzieren künstliche Gelenkprothesen Partikel, welche bis zu einer gewissen Belastung von Immunzellen beseitigt werden können und erst darüber hinaus die osteolytische Kaskade in Gang setzen. Auf eine überschießende

Entzündung folgt schließlich eine gestörte Knochenformation und -regeneration und die Verschiebung des ausgeglichenen Bone Remodelings in Richtung vermehrter Knochenresorption. Eine leichte Osteolyse wird mit einer Abriebrate von unter 80 mm³ assoziiert, eine leichte bis mittlere mit 80 - 140 mm³; über 140 mm³ spricht man von einem erhöhten Grad an Osteolyse[157]. Titanlegierungen in Festform rufen eine geringere inflammatorische Antwort und schädliche Effekte wie Zytotoxizität als Beiprodukte wie Partikel und Ionen hervor[151].

5.9. Limitationen und Ausblick

Der geringe Einfluss der dynamischen Kultivierung von hOB auf Ti6Al4V-Scaffolds in Studie I ist auf eine zu geringe Fließrate und das Bioreaktordesign zurückzuführen. Vergleichende Untersuchungen sollten daher mit einem bereits zur Verfügung stehenden System, welches eine direkte Perfusion des Scaffolds und erhöhte Fließraten erlaubt, z. B. bei oszillatorischer Strömung durchgeführt werden. Für weitere Partikelexpositionsversuche sollten neben kommerziell erhältlichen Materialien, auch Abriebpartikel aus Simulatorversuchen oder isoliert aus Gewebe verwendet werden. Die Variation von Partikeltypen, -konzentrationen und -größen sollte ausgedehnt und zudem Metallionen zur zellbiologischen Untersuchung herangezogen werden. Die Untersuchung von Vollmaterialien erfordert den Einsatz verschiedener Zelltypen, um auch zellspezifische Reaktionen auf Materialien bewerten zu können. Humanzellen sind aufgrund der höheren Aussagekraft und Spenderindividualität Zelllinien vorzuziehen. Das angewendete Methodenspektrum kann zur Beurteilung der Biokompatibilität noch erweitert werden, um weiterführende Aussagen ableiten zu können. Dazu könnte im Zuge von Partikelversuchen die Anwendung eines konfokalen Mikroskopes und spezieller Phagozytose-Assays erfolgen, um die zelluläre Aufnahme der Partikel detaillierter betrachten zu können. Bei Versuchen mit differenzierenden Zellen (MP, OK) sollte eine vorhergehende Zellsortierung, z. B. mittels Fluoreszenzmarkierung, vorgenommen werden, um Differenzierungsstadien genauer abgrenzen und untersuchen zu können. Die Charakterisierung der humanen Osteoklasten kann auf die durchflusszytometrische Bestimmung spezifischer immunphänotypischer Oberflächenmerkmale, die Anfärbung des Aktinringes sowie eine rasterelektronenmikroskopische Darstellung der Ruffled Border als auch von Resorptionslakunen, z. B. auf Dentin, ausgedehnt werden. Auch zur genauen Betrachtung der oberflächlichen Besiedlung durch unterschiedliche Zelltypen sollte auf das Rasterelektronenmikroskop zurückgegriffen werden; die Ausrichtung des Zytoskeletts (z. B. Aktin) und Integrine der Zelladhäsion untersucht werden. Vorherige Materialcharakterisierungen hinsichtlich detaillierter Elementzusammensetzung, Oberflächenladung sowie hydrophiler bzw. hydrophober Eigenschaften sollten zur besseren Einordnung erlangter Ergebnisse durchgeführt werden. Untersuchungen auf DNA-, RNA- sowie Gen- und Proteinebene sowie entsprechende Marker sollten ausgedehnt und zellspezifisch angepasst werden.

6 Zusammenfassung

Lasttragende Bereiche erfordern den Einsatz mechanisch stabiler, metallischer Implantate, um geschädigte Körperfunktionen zu behandeln. Deren mechanische Eigenschaften sowie eine gute Biokompatibilität sind dabei ausschlaggebend. Ti6Al4V-Legierungen können für die Herstellung poröser Scaffolds zur Behandlung großer Knochendefekte verwendet werden (Studie I). Die Modifizierung strukturierter 3D-Formkörper hinsichtlich Porendesign, Porengröße, Porosität sowie Interkonnektivität ist mittels additiver Fertigungsverfahren möglich. Vier unterschiedlich konfigurierte Ti6Al4V-Scaffolds wurden bezüglich ihrer Besiedlung mit Osteoblasten im statischen und dynamischen System beurteilt, um die optimale Struktur und Kulturbedingung zu ermitteln (Studie I). Das Scaffold mit pyramidalem Porendesign, kleinster Porengröße und größter Porosität erwies sich aufgrund der signifikant höheren metabolischen Aktivität, guter Kollagensynthese und Zellmigration als geeignete Leitstruktur. Das gewählte Bioreaktorsystem erlaubt keine eindeutige Aussage über einen signifikanten Vorteil der dynamischen Kultivierung; dennoch zeigte sich partiell ein leicht positiver Einfluss. Weiterhin ermöglichen Formgedächtnislegierungen neuartige medizinische Anwendungen. Im Rahmen der Entwicklung eines adaptiven Endoprothesensystems erfolgte die molekular- und zellbiologische Beurteilung zweier Nitinol- und Ti6Al4V-Oberflächen mit verschiedenen Humanzellen hinsichtlich Zellaktivität, Genexpression und Proteinsynthese als auch inflammatorischem Potential (Studie II). Es konnte gezeigt werden, dass Nitinol, abhängig von seiner Oberflächenmodifikation, eine Alternative zum häufig verwendeten Ti6Al4V darstellt. Spezielle β-Stabilisatoren wie Niob, verbessern die Materialeigenschaften von Titanlegierungen. Daher stellen Niob und seine Legierungen (v. a. Ti-42Nb) attraktive neue Biomaterialien dar. Vier verschiedene Oberflächen und vor dem Hintergrund der aseptischen Implantatlockerung erstmals entsprechende Partikel dieser Materialien wurden daher auf ihre zeit-, dosis- und typabhängige Wirkung auf Humanzellen untersucht (Studie III). Die verwendeten Materialien zeigen vielversprechende Ergebnisse. Es treten Unterschiede und Abhängigkeiten zwischen den jeweiligen Vollmaterialien und deren Pulverformen auf. Besonders Ti-42Nb kann als Vollmaterial sowie als großkörniges Pulver mit positiven Ergebnissen hinsichtlich Zellaktivität, Kollagensynthese und Inflammation überzeugen und bietet sich so als aussichtsreiche Alternative für Ti6Al4V an. Um das Problem der aseptischen Lockerung erneut aufzugreifen, wurden reife, humane OK mit Titan- und Zirkoniumoxidpartikeln kultiviert und bezüglich Dosis-, Partikel- und Zeitabhängigkeit ausgewertet (Studie IV). Es konnte gezeigt werden, dass reife OK aktiv am Prozess der Osteolyse als Ursache aseptischer Implantatlockerung beteiligt sind und dabei dosis-, zeit- und typabhängig auf die jeweiligen Abriebpartikel reagieren. Zur weiterführenden Analyse und Modifikation der neuartigen metallischen Biomaterialien sollten weitere Studien mit veränderten Parametern und weiteren methodischen Verfahren durchgeführt werden.

7 Literaturverzeichnis

1. Agarwal R, García AJ. Biomaterial strategies for engineering implants for enhanced osseointegration and bone repair. Adv Drug Deliv Rev 2015;94:53–62.
2. McEntire BJ, Bal BS, Rahaman MN, Chevalier J, Pezzotti G. Ceramics and ceramic coatings in orthopaedics. J Eur Ceram Soc 2015;35:4327–4369.
3. Xiao W, Wang Y, Pacios S, Li S, Graves DT. Cellular and Molecular Aspects of Bone Remodeling. Front Oral Biol 2016;18:9–16.
4. Florencio-Silva R, Sasso, Gisela Rodrigues da Silva, Sasso-Cerri E, Simoes MJ, Cerri PS. Biology of Bone Tissue: Structure, Function, and Factors That Influence Bone Cells. Biomed Res Int 2015;2015:421746.
5. Manolagas SC. Birth and death of bone cells: basic regulatory mechanisms and implications for the pathogenesis and treatment of osteoporosis. Endocr Rev 2000;21:115–137.
6. Stepien E. Acceleration of New Biomarkers Development and Discovery in Synergistic Diagnostics of Coronary Artery Disease. In: Branislav B, editor. Coronary Angiography - Advances in Noninvasive Imaging Approach for Evaluation of Coronary Artery Disease: InTech; 2011.
7. Sims NA, Martin TJ. Coupling the activities of bone formation and resorption: a multitude of signals within the basic multicellular unit. Bonekey Rep 2014;3:481.
8. Lewiecki EM. New targets for intervention in the treatment of postmenopausal osteoporosis. Nat Rev Rheumatol 2011;7:631–638.
9. Raggatt LJ, Partridge NC. Cellular and molecular mechanisms of bone remodeling. J Biol Chem 2010;285:25103–25108.
10. Boyce BF, Rosenberg E, Papp AE de, Le Duong T. The osteoclast, bone remodelling and treatment of metabolic bone disease. Eur J Clin Invest 2012;42:1332–1341.
11. Arboleya L, Castañeda S. Osteoimmunology: The Study of the Relationship Between the Immune System and Bone Tissue. Reumatología Clinica (English Edition) 2013;9:303–315.
12. Kular J, Tickner J, Chim SM, Xu J. An overview of the regulation of bone remodelling at the cellular level. Clin Biochem 2012;45:863–873.
13. Aherwar A, K Singh A, Patnaik A. Current and future biocompatibility aspects of biomaterials for hip prosthesis. AIMS Bioengineering 2015;3:23–43.
14. Li Y, Yang C, Zhao H, Qu S, Li X, Li Y. New Developments of Ti-Based Alloys for Biomedical Applications. Materials 2014;7:1709–1800.
15. Bitar D, Parvizi J. Biological response to prosthetic debris. World J Orthop 2015;6:172–189.
16. Chang J-D. Future bearing surfaces in total hip arthroplasty. Clin Orthop Surg 2014;6:110–116.
17. Nine M, Choudhury D, Hee A, Mootanah R, Osman N. Wear Debris Characterization and Corresponding Biological Response: Artificial Hip and Knee Joints. Materials 2014;7:980–1016.

18. MacInnes SJ, Gordon A, Wilkinson MJ. Risk Factors for Aseptic Loosening Following Total Hip Arthroplasty. In: Recent Advances in Arthroplasty: InTech; 2012.
19. Bosshardt DD, Chappuis V, Buser D. Osseointegration of titanium, titanium alloy and zirconia dental implants: Current knowledge and open questions. Periodontol 2000 2017;73:22–40.
20. Affatato S, Ruggiero A, Merola M. Advanced biomaterials in hip joint arthroplasty. A review on polymer and ceramics composites as alternative bearings. Composites Part B: Engineering 2015;83:276–283.
21. Wang W, Ouyang Y, Poh CK. Orthopaedic implant technology: Biomaterials from past to future. Ann Acad Med Singap 2011;40:237–244.
22. Bahraminasab M, Sahari BB, Edwards KL, Farahmand F, Arumugam M, Hong TS. Aseptic loosening of femoral components – A review of current and future trends in materials used. Materials & Design 2012;42:459–470.
23. Chug A, Shukla S, Mahesh L, Jadwani S. Osseointegration—Molecular events at the bone–implant interface: A review. Journal of Oral and Maxillofacial Surgery, Medicine, and Pathology 2013;25:1–4.
24. Jain R, Kapoor D. The dynamic interface: A review. J Int Soc Prev Community Dent 2015;5:354–358.
25. Ratner BD. The biocompatibility manifesto: Biocompatibility for the twenty-first century. J Cardiovasc Transl Res 2011;4:523–527.
26. Goriainov V, Cook R, M. Latham J, G. Dunlop D, Oreffo RO. Bone and metal: An orthopaedic perspective on osseointegration of metals. Acta Biomater 2014;10:4043–4057.
27. Elshahawy W. Biocompatibility. In: Sikalidis C, editor. Advances in Ceramics - Electric and Magnetic Ceramics, Bioceramics, Ceramics and Environment: InTech; 2011.
28. Klineberg I, Henry P. Per-Ingvar Brånemark: 3 May 1929--20 December 2014. Aust Dent J 2015;60:133.
29. Alford AI, Kozloff KM, Hankenson KD. Extracellular matrix networks in bone remodeling. Int J Biochem Cell Biol 2015;65:20–31.
30. Capulli M, Paone R, Rucci N. Osteoblast and osteocyte: games without frontiers. Arch Biochem Biophys 2014;561:3–12.
31. Del Fattore A, Capannolo M, Rucci N. Bone and bone marrow: the same organ. Arch Biochem Biophys 2010;503:28–34.
32. Jayakumar P, Di Silvio L. Osteoblasts in bone tissue engineering. Proc Inst Mech Eng H 2010;224:1415–1440.
33. Fakhry M, Hamade E, Badran B, Buchet R, Magne D. Molecular mechanisms of mesenchymal stem cell differentiation towards osteoblasts. World J Stem Cells 2013;5:136–148.
34. Schaffler MB, Cheung W-Y, Majeska R, Kennedy O. Osteocytes: master orchestrators of bone. Calcif Tissue Int 2014;94:5–24.

35. Lee CH, Shah B, Moioli EK, Mao JJ. CTGF directs fibroblast differentiation from human mesenchymal stem/stromal cells and defines connective tissue healing in a rodent injury model. J Clin Invest 2010;120:3340–3349.
36. Pacifici R. The immune system and bone. Arch Biochem Biophys 2010;503:41–53.
37. Soysa NS, Alles N, Aoki K, Ohya K. Osteoclast formation and differentiation: an overview. J Med Dent Sci 2012;59:65–74.
38. Endo-Munoz L, Evdokiou A, Saunders NA. The role of osteoclasts and tumour-associated macrophages in osteosarcoma metastasis. Biochim Biophys Acta 2012;1826:434–442.
39. Lee NK. Molecular Understanding of Osteoclast Differentiation and Physiology. Endocrinol Metab 2010;25:264.
40. Abu-Amer Y. NF-kappaB signaling and bone resorption. Osteoporos Int 2013;24:2377–2386.
41. Del Fattore A, Teti A, Rucci N. Bone cells and the mechanisms of bone remodelling. Front Biosci (Elite Ed) 2012;4:2302–2321.
42. Edwards JR, Mundy GR. Advances in osteoclast biology: old findings and new insights from mouse models. Nat Rev Rheumatol 2011;7:235–243.
43. Chambers TJ, Fuller K. How are osteoclasts induced to resorb bone? Ann NY Acad Sci 2011;1240:1–6.
44. Søe K, Delaissé J-M. Time-lapse reveals that osteoclasts can move across the bone surface while resorbing. J Cell Sci 2017;130:2026–2035.
45. Gruber R. Molecular and cellular basis of bone resorption. Wien Med Wochenschr 2015;165:48–53.
46. Blair HC, Zaidi M. Osteoclastic differentiation and function regulated by old and new pathways. Rev Endocr Metab Disord 2006;7:23–32.
47. Kikuta J, Ishii M. Osteoclast migration, differentiation and function: novel therapeutic targets for rheumatic diseases. Rheumatology (Oxford) 2013;52:226–234.
48. Novinec M, Lenarcic B. Cathepsin K: a unique collagenolytic cysteine peptidase. Biol Chem 2013;394:1163–1179.
49. Paiva KBS, Granjeiro JM. Bone tissue remodeling and development: focus on matrix metalloproteinase functions. Arch Biochem Biophys 2014;561:74–87.
50. Atkins GJ, Haynes DR, Howie DW, Findlay DM. Role of polyethylene particles in peri-prosthetic osteolysis: A review. World J Orthop 2011;2:93–101.
51. Alidousti H, Taylor M, Bressloff NW. Periprosthetic wear particle migration and distribution modelling and the implication for osteolysis in cementless total hip replacement. J Mech Behav Biomed Mater 2014;32:225–244.
52. Beck RT, Illingworth KD, Saleh KJ. Review of periprosthetic osteolysis in total joint arthroplasty: an emphasis on host factors and future directions. J Orthop Res 2012;30:541–546.

53. Otto M, Kriegsmann J, Gehrke T, Bertz S. Abriebpartikel. Schlüssel der aseptischen Prothesenlockerung? Pathologe 2006;27:447–460.
54. Wang Z, Wang C, Li C, Qin Y, Zhong L, Chen B, Li Z, Liu H, Chang F, Wang J. Analysis of factors influencing bone ingrowth into three-dimensional printed porous metal scaffolds: A review. J Alloys Compd 2017;717:271–285.
55. Chan CW, Hussain I, Waugh DG, Lawrence J, Man HC. Effect of laser treatment on the attachment and viability of mesenchymal stem cell responses on shape memory NiTi alloy. Mater Sci Eng C Mater Biol Appl 2014;42:254–263.
56. Matassi F, Botti A, Sirleo L, Carulli C, Innocenti M. Porous metal for orthopedics implants. Clin Cases Miner Bone Metab 2013;10:111–115.
57. Chen J, Paetzell E, Zhou J, Lyons L, Soboyejo W. Osteoblast-like cell ingrowth, adhesion and proliferation on porous Ti-6Al-4V with particulate and fiber scaffolds. Mater Sci Eng C Mater Biol Appl 2010;30:647–656.
58. Murphy CM, O'Brien FJ. Understanding the effect of mean pore size on cell activity in collagen-glycosaminoglycan scaffolds. Cell Adh Migr 2010;4:377–381.
59. St-Pierre J-P, Gauthier M, Lefebvre L-P, Tabrizian M. Three-dimensional growth of differentiating MC3T3-E1 pre-osteoblasts on porous titanium scaffolds. Biomaterials 2005;26:7319–7328.
60. O'Brien B, Stinson J, Carroll W. Development of a new niobium-based alloy for vascular stent applications. J Mech Behav Biomed Mater 2008;1:303–312.
61. Warnke PH, Douglas T, Wollny P, Sherry E, Steiner M, Galonska S, Becker ST, Springer IN, Wiltfang J, Sivananthan S. Rapid prototyping: Porous titanium alloy scaffolds produced by selective laser melting for bone tissue engineering. Tissue Eng Part C Methods 2009;15:115–124.
62. Dabrowski B, Swieszkowski W, Godlinski D, Kurzydlowski KJ. Highly porous titanium scaffolds for orthopaedic applications. J Biomed Mater Res B Appl Biomater 2010;95:53–61.
63. Volkmer E, Drosse I, Otto S, Stangelmayer A, Stengele M, Kallukalam BC, Mutschler W, Schieker M. Hypoxia in static and dynamic 3D culture systems for tissue engineering of bone. Tissue Eng Part A 2008;14:1331–1340.
64. Ban Y, Wu Y-y, Yu T, Geng N, Wang Y-y, Liu X-g, Gong P. Response of osteoblasts to low fluid shear stress is time dependent. Tissue Cell 2011;43:311–317.
65. Zhang Z, Yuan L, Lee PD, Jones E, Jones JR. Modeling of time dependent localized flow shear stress and its impact on cellular growth within additive manufactured titanium implants. J Biomed Mater Res B Appl Biomater 2014;102:1689–1699.
66. Cartmell SH, Porter BD, García AJ, Guldberg RE. Effects of medium perfusion rate on cell-seeded three-dimensional bone constructs in vitro. Tissue Eng 2003;9:1197–1203.
67. Jaasma MJ, O'Brien FJ. Mechanical stimulation of osteoblasts using steady and dynamic fluid flow. Tissue Eng Part A 2008;14:1213–1223.

68. Du D, Furukawa KS, Ushida T. 3D culture of osteoblast-like cells by unidirectional or oscillatory flow for bone tissue engineering. Biotechnol Bioeng 2009;102:1670–1678.
69. Mikulewicz M, Chojnacka K. Cytocompatibility of medical biomaterials containing nickel by osteoblasts: A systematic literature review. Biol Trace Elem Res 2011;142:865–889.
70. Fili P, Lausmaa J, Musialek J, Mazanec K. Structure and surface of TiNi human implants. Biomaterials 2001;22:2131–2138.
71. Bernard SA, Balla VK, Davies NM, Bose S, Bandyopadhyay A. Bone cell–materials interactions and Ni ion release of anodized equiatomic NiTi alloy. Acta Biomater 2011;7:1902–1912.
72. Alvarez K, Nakajima H. Metallic Scaffolds for Bone Regeneration. Materials 2009;2:790–832.
73. Bai Y, Deng Y, Zheng Y, Li Y, Zhang R, Lv Y, Zhao Q, Wei S. Characterization, corrosion behavior, cellular response and in vivo bone tissue compatibility of titanium-niobium alloy with low Young's modulus. Mater Sci Eng C Mater Biol Appl 2016;59:565–576.
74. Woo KD. Microstructures and Mechanical Properties of Biocompatible Ti-42 wt.%Nb P/M Alloy. Met. Mater. -Int. 2008;14:327–333.
75. Niinomi M, Narushima T, Nakai M, editors (2015). Advances in Metallic Biomaterials: Tissues, Materials and Biological Reactions. Springer Series in Biomaterials Science and Engineering 3. Berlin Heidelberg: Springer Berlin Heidelberg. X, 348 p.
76. Lochner K, Fritsche A, Jonitz A, Hansmann D, Mueller P, Mueller-Hilke B, Bader R. The potential role of human osteoblasts for periprosthetic osteolysis following exposure to wear particles. Int J Mol Med 2011;28:1055–1063.
77. Liu X, Chu P, Ding C. Surface modification of titanium, titanium alloys, and related materials for biomedical applications. Mater Sci Eng R Reports 2004;47:49–121.
78. Saini M, Singh Y, Arora P, Arora V, Jain K. Implant biomaterials: A comprehensive review. World J Clin Cases 2015;3:52–57.
79. Shah FA, Trobos M, Thomsen P, Palmquist A. Commercially pure titanium (cp-Ti) versus titanium alloy (Ti6Al4V) materials as bone anchored implants - Is one truly better than the other? Mater Sci Eng C Mater Biol Appl 2016;62:960–966.
80. Wang X, Xu S, Zhou S, Xu W, Leary M, Choong P, Qian M, Brandt M, Xie YM. Topological design and additive manufacturing of porous metals for bone scaffolds and orthopaedic implants: A review. Biomaterials 2016;83:127–141.
81. Lin L, Wang H, Ni M, Rui Y, Cheng T-Y, Cheng C-K, Pan X, Li G, Lin C. Enhanced osteointegration of medical titanium implant with surface modifications in micro/nanoscale structures. J Orthop Translat 2014;2:35–42.
82. Sidambe A. Biocompatibility of Advanced Manufactured Titanium Implants - A Review. Materials 2014;7:8168–8188.

83. Matena J, Petersen S, Gieseke M, Kampmann A, Teske M, Beyerbach M, Murua Escobar H, Haferkamp H, Gellrich N-C, Nolte I. SLM produced porous titanium implant improvements for enhanced vascularization and osteoblast seeding. Int J Mol Sci 2015;16:7478–7492.
84. Haslauer CM, Springer JC, Harrysson OLA, Loboa EG, Monteiro-Riviere NA, Marcellin-Little DJ. In vitro biocompatibility of titanium alloy discs made using direct metal fabrication. Med Eng Phys 2010;32:645–652.
85. Karageorgiou V, Kaplan D. Porosity of 3D biomaterial scaffolds and osteogenesis. Biomaterials 2005;26:5474–5491.
86. Stangl R, Rinne B, Kastl S, Hendrich C. The influence of pore geometry in cp Ti-implants--a cell culture investigation. Eur Cell Mater 2001;2:1–9.
87. Jonitz-Heincke A, Wieding J, Schulze C, Hansmann D, Bader R. Comparative Analysis of the Oxygen Supply and Viability of Human Osteoblasts in Three-Dimensional Titanium Scaffolds Produced by Laser-Beam or Electron-Beam Melting. Materials 2013;6:5398–5409.
88. Hollander DA, Walter M von, Wirtz T, Sellei R, Schmidt-Rohlfing B, Paar O, Erli H-J. Structural, mechanical and in vitro characterization of individually structured Ti-6Al-4V produced by direct laser forming. Biomaterials 2006;27:955–963.
89. Salinas AJ, Vallet-Reg M. Bioactive ceramics: From bone grafts to tissue engineering. RSC Adv. 2013;3:11116.
90. Frosch K-H, Barvencik F, Viereck V, Lohmann CH, Dresing K, Breme J, Brunner E, Stürmer KM. Growth behavior, matrix production, and gene expression of human osteoblasts in defined cylindrical titanium channels. J Biomed Mater Res 2004;68:325–334.
91. Müller U, Imwinkelried T, Horst M, Sievers M, Graf-Hausner U. Do human osteoblasts grow into open-porous titanium? Eur Cell Mater 2006;11:8–15.
92. Egger D, Fischer M, Clementi A, Ribitsch V, Hansmann J, Kasper C. Development and Characterization of a Parallelizable Perfusion Bioreactor for 3D Cell Culture. Bioengineering 2017;4:51.
93. Grayson WL, Bhumiratana S, Cannizzaro C, Chao P-HG, Lennon DP, Caplan AI, Vunjak-Novakovic G. Effects of initial seeding density and fluid perfusion rate on formation of tissue-engineered bone. Tissue Eng Part A 2008;14:1809–1820.
94. Bancroft GN, Sikavitsas VI, van den Dolder J, Sheffield TL, Ambrose CG, Jansen JA, Mikos AG. Fluid flow increases mineralized matrix deposition in 3D perfusion culture of marrow stromal osteoblasts in a dose-dependent manner. Proc Natl Acad Sci USA 2002;99:12600–12605.
95. Sailon AM, Allori AC, Davidson EH, Reformat DD, Allen RJ, Warren SM. A novel flow-perfusion bioreactor supports 3D dynamic cell culture. J Biomed Biotechnol 2009;2009:873816.
96. Gaspar DA, Gomide V, Monteiro FJ. The role of perfusion bioreactors in bone tissue engineering. Biomatter 2012;2:167–175.

97. Zhang D, Wong CS, Wen C, Li Y. Cellular responses of osteoblast-like cells to 17 elemental metals. J Biomed Mater Res A 2017;105:148–158.
98. Abdel-Hady Gepreel M, Niinomi M. Biocompatibility of Ti-alloys for long-term implantation. J Mech Behav Biomed Mater 2013;20:407–415.
99. Wen CE, Xiong JY, Li YC, Hodgson PD. Porous shape memory alloy scaffolds for biomedical applications: A review. Phys. Scr. 2010;T139:14070.
100. Cortizo MC, De Mele, Monica Fernandez L, Cortizo AM. Metallic dental material biocompatibility in osteoblastlike cells: correlation with metal ion release. Biol Trace Elem Res 2004;100:151–168.
101. Geetha M, Singh AK, Asokamani R, Gogia AK. Ti based biomaterials, the ultimate choice for orthopaedic implants – A review. Progress in Materials Science 2009;54:397–425.
102. Es-Souni M, Fischer-Brandies H. Assessing the biocompatibility of NiTi shape memory alloys used for medical applications. Anal Bioanal Chem 2005;381:557–567.
103. Sevcikova J, Pavkova Goldbergova M. Biocompatibility of NiTi alloys in the cell behaviour. Biometals 2017;30:163–169.
104. Elahinia MH, Hashemi M, Tabesh M, Bhaduri SB. Manufacturing and processing of NiTi implants: A review. Prog Mater Sci 2012;57:911–946.
105. Hahn A, Fuhlrott J, Loos A, Barcikowski S. Cytotoxicity and ion release of alloy nanoparticles. J Nanopart Res 2012;14:1–10.
106. Hang R, Liu Y, Liu S, Bai L, Gao A, Zhang X, Huang X, Tang B, Chu PK. Size-dependent corrosion behavior and cytocompatibility of Ni–Ti–O nanotubes prepared by anodization of biomedical NiTi alloy. Corrosion Science 2016;103:173–180.
107. Fage SW, Muris J, Jakobsen SS, Thyssen JP. Titanium: a review on exposure, release, penetration, allergy, epidemiology, and clinical reactivity. Contact Dermatitis 2016;74:323–345.
108. Branzoi IV, Iordoc M, Branzoi F, Vasilescu-Mirea R, Sbarcea G. Influence of diamond-like carbon coating on the corrosion resistance of the NITINOL shape memory alloy. Surf. Interface Anal. 2010;42:502–509.
109. Lackner JM, Waldhauser W. Diamond and Diamond-like Carbon Coated Surfaces as Biomaterials. Berg Huettenmaenn Monatsh 2010;155:528–533.
110. Li Q, Xia Y-Y, Tang J-C, Wang R-Y, Bei C-Y, Zeng Y. In vitro and in vivo biocompatibility investigation of diamond-like carbon coated nickel-titanium shape memory alloy. Artif Cells Blood Substit Immobil Biotechnol 2011;39:137–142.
111. Roy RK, Lee K-R. Biomedical applications of diamond-like carbon coatings: A review. J Biomed Mater Res B Appl Biomater 2007;83:72–84.
112. Shabalovskaya S, Anderegg J, van Humbeeck J. Critical overview of Nitinol surfaces and their modifications for medical applications. Acta Biomater 2008;4:447–467.

113. Ponsonnet L., Tréheux D., Lissac M., Jaffrezic N., Grosgogeat B. Review of in vitro studies on the biocompatibility of NiTi alloys. Int J Appl Electrom 2006;23:147–151.
114. Michiardi A, Engel E, Aparicio C, Planell JA, Gil FJ. Oxidized NiTi surfaces enhance differentiation of osteoblast-like cells. J Biomed Mater Res A 2008;85:108–114.
115. Fleischmann L, Crismani A, Falkensammer F, Bantleon H-P, Rausch-Fan X, Andrukhov O. Behavior of osteoblasts on TI surface with two different coating designed for orthodontic devices. J Mater Sci Mater Med 2015;26:5335.
116. Tabish T.A., Butt M.T, Ali M. Biocompatibility behavior and biomedical applications of Ti-Ni based shape memory alloys: a brief review. JFET 2006;19.
117. Bogdanski D, Koller M, Bram M, Stöver D, Buchkremer HP, Choi J, Epple M, Muhr G. Schnelle Analyse der Biokompatibilität mittels gradierter Probekörper am Beispiel von Ni-NiTi-Ti. Biomed Tech/Biomed Eng 2002;47:500–502.
118. McMahon RE, Ma J, Verkhoturov SV, Munoz-Pinto D, Karaman I, Rubitschek F, Maier HJ, Hahn MS. A comparative study of the cytotoxicity and corrosion resistance of nickel-titanium and titanium-niobium shape memory alloys. Acta Biomater 2012;8:2863–2870.
119. Rocher P, El Medawar L, Hornez J-C, Traisnel M, Breme J, Hildebrand H. Biocorrosion and cytocompatibility assessment of NiTi shape memory alloys. Scripta Materialia 2004;50:255–260.
120. Vasilescu E, Drob P, Raducanu D, Cojocaru VD, Cinca I, Iordachescu D, Ion R, Popa M, Vasilescu C. In vitro biocompatibility and corrosion resistance of a new implant titanium base alloy. J Mater Sci Mater Med 2010;21:1959–1968.
121. Li Y, Wong C, Xiong J, Hodgson P, Wen C. Cytotoxicity of titanium and titanium alloying elements. J Dent Res 2010;89:493–497.
122. Xiong J, Li Y, Hodgson PD, Wen C. In vitro osteoblast-like cell proliferation on nano-hydroxyapatite coatings with different morphologies on a titanium-niobium shape memory alloy. J Biomed Mater Res A 2010;95:766–773.
123. Guo Y, Georgarakis K, Yokoyama Y, Yavari AR. On the mechanical properties of TiNb based alloys. J Alloys Compd 2013;571:25–30.
124. O'Brien B. Niobium Biomaterials. In: Niinomi M, Narushima T, Nakai M, editors. Advances in Metallic Biomaterials: Tissues, Materials and Biological Reactions. Springer Berlin Heidelberg; 2015.
125. Hofstetter W, Sehr H, Wild M de, Portenier J, Gobrecht J, Hunziker EB. Modulation of human osteoblasts by metal surface chemistry. J Biomed Mater Res A 2013;101:2355–2364.
126. Park YJ, Song YH, An JH, Song HJ, Anusavice KJ. Cytocompatibility of pure metals and experimental binary titanium alloys for implant materials. J Dent 2013;41:1251–1258.
127. Andrade DP de, de Vasconcellos, Luana Marotta Reis, Carvalho ICS, Forte, Lilibeth Ferraz de Brito Penna, de Souza Santos, Evelyn Luzia, Prado RFd, Santos DRD, Cairo CAA,

Carvalho YR. Titanium-35niobium alloy as a potential material for biomedical implants: In vitro study. Mater Sci Eng C Mater Biol Appl 2015;56:538–544.

128. do Prado RF, Rabelo SB, Andrade DP de, Nascimento RD, Henriques VAR, Carvalho YR, Cairo CAA, de Vasconcellos, Luana Marotta Reis. Porous titanium and Ti-35Nb alloy: effects on gene expression of osteoblastic cells derived from human alveolar bone. J Mater Sci Mater Med 2015;26:259.
129. Cremasco A, Messias AD, Esposito AR, Duek, Eliana Aparecida de Rezende, Caram R. Effects of alloying elements on the cytotoxic response of titanium alloys. Mater Sci Eng C Mater Biol Appl 2011;31:833–839.
130. Jirka I, Vandrovcova M, Frank O, Tolde Z, Plsek J, Luxbacher T, Bacakova L, Stary V. On the role of Nb-related sites of an oxidized beta-TiNb alloy surface in its interaction with osteoblast-like MG-63 cells. Mater Sci Eng C Mater Biol Appl 2013;33:1636–1645.
131. Kim SE, Jeong HW, Hyun YT, Lee YT, Jung CH, Kim SK, Song JS, Lee JH. Elastic modulus and in vitro biocompatibility of Ti−xNb and Ti−xTa alloys. Met Mater Int 2007;13:145–149.
132. Sista S, Wen C, Hodgson PD, Pande G. Expression of cell adhesion and differentiation related genes in MC3T3 osteoblasts plated on titanium alloys: role of surface properties. Mater Sci Eng C Mater Biol Appl 2013;33:1573–1582.
133. Shapira L, Klinger A, Tadir A, Wilensky A, Halabi A. Effect of a niobium-containing titanium alloy on osteoblast behavior in culture. Clin Oral Implants Res 2009.
134. Treves C, Martinesi M, Stio M, Gutierrez A, Jimenez JA, Lopez MF. In vitro biocompatibility evaluation of surface-modified titanium alloys. J Biomed Mater Res A 2010;92:1623–1634.
135. Obata A, Takahashi Y, Miyajima T, Ueda K, Narushima T, Kasuga T. Effects of niobium ions released from calcium phosphate invert glasses containing Nb2O5 on osteoblast-like cell functions. ACS Appl Mater Interfaces 2012;4:5684–5690.
136. Neacsu P, Gordin D-M, Mitran V, Gloriant T, Costache M, Cimpean A. In vitro performance assessment of new beta Ti-Mo-Nb alloy compositions. Mater Sci Eng C Mater Biol Appl 2015;47:105–113.
137. Wirth C, Grosgogeat B, Lagneau C, Jaffrezic-Renault N, Ponsonnet L. Biomaterial surface properties modulate in vitro rat calvaria osteoblasts response: Roughness and or chemistry? Mater Sci Eng C Mater Biol Appl 2008;28:990–1001.
138. Fini M, Giardino R, Borsari V, Torricelli P, Rimondini L, Giavaresi G, Nicoli Aldini N. In vitro behaviour of osteoblasts cultured on orthopaedic biomaterials with different surface roughness, uncoated and fluorohydroxyapatite-coated, relative to the in vivo osteointegration rate. Int J Artif Organs 2003;26:520–528.
139. Eisenbarth E, Velten D, Muller M, Thull R, Breme J. Nanostructured niobium oxide coatings influence osteoblast adhesion. J Biomed Mater Res A 2006;79:166–175.
140. Mavrogenis AF, Dimitriou R, Parvizi J, Babis GC. Biology of implant osseointegration. J Musculoskelet Neuronal Interact 2009;9:61–71.

141. Zhang H, Han J, Sun Y, Huang Y, Zhou M. MC3T3-E1 cell response to stainless steel 316L with different surface treatments. Mater Sci Eng C Mater Biol Appl 2015;56:22–29.
142. Lohmann CH, Bonewald LF, Sisk MA, Sylvia VL, Cochran DL, Dean DD, Boyan BD, Schwartz Z. Maturation state determines the response of osteogenic cells to surface roughness and 1,25-dihydroxyvitamin D3. J Bone Miner Res 2000;15:1169–1180.
143. Kunzler TP, Drobek T, Schuler M, Spencer ND. Systematic study of osteoblast and fibroblast response to roughness by means of surface-morphology gradients. Biomaterials 2007;28:2175–2182.
144. Chrzanowski W, Neel EA, Armitage DA, Zhao X, Knowles JC, Salih V. In vitro studies on the influence of surface modification of Ni-Ti alloy on human bone cells. J Biomed Mater Res A 2010 Jun 15;93(4):1596-608.
145. Kapanen A, Danilov A, Lehenkari P, Ryhänen J, Jämsä T, Tuukkanen J. Effect of metal alloy surface stresses on the viability of ROS-17/2.8 osteoblastic cells. Biomaterials 2002;23:3733–3740.
146. Waugh DG, Lawrence J, Chan CW, Hussain I, Man HC. Laser melting of NiTi and its effects on in vitro mesenchymal stem cell responses. In: Laser Surface Engineering: Elsevier; 2015. p 653–676.
147. Refai AK, Textor M, Brunette DM, Waterfield JD. Effect of titanium surface topography on macrophage activation and secretion of proinflammatory cytokines and chemokines. J Biomed Mater Res 2004;70:194–205.
148. Soskolne WA, Cohen S, Sennerby L, Wennerberg A, Shapira L. The effect of titanium surface roughness on the adhesion of monocytes and their secretion of TNF-alpha and PGE2. Clin Oral Implants Res 2002;13:86–93.
149. Kzhyshkowska J, Gudima A, Riabov V, Dollinger C, Lavalle P, Vrana NE. Macrophage responses to implants: Prospects for personalized medicine. J Leukoc Biol 2015;98:953–962.
150. Xia Z, Triffitt JT. A review on macrophage responses to biomaterials. Biomed Mater 2006;1:R1-9.
151. Gibon E, Amanatullah DF, Loi F, Pajarinen J, Nabeshima A, Yao Z, Hamadouche M, Goodman SB. The biological response to orthopaedic implants for joint replacement: Part I: Metals. J Biomed Mater Res B Appl Biomater 2016.
152. Yang S-Y, Ren W, Park Y, Sieving A, Hsu S, Nasser S, Wooley PH. Diverse cellular and apoptotic responses to variant shapes of UHMWPE particles in a murine model of inflammation. Biomaterials 2002;23:3535–3543.
153. Ren W, Yang S-Y, Fang H-W, Hsu S, Wooley PH. Distinct gene expression of receptor activator of nuclear factor-kappaB and rank ligand in the inflammatory response to variant morphologies of UHMWPE particles. Biomaterials 2003;24:4819–4826.

154. Kuroda S, Takeda S, Nakamura M. Effects of six particulate metals on osteoblast-like MG-63 and HOS cells in vitro. Dent Mater J 2003;22:507–520.
155. Sakai T, Takeda S, Nakamura M. The effects of particulate metals on cell viability of osteoblast-like cells in vitro. Dent Mater J 2002;21:133–146.
156. Nich C, Takakubo Y, Pajarinen J, Ainola M, Salem A, Sillat T, Rao AJ, Raska M, Tamaki Y, Takagi M, Konttinen YT, Goodman SB, Gallo J. Macrophages-Key cells in the response to wear debris from joint replacements. J Biomed Mater Res A 2013;101:3033–3045.
157. Sukur E, Akman YE, Ozturkmen Y, Kucukdurmaz F. Particle Disease: A Current Review of the Biological Mechanisms in Periprosthetic Osteolysis After Hip Arthroplasty. Open Orthop J 2016;10:241–251.
158. Neale SD, Haynes DR, Howie DW, Murray DW, Athanasou NA. The effect of particle phagocytosis and metallic wear particles on osteoclast formation and bone resorption in vitro. J Arthroplasty 2000;15:654–662.
159. Zhang H, Ricciardi BF, Yang X, Shi Y, Camacho NP, Bostrom MG. Polymethylmethacrylate particles stimulate bone resorption of mature osteoclasts in vitro. Acta Orthop 2008;79:281–288.
160. Greenfield EM, Bi Y, Ragab AA, Goldberg VM, van de Motter RR. The role of osteoclast differentiation in aseptic loosening. J Orthop Res 2002;20:1–8.
161. Bi Y, van de Motter RR, Ragab AA, Goldberg VM, Anderson JM, Greenfield EM. Titanium particles stimulate bone resorption by inducing differentiation of murine osteoclasts. J Bone Joint Surg Am 2001;83-A:501–508.
162. Oursler MJ. Recent advances in understanding the mechanisms of osteoclast precursor fusion. J Cell Biochem 2010;110:1058–1062.
163. Sun SX, Guo HH, Zhang J, Yu B, Sun KN, Jin QH. BMP-2 and titanium particles synergistically activate osteoclast formation. Braz J Med Biol Res 2014;47:461–469.
164. Otera H, Mihara K. Molecular mechanisms and physiologic functions of mitochondrial dynamics. J Biochem 2011;149:241–251.
165. Ollivere B, Wimhurst JA, Clark IM, Donell ST. Current concepts in osteolysis. J Bone Joint Surg Br 2012;94:10–15.
166. Hill PA, Murphy G, Docherty AJ, Hembry RM, Millican TA, Reynolds JJ, Meikle MC. The effects of selective inhibitors of matrix metalloproteinases (MMPs) on bone resorption and the identification of MMPs and TIMP-1 in isolated osteoclasts. J Cell Sci 1994;107 (Pt 11):3055–3064.
167. Liu Y, Song F, Sun J, Yu H, Liu SS-Y. Suture compression induced bone resorption with intensified MMP-1 and 13 expressions. Bone 2012;51:695–703.
168. Geoffroy V, Marty-Morieux C, Le Goupil N, Clement-Lacroix P, Terraz C, Frain M, Roux S, Rossert J, Vernejoul MC de. In vivo inhibition of osteoblastic metalloproteinases leads to increased trabecular bone mass. J Bone Miner Res 2004;19:811–822.

169. Schiltz C, Prouillet C, Marty C, Merciris D, Collet C, Vernejoul M-C de, Geoffroy V. Bone loss induced by Runx2 over-expression in mice is blunted by osteoblastic over-expression of TIMP-1. J Cell Physiol 2010;222:219–229.
170. Carter LC, Carter JM, Nickerson PA, Wright JR, Baier RE. Particle-induced Phagocytic Cell Responses are Material Dependent: Foreign Body Giant Cells Vs. Osteoclasts from a Chick Chorioallantoic Membrane Particle-implantation Model. J Adhes 2000;74:53–77.
171. Markhoff J, Zietz C, Fabry C, Fulda G, Bader R. Influence of analyzed lubricant volumes on the amount and characteristics of generated wear particles from three different types of polyethylene liner materials. J Biomed Mater Res B Appl Biomater 2017.
172. Foged C, Brodin B, Frokjaer S, Sundblad A. Particle size and surface charge affect particle uptake by human dendritic cells in an in vitro model. Int J Pharm 2005;298:315–322.
173. Fröhlich E. The role of surface charge in cellular uptake and cytotoxicity of medical nanoparticles. Int J Nanomedicine 2012;7:5577–5591.

8 Verwendete Originalarbeiten zur kumulativen Dissertation

Folgende Arbeiten wurden für die kumulative Dissertation herangezogen:

[I] **J. Markhoff**, J. Wieding, V. Weissmann, J. Pasold, A. Jonitz-Heincke, R. Bader. Influence of different three-dimensional open porous titanium scaffold designs on human osteoblasts behavior in static and dynamic cell investigations. Materials 2015, 8, 5490-5507. DOI: 10.3390/ma8085259.

[II] **J. Markhoff**, M. Krogull, C. Schulze, C. Rotsch, S. Hunger, Rainer Bader. Biocompatibility and inflammatory potential of titanium alloys cultivated with human osteoblasts, fibroblasts and macrophages. Special Issue “Biocompatibility of Materials”, Materials 2017, 10(1), 52. (17 Seiten), DOI: 10.3390/ma10010052.

[III] **J. Markhoff**, M. Weinmann, C. Schulze, R. Bader. Influence of different grained powders and pellets made of niobium and Ti-42Nb on human cell viability. Materials Science and Engineering C 73 (2017) 756–766. DOI: 10.1016/j.msec.2016.12.098.

[IV] J. Pasold, **J. Markhoff**, J. Tillmann, M. Krogull, P. Pisowocki, R. Bader. Direct influence of titanium and zirconia particles on the morphology and functionality of mature human osteoclasts. Journal of Biomedical Materials Research Part A. 2017 Sep;105(9):2608-2615. DOI: 10.1002/jbm.a.36114.

Abkürzungsverzeichnis

AG	Antigen
AK	Antikörper
BMI	Body-Mass-Index
BMU	Basic multicellular unit
C1CP	Pro-Kollagen Typ I
cDNA	complementary deoxyribonucleic acid, komplementäre Desoxyribonukleinsäure
CoCrMo	Cobalt-Chrom-Molybdän
cpTi	commercially pure Titanium
CTSK	Cathepsin K
DLC	diamond-like carbon (coating)
EBM	Elektronenstrahlschmelzen
ELISA	Enzyme-linked Immunosorbent Assay
FB	Fibroblast
FBGC	foreign body giant cell, Fremdkörperriesenzelle
GPa	Gigapascal
hFB	humane Fibroblasten
hMP	humane Makrophagen
hOB	humane Osteoblasten
hOK	humane Osteoklasten
HRP	Horseradish-Peroxidase (Meerrettich-Peroxidase)
IL	Interleukin
MCP-1	Monocyte chemoattractant protein-1
M-CSF	Macrophage colony-stimulating factor
MITF	Microphthalmia-associated transcription factor
MP	Makrophage
MMP	Matrix Metalloproteinase
MSC	Mesenchymal stem cell
Nb	Niob
NFATc1	Nuclear factor of activated T-cells cytoplasmic 1
NiTi	Nitinol
NOL	Naval Ordinance Laboratory
OB	Osteoblast
OK	Osteoklast
OPG	Osteoprotegerin
PBS	Phosphat buffered solution
qRT-PCR	quantitative Real time-Polymerase-Kettenreaktion
PE	Polyethylen
Ra	mittlerer Rauheitswert
RANK	Receptor Activator of NF-κB

RANKL	Receptor Activator of NF-κB Ligand
RNA	Ribonucleic acid, Ribonukleinsäure
Rz	Mittelwert der Einzelrautiefen
SEM	Standard error of the mean
SLM	Selektives Laserstrahlschmelzen
Ti6Al4V	Titan-Aluminium (6 %)-Vanadium (4 %)
Ti-42Nb	Titan-42Niob
TIMP	Tissue inhibitor of Matrix Metalloproteinase
TNF	Tumor necrosis factor
TRAcP/TRAP	Tartrate resistant acid phosphatase
UHMWPE	Ultra-high-molecular-weight-polyethylene
VEGF	Vascular Endothelial Growth Factor
VNR	Vitronectin-Rezeptor
wt%	Gewichtsprozent
WST-1	4-3-(4-Iodo-phenyl)-2-(4-Nitrophenyl)-2H-5-Tetrazolium-1,3-Benzendisulfonat
ZrO_2	Zirkoniumoxid

Erklärung

Ich erkläre, dass ich die eingereichte Dissertation selbstständig und ohne fremde Hilfe verfasst, andere als die von mir angegebenen Quellen und Hilfsmittel nicht benutzt und die den benutzten Werken wörtlich oder inhaltlich entnommenen Stellen als solche kenntlich gemacht habe.

Rostock, August 2017

Jana Markhoff

Erklärung

Hiermit erkläre ich, dass ich mich bisher noch keinem Promotionsverfahren unterzogen oder um eine Zulassung zu solchem beworben habe. Die eingereichte Schrift wurde an keiner anderen Hochschule vorgelegt.

Rostock, August 2017

Jana Markhoff

Eigene Publikationsliste

Originalarbeiten

J. Markhoff, A. Jonitz, C. Zietz, K. Lochner, D. Hansmann, R. Bader. Establishment of a novel in vitro test setup exposing adherent cells to wear particles made of polyethylene. Polymer Testing 32 (2013) 982-986; DOI: 10.1016/j.polymertesting.2013.05.005. IF 2,464

E. Mick, **J. Markhoff**, A. Mitrovic, A. Jonitz, R. Bader. New coating technique of ceramic implants with different glass solder matrices for improved osseointegration-mechanical investigations. Materials 2013, 6, 4001-4010; DOI: 10.3390/ma6094001. IF 2,654

J. Markhoff, E. Mick, A. Mitrovic, J. Pasold, K. Wegner, R. Bader. Surface modifications of dental ceramic implants with different glass solder matrices: *In vitro* analyses with human primary osteoblasts and epithelial cells. Special Issue „Osteogenic Biomaterials in Contemporary Dentistry“, Biomed Res Int. 2014;2014:742180. DOI: 10.1155/2014/742180. IF 2,476

J. Markhoff, J. Wieding, V. Weissmann, J. Pasold, A. Jonitz-Heincke, R. Bader. Influence of different three-dimensional open porous titanium scaffold designs on human osteoblasts behavior in static and dynamic cell investigations. Materials 2015, 8(8), 5490-5507; DOI: 10.3390/ma8085259. IF 2,654

J. Markhoff, M. Krogull, C. Schulze, C. Rotsch, S. Hunger, Rainer Bader. Biocompatibility and inflammatory potential of titanium alloys cultivated with human osteoblasts, fibroblasts and macrophages. Special Issue “Biocompatibility of Materials 2016”, Materials 2017, 10(1), 52; DOI: 10.3390/ma10010052. IF 2,654

J. Markhoff, M. Weinmann, C. Schulze, R. Bader. Influence of different grained powders and pellets made of Niobium and Ti-42Nb on human cell viability. Materials Science and Engineering C 73 (2017) 756–766; DOI: 10.1016/j.msec.2016.12.098. IF 4,164

J. Pasold, **J. Markhoff**, J. Tillmann, M. Krogull, P. Pisowocki, R. Bader. Direct influence of titanium and zirconia particles on the morphology and functionality of mature human osteoclasts. Journal of Biomedical Materials Research Part A. 2017 Sep;105(9):2608-2615; DOI: 10.1002/jbm.a.36114. IF 3,076

J. Markhoff, C. Zietz, C. Fabry, G. Fulda, R. Bader. Influence of analyzed lubricant volumes on the amount and characteristics of generated wear particles from three different types of

polyethylene liner materials. Journal of Biomedical Materials Research Part B: Applied Biomaterials. 2018 Apr;106(3):1299-1306. doi: 10.1002/jbm.b.33944. IF 3,189

M. Weinmann, C. Schnitter, M. Stenzel, **J. Markhoff**, C. Schulze, R. Bader. Development of bio-compatible refractory Ti/Nb(/Ta) alloys for application in patient-specific orthopaedic implants. International Journal of Refractory Metals & Hard Materials 75 (2018) 126–136. doi: 10.1016/j.ijrmhm.2018.03.018. IF 2,155

J. Markhoff, J. Pasold, J. Tillmann, M. Krogull, R. Bader. Influence of metallic and ceramic particles on the differentiation of human mononuclear cells into osteoclasts. (in revision).

A. Klinder*, **J. Markhoff***, J. Pasold, P. Sterna, A. Salamon, A. Jonitz-Heincke, R. Bader. Comparison of different cell culture dishes for the enrichment of non-adherent human mononuclear cells. (in revision).

Kongressbeiträge (* persönliche Teilnahme und Präsentation)

Vorträge

J. Markhoff *, J. Wieding, J. Pasold, A. Jonitz-Heincke, R. Bader. Kultivierung humaner Osteoblasten auf Titanformkörpern unterschiedlicher Mikrostruktur unter statischen und dynamischen Bedingungen. IV. Münchener Symposium für experimentelle Orthopädie, Unfallchirurgie und muskuloskelettale Forschung, 13.-14.02.2014, München, Deutschland.

J. Markhoff *, J. Pasold, B. Heskamp, P. Sterna, J. Tillmann, A. Salamon, D. Hansmann, P. Müller, A. Jonitz-Heincke, R. Bader. Hydrophilic cell culture surfaces enable the enrichment of human mononuclear cells for subsequent exposure to metallic and ceramic particles. 18. Chirurgische Forschungstage, 09.-11.10.2014, Hannover, Deutschland.

J. Wieding, **J. Markhoff ***, T. Lindner, P. Bergschmidt, R. Bader. µ-CT-Untersuchung des Knocheneinwachsens von additiv gefertigten offenporigen Scaffolds im Schafmodell. 18. Chirurgische Forschungstage, 09.-11.10.2014, Hannover, Deutschland.

J. Wieding, T. Lindner, P. Bergschmidt, **J. Markhoff *,** E.-D. Klinkenberg, A. Quade, R. Bader. Oberflächenbeschichtung mit CaP und PPAAm verbessert die knöcherne Integration offenporiger Titanformkörper im Schafmodell. Deutsche Gesellschaft für Biomaterialien, 06.-08.11.2014, Dresden, Deutschland, BioNanoMat. 2014; 15 (S1), S. 70, DOI: 10.1515/bnm-2014-9010, ISSN Online 2193-066X.

J. Markhoff *, J. Pasold, J. Tillmann, R. Bader. The functional properties of human mature osteoclasts are influenced by phagocytosis of metallic and ceramic wear particles. 19. Chirurgische Forschungstage, 08.-10.10.2015, Würzburg, Deutschland.

J. Markhoff *, C. Zietz, C. Fabry, G. Fulda, R. Bader. Type and composition of polyethylene material determine the amount and properties of generated wear particles. Deutsche Gesellschaft für Biomaterialien, 12.-14.11.2015, Freiburg, Deutschland, BioNanoMat. 2015; 16 (2-3): S. 154, DOI: 10.1515/bnm-2015-9014.

J. Markhoff *, M. Weinmann, C. Schulze, B. Nebe, R. Bader. Human osteoblast viability under the influence of different grained powders and pellets made of Niobium and Ti-42Nb. EORS, 25th Annual Meeting of the European Orthopaedic. Research Society, 13.-15.09.2017, München, Deutschland.

Poster/Abstracts

M. Lantow, T. Rharass, **J. Markhoff**, C. Mihoc, D. G. Weiss, E. Burkel. Biocompatibility tests on quasicrystal-ultrahigh molecular weight polyethylene (UHMWPE) composites in human MG63 osteoblast-like cell cultures. Nanobio-Europe, 15.-17.06.2010, Münster, Deutschland.

J. Markhoff, A. Jonitz, K. Lochner, C. Zietz, D. Hansmann, R. Bader. Establishment of an in-vitro test setup exposing human osteoblasts to ultra-high molecular weight polyethylene particles. 4th International Symposium Interface Biology of Implants (IBI), 9.-11.05.2012, Rostock, Deutschland. ISBN 978-3-00-038220-8, Seite 53.

J. Markhoff, B. Heskamp, P. Sterna, A. Jonitz-Heincke, R. Bader. Cultivation of human mononuclear cells in modified cell culture plates to prevent adhesion-induced differentiation. Osteologie Kongress, 13.-15.3.2014, München, Deutschland. Osteologie 2014; 23 (Suppl 1): S1–S57, ISSN 1019-1291, Seite 44.

J. Markhoff, E. Mick, A. Mitrovic, A. Jonitz, R. Bader. Surface coating of ceramic implants with different glass solder matrices for improved osseointegration - mechanical and cell biological investigations. Orthopaedic Research Society, 15.-18.3.2014, New Orleans, Louisiana, USA.

E. Mick, **J. Markhoff**, A. Mitrovic, A. Jonitz-Heincke, R. Bader. Novel surface modification of ceramic implants with glass solder matrices for improved osseointegration. European Orthopaedic Research Society, 22nd Annual Meeting, 02.-04.07.2014, Nantes, Frankreich.

J. Markhoff *, J. Wieding, V. Weissmann, J. Pasold, R. Bader. Microstructure of titanium scaffolds influences human osteoblasts behavior in static and dynamic culture. Deutsche Gesellschaft für Biomaterialien 06.-08.11.2014, Dresden, Deutschland. BioNanoMat. 2014; 15 (S1), S. 191, DOI 10.1515/bnm-2014-9018.

J. Markhoff, J. Pasold, J. Tillmann, R. Bader. Influence of metallic and ceramic wear particles on differentiation and functionality of human osteoclasts. International Conference of Tissue Engineering, 25.-27.06.2015, Lissabon, Portugal.

J. Markhoff, J. Pasold, J. Tillmann, R. Bader. The differentiation of human monocytes into osteoclasts is upregulated after phagocytosis of metallic and ceramic wear particles. BMT, 49th DGBMT Annual Conference, 16.-18.09.2015, Lübeck, Deutschland.

V. Weissmann, **J. Markhoff**, R. Bader, H. Hansmann. Einfluss geometrischer Faktoren auf die mechanischen Eigenschaften offenporiger, mittels AM-Technologie gefertigter TiAl6V4 Strukturelemente für biomedizinische Anwendungen. 3. Forschungscamp der Universität Rostock, 26.11.2015, Rostock, Deutschland.

J. Pasold, **J. Markhoff**, J. Tillmann, P. Pisowocki, R. Bader. Enhanced activation and fusion of human osteoclasts after exposure to metallic and ceramic particles. Orthopaedic Research Society, 05.-08.03.2016, Orlando, Florida, USA.

J. Markhoff *, J. Pasold, J. Tillmann, B. Nebe, R. Bader. Differentiation and functionality of human osteoclasts under the influence of titanium and zirconium oxide wear particles. 28th Annual Meeting of the European Society for Biomaterials. 04.-08.09.2017, Athen, Griechenland.

Workshops

GoBone Summer Workshop - “Treatment of large bone defects – From innovation to clinics”, (nach Auswahlverfahren, zusätzlich: Reisestipendium der Deutschen Gesellschaft für Biomaterialien), 17.-22.09.2017, Krakau, Polen.

Materials **2015**, *8*, 5490-5507; doi:10.3390/ma8085259

OPEN ACCESS

materials

ISSN 1996-1944

www.mdpi.com/journal/materials

Article

Influence of Different Three-Dimensional Open Porous Titanium Scaffold Designs on Human Osteoblasts Behavior in Static and Dynamic Cell Investigations

Jana Markhoff [1,*], Jan Wieding [1], Volker Weissmann [2], Juliane Pasold [1], Anika Jonitz-Heincke [1] and Rainer Bader [1]

[1] University Medicine Rostock, Department of Orthopaedics, Biomechanics and Implant Technology Laboratory, Doberaner Strasse 142, Rostock 18057, Germany;
E-Mails: jan.wieding@med.uni-rostock.de (J.W.); juliane.pasold@med.uni-rostock.de (J.P.); anika.jonitz@med.uni-rostock.de (A.J.-H.); rainer.bader@med.uni-rostock.de (R.B.)

[2] Institute for Polymer Technology, Alter Holzhafen 19, Wismar 23966, Germany;
E-Mail: weissmann@ipt-wismar.de

* Author to whom correspondence should be addressed; E-Mail: jana.markhoff@med.uni-rostock.de; Tel.: +49-381-494-9338.

Academic Editor: Sudipta De

Received: 26 May 2015 / Accepted: 13 August 2015 / Published: 24 August 2015

Abstract: In the treatment of osseous defects micro-structured three-dimensional materials for bone replacement serve as leading structure for cell migration, proliferation and bone formation. The scaffold design and culture conditions are crucial for the limited diffusion distance of nutrients and oxygen. In static culture, decreased cell activity and irregular distribution occur within the scaffold. Dynamic conditions entail physical stimulation and constant medium perfusion imitating physiological nutrient supply and metabolite disposal. Therefore, we investigated the influence of different scaffold configurations and cultivation methods on human osteoblasts. Cells were seeded on three-dimensional porous Ti-6Al-4V scaffolds manufactured with selective laser melting (SLM) or electron beam melting (EBM) varying in porosity, pore size and basic structure (cubic, diagonal, pyramidal) and cultured under static and dynamic conditions. Cell viability, migration and matrix production were examined via mitochondrial activity assay, fluorescence staining and ELISA. All scaffolds showed an increasing cell activity and matrix production under static conditions over time. Expectations about the dynamic culture were only partially fulfilled, since it enabled proliferation alike the static one and enhanced cell migration. Overall, the

SLM manufactured scaffold with the highest porosity, small pore size and pyramidal basic structure proved to be the most suitable structure for cell proliferation and migration.

Keywords: scaffold; Ti-6Al-4V; microstructure; bioreactor; human osteoblasts; static culture; dynamic culture; additive manufacturing

1. Introduction

The application of synthetic, micro-structured three-dimensional scaffolds for the treatment of large bone defects has become an adequate alternative to bone autografts and allografts with their limited availability and risk of infection or rejection [1,2]. Due to good mechanical properties and excellent biocompatibility resulting from a formed oxide layer, metallic materials, e.g., Ti-6Al-4V, are mainly used in orthopedic surgery [3,4].

Porous metallic materials can exhibit compression strength similar to cortical bone [5] and are, in contrast to ceramics and polymers, applicable for load-bearing areas [6]. Metallic materials are inserted in form of titanium foams, [4,7] fiber meshes [8,9] or open-porous scaffolds with regular structure [1,5,6,10]. Thereby, the cell growth is influenced by the roughness of surfaces [3,11] and the structure of pores, *i.e.*, pore size, shape, porosity and interconnectivity [12]. These requirements can be controlled by the manufacturing methods. Fabrication of porous three-dimensional structures based on metal and alloy is hindered by reasons of their chemical reactivity and high melting/sintering temperatures [13]. Techniques like plasma-spraying, sintering, shot-blasting or acid-etching [9] only allow limited control over the pore structure on the scaffold surface [14,15]. As against conventional material forming processes, the lower-cost and faster additive-manufacturing processes, e.g., laser- or electron-beam-melting [1,16] permit gradual-building of solid metallic material from powder [17] and enable a controllable microstructure; an interconnective porosity with defined pore size [18,19]. By modifying the micro-structure of these porous constructs an adjustment of the mechanical properties is possible; e.g., similar to these of bone [19]. However, the scaffold's porosity determines the permeability [20], but also the mechanical properties and is therefore limited [12]. For optimal cell growth, pore sizes in the range of mainly 50 to 500 µm [3,14,21,22] and an interconnective porosity of 60% to 75% [1,23] are mentioned. These parameters are crucial for cell seeding, migration, nutrient transport, matrix deposition and vascularization [3]. On the one hand, smaller pores result in increased proliferation due to a greater material surface for adhesion and growth [12] and also enable cell bridging over the pores [24] as well as an efficient cell seeding [18] considering that pore size is cell specific [25]. On the other hand, small pores limit scaffold permeability and thus, nutrient and waste exchange [18] as well as cell migration into the scaffold and vascularization [20].

Besides structural properties, scaffold colonization *in vitro* is determined by cultivation conditions. In static culture, cells on porous scaffolds are submitted to limited nutrient and oxygen supply as well as waste removal in the centre [26,27]. The resulting hypoxia decreases matrix production and cell viability and causes cell necrosis [28,29]. Furthermore, cells mainly adhere and proliferate at the outer face of the scaffold and tend to obstruct the upper pores, which avoids cell migration and diffusion processes into the scaffold [4]. To solve this problem, dynamic cultivation in bioreactors, e.g.,

spinner flasks, rotating wall vessels or cylindrical or vertical perfusion systems is used [30,31]. By applying a constant fluid flow *in vitro*, shear stress is carried out to the cells and mechanotransduction is initiated [32], so physical signals are converted into biochemical ones [33]. Increased cell proliferation, differentiation, migration, uniform cell distribution and matrix formation are proved in consequence of dynamic cultivation [34–36], which is due to enhanced nutrient and oxygen supply and waste removal [8]. Nevertheless, high flow rates can also lead to increased cell detachment or damage [35].

The aim of the present *in vitro* study was to compare the behavior of human osteoblasts on three-dimensional porous Ti-6Al-4V scaffolds of two manufacturing methods with different structural design features including pore size, porosity and basic structure under static and dynamic cultivation conditions.

2. Materials and Methods

2.1. Generation and Fabrication of Micro-Structured Titanium Scaffolds

The choice of structures and scaffold parameters was preceded by previous biomechanical studies [5,37]. Three scaffold designs were generated by means of CAD software (SolidWorks, SolidWorks Corporation, Concord, MA, USA) differing in their basic structure (Figure 1) as well as in porosity, pore size and strut design. The geometrical parameters of the scaffolds are constituted in Table 1. The cubic structure is characterized by rectangular pores in vertical orientation, while the pyramidal basic structure exhibited trapezoidal pores in both directions of the z-axis. Another basic structure is marked by diagonally-orientated struts and checked-like pores [5].

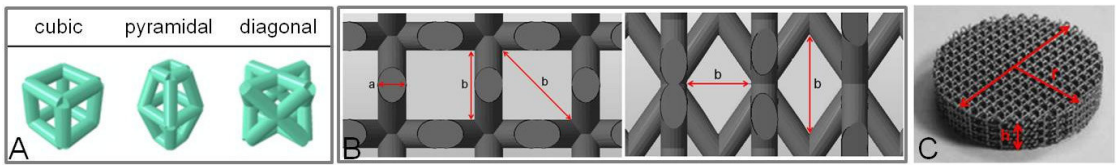

Figure 1. (**A**) Basic structures of the generated Ti-6Al-4V scaffolds (cubic, pyramidal and diagonal); (**B**) Span of strut thickness (a) and pore size (b) in µm exemplary for the cubic (left) and diagonal scaffold (right); (**C**) Manufactured Ti-6Al-4V scaffold with pyramidal basic structure.

Table 1. Geometrical parameters of the generated Ti-6Al-4V scaffolds.

	Basic Structure			Scaffold Dimensions			
Scaffold Design	**Strut Thickness [a] [µm]**	**Strut Cross-Sectional Area [mm²]**	**Pore Size [b] [µm]**	**Radius [r] [mm]**	**Height [h] [mm]**	**Surface Area [mm²]**	**Porosity [%]**
cubic	700 *	0.490	700 × 700	17.5	5.5	~12200	~51
pyramidal	400 **	0.126	400–620	17	9.4	~18000	~76
diagonal	400 **	0.126	400–1000	17	10.4	~20800	~75

Notes: * struts exhibited a rectangular cross-section; ** struts exhibited a circular cross-section. Elevated letters are associated with Figure 1B,C.

The scaffolds were fabricated of titanium powder (Ti-6Al-4V) using two different additive manufacturing processes (AM), selective laser melting (SLM) (SLM solutions GmbH, Luebeck, Germany) as well as electron-beam melting (EBM) (Institute for Materials Science, University of Erlangen-Nuremberg, Erlangen, Germany) (Figure 2). Thereby, the scaffolds are created in an inert gas or vacuum atmosphere by layerwise melting of the loose powder particles with a layer thickness of approximately 40 μm, depending on the process parameters [17].

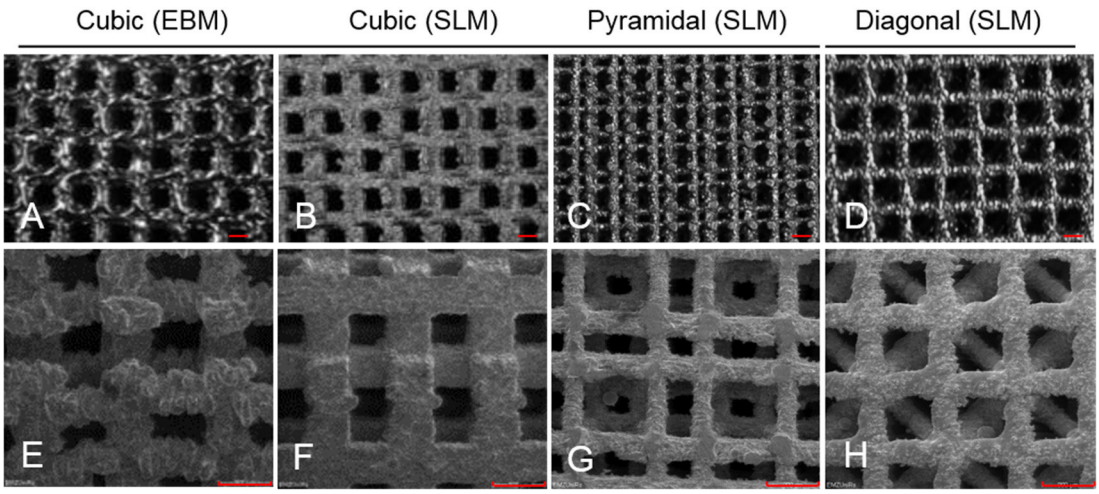

Figure 2. Light microscope (**A**–**D**; scale bar: 700 μm) and scanning electron microscope pictures (**E**–**H**; scale bar: 900 μm) of the Ti-6Al-4V scaffolds with four basic structures and fabricated with two different processes (EBM: electron beam melting; SLM: selective laser melting).

2.2. Isolation and Cultivation of Human Primary Osteoblasts

Isolation of human primary osteoblasts followed the procedure described previously by Lochner *et al.* [38]. Briefly, cells were isolated from the spongiosa of the femoral heads of patients undergoing primary total hip replacement. The samples were collected with patient agreement and approval by the Local Ethical Committee (registration number: A 2010-10). Cultivation was done in osteogenic cell culture medium (MEM Dulbecco, Biochrom AG, Berlin, Germany) with 10% FCS, 1% penicillin/streptomycin, 1% amphotericin B, 1% HEPES buffer (all: Gibco®-Invitrogen, Darmstadt, Germany) including osteogenic additives (dexamethason (100 mM), L-ascorbic acid (50 mg/mL) and β-glycerophosphate (10 mM) (all from Sigma-Aldrich, Munich, Germany)). Alkaline phosphatase staining with fuchsin substrate chromogen (DAKO, Hamburg, Germany) was done to verify the osteogenic character of the isolated cells. Cultivation was carried out in an incubator (Binder GmbH, Tuttlingen, Germany) at simulated *in vivo* conditions 37 °C, 5% CO_2 and 21% O_2 for one week.

A total of seventeen different donors (10 ♂, 7 ♀) were used for all experiments. The average age was 66 ± 9.4 years. Cells were not pooled; one donor was used for one scaffold per experiment.

2.3. Test Setup

Titanium scaffolds were placed in standard six well culture plates and saturated with medium to avoid air bubbles within the pores. After the pre-cultivation, osteoblasts in the second passage were detached from the flask bottom using trypsin/EDTA (Gibco®-Invitrogen, Darmstadt, Germany) after being rinsed with phosphate buffered solution (PBS) (PAA, Coelbe, Germany). Cell suspension was adjusted to 4×10^5 cells in 100 µL per scaffold and homogenously distributed onto the scaffold surface in 10 µL drops. After cells adhered for 30 min, medium was added until the scaffolds were completely covered. Static cultivation was done over eight days with medium changes after two, four and seven days.

For dynamic cultivation, cells were allowed to adhere for 24 h on a scaffold in static culture, which then was transferred to a per(i)fusion-chamber (Minucells and Minutissue Vertriebs GmbH, Bad Abbach, Germany) under sterile conditions. Thereby, the scaffold was placed in specific retainers made of polycarbonate and were placed horizontally in the medium-filled reactor (Figure 3A,B). The system (containing of bioreactor and hose connections) was refilled with additional medium and was hermetically closed via gasket and clamps (Figure 3C). The cell seeded surface was orientated towards the fresh medium influx. Gas permeable silicon tubes for CO_2 exchange (PharMed® BPT, ID 0.25 mm, Ismatec, IDEX Health & Science GmbH, Wertheim, Germany) and luer-lock pins enabled connection to a shaded and constantly cooled medium reservoir flask and a waste flask (Figure 3D). By means of a peristaltic pump (MCP, Ismatec, IDEX Health & Science GmbH, Wertheim, Germany) a constant upwards medium flow rate (50 µL/min) through the chamber was maintained. This flow rate is deduced from previous works of this research group [39]. The complete system is illustrated in Figure 4. The appropriate level of shear stress cannot be elevated in this system. Cells were cultured for further 72 h in the dynamic system and then the scaffold was transferred back to a 6-well plate for analyzing.

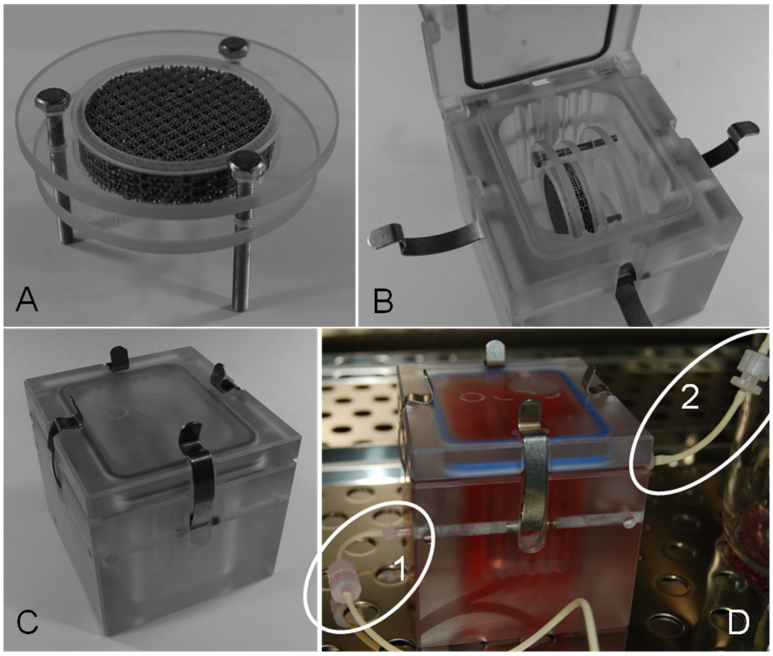

Figure 3. Scaffold placement. (**A**) Titanium scaffold fixed in polycarbonate disks; (**B**) Bioreactor with inserted scaffold; (**C**) Closed bioreactor. (**D**) Dynamic cultivation of a scaffold placed in the closed per(i)fusion system. 1D—medium influx. 2D—medium efflux.

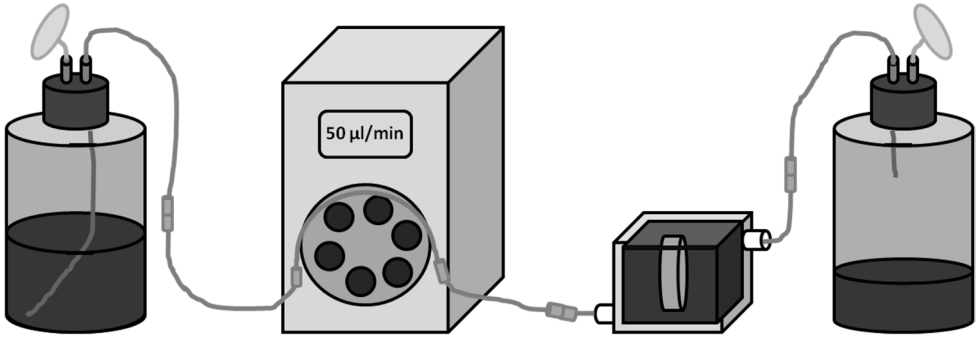

Figure 4. Test system. From left to right: Cooled medium reservoir with air filter, ISMATEC peristaltic pump, reactor with scaffold, waste container. Connections via gas permeable silicon tubes and luer-lock pins.

2.4. Cell Biological Tests

Analyses of cell viability and migration were carried out after one, four and eight days to evaluate chronological sequence of cell behavior. The colorimetric WST-1 assay was conducted to examine cell viability on the four different types of titanium scaffolds. The tetrazolium salt WST is transformed to formazan by mitochondrial succinate dehydrogenase of metabolic active cells. The adsorption is measured at 450 nm in a microplate reader (Opsys MRTM, Dynex Technologies GmbH, Denkendorf, Germany) and is directly proportional to the metabolic cell activity. Qualitative cell viability was analyzed by means of live/dead staining with the two fluorescence dyes calcein AM for vital cells and ethidium homodimer-1 for dead ones (Live/Dead Cell Viability Assay, Invitrogen, Darmstadt, Germany). An enzyme linked immunosorbent assay (Metra C1CP EIA Kit, Quidel, Buende, Germany) was done to verify synthesis of pro-collagen type 1 by the osteoblasts after static culture. A detection of collagen in the cell supernatant while or after dynamic cultivation was not possible due to the reactor construction and continuous medium flow.

2.5. Statistical Analysis

The statistical significance of the influence of the manufacturing processes comparing the cubic EBM and SLM scaffolds was evaluated by ANOVA Post-Hoc-LSD using IBM® SPSS® Statistics Version 20 (IBM Corp., New York, NY, USA). Furthermore, the structural influence was assessed between the SLM scaffolds with cubic, pyramidal and diagonal designs. The significance level was set to $p < 0.05$.

3. Results

3.1. Cubic Structure—Influence of the Manufacturing Method

Titanium scaffolds with cubic microstructure (pore size 700 µm, porosity ~51%) manufactured with EBM and SLM were seeded with human osteoblasts and cultured under static and dynamic conditions. Static cultivation showed no significant differences of metabolic cell activity between the manufacturing methods investigated over time, but revealed a significant increase for both structures in general after eight days ($p \leqslant 0.001$) (Figure 5).

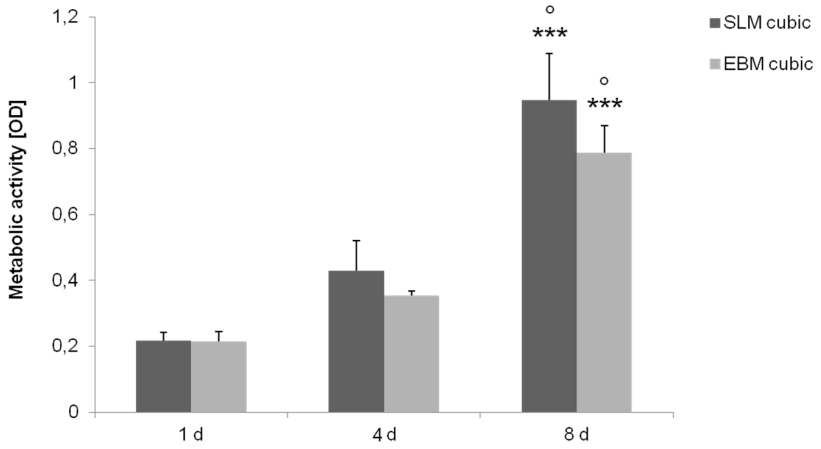

Figure 5. Metabolic activity of human osteoblasts cultured under static conditions over eight days on cubic structures (SLM, EBM). Values are means ± SD ($n \geqslant 3$). ANOVA Post-Hoc-LSD: Statistical significance levels (° $p < 0.05$, *** $p \leqslant 0.001$) compared to the respective four days (°) and one day (*). No significant differences revealed between the several manufacturing methods.

Live/dead staining illustrated an increase of living (green), but also dead cells (red) as well as higher cell density over time (Figure 6). Furthermore, living cells in lower layers are mainly visible at the pyramidal and the diagonal structured scaffolds. After eight days migrated cells can only be assumed in lower layers, but seem to have died off lacking supply with oxygen and nutrients.

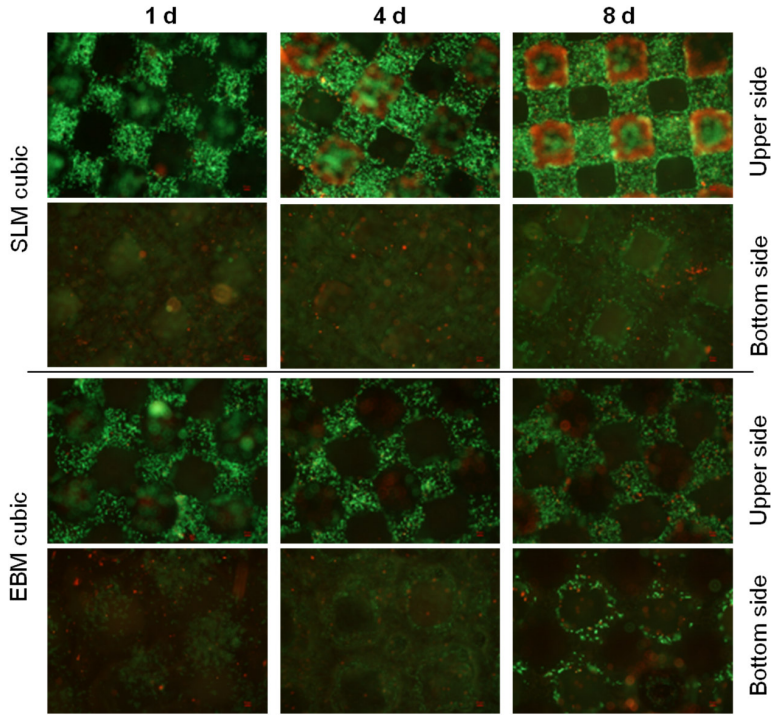

Figure 6. Live/dead staining of cubic scaffolds after static cultivation (one day, four days and eight days). Living cells are displayed in green, dead ones in red. Magnification: 40×. Scale bar: 50 µm (down right).

Due to the design of the bioreactor, measurement of collagen synthesis could only be done after static cultivation. Detection of collagen type 1 production revealed a significant increase over time for both cubic scaffolds (SLM: $p < 0.008$; EBM: $p < 0.019$), but no significant difference between, confirming a missing influence of the manufacturing method on protein synthesis (Figure 7).

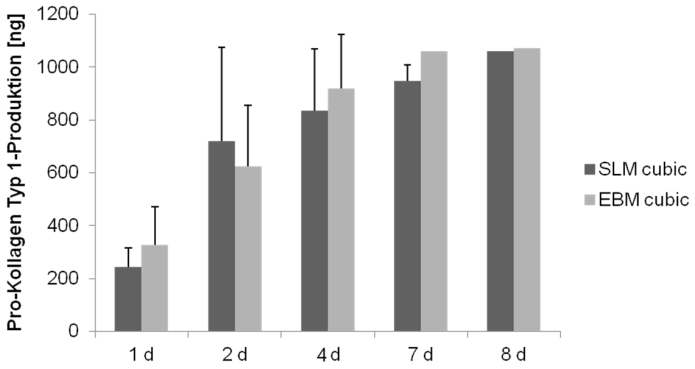

Figure 7. Collagen synthesis of human osteoblasts cultured under static conditions over eight days. Values are means ± SD. ($n \geqslant 1$): ANOVA Post-Hoc-LSD. Statistical significance levels ($p < 0.05$).

In case of dynamic cultivation the cubic scaffolds were placed in a bioreactor after 24 h static pre-cultivation and cultured for further three days. Human osteoblasts on the SLM and EBM manufactured scaffolds exhibited no significant increased metabolic activity after dynamic cultivation compared to the static one (Figure 8). Comparison between both types of scaffolds after dynamic cultivation showed also no significant differences.

Cells on the upper side of the scaffolds showed dense cell collectives, but cell migration to the bottom side of the scaffold can only be observed for the EBM scaffold detecting dead cells (Figure 8).

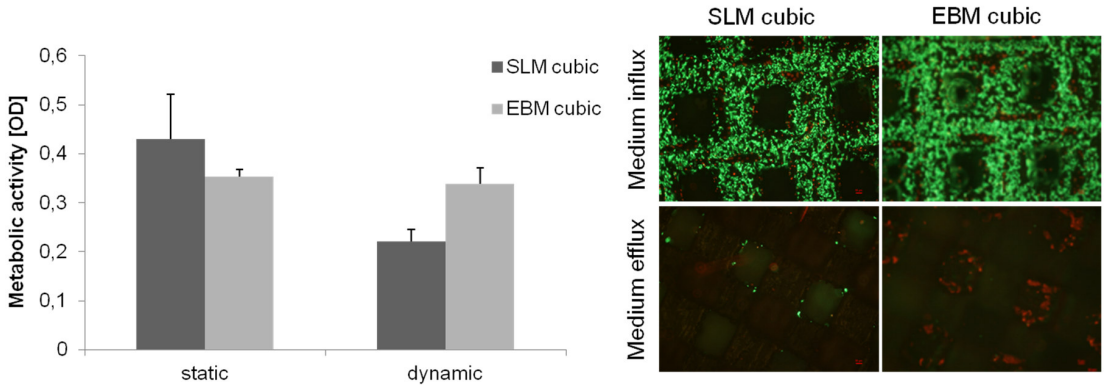

Figure 8. (**a**) Metabolic activity of human osteoblasts cultured on cubic scaffold designs under dynamic and static conditions after four days of cultivation. Values are means ± SD ($n \geqslant 3$). Statistic revealed no significant differences between static and dynamic cultivation. (**b**) Live/dead staining of cubic scaffolds after dynamic cultivation after total five days. Living cells are displayed in green, dead ones in red. Magnification: 40×. Scale bar: 50 µm (down right).

3.2. Fabrication via Selective Laser-Melting—Comparison of Different Structures

Based on the results of the comparison between the two manufacturing methods and the biomechanical investigations [5,37], the selective-laser melting was used for further structures to compare. Titanium scaffolds manufactured via SLM with three different microstructures (cubic, pyramidal, diagonal) were seeded with human osteoblasts and cultured under static and dynamic conditions. Static cultivation showed a significant higher metabolic cell activity on the pyramidal scaffold compared to the other ones after four and eight days (cubic *vs.* pyramidal: $p = 0.002$, $p = 0.013$; diagonal *vs.* pyramidal: $p \leqslant 0.001$, $p \leqslant 0.001$). No significant differences could be determined between the cubic and diagonal structure at any point. In general, a significant increase of activity was detected for all structures over time (all: $p \leqslant 0.001$) (Figure 9).

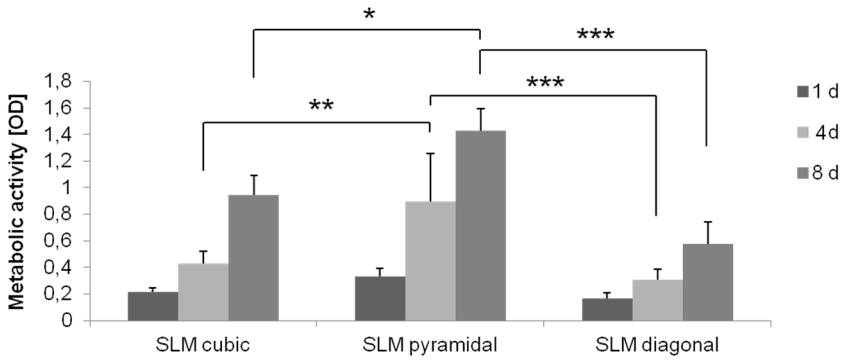

Figure 9. Metabolic activity of human osteoblasts cultured under static conditions over eight days on SLM manufactured structures with several designs (cubic, pyramidal, diagonal). Values are means ± SD ($n \geqslant 3$). ANOVA Post-Hoc-LSD: Statistical significance levels (* $p < 0.05$, ** $p < 0.01$, *** $p < 0.001$).

Live/dead staining illustrated an increase of living (green), but also dead cells (red) as well as higher cell density over time (Figure 10) and especially, living cells in lower layers for the diagonal and pyramidal structures. Over time migrated cells can mainly be observed in lower layers of the pyramidal and diagonal structures, but not in the cubic one, possibly due to lacking supply with oxygen and nutrients.

Detection of collagen type 1 production revealed a significant increase over time for all three scaffold structures (cubic: $p < 0.008$; pyramidal: $p = 0.002$; diagonal: $p = 0.001$), but a significant lower synthesis on the diagonal one over time ($p \leqslant 0.008$) (Figure 11).

Dynamic cultivation was done as described previously. Human osteoblasts on the SLM manufactured scaffold structures revealed no significant differences between the cultivation methods for all structures, but showed a significant higher activity on the pyramidal scaffold ($p < 0.001$) after dynamic cultivation compared to the other structures (Figure 12).

Live/dead staining illustrated a high cell density after dynamic cultivation, partly in lower layers of the scaffolds (Figure 12). The pyramidal structure with the highest metabolic activity also exhibits living cells at the side of medium efflux as well as ones in overlying layers, hence a cell migration through the scaffold without cell dying can be assumed.

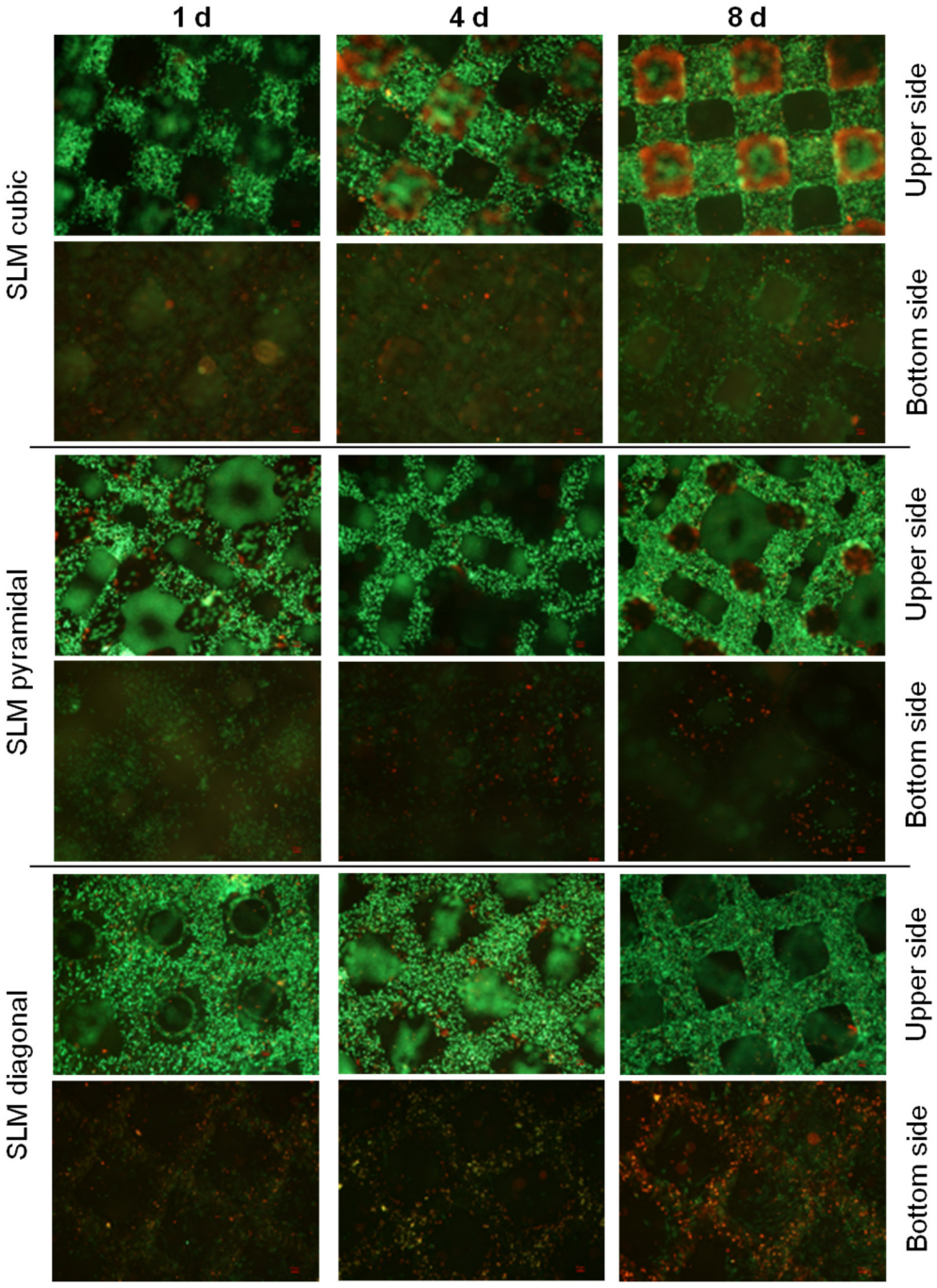

Figure 10. Live/dead staining of SLM manufactured scaffolds with several designs after static cultivation (one day, four days and eight days). Living cells are displayed in green, dead ones in red. Magnification: 40×. Scale bar: 50 µm (down right).

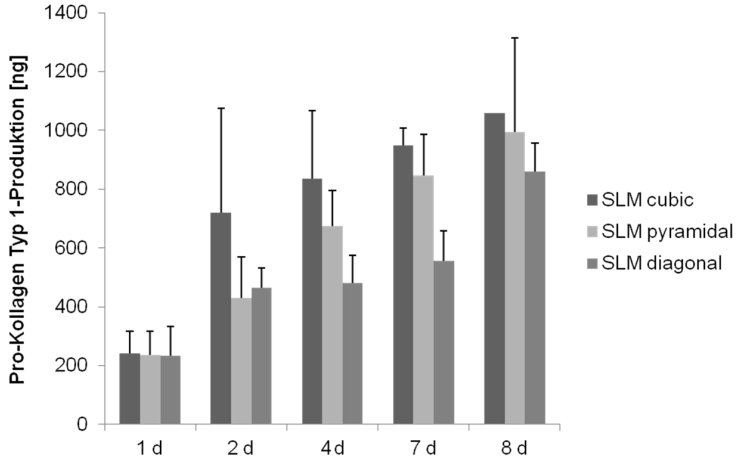

Figure 11. Collagen synthesis of human osteoblasts cultured under static conditions over eight days. Values are means ± SD. ($n \geqslant 1$): ANOVA Post-Hoc-LSD. Statistical significance levels ($p < 0.05$).

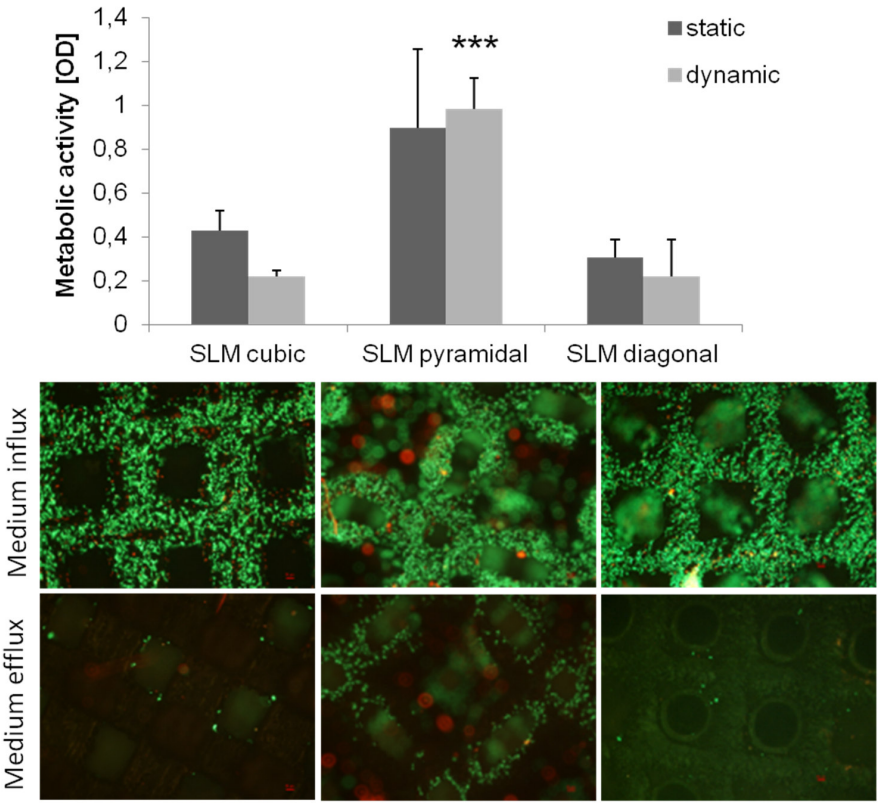

Figure 12. Metabolic activity of human osteoblasts cultured on SLM manufactured scaffold with several designs under dynamic and static conditions after four days of cultivation. Values are means ± SD ($n \geqslant 3$). ANOVA Post-Hoc-LSD: Statistical significance levels (*** $p < 0.001$) compared to the further designs after dynamic cultivation. Statistic revealed no significant differences between static and dynamic cultivation (above). Live/dead staining of SLM manufactured scaffolds after dynamic cultivation after four days. Living cells are displayed in green, dead ones in red. Magnification: 40×. Scale bar: 50 µm (down right) (below).

4. Discussion

Synthetic, open-porous three-dimensional scaffolds are used for the treatment of large bone defects in consequence of trauma, tumors, tissue degeneration or congenital deformation [30]. In our study, we compared four different types of titanium scaffolds concerning the colonization with human osteoblasts during cultivation under static and dynamic conditions. First of all, we showed that titanium is an adequate material for three-dimensional scaffold fabrication by AM processes and for cellular biocompatibility as previously described [5,40].

4.1. Static Cultivation

During static cell cultivation, no significant differences in metabolic activity between the different manufactured scaffolds (SLM, EBM) were found over time. Hence, no distinct predominance of one manufacturing method could be found regarding the cubic structures, which was previously described [16]. However, selective-laser-melting revealed a more accurate and regular geometry of pores and struts (Figure 2F). Surface roughness by all means enhances osteoblastic adhesion and proliferation as pointed out by Karageorgiou and Kaplan [9]. Ingrowth in rough and porous structures is favored by osteoblasts [41]. The illustrated surfaces of the tested titanium scaffolds (Figure 2E–H) allude to different surface roughness with a possible influence on cell adhesion. Though, a higher roughness of the electron beam-melted titanium can be assumed and could be proven in exemplary tests in our research group, preferred by osteoblasts to adhere, actually [41]. Static cultivation of the SLM manufactured structures (cubic, pyramidal, diagonal) revealed no significant differences in metabolic cell activity after one day. With increasing cultivation duration, however, cellular activity of the human osteoblasts significantly increased on the SLM manufactured scaffold with pyramidal basic structure after 96 h and eight days. In contrast, at none of the other time periods significant differences occurred between the two other structures. An increasing proliferation and cell spreading was proven for a similar period by Chen *et al.* [12] and also up to 14 days by Hollander *et al.* [42]. Furthermore, in this work the scaffold with the highest porosity (76%) and smallest pores (400 to 620 µm) enabled the highest metabolic activity and ingrowth of the human osteoblasts over time. Smaller pores are proved to enhance cell proliferation and migration due to a higher surface for initial cell adhesion and relieved cell bridging [12,20,24]. However, a hundred percent plugging of the voids is designated for pores with 450–500 µm, [10] but was not detected on our scaffolds. At the top layer of the scaffolds used in our *in vitro* tests, growth of human cells was clearly cognizable along the struts for every structure, as indicated for increasing pore sizes [10]. High porosities up to 75% as used for the pyramidal and diagonal structures are referred to be necessary for sufficient permeability and cause Young's modulus and compressive strength comparable to cancellous bone [23]. Advantage to the diagonal structure with similar values of porosity and pore size might be due to its basic structure narrowing the pore void and thereby inhibiting oxygen, nutrient and waste transport as well as cell migration. Furthermore, the mechanical stiffness might have influence on growth and matrix synthesis since osteoblasts are mechano-sensitive. The appropriate mechanical tests are published by Wieding *et al.* [43]. The slightly increased metabolic activity on the cubic structures compared to the diagonal one results from the lower porosity and four times wider struts leading to a larger surface area for initial adhesion [20].

The increase of dead cells in lower layers (see Figures 6 and 10) and absent of cell migration during static cultivation is due to the initially seeded dense and thick cell layers on the top layer clogging the underlying pores [4]. With a lack of a supplemental continuous medium flow, nutrient supply is inhibited and, thereby, acidification of media in the scaffold centre and deficient provision with oxygen promoted [16,44].

We detected an increase of collagen production over time during cultivation under static conditions for the structures as well as manufacturing methods, significantly lower in the diagonal structured scaffold due to its basic structure, presumably, as mentioned above. Contrary to the expectations, collagen synthesis of cells on the pyramidal scaffold was not significantly higher compared to the other structures. Hence, as previously described, collagen synthesis is not influenced by the scaffold's pore size [45].

4.2. Dynamic Cultivation

In our present study, dynamic cultivation supported an increased cell activity as well as migration through the pyramidal scaffold. Possible reasons were mentioned above considering porosity, pore size and basic scaffold structure. An adequate medium flow through the pyramidal structured scaffold can be assumed due to the high porosity and the open basic structure [23]. McCoy *et al.* [46] stated that pore size had no effect on the shear stress transferred to the cells by fluid flow. In contrast to previous studies [28,44], we could not confirm improved bone cell activity after dynamic cultivation compared to static conditions testing all four scaffold designs. Nevertheless, enhanced cell migration due to flow conditions was demonstrated in this work and is also proven by others [35,47]. So, a beneficial influence of our bioreactor is partially given depending on the chosen structure, but could be improved with appropriate adaptations and modifications, mentioned below. Several *in vitro* studies [27,28,32,48] were carried out with perfusion systems using flow rate intensities from 0.01 mL/min to 4 mL/min, mainly in excess of 0.1 mL/min. Overall, possibly the flow rate of 50 µL/min (=0.05 mL/min) was chosen too low in that case, but is similar to Jaasma *et al.* (0.05 mL/min) [49]. The flow rate and frequency influences the cell response and cause cell detachment and necrosis at too high levels [28]. In oscillatory or pulsatile perfusion systems, rather according to physiological fluid flow profiles [50], flow rates even up to 10 mL/min were used [30]. Osteoblasts are shown to be more mechano-responsive to those forms of perfusion as to steady one [49,50]. It must be pointed out that velocities and shear rates of the culture medium may differ in several zones of the scaffold, for instance those might be higher in the boundary area. In case of that, cell response will slightly differ in the appropriate areas. That should be simulated and determined for further studies.

In future studies an adaptation and a variation of the flow rate and cultivation period can be conducted in order to assess the influence of flow rate intensity and of time to cell behavior on the titanium scaffolds. Furthermore, a novel perfusion system will be tested, to enforce the medium to flow through the scaffold. Volkmer *et al.* [51] modified the same model of bioreactor used in this work from a per(i)fusion to perfusion system avoiding that medium flows around the scaffold promoting an enhanced oxygen supply. Moreover, cell growth on and into the scaffold is limited by its height and width [27]. In addition, evaluation of broader parameters will be necessary to understand the impact of the structural conditions used. For instance, protein expression as well as mRNA analysis would help to identify the osteogenic phenotype of the cells. So far, RNA isolation from the titanium scaffolds proved to be

difficult and afforded to low yields for further steps like qRT-PCR. Thus, protein-analysis via ELISA while or after dynamic cultivation was constricted by the current reactor construction and a too heavily diluted supernatant in the waste container, moreover, containing synthesized proteins from the whole test duration making a defined evaluation for one time point difficult. Additionally, levels of alkaline phosphatase, osteocalcin and intracellular calcium could be detected [35]. As previously done by other groups [26,51], evaluation of oxygen amount and pH-value seems to be a needful control for supply in the scaffold centre while dynamic cultivation.

5. Conclusions

Three-dimensional open-porous titanium scaffolds of two manufacturing methods with three different structural designs, porosities and pore sizes were examined as most suitable structure for human osteoblasts under static and dynamic conditions. Titanium proved to be an adequate scaffold material for *in vitro* cell tests targeting to bridge large bone defects *in vivo*. Moreover, at choice of an additive manufacturing method selective-laser-melting could be preferred as suitable generative process with more defined structure borders. This study could not point out a cultivation method (static *vs.* dynamic) enhancing the cellular proliferation more than the other one using the per(i)fusion flow bioreactor at 50 micro litres per mL. However, dynamic cultivation resulted in an improved cell migration through the porous titanium scaffold. Altogether, the structure, porosity and pore size of a scaffold influences cell growth behavior. The scaffold with smaller pores (400 to 620 μm), a high porosity (75%) and an open-porous pyramidal basic structure enabled the highest metabolic cell activity and migration and is proved be the most suitable leading structure so far. This has to be verified in further animal tests.

Acknowledgments

The authors gratefully thank the European Union and the Ministry of Economic Affairs, Employment and Tourism of Mecklenburg-Western Pomerania, Germany for financial support within the project "Tissue Regeneration", sub-project "TiFoBone". Further thanks go to SLM solutions GmbH and the Institute for Materials Science, University of Erlangen-Nuremberg for scaffold fabrication as well as Institute for Polymer Technology e.V. We thank the Electron microscopy centre of the University medicine Rostock for enabling scanning electron microscopy and Doris Hansmann for technical support.

Conflicts of Interest

The authors declare no conflict of interest.

References

1. Bonfield, W. Designing porous scaffolds for tissue engineering. *Philos. Trans. A Math. Phys. Eng. Sci.* **2006**, *364*, 227–232. [CrossRef] [PubMed]
2. Hutmacher, D.W. Scaffolds in tissue engineering bone and cartilage. *Biomaterials* **2000**, *21*, 2529–2543. [CrossRef]
3. Alvarez, K.; Nakajima, H. Metallic Scaffolds for Bone Regeneration. *Materials* **2009**, *2*, 790–832. [CrossRef]

4. Muller, U.; Imwinkelried, T.; Horst, M.; Sievers, M.; Graf-Hausner, U. Do human osteoblasts grow into open-porous titanium? *Eur. Cell Mater.* **2006**, *11*, 8–15. [PubMed]
5. Wieding, J.; Jonitz, A.; Bader, R. The effect of structural design on mechanical properties and cellular response of additive manufactured titanium scaffolds. *Materials* **2012**, *5*, 1336–1347. [CrossRef]
6. Ryan, G.E.; Pandit, A.S.; Apatsidis, D.P. Porous titanium scaffolds fabricated using a rapid prototyping and powder metallurgy technique. *Biomaterials* **2008**, *29*, 3625–3635. [CrossRef] [PubMed]
7. Nakajima, H. Fabrication, properties, and applications of porous metals with directional pores. *Proc. Jpn. Acad. Ser. B Phys. Biol. Sci.* **2010**, *86*, 884–899. [CrossRef] [PubMed]
8. Sikavitsas, V.I.; Bancroft, G.N.; Holtorf, H.L.; Jansen, J.A.; Mikos, A.G. Mineralized matrix deposition by marrow stromal osteoblasts in 3D perfusion culture increases with increasing fluid shear forces. *Proc. Natl. Acad. Sci. USA* **2003**, *100*, 14683–14688. [CrossRef] [PubMed]
9. Karageorgiou, V.; Kaplan, D. Porosity of 3D biomaterial scaffolds and osteogenesis. *Biomaterials* **2005**, *26*, 5474–5491. [CrossRef] [PubMed]
10. Warnke, P.H.; Douglas, T.; Wollny, P.; Sherry, E.; Steiner, M.; Galonska, S.; Becker, S.T.; Springer, I.N.; Wiltfang, J.; Sivananthan, S. Rapid prototyping: Porous titanium alloy scaffolds produced by selective laser melting for bone tissue engineering. *Tissue Eng. Part C Methods* **2009**, *15*, 115–124. [CrossRef] [PubMed]
11. Lincks, J.; Boyan, B.D.; Blanchard, C.R.; Lohmann, C.H.; Liu, Y.; Cochran, D.L.; Dean, D.D.; Schwartz, Z. Response of MG63 osteoblast-like cells to titanium and titanium alloy is dependent on surface roughness and composition. *Biomaterials* **1998**, *19*, 2219–2232. [CrossRef]
12. Chen, J.; Paetzell, E.; Zhou, J.; Lyons, L.; Soboyejo, W. Osteoblast-like cell ingrowth, adhesion and proliferation on porous Ti-6Al-4V with particulate and fiber scaffolds. *Mater. Sci. Eng. C* **2010**, *30*, 647–656. [CrossRef]
13. Murr, L.E.; Gaytan, S.M.; Martinez, E.; Medina, F.; Wicker, R.B. Next generation orthopaedic implants by additive manufacturing using electron beam melting. *Int. J. Biomater.* **2012**, *2012*, 245727:1–245727:14. [CrossRef] [PubMed]
14. Heinl, P.; Muller, L.; Korner, C.; Singer, R.F.; Muller, F.A. Cellular Ti-6Al-4V structures with interconnected macro porosity for bone implants fabricated by selective electron beam melting. *Acta Biomater.* **2008**, *4*, 1536–1544. [CrossRef] [PubMed]
15. Van der Stok, J.; van der Jagt, O.P.; Amin, Y.S.; de Haas, M.F.; Waarsing, J.H.; Jahr, H.; van Lieshout, E.M.; Patka, P.; Verhaar, J.A.; Zadpoor, A.A.; *et al.* Selective laser melting-produced porous titanium scaffolds regenerate bone in critical size cortical bone defects. *J. Orthop. Res.* **2013**, *31*, 792–799. [CrossRef] [PubMed]
16. Jonitz-Heincke, A.; Wieding, J.; Schulze, C.; Hansmann, D.; Bader, R. Comparative Analysis of the Oxygen Supply and Viability of Human Osteoblasts in Three-Dimensional Titanium Scaffolds Produced by Laser-Beam or Electron-Beam Melting. *Materials* **2013**, *6*, 5398–5409. [CrossRef]
17. Koike, M.; Greer, P.; Owen, K.; Lilly, G.; Murr, L.E.; Gaytan, S.M.; Martinez, E.; Okabe, T. Evaluation of Titanium Alloys Fabricated Using Rapid Prototyping Technologies-Electron Beam Melting and Laser Beam Melting. *Materials* **2011**, *4*, 1776–1792. [CrossRef]

18. Van, B.S.; Chai, Y.C.; Truscello, S.; Moesen, M.; Kerckhofs, G.; Van, O.H.; Kruth, J.P.; Schrooten, J. The effect of pore geometry on the *in vitro* biological behavior of human periosteum-derived cells seeded on selective laser-melted Ti6Al4V bone scaffolds. *Acta Biomater.* **2012**, *8*, 2824–2834.
19. Yavari, S.A.; Wauthle, R.; Van der Stok, J.; Riemslag, A.C.; Janssen, M.; Mulier, M.; Kruth, J.P.; Schrooten, J.; Weinans, H.; Zadpoor, A.A. Fatigue behavior of porous biomaterials manufactured using selective laser melting. *Mater. Sci. Eng. C Mater. Biol. Appl.* **2013**, *33*, 4849–4858. [CrossRef] [PubMed]
20. Murphy, C.M.; O'Brien, F.J. Understanding the effect of mean pore size on cell activity in collagen-glycosaminoglycan scaffolds. *Cell Adhes. Migr.* **2010**, *4*, 377–381. [CrossRef] [PubMed]
21. Otsuki, B.; Takemoto, M.; Fujibayashi, S.; Neo, M.; Kokubo, T.; Nakamura, T. Pore throat size and connectivity determine bone and tissue ingrowth into porous implants: Three-dimensional micro-CT based structural analyses of porous bioactive titanium implants. *Biomaterials* **2006**, *27*, 5892–5900. [CrossRef] [PubMed]
22. Teixeira, L.N.; Crippa, G.E.; Lefebvre, L.P.; de Oliveira, P.T.; Rosa, A.L.; Beloti, M.M. The influence of pore size on osteoblast phenotype expression in cultures grown on porous titanium. *Int. J. Oral Maxillofac. Surg.* **2012**, *41*, 1097–1101. [CrossRef] [PubMed]
23. Dabrowski, B.; Swieszkowski, W.; Godlinski, D.; Kurzydlowski, K.J. Highly porous titanium scaffolds for orthopaedic applications. *J. Biomed. Mater. Res. B Appl. Biomater.* **2010**, *95*, 53–61. [CrossRef] [PubMed]
24. St-Pierre, J.P.; Gauthier, M.; Lefebvre, L.P.; Tabrizian, M. Three-dimensional growth of differentiating MC3T3-E1 pre-osteoblasts on porous titanium scaffolds. *Biomaterials* **2005**, *26*, 7319–7328. [CrossRef] [PubMed]
25. Burg, K.J.; Porter, S.; Kellam, J.F. Biomaterial developments for bone tissue engineering. *Biomaterials* **2000**, *21*, 2347–2359. [CrossRef]
26. Malda, J.; Klein, T.J.; Upton, Z. The roles of hypoxia in the *in vitro* engineering of tissues. *Tissue Eng.* **2007**, *13*, 2153–2162. [CrossRef] [PubMed]
27. Sailon, A.M.; Allori, A.C.; Davidson, E.H.; Reformat, D.D.; Allen, R.J.; Warren, S.M. A novel flow-perfusion bioreactor supports 3D dynamic cell culture. *J. Biomed. Biotechnol.* **2009**, *2009*, 873816:1–873816:7. [CrossRef] [PubMed]
28. Cartmell, S.H.; Porter, B.D.; Garcia, A.J.; Guldberg, R.E. Effects of medium perfusion rate on cell-seeded three-dimensional bone constructs *in vitro*. *Tissue Eng.* **2003**, *9*, 1197–1203. [CrossRef] [PubMed]
29. Gomes, M.E.; Holtorf, H.L.; Reis, R.L.; Mikos, A.G. Influence of the porosity of starch-based fiber mesh scaffolds on the proliferation and osteogenic differentiation of bone marrow stromal cells cultured in a flow perfusion bioreactor. *Tissue Eng.* **2006**, *12*, 801–809. [CrossRef] [PubMed]
30. Gaspar, D.A.; Gomide, V.; Monteiro, F.J. The role of perfusion bioreactors in bone tissue engineering. *Biomatter* **2012**, *2*, 167–175. [CrossRef] [PubMed]
31. Iwashiro, H.; Hosoya, S.; Hirai, K.; Mima, T.; Ohashi, S.; Aihara, T.; Ito, S.; Ohara, S.; Adachi, E. Characterization of dense artificial connective tissues generated in a newly designed bioreactor. *Connect. Tissue Res.* **2011**, *52*, 340–352. [CrossRef] [PubMed]

32. Bancroft, G.N.; Sikavitsas, V.I.; van den Dolder, J.; Sheffield, T.L.; Ambrose, C.G.; Jansen, J.A.; Mikos, A.G. Fluid flow increases mineralized matrix deposition in 3D perfusion culture of marrow stromal osteoblasts in a dose-dependent manner. *Proc. Natl. Acad. Sci. USA* **2002**, *99*, 12600–12605. [CrossRef] [PubMed]
33. Morris, H.L.; Reed, C.I.; Haycock, J.W.; Reilly, G.C. Mechanisms of fluid-flow-induced matrix production in bone tissue engineering. *Proc. Inst. Mech. Eng. H* **2010**, *224*, 1509–1521. [CrossRef] [PubMed]
34. Van den Dolder, J.; Bancroft, G.N.; Sikavitsas, V.I.; Spauwen, P.H.; Jansen, J.A.; Mikos, A.G. Flow perfusion culture of marrow stromal osteoblasts in titanium fiber mesh. *J. Biomed. Mater. Res. A* **2003**, *64*, 235–241. [CrossRef] [PubMed]
35. Ban, Y.; Wu, Y.Y.; Yu, T.; Geng, N.; Wang, Y.Y.; Liu, X.G.; Gong, P. Response of osteoblasts to low fluid shear stress is time dependent. *Tissue Cell* **2011**, *43*, 311–317. [CrossRef] [PubMed]
36. Chao, P.H.; Grayson, W.; Vunjak-Novakovic, G. Engineering cartilage and bone using human mesenchymal stem cells. *J. Orthop. Sci.* **2007**, *12*, 398–404. [CrossRef] [PubMed]
37. Wieding, J.; Souffrant, R.; Mittelmeier, W.; Bader, R. Finite element analysis on the biomechanical stability of open porous titanium scaffolds for large segmental bone defects under physiological load conditions. *Med. Eng. Phys.* **2013**, *35*, 422–432. [CrossRef] [PubMed]
38. Lochner, K.; Fritsche, A.; Jonitz, A.; Hansmann, D.; Mueller, P.; Mueller-Hilke, B.; Bader, R. The potential role of human osteoblasts for periprosthetic osteolysis following exposure to wear particles. *Int. J. Mol. Med.* **2011**, *28*, 1055–1063. [CrossRef] [PubMed]
39. Lochner, K.; Jonitz-Heincke, A.; Lindner, T.; Weissmann, V.; Hansmann, D.; Mittelmeier, W.; Bader, R. Kultivierung von Humanen Osteoblasten auf großflächigen, Porösen Knochenersatz-materialien: Analyse Unterschiedlicher Statischer und Dynamischer Kultivierungsbedingungen. In *Knöcherne Geweberegeneration*; Neumann, H.G., Klinkenberg, E.D., Eds.; Deutsche NationalBibliothek: Shaker Verlag, Aachen, 2014; pp. 113–130.
40. Ponader, S.; Vairaktaris, E.; Heinl, P.; Wilmowsky, C.V.; Rottmair, A.; Korner, C.; Singer, R.F.; Holst, S.; Schlegel, K.A.; Neukam, F.W.; *et al*. Effects of topographical surface modifications of electron beam melted Ti-6Al-4V titanium on human fetal osteoblasts. *J. Biomed. Mater. Res. A* **2008**, *84*, 1111–1119. [CrossRef] [PubMed]
41. Stangl, R.; Rinne, B.; Kastl, S.; Hendrich, C. The influence of pore geometry in cp Ti-implants—A cell culture investigation. *Eur. Cells Mater.* **2001**, *2*, 1–9.
42. Hollander, D.A.; von, W.M.; Wirtz, T.; Sellei, R.; Schmidt-Rohlfing, B.; Paar, O.; Erli, H.J. Structural, mechanical and *in vitro* characterization of individually structured Ti-6Al-4V produced by direct laser forming. *Biomaterials* **2006**, *27*, 955–963. [CrossRef] [PubMed]
43. Wieding, J.; Wolf, A.; Bader, R. Numerical optimization of open-porous bone scaffold structures to match the elastic properties of human cortical bone. *J. Mech. Behav. Biomed. Mater.* **2014**, *37*, 56–68. [CrossRef] [PubMed]
44. Volkmer, E.; Drosse, I.; Otto, S.; Stangelmayer, A.; Stengele, M.; Kallukalam, B.C.; Mutschler, W.; Schieker, M. Hypoxia in static and dynamic 3D culture systems for tissue engineering of bone. *Tissue Eng. Part A* **2008**, *14*, 1331–1340. [CrossRef] [PubMed]

45. Frosch, K.H.; Barvencik, F.; Viereck, V.; Lohmann, C.H.; Dresing, K.; Breme, J.; Brunner, E.; Sturmer, K.M. Growth behavior, matrix production, and gene expression of human osteoblasts in defined cylindrical titanium channels. *J. Biomed. Mater. Res. A* **2004**, *68*, 325–334. [CrossRef] [PubMed]
46. McCoy, R.J.; Jungreuthmayer, C.; O'Brien, F.J. Influence of flow rate and scaffold pore size on cell behavior during mechanical stimulation in a flow perfusion bioreactor. *Biotechnol. Bioeng.* **2012**, *109*, 1583–1594. [CrossRef] [PubMed]
47. Zhang, Z.; Yuan, L.; Lee, P.D.; Jones, E.; Jones, J.R. Modeling of time dependent localized flow shear stress and its impact on cellular growth within additive manufactured titanium implants. *J. Biomed. Mater. Res. B Appl. Biomater.* **2014**, *102*, 1689–1699. [CrossRef] [PubMed]
48. Grayson, W.L.; Bhumiratana, S.; Cannizzaro, C.; Chao, P.H.; Lennon, D.P.; Caplan, A.I.; Vunjak-Novakovic, G. Effects of initial seeding density and fluid perfusion rate on formation of tissue-engineered bone. *Tissue Eng Part A* **2008**, *14*, 1809–1820. [CrossRef] [PubMed]
49. Jaasma, M.J.; O'Brien, F.J. Mechanical stimulation of osteoblasts using steady and dynamic fluid flow. *Tissue Eng Part A* **2008**, *14*, 1213–1223. [CrossRef] [PubMed]
50. Du, D.; Furukawa, K.S.; Ushida, T. 3D culture of osteoblast-like cells by unidirectional or oscillatory flow for bone tissue engineering. *Biotechnol. Bioeng.* **2009**, *102*, 1670–1678. [CrossRef] [PubMed]
51. Volkmer, E.; Otto, S.; Polzer, H.; Saller, M.; Trappendreher, D.; Zagar, D.; Hamisch, S.; Ziegler, G.; Wilhelmi, A.; Mutschler, W.; *et al*. Overcoming hypoxia in 3D culture systems for tissue engineering of bone *in vitro* using an automated, oxygen-triggered feedback loop. *J. Mater. Sci. Mater. Med.* **2012**, *23*, 2793–2801. [CrossRef] [PubMed]

materials

MDPI

Article

Biocompatibility and Inflammatory Potential of Titanium Alloys Cultivated with Human Osteoblasts, Fibroblasts and Macrophages

Jana Markhoff [1,*], Martin Krogull [1], Christian Schulze [1], Christian Rotsch [2], Sandra Hunger [2] and Rainer Bader [1]

1 Biomechanics and Implant Technology Laboratory, Department of Orthopaedics, University Medicine Rostock, Doberaner Strasse 142, 18057 Rostock, Germany; martin.krogull2@uni-rostock.de (M.K.); christian_schulze@med.uni-rostock.de (C.S.); rainer.bader@med.uni-rostock.de (R.B.)

2 Department Medical Engineering, Fraunhofer Institute for Machine Tools and Forming Technology IWU, Nöthnitzer Strasse 44, 01187 Dresden, Germany; christian.rotsch@iwu.fraunhofer.de (C.R.); sandra.hunger@iwu.fraunhofer.de (S.H.)

* Correspondence: markhoffj@gmail.com; Tel.: +49-381-494-9338; Fax: +49-381-494-9308

Academic Editor: Mohan Jacob
Received: 13 October 2016; Accepted: 4 January 2017; Published: 10 January 2017

Abstract: The biomaterials used to maintain or replace functions in the human body consist mainly of metals, ceramics or polymers. In orthopedic surgery, metallic materials, especially titanium and its alloys, are the most common, due to their excellent mechanical properties, corrosion resistance, and biocompatibility. Aside from the established Ti6Al4V alloy, shape memory materials such as nickel-titanium (NiTi) have risen in importance, but are also discussed because of the adverse effects of nickel ions. These might be reduced by specific surface modifications. In the present in vitro study, the osteoblastic cell line MG-63 as well as primary human osteoblasts, fibroblasts, and macrophages were cultured on titanium alloys (forged Ti6Al4V, additive manufactured Ti6Al4V, NiTi, and Diamond-Like-Carbon (DLC)-coated NiTi) to verify their specific biocompatibility and inflammatory potential. Additive manufactured Ti6Al4V and NiTi revealed the highest levels of metabolic cell activity. DLC-coated NiTi appeared as a suitable surface for cell growth, showing the highest collagen production. None of the implant materials caused a strong inflammatory response. In general, no distinct cell-specific response could be observed for the materials and surface coating used. In summary, all tested titanium alloys seem to be biologically appropriate for application in orthopedic surgery.

Keywords: NiTi; DLC; Ti6Al4V; cell viability; human osteoblasts; macrophages

1. Introduction

Biomaterials are used to maintain or replace a wide range of functions in the human body that have been lost due to tumors, fractures, infections, or aging [1–3]. In orthopedic surgery, the materials used consist mainly of metals, ceramics, or polymers [4]. Thereby, metallic materials can be made of stainless steel, titanium or alloys of titanium, cobalt–chromium, magnesium, tantalum, or niobium, for example [5]. Titanium and its alloys are the most common materials, comprising 70%–80% of all used materials [6–8]. Due to their excellent mechanical properties, corrosion resistance, and biocompatibility, these materials are used in load-bearing areas such as orthodontics, orthopedics, and gastroenterology as well as for cardiovascular and reconstructive purposes [5,6,9–12]. Furthermore, components made of titanium can be easily manufactured in various shapes and textures [6]. Commercial pure titanium and Ti6Al4V were established in the 1950s and offer excellent physical

and chemical properties; then, shape memory alloys like nickel-titanium (as nitinol with a nickel content of 49%–51%) were first reported in the late 1960s [13] and have risen in importance in the last decades [14]. This is related to their favorable properties like the shape memory effect (SME), good biocompatibility, and superelasticity of up to 8% [15], with mechanical values (elastic modulus and compressive strength) close to those of bone tissue [16–18] as well as beneficial corrosion and wear resistance [15]. Nevertheless, fabrication of NiTi is difficult and expensive [5,15]. NiTi alloys are also discussed, because of the possible toxic, allergenic, and carcinogenic properties of nickel ions [5,16,19]. To create an ion diffusion barrier, several surface modifications have been taken into account [14,16], for example chemical, electrochemical, or heat treatment as well as irradiation or coatings like diamond-like carbon (DLC) [14,20–22]. DLC coatings are reported to be chemically inert with good biocompatibility [20]. For initial cell attachment and growth, the surface properties (roughness, surface chemical structure, and wettability) play an important role [6,14], since they even result in a cell-specific response [10,23]. It is known that osteoblasts prefer rougher surfaces while fibroblast growth is increased on smoother ones, for example [10]. Since human tissue comprises specific cell types, cells of different origins and with various functions should be considered for preclinical testing of specific biomaterials. Primary human cells may be preferred since cell lines may not fully display the physiological situation [24]. Osteoblasts are cells of the lineage of mesenchymal stem cells and are responsible for the formation of new bone [25]. Fibroblasts and mesenchymal stromal cells are involved in inflammatory processes occurring in all types of tissues [26]. Macrophages play a dominant role in inflammation and interaction with implanted materials and represent an important type of cell for biocompatibility testing [27]. Macrophages develop from monocytic cells, which are a multifunctional fraction of peripheral blood mononuclear cells (PBMCs) [28].

In the present in vitro study, the osteoblastic cell line MG-63 as well as human osteoblasts, human fibroblasts, and human macrophages were cultured on four titanium alloys (forged Ti6Al4V, additive manufactured Ti6Al4V, NiTi, and DLC-coated NiTi) to verify their specific biocompatibility and inflammatory potential.

2. Materials and Methods

2.1. Test Samples

The forged Ti6Al4V samples were provided by DOT GmbH, Rostock, Germany. The selective laser melted (SLM)-manufactured Ti6Al4V pellets were manufactured with an EOS M 280 and provided by Proto Labs Eschenlohe GmbH, Eschenlohe, Germany. The samples were heat-treated after the manufacturing process (protective gas atmosphere argon, slow cooling in oven under inert gas) and run through a multi-level post-processing (removing the support-structures, grinding of supported surfaces, sandblasting of the samples with 20–45 µm grain size), cleaning (removing of loose particles) and sterilization process. We used NiTi-samples (Memry GmbH, Weil, Germany), which are biocompatible commercially available materials. NiTi-samples were oxide-free etched by the manufacturer. The DLC coating of the conventionally available biocompatible NiTi (Type "S" by Memry GmbH) with a nickel content of about 50% was provided by EC EUROP COATING GmbH (Hohenlockstedt, Germany). The coating was realized by a physical vapor deposition (PVD) process (dc magnetron sputtering; coating temperature: 180–200 °C; coating thickness: about 2–4 µm).

All test samples exhibited similar geometries and were cleaned in an ultrasonic bath and sterilized via gamma sterilization with 25 kGy. Surface roughness was measured using a profilometer (Hommel–Etamic T1000, Jenoptik AG, Jena, Germany). The parameters "mean roughness index" (Ra) and "average surface roughness" (Rz) were determined (Table 1).

Table 1. Dimensions as well as values of roughness of the test samples.

Test Pellet	Dimensions (mm^2)	Rz (µm) Mean ± SD	Ra (µm) Mean ± SD
Ti6Al4V	10 × 2	15.71 ± 1.27	2.38 ± 0.15
Ti6Al4V SLM	10 × 2	68.82 ± 10.59	13.53 ± 2.55
NiTi	10 × 1	1.12 ± 0.26	0.15 ± 0.03
NiTi + DLC	10 × 1	1.13 ± 0.32	0.15 ± 0.02

Field emission scanning electron microscopy (FESEM) images of the sample surfaces were generated using a sputter coater (Leica SCD004, Wetzlar, Germany) and Merlin VP compact microscope (Carl Zeiss AG, Oberkochen, Germany) (Figure 1).

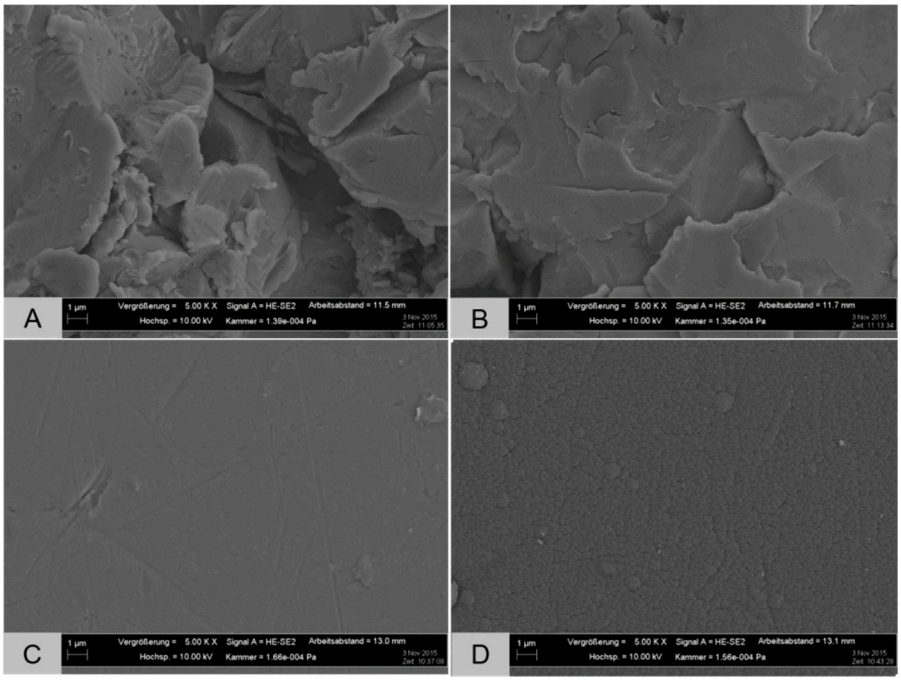

Figure 1. FESEM images of the test pellets: (**A**) Ti6Al4V; (**B**) Ti6Al4V SLM; (**C**) NiTi; and (**D**) NiTi + DLC (magnification: 5.00 kX, bar: 1 µm).

2.2. Cell Isolation

For the in vitro tests, a cell line and three human types of cells were used. The use of all human cell types was approved by the Local Ethical Committee of the University Medicine Rostock (registration numbers: for osteoblasts: A 2010-10; for fibroblasts: A 2013-0092; and for macrophages: A 2011-140). Characteristics of the human cell donors are mentioned in Table 2. Cell cultivation was carried out in an incubator (Binder GmbH, Tuttlingen, Germany) under simulated in vivo conditions at 5% CO_2, 21% O_2, and 37 °C with regular medium changes unless otherwise stated. Tissue culture polystyrene (TCPS) served as a common surface for growth control.

Table 2. Characteristics of the human cell donors used for cell experiments.

Human Cells	Donors	Gender	Average Age
Osteoblasts	$n = 8$	4 ♂/4 ♀	71.88 ± 7.88
Fibroblasts	$n = 4$	− ♂/2 ♀(2 n/a)	40 ± 7.07 (2 n/a)
Macrophages	$n = 4$	n/a	n/a

The bone cell line MG-63 was ordered from ATCC (American Type Culture Collection, Manassas, VA, USA). MG-63 is an established cell line, isolated from the osteosarcoma of a 14-year old Caucasian male patient. MG-63 cells were cultured in Dulbecco's Modified Eagle's Medium (DMEM) with 10% fetal calf serum (FCS), 1% penicillin/streptomycin, 1% amphotericin B, 1% HEPES buffer (2-(4-(2-hydroxyethyl)-1-piperazineethanesulfonic acid) (all: Gibco-Invitrogen, Darmstadt, Germany). The test samples were directly seeded with MG-63 cells at a density of 20,000 cells per 48 wells in 500 µL of culture medium in two wells per donor for every configuration.

The isolation of human primary osteoblasts was performed as previously described by Lochner et al. [29]. After patient agreement, the femoral heads of the patients undergoing primary total hip replacement in our in-house operating theatre were collected and cells were isolated from the spongiosa. Cultivation was done in osteogenic cell culture medium (Minimum Essential Medium (MEM) Dulbecco, Biochrom AG, Berlin, Germany) with 10% FCS, 1% penicillin/streptomycin, 1% amphotericin B, and 1% HEPES buffer (all from Gibco-Invitrogen, Darmstadt, Germany), including osteogenic additives (dexamethasone (100 nM), L-ascorbic acid (50 µg/mL), and β-glycerophosphate (10 mM) (all from Sigma-Aldrich, Munich, Germany)). To verify the osteogenic character of the isolated cells, alkaline phosphatase staining with fuchsin substrate chromogen (DAKO, Hamburg, Germany) was carried out. The test samples were directly seeded with osteoblasts at a density of 20,000 cells (third passage) per 48 wells in 500 µL of culture medium with two wells per donor for every configuration (Figure 2b). Furthermore, to verify whether cytopathic substances are emitted into the culture medium, all test samples were incubated in culture medium during 72 h with an additional medium control without pellet. Afterwards, the supernatants were transferred onto human osteoblasts (20,000 cells per 48 wells in 500 µL) for a further 72 h of cultivation in two wells per donor for every configuration (Figure 2a).

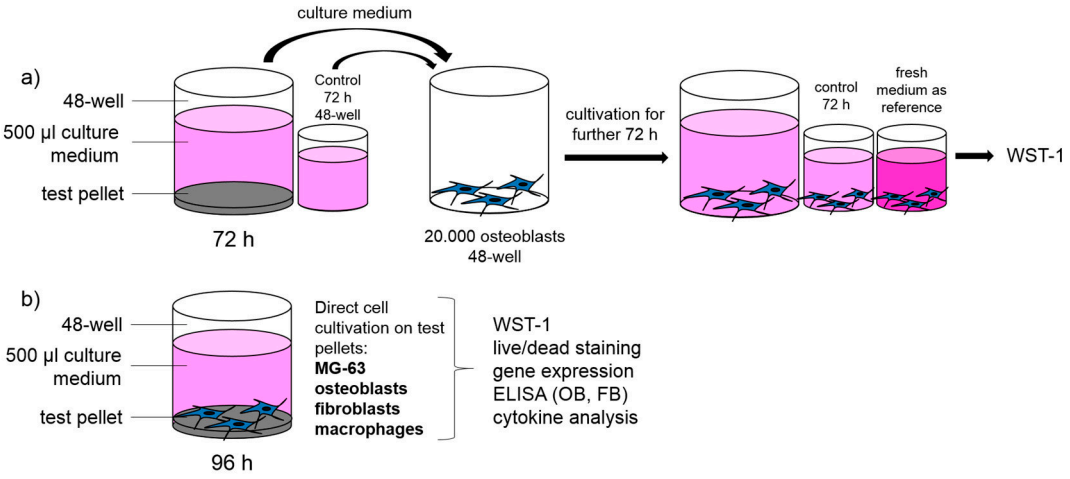

Figure 2. Schematic experiment set-up: (**a**) verification of potential cytopathic substances; and (**b**) analysis of biocompatibility of different titanium alloys with four types of cells.

Human fibroblasts were isolated from skin biopsies (breast, eyelid) provided by a local clinic for aesthetic surgeries. Redundant adipose tissue was removed and the remaining tissue was cut into equal segments (edge length: 2–3 mm). Then, skin pieces were transferred to six-well plates (2–3 bits per well) with the epidermis upwards. After 20 min of surface drying, skin was overlaid with 3 mL of DMEM medium (with Glutamax, 10% FCS, 1% penicillin/streptomycin, and 1% amphotericin B (all from Gibco-Invitrogen, Darmstadt, Germany)). After three weeks, cells were transferred to tissue culture flasks and cryo-preserved after further confluence. The test pellets were directly seeded with fibroblasts at a density of 20,000 cells (fifth passage) per 48 wells in 500 µL of culture medium in two wells per donor for every configuration.

Furthermore, human buffy coats from blood donations were provided by the Institute of Transfusion Medicine, University Medicine Rostock and used after patient agreement for isolation of PBMCs. The buffy coats were separated in different directions by means of density gradient centrifugation (Ficoll Hypaque method) by lymphocyte separation medium (Histopaque-1077, Sigma-Aldrich, Hamburg, Germany). The interphase containing the PBMC-like lymphocytes and monocytes (density: 1.07 g/mL) was extracted by means of a Pasteur pipette. After two washing steps in phosphate-buffered saline (PBS, Biochrom GmbH, Berlin, Germany), the cells were seeded in monolayers (1×10^7 cells per well in 3 mL) in six-well suspension culture plates (Cellstar cell-repellent surface, Greiner Bio-One, Frickenhausen, Germany) using Roswell Park Memorial Institute (RPMI) medium 1640 (Biochrom, Berlin, Germany) containing 10% FCS, 1% penicillin/streptomycin (all from Gibco-Invitrogen, Darmstadt, Germany), and 2% L-glutamine (PAA Laboratories GmbH, Coelbe, Germany). After seven days of cultivation, suspension cells were transferred to a standard 48-well culture plate and directly cultured on test pellets with a density of 4×10^5 cells per well in 500 µL of (MEM Alpha-Medium (1×), Life Technologies GmbH, Darmstadt, Germany) with 10% FCS and 2% penicillin/streptomycin in two wells per donor for every configuration.

2.3. Cell Biological Testing

2.3.1. Metabolic Activity and Live/Dead Staining

The metabolic activity of cells was determined via mitochondrial dehydrogenase activity (WST-1 test) (Roche, Grenzach–Wyhlen, Germany) after 96 h. The tetrazolium salt WST (water soluble tetrazolium) is transformed into formazan by mitochondrial succinate dehydrogenase from metabolically active cells. The adsorption, which was directly proportional to the metabolic cell activity, was measured at 450 nm in a Tecan reader (Infinite F200 Pro, Männedorf, Switzerland). Qualitative cell viability was analyzed by live/dead staining with two fluorescent dyes. Calcein-Acetyoxymethyl (AM) visualizes vital cells and ethidium homodimer-1 visualizes dead ones (Live/Dead Cell Viability Assay, Invitrogen, Darmstadt, Germany). For imaging, an inverted microscope (Nikon TS 100, Nikon GmbH, Duesseldorf, Germany) was used.

2.3.2. Gene Expression Analysis

Human osteoclasts, fibroblasts, and macrophages were isolated from the test pellets to obtain the total RNA via TRIzol reagent (Invitrogen, Darmstadt, Germany) and the Direct-zol RNA kit (Zymo Research, Freiburg, Germany), according to the manufacturer's instructions, with optional DNAse digestion. RNA concentrations were determined using Tecan's NanoQuant plate and the Tecan reader (Infinite F200 Pro, Männedorf, Switzerland). Afterwards, 250 ng of total RNA was retrotranscribed to cDNA using the High Capacity cDNA Reverse Transcription Kit (Applied Biosystems, Darmstadt, Germany) with 10× RT buffer, 25× dNTP Mix (100 mM), RT random primers, MultiScribe® Reverse Transcriptase (50 U/µL), and Diethylpyrocarbonate (DEPC) water in a final volume of 20 µL. This suspension was incubated for 10 min at 25 °C, 120 min at 37 °C, and finally 15 s at 85 °C in a thermocycler (Personal Thermocycler, Biometra, Göttingen, Germany). One microliter of cDNA was used as the template for polymerase chain reaction (PCR) in triple. These reactions were performed with DEPC water, 0.5 µL of each forward and reverse primer (Sigma-Aldrich, Hamburg, Germany), and innuMIX qPCR MasterMix SyGreen (Analytik Jena, Jena, Germany) including high specific Taq DNA polymerase, high quality dNTPs, and intercalating dyestuff, in a final reaction volume of 20 µL. The primer details are summarized in Table 3. The quantitative PCR reaction was performed at 95 °C for 3 min, 95 °C for 5 s, and 60 °C for 30 s over 40 cycles via qTower 2.0 (Analytik Jena, Jena, Germany). β-actin (osteoblasts and fibroblasts) and Hypoxanthine-guanine phosphoribosyltransferase (HPRT) (macrophages) were chosen as housekeeping genes.

Table 3. Primers and Primer sequences used for gene expression analysis.

Primer	Primer Sequence
β-Actin	Forward primer: 5′-CTTCCTGGGCATGGAGTC-3′ Reverse primer: 5′-AGCACTGTGTTGGCGTACAG-3′
Collagen I	Forward primer: 5′-ACGAAGACATCCCACCAATC-3′ Reverse primer 5′-AGATCACGTCATCGCACAAC-3′
HPRT	Forward primer: 5′-CCCTGGCGTCGTGATTAGTG-3′ Reverse primer: 5′-TCGAGCAAGACGTTCAGTCC-3′
IL-6	Forward primer: 5′-TGGATTCAATGAGGAGACTTGCC-3′ Reverse primer: 5′-CTGGCATTTGTGGTTGGGTC-3′
IL-8	Forward primer: 5′-TCTGTGTGAAGGTGCAGTTTTG-3′ Reverse primer: 5′-ATTTCTGTGTTGGCGCAGTG-3′
MCP-1	Forward primer: 5′-CCGAGAGGCTGAGACTAACC-3′ Reverse primer: 5′-GGCATTGATTGCATCTGGCTG-3′
MMP-1	Forward primer: 5′-AGAGCAGATGTGGACCATGC-3′ Reverse primer 5′-TCCCGATGATCTCCCCTGAC-3′
TNF-α	Forward primer: 5′-GTTGTAGCAAACCCTCAAGCTG-3′ Reverse primer: 5′-GAGGTACAGGCCCTCTGATG-3′

IL: interleukin; MCP-1: monocyte chemoattractant protein-1; MMP-1: matrix metalloproteinase-1; TNF-α: tumor necrosis factor-α.

2.3.3. Enzyme-Linked Immunosorbent Assays

Enzyme-linked immunosorbent assays (ELISAs) were used to verify protein syntheses of pro-collagen type I (Metra C1CP EIA Kit, Quidel, Buende, Germany) and MMP-1 (Human MMP-1 ELISA, RayBiotech, Köln, Germany) in human osteoblasts and fibroblasts. Protein content in the culture supernatants was determined according to the manufacturer's instructions after 96 h of cultivation.

2.3.4. Cytokine Analysis

A cytokine multiplex assay (IL-6, IL-8, MCP-1, TNF-α) (Bio-Rad, Munich, Germany) was done according to the manufacturer's instructions to verify a possible immune-stimulatory effect of the test pellets. In brief, multi-cytokine detection in the culture supernatants was conducted by means of microsphere beads interlinking several cytokines via specific monoclonal antibodies and fluorescent dyes. The appropriate cytokine concentration was measured using the BioPlex 200 System (Bio-Rad, Munich, Germany) and calculated based on a recombinant standard curve of the assay. The reader combines two lasers (reporter laser 532 nm, classification laser 635 nm) and high-throughput fluidics (<100 μL/s) to distinguish several color-coded beads.

2.3.5. Statistical Analysis

The statistical significance was calculated using IBM® SPSS® Statistics Version 20 (IBM Corp., New York, NY, USA). Multiple comparison procedures were carried out by the ANOVA Post Hoc LSD test. Data are shown as box plots. Boxes denote interquartile ranges, horizontal lines within the boxes denote medians, and whiskers denote minimum and maximum values. Values of $p < 0.05$ were set to be significant.

3. Results

Various cell types (MG-63; human osteoblasts, fibroblasts, and macrophages) were used to verify the biocompatibility of several metallic test samples (forged Ti6Al4V, Ti6Al4V SLM, NiTi, and NiTi + DLC coating). After cultivation of human osteoblasts for 72 h in pre-incubated sample medium, all groups including the 72 h medium control showed a significant decrease of metabolic activity of nearly 40% compared to the fresh medium reference (Figure 3).

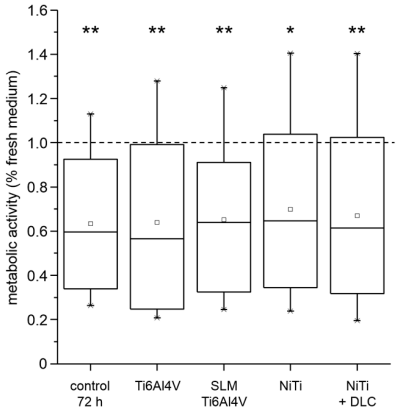

Figure 3. Metabolic activity of human osteoblasts (n = 4) cultured in pre-incubated (72 h) cell culture medium and incubated supernatants (72 h) of different test pellets (forged Ti6Al4V, Ti6Al4V SLM, NiTi, and NiTi + DLC) compared to fresh medium as reference (dotted line). Boxes denote interquartile ranges, horizontal lines within the boxes denote medians, and whiskers denote minimum and maximum values. For statistical analysis, ANOVA was conducted. Data were compared to the fresh medium control (100%, * p). * $p < 0.05$, ** $p < 0.01$.

All cell types were seeded directly on the test samples using TCPS as a common surface for growth control. Except for macrophages, the metabolic activity of cells cultured on the metallic test samples was significantly lower than the growth control. Cultivation of cell line MG-63 on the test samples revealed no significant differences between the test pellets, but compared to the growth control, metabolic activity was significantly decreased by half for all groups (Figure 4, white bars). In general, the human cells showed similar results regarding differences between materials. The forged Ti6Al4V and NiTi + DLC coating resulted in significantly lower activities compared to Ti6Al4V SLM and NiTi, respectively (Figure 4, all gray bars). Metabolic activity on Ti6Al4V SLM and NiTi was similar for human osteoblasts (66% and 63%) and highest on Ti6Al4V SLM with human fibroblasts (59%) and especially human macrophages (115%). These results are partly confirmed by live/dead staining (Figure 5).

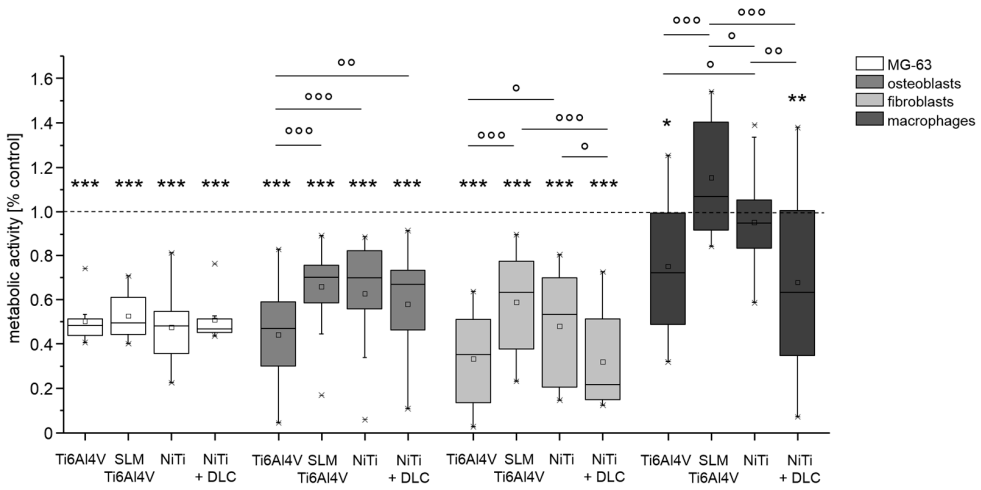

Figure 4. Metabolic activity of MG63 cells (n = 8), human osteoblasts (n = 8), human fibroblasts (n = 4), and human macrophages (n = 4) after 96 h of cultivation on several test pellets (forged Ti6Al4V, Ti6Al4V SLM, NiTi, NiTi + DLC). Boxes denote interquartile ranges, horizontal lines within the boxes denote medians, and whiskers denote minimum and maximum values. For statistical analysis, ANOVA was conducted. Data were compared to the respective growth control (100%, * p) and against each other (° p). * $p < 0.05$, ** $p < 0.01$, *** $p \leq 0.001$; ° $p < 0.05$, °° $p < 0.01$, °°° $p \leq 0.001$.

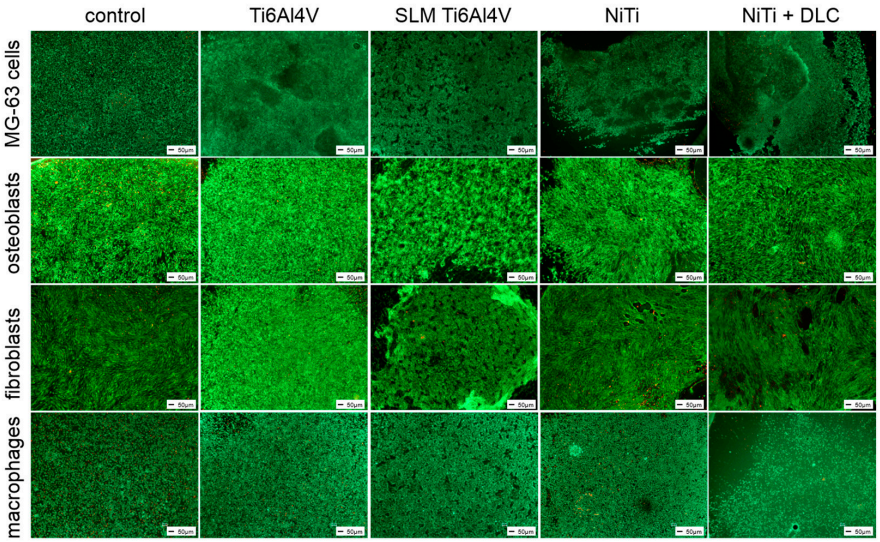

Figure 5. Live/dead staining of MG-63 cells, human osteoblasts, fibroblasts, and macrophages on different test pellets (forged Ti6Al4V, Ti6Al4V SLM, NiTi, and NiTi + DLC). Living cells are displayed in green, dead ones in red. Scale bar: 50 µm.

Gene expression analysis was conducted for pro-collagen type I as the main component of bone matrix, MMP-1 as its degrading enzyme, and several cytokines (IL-6, IL-8, MCP-1, and TNF-α) to verify inflammatory cytokine secretion. Both human osteoblasts and fibroblasts presented a decreased expression of pro-collagen type I for all groups in similar to TCPS and without significant differences between the several test samples (Figures 6 and 7, both white bars). MMP-1 expression was increased on forged Ti6Al4V and decreased on SLM manufactured Ti6Al4V for both types of cells compared to the control. Expression of MMP-1 on NiTi surfaces with and without DLC coating was slightly increased in osteoblasts and obviously higher compared to control in fibroblasts, but without distinct differences. Cytokine expression was similar for those cells, as IL-6 and IL-8 were increased with forged Ti6Al4V and NiTi as well as decreased with SLM Ti6Al4V and NiTi + DLC, and thus varied among the test samples. Furthermore, expression of MCP-1 was slightly higher on the Ti6Al4V surfaces compared to the control and similar or lower on NiTi surfaces.

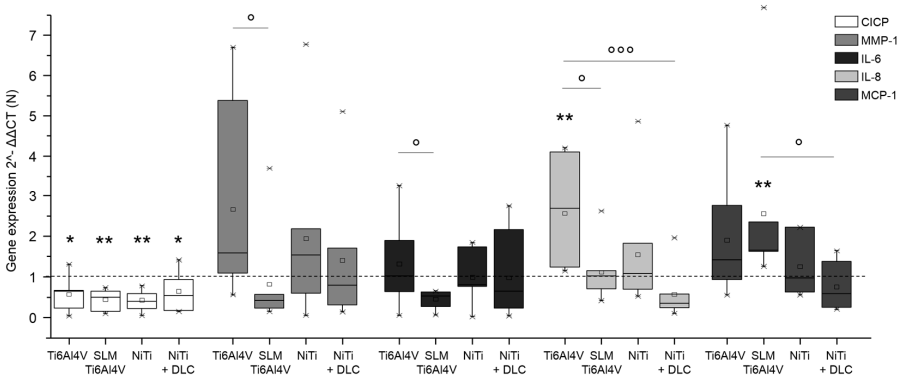

Figure 6. Gene expression (CICP, MMP-1, IL-6, IL-8, and MCP-1) of human osteoblasts (n = 8) after 96 h of cultivation on several test pellets (forged Ti6Al4V, Ti6Al4V SLM, NiTi, and NiTi + DLC). Boxes denote interquartile ranges, horizontal lines within the boxes denote medians, and whiskers denote minimum and maximum values. Data are normalized to the growth control (=100%, dotted line). For statistical analysis, ANOVA was conducted. A p-value < 0.05 was considered statistically significant. Comparison to respective growth control: * $p < 0.05$, ** $p < 0.01$. Comparison between several test pellets: ° $p < 0.05$, °°° $p \leq 0.001$.

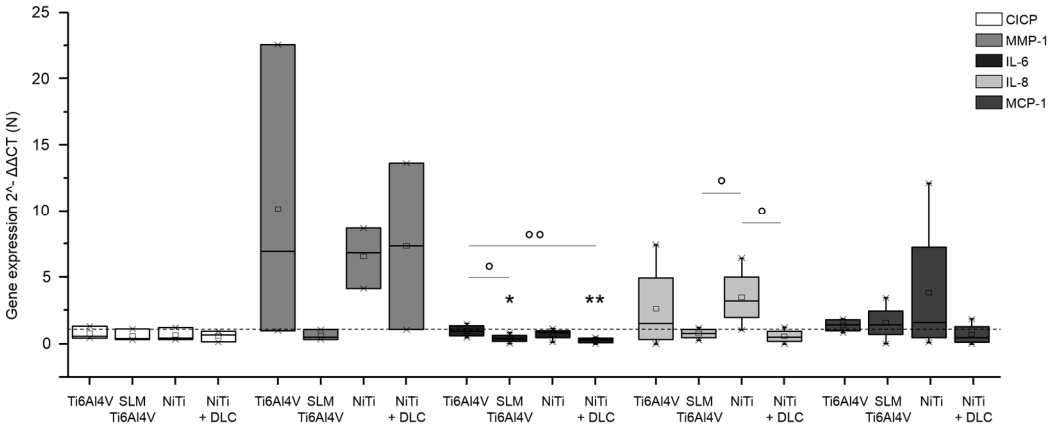

Figure 7. Gene expression (CICP, MMP-1, IL-6, IL-8, and MCP-1) of human fibroblasts ($n \geq 3$) after 96 h of cultivation on several test pellets (forged Ti6Al4V, Ti6Al4V SLM, NiTi, and NiTi + DLC). Boxes denote interquartile ranges, horizontal lines within the boxes denote medians, and whiskers denote minimum and maximum values. Data are normalized to the growth control (=100%, dotted line). For statistical analysis, ANOVA was conducted. A p-value < 0.05 was considered statistically significant. Comparison to growth control: * $p < 0.05$, ** $p < 0.01$. Comparison between several test pellets: ° $p < 0.05$, °° $p < 0.01$.

Gene expression analysis for macrophages on metallic test samples revealed similar or significantly decreased expression compared to the control for all proved cytokines (Figure 8). In general, the highest expression of all cytokines was proven with forged Ti6Al4V. Macrophages on SLM Ti6Al4V expressed the lowest levels of IL-6 and TNF-α and expression of IL-8 and MCP-1 was the lowest with NiTi.

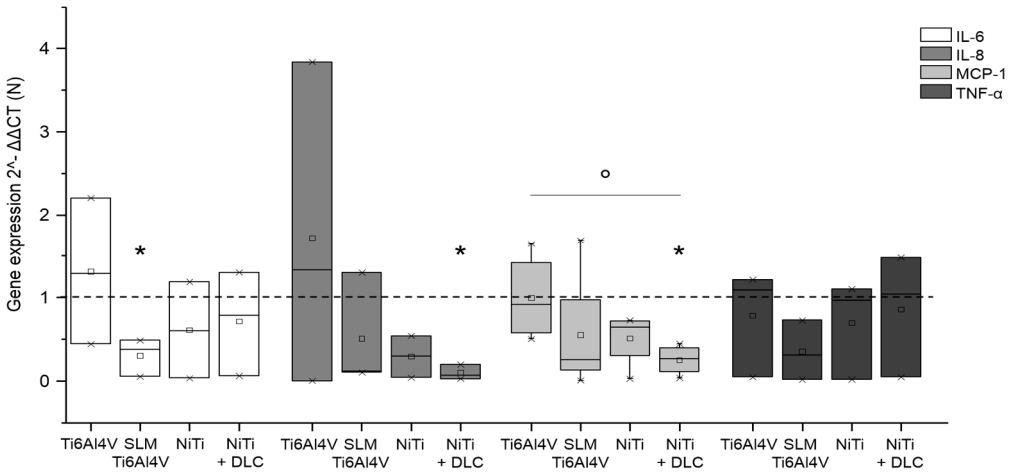

Figure 8. Gene expression (IL-6, IL-8, MCP-1, and TNF-α) of human macrophages ($n \geq 3$) after 96 h of cultivation on several test pellets (forged Ti6Al4V, Ti6Al4V SLM, NiTi, and NiTi + DLC). Boxes denote interquartile ranges, horizontal lines within the boxes denote medians, and whiskers denote minimum and maximum values. Data are normalized to the growth control (=100%, dotted line). For statistical analysis, ANOVA was conducted. A p-value < 0.05 was considered statistically significant. Comparison to growth control: * $p < 0.05$. Comparison between several test pellets: ° $p < 0.05$.

For osteoblasts and fibroblasts, protein synthesis of pro-collagen type I and MMP-1 was determined. Collagen synthesis of human osteoblasts was nearly unaffected on Ti6Al4V surfaces, but was increased on NiTi ones compared to TCPS (Figure 9, left, white bars). In contrast, MMP-1 synthesis was increased in all groups, being highest on forged Ti6Al4V and similar in the other groups (Figure 9, left, gray bars). The pro-collagen type I synthesis of human fibroblasts was higher than on TCPS, with synthesis of all test samples being significantly increased on NiTi + DLC (Figure 9, right, white bars). MMP-1

synthesis was increased on NiTi surfaces compared to TCPS, and was highest on NiTi + DLC (Figure 9, right, gray bars).

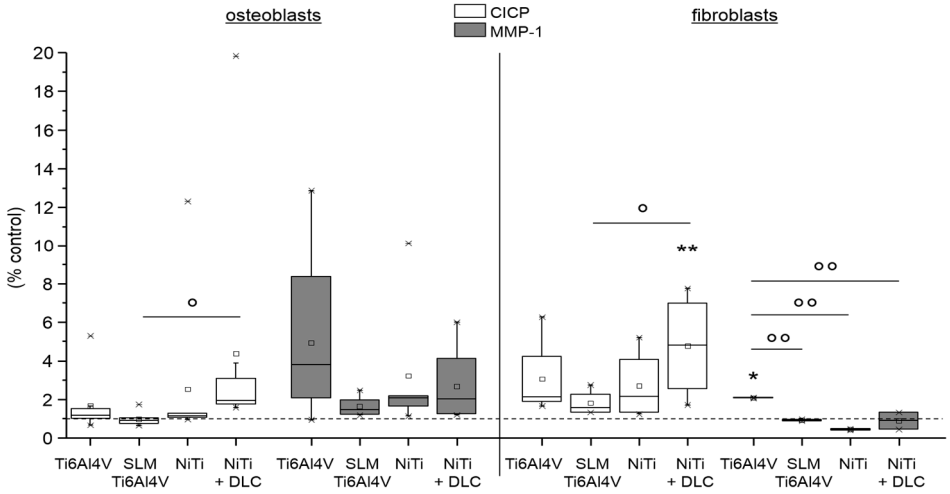

Figure 9. Pro-collagen type I synthesis (white) and MMP-1 synthesis (gray) of human osteoblasts (n = 8, left) and human fibroblasts ($n \geq 2$, right) after 96 h of cultivation on several test pellets (forged Ti6Al4V, Ti6Al4V SLM, NiTi, NiTi + DLC). Boxes denote interquartile ranges, horizontal lines within the boxes denote medians, and whiskers denote minimum and maximum values. For statistical analysis, ANOVA was conducted. Data were compared with the respective growth control (100%, * p) and with each other (° p). * $p < 0.05$, ** $p < 0.01$; ° $p < 0.05$, °° $p < 0.01$.

In addition, a cytokine multiplex was conducted to verify the inflammatory cytokine secretion on the metallic test samples. Interleukin syntheses were increased for human osteoblasts cultured on SLM Ti6Al4V and NiTi + DLC (Figure 10, left diagram) compared to the control, while forged Ti6Al4V and NiTi did not show relevant interleukin release. Furthermore, syntheses of MCP-1 and VEGF were higher than on control TCPS for all surfaces except forged Ti6Al4V (Figure 10, right-hand diagram).

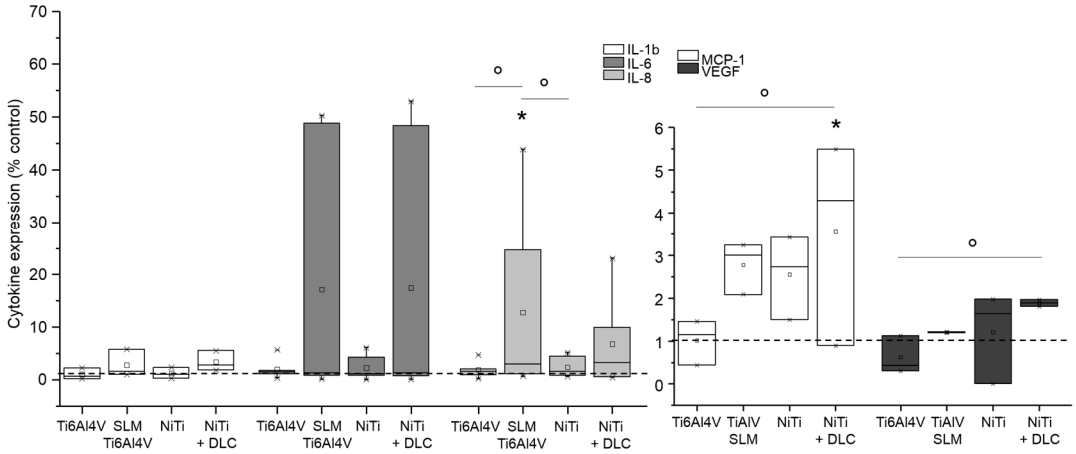

Figure 10. Cytokine level of IL-1b, IL-6, IL-8, MCP-1, and VEGF in supernatants of human osteoblasts ($n \geq 2$) after 96 h of cultivation on several test pellets (forged Ti6Al4V, Ti6Al4V SLM, NiTi, and NiTi + DLC). Data were normalized to the growth control (=100%, dotted line). Boxes denote interquartile ranges, horizontal lines within the boxes denote medians, and whiskers denote minimum and maximum values. For statistical analysis, ANOVA was conducted. A p-value < 0.05 was considered statistically significant. Comparison to growth control: * $p < 0.05$. Comparison between several test pellets: ° $p < 0.05$.

Cultivation of human fibroblasts on the metallic surfaces resulted in slightly increased syntheses of interleukins and MCP-1 mainly on NiTi surfaces compared to the control (Figure 11). In comparison, syntheses were similar to the control or slightly decreased on Ti6Al4V surfaces.

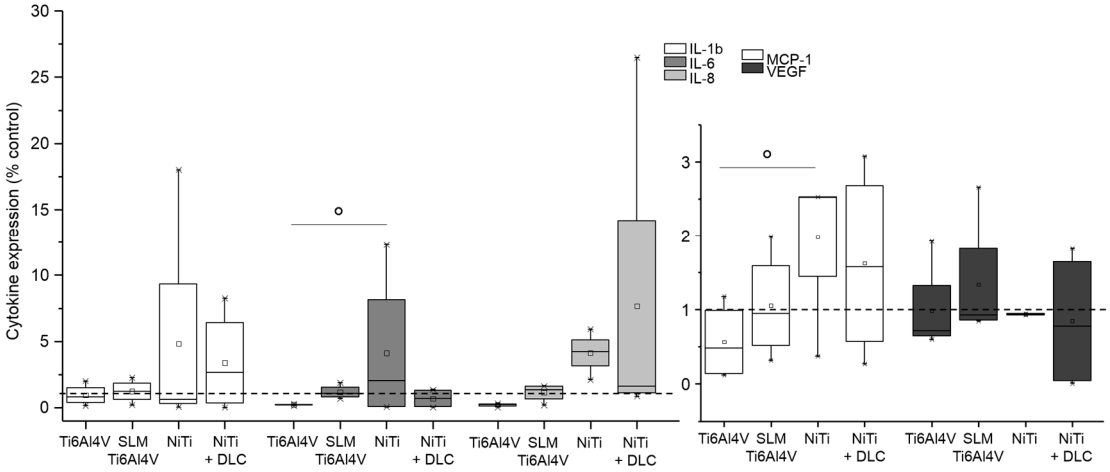

Figure 11. Cytokine level of IL-1b, IL-6, IL-8, MCP-1, and VEGF in supernatants of human fibroblasts (n = 4) after 96 h of cultivation on several test pellets (forged Ti6Al4V, Ti6Al4V SLM, NiTi, and NiTi + DLC). Data were normalized to the growth control (=100%, dotted line). Boxes denote interquartile ranges, horizontal lines within the boxes denote medians, and whiskers denote minimum and maximum values. For statistical analysis, ANOVA was conducted. A p-value < 0.05 was considered statistically significant. Comparison to growth control: no significances. Comparison between several test pellets: $^{\circ}$ $p < 0.05$.

NiTi surfaces with and without DLC coating resulted in increased interleukin and MCP-1 values compared to controls. This trend was also observed in human macrophages (Figure 12). Cytokine syntheses were not caused by the Ti6Al4V surfaces. Altogether, VEGF syntheses were below the control level for all surfaces.

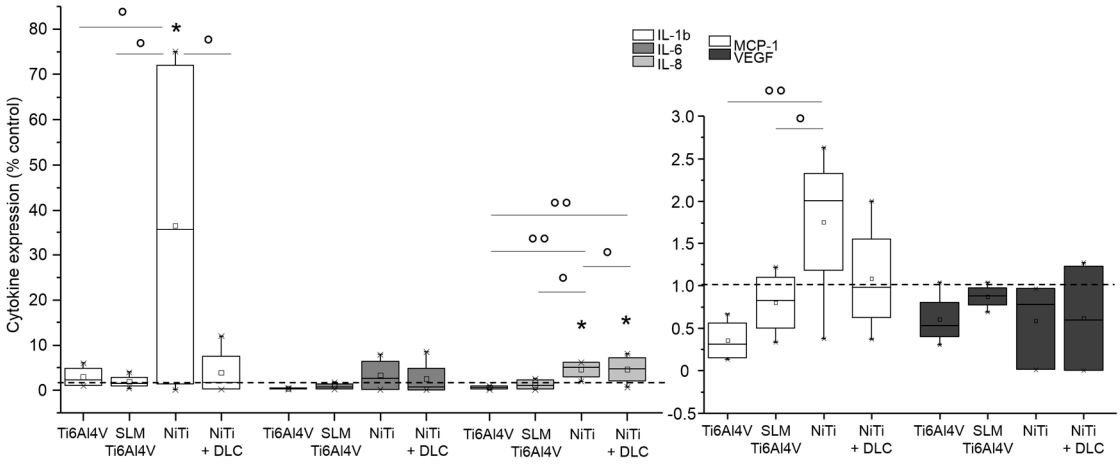

Figure 12. Cytokine levels of IL-1b, IL-6, IL-8, MCP-1, and VEGF in supernatants of human macrophages ($n \geq 3$) after 96 h of cultivation on several test pellets (forged Ti6Al4V, Ti6Al4V SLM, NiTi, and NiTi + DLC). Data were normalized to the growth control (=100%, dotted line). Boxes denote interquartile ranges, horizontal lines within the boxes denote medians, and whiskers denote minimum and maximum values. For statistical analysis, ANOVA was conducted. A p-value < 0.05 was considered statistically significant. Comparison to growth control: * $p < 0.05$. Comparison between several test pellets: $^{\circ}$ $p < 0.05$, $^{\circ\circ}$ $p < 0.01$.

4. Discussion

Four titanium alloys were analyzed with regard to their biocompatibility and inflammatory potential using an osteosarcoma cell line (MG-63) and three human cell types (osteoblasts, fibroblasts, and macrophages). Forged Ti6Al4V, SLM manufactured Ti6Al4V, and NiTi with and without DLC coating samples were used. The elements aluminum and vanadium of the Ti6Al4V alloy may cause neurodegenerative diseases and genotoxicity [19,30]. However, the biological properties of metals like titanium, cobalt-chromium alloys, and stainless steel are well known, since pure titanium and its alloys are associated with the highest biocompatibilities [7,31]. NiTi materials with their high nickel content are also under discussion [31], but their biocompatibility has been proven [15]. When in contact with body fluid (blood, urine, saliva, and serum) or culture medium, all metals tend to corrode, releasing ions into their environments [3,32]. Nevertheless, the intensity of ion dissolution is dependent on the properties of the medium (pH, temperature, and chemical composition) [11,33–35] and the dissolution rate and roughness of the metal [34,36]. Although nickel is an essential body element, daily uptake is limited to 600 µg [14]. Hence, in our present in vitro study, all test samples were pre-incubated in culture medium for further cell cultivation in it. Thereby, no negative effect of any of the alloys could be observed compared to the control medium. Supernatants were analyzed after 72 h via Inductively Coupled Plasma–Atomic Emission Spectrometry (ICP-EOS) for testing purposes using an ICP Optical Emission Spectrometers (Varian/Agilent 715-ES, Waldbronn, Germany). Sample digestion and dilution were done with HNO_3 and with H_2O_2 and H_2O, respectively. Due to technical incidents a high dilution of samples was necessary, so all tested supernatants were under the detectable limit. Cortizo et al. [34] tested ion release from NiTi after 48 h and found that it was also below the detectable limit. Further work revealed little or no influence on cells due to nickel release [37,38]. To avoid a possible ion release, corrosion resistance can be improved by, for example, DLC coating [20,27]. There are opposing statements concerning the influence of uncoated and coated NiTi surfaces. On the one hand, surface coating with DLC is associated with an increased proliferation of osteoblasts and mesenchymal precursors and a higher biocompatibility [22,39–41]. Conversely, untreated implant surfaces seemed to be more favorable in other studies [42,43]. In general, DLC coatings are proven to be biocompatible without inducing inflammatory reactions in osteoblasts, fibroblasts, and macrophages and in vivo [27]. In the present in vitro study, the metabolic activity of fibroblasts and macrophages was the lowest with the NiTi sample coated with DLC, but pro-collagen type I synthesis was increased in osteoblasts and fibroblasts. MMP-1 synthesis was significantly increased in osteoblasts, which might explain the low level of collagen 1 synthesis, since MMP-1 is one of the main enzymes degrading collagen 1. In general, MMP-1 synthesis shows similar levels for all configurations, despite a high variability for Ti6Al4V. Nevertheless, results of protein synthesis of CICP and MMP-1 correspond with the results of the appropriate gene expression analysis. Fibroblasts show a nearly reverse behavior, since collagen 1 synthesis is obviously higher than MMP-1 synthesis, although, collagen expression is still slightly decreased on gene level. MMP-1 expression shows extreme variability, but only minor protein synthesis, finally. In gene expression analyses, no inflammatory response was indicated among the samples, but inflammation was slightly detectable in all cell types through the measurement of cytokine and chemokine concentrations in supernatants. Moreover, cell density was the lowest with NiTi coated with DLC for MG-63 cells and macrophages but was unaffected for osteoblasts and fibroblasts. Hence, DLC coating on NiTi seems to be biocompatible, inducing collagen production, but with slight inflammatory reactions. Moreover, our results indicate a promising biocompatibility of SLM manufactured Ti6Al4V and uncoated NiTi since they revealed the highest values of metabolic activity in all tested human cell types and only minor inflammatory reactions, but without an obvious influence on matrix production. Good biocompatibility of NiTi with MG-63 cells [42], osteoblasts [34,43–47], and fibroblasts [33,43,47,48] as well as hMSCs [49] has been proven previously. Furthermore, coated Ti6AlV4 and titanium nitride (TiN)-coated Ti were approved as suitable surfaces by Fleischmann et al. [50]. Fage et al. reported that titanium material can activate macrophages by secreting inflammatory cytokines [12]. NiTi seems to show good biocompatibility in vivo [51–53]; however, a slight cytotoxicity of NiTi material to fibroblasts

was observed in vitro [54,55]. In general, biocompatibility might depend on the nickel content in the alloy since Bogdanski et al. recommended a content up to about 50% [56] and biocompatibility might result from a TiO_2 layer created on the material surface similar to titanium [35,57]. Several studies have indicated that the biocompatibility of NiTi is equal to that of pure titanium [32,35,41,53,58,59]. Rocher et al. found that Ti6Al4V and NiTi were the most cytocompatible materials and were equal to cp-Ti [58]. In the end, the cellular response to materials depends on the specific cell types, materials processing, and testing conditions [10,32,60]. Furthermore, surface roughness, topography, and chemistry are crucial factors for cell adhesion, proliferation, and differentiation [3,8,14,61–65]. In our present in vitro study, the Ti6Al4V and NiTi alloys also differed strongly in roughness values. Interestingly, metabolic activity was the highest on the SLM Ti6Al4V samples followed by uncoated NiTi. Although the roughness value Rz varied up to 70 µm, matrix production and inflammatory reactions seemed to be unaffected by surface roughness. Nevertheless, a cell-specific effect on materials with varying surface roughness is well known, as shown in the following. However, adhesion of MG-63 cells is not affected by surface roughness [42]. In contrast, inhibition of MG-63 proliferation and increased osteoblastic differentiation are demonstrated with higher titanium roughness [66]. However, osteoblasts may prefer rougher surfaces [67], but this has not been fully confirmed by other studies [10,21,68]. Kapanen et al. demonstrated the highest cell detachment on rough NiTi and smooth titanium alloyed samples [69]. Moreover, the cell response of osteoblasts to surface roughness depends on their state of maturation [70]. In contrast, a preference for smooth surfaces is clearly displayed by fibroblasts [60,67,68], whereas activation of monocytes/macrophages is caused by rough surfaces [71,72]. Since surface properties of materials are a main factor influencing cell behavior, a variability of results might be based on the use of primary cells. Compared to cell lines, which are cultivated for years, primary cells react in a more specific and sensitive manner. While every single donor can cause variations, even single cells should be taken into account. Further tests could be done analyzing impact of gender or age of the several donors in detail. For example, a high metabolic activity in WST-1 test can be the result of many cells with low or similar activity or of fewer cells with a much higher metabolic activity.

Furthermore, sample specific differences (surface irregularities, residues from manufacturing or cleaning) might influence variability, since a broad range of different manufacturers and processes were deployed.

5. Conclusions

In the present in vitro study, the osteoblastic cell line MG-63 as well as human osteoblasts, fibroblasts, and macrophages were cultured on four titanium alloys (forged Ti6Al4V, Ti6Al4V SLM, NiTi, and DLC-coated NiTi) to verify cell-specific biocompatibility and inflammatory potential. Thereby, Ti6Al4V SLM and NiTi revealed the best results regarding metabolic activity. DLC-coated NiTi appeared to be a suitable surface for cell cultivation, with good results for osteoblasts and macrophages. Uncoated NiTi resulted in high collagen production in both mesenchymal cell types. In contrast, forged Ti6Al4V caused an increase of MMP-1 production in osteoblasts and fibroblasts on gene and protein levels. The materials used caused a cell- and surface-dependent inflammatory response. In general, no distinct cell-specific response could be observed regarding the surface material, coating, or roughness. In summary, all of the tested titanium alloys seem to be biologically appropriate for application as orthopedic implants.

Acknowledgments: The authors thank Jürgen Weber (Ästhetik-Klinik Rostock) for allocation of tissues for fibroblast isolation. We kindly thank the Institute of Transfusion Medicine, University Medicine Rostock, for allocation of the Buffy Coats. We would like to thank the electron microscopy center Rostock for enabling the acquisition of FESEM images. We thank DOT GmbH Rostock, Germany, for providing the forged Ti6Al4V test pellets; EC Europ Coating GmbH Hohenlockstedt, Germany, for the DLC coating of the NiTi probes; Proto Labs Eschenlohe GmbH, Eschenlohe, Germany, for the SLM Ti6Al4V probes. Furthermore, we kindly thank Doris Hansmann, Petra Mueller, Philipp Pisowocki and Mario Jackszis for technical support with the measurements and FESEM images. We thank PD Wolfgang Baumann (Leibniz Institute for Catalysis, Rostock) for performing

ICP-OES measurements. This work was supported by the German Federation of Industrial Research Associations (AiF) (grant number IGF 17906 BR).

Author Contributions: Jana Markhoff conceived and designed the experiments; Jana Markhoff and Martin Krogull performed the experiments and analyzed the data; Christian Schulze contributed analysis tools; Christian Rotsch and Sandra Hunger are responsible for the design and development of the test materials (NiTi, DLC-coated NiTi, Ti6Al4V SLM) and manufacturing technologies; Jana Markhoff wrote the paper; Rainer Bader organized the founding.

Conflicts of Interest: The authors declare no conflict of interest.

References

1. Davis, J.R. (Ed.) *Handbook of Materials for Medical Devices*, 4th ed.; ASM International: Novelty, OH, USA, 2006.
2. Lewallen, E.A.; Riester, S.M.; Bonin, C.A.; Kremers, H.M.; Dudakovic, A.; Kakar, S.; Cohen, R.C.; Westendorf, J.J.; Lewallen, D.G.; van Wijnen, A.J. Biological strategies for improved osseointegration and osteoinduction of porous metal orthopedic implants. *Tissue Eng. Part B Rev.* **2015**, *21*, 218–230. [CrossRef] [PubMed]
3. Geetha, M.; Singh, A.K.; Asokamani, R.; Gogia, A.K. Ti based biomaterials, the ultimate choice for orthopaedic implants—A review. *Prog. Mater. Sci.* **2009**, *54*, 397–425. [CrossRef]
4. Kulkarni, M.; Mazare, A.; Schmuki, P.; Iglic, A. (Eds.) Biomaterial surface modification of titanium and titanium alloys for medical applications. In *Nanomedicine*; One Central Press: Manchester, UK, 2014.
5. Niinomi, M.; Narushima, T.; Nakai, M. *Advances in Metallic Biomaterials*; Springer: Berlin/Heidelberg, Germany, 2015.
6. De Vasconcellos, L.M.R.; Rodarte, Y.; do Prado, R.F.; de Vasconcellos, L.G.O.; Alencastro Graa, M.L.D.; Alves Cairo, C.A. Porous titanium by powder metallurgy for biomedical application: Characterization, cell citotoxity and in vivo tests of osseointegration. In *Biomedical Engineering—Technical Applications in Medicine*; Hudak, R., Ed.; InTech: Rijeka, Croatia, 2012.
7. Niinomi, M.; Nakai, M.; Hieda, J. Development of new metallic alloys for biomedical applications. *Acta Biomater.* **2012**, *8*, 3888–3903. [CrossRef] [PubMed]
8. Cremasco, A.; Messias, A.D.; Esposito, A.R.; Eliana Aparecida de Rezende, D.; Caram, R. Effects of alloying elements on the cytotoxic response of titanium alloys. *Mater. Sci. Eng. C* **2011**, *31*, 833–839. [CrossRef]
9. Goyenvalle, E.; Aguado, E.; Cognet, R.; Bourges, X.; Daculsi, G. Calcium phosphate ceramic blasting on titanium surface improve bone ingrowth. *KEM* **2008**, *361*, 1351–1354. [CrossRef]
10. Chan, C.W.; Hussain, I.; Waugh, D.G.; Lawrence, J.; Man, H.C. Effect of laser treatment on the attachment and viability of mesenchymal stem cell responses on shape memory NiTi alloy. *Mater. Sci. Eng. C* **2014**, *42*, 254–263. [CrossRef] [PubMed]
11. Fage, S.W.; Muris, J.; Jakobsen, S.S.; Thyssen, J.P. Titanium: A review on exposure, release, penetration, allergy, epidemiology, and clinical reactivity. *Contact Dermat.* **2016**, *74*, 323–345. [CrossRef] [PubMed]
12. Tabish, T.A.; Butt, M.T.; Ali, M. Biocompatibility behavior and biomedical applications of Ti-Ni based shape memory alloys: A brief review. *J. Fac. Eng. Technol.* **2006**, *19*, 135–140.
13. Fonte, M.; Saigal, A. Crystallographic texture of nitinol and its effects on macrophage. In Proceedings of the ASME 2010 International Mechanical Engineering Congress and Exposition, Vancouver, BC, Canada, 12–18 November 2010; pp. 1–8.
14. Bernard, S.A.; Balla, V.K.; Davies, N.M.; Bose, S.; Bandyopadhyay, A. Bone cell-materials interactions and Ni ion release of anodized equiatomic NiTi alloy. *Acta Biomater.* **2011**, *7*, 1902–1912. [CrossRef] [PubMed]
15. Elahinia, M.H.; Hashemi, M.; Tabesh, M.; Bhaduri, S.B. Manufacturing and processing of NiTi implants: A review. *Prog. Mater. Sci.* **2012**, *57*, 911–946. [CrossRef]
16. Alvarez, K.; Nakajima, H. Metallic scaffolds for bone regeneration. *Materials* **2009**, *2*, 790–832. [CrossRef]
17. Bansiddhi, A.; Sargeant, T.D.; Stupp, S.I.; Dunand, D.C. Porous NiTi for bone implants: A review. *Acta Biomater.* **2008**, *4*, 773–782. [CrossRef] [PubMed]
18. Chu, C.; Chung, C.; Lin, P.; Wang, S. Fabrication of porous NiTi shape memory alloy for hard tissue implants by combustion synthesis. *Mater. Sci. Eng. A* **2004**, *366*, 114–119. [CrossRef]
19. Biesiekierski, A.; Wang, J.; Abdel-Hady Gepreel, M.; Wen, C. A new look at biomedical Ti-based shape memory alloys. *Acta Biomater.* **2012**, *8*, 1661–1669. [CrossRef] [PubMed]

20. Branzoi, I.V.; Iordoc, M.; Branzoi, F.; Vasilescu-Mirea, R.; Sbarcea, G. Influence of diamond-like carbon coating on the corrosion resistance of the NITINOL shape memory alloy. *Surf. Interface Anal.* **2010**, *42*, 502–509. [CrossRef]
21. Chrzanowski, W.; Neel, E.A.A.; Armitage, D.A.; Zhao, X.; Knowles, J.C.; Salih, V. In vitro studies on the influence of surface modification of Ni-Ti alloy on human bone cells. *J. Biomed. Mater. Res.* **2009**, *9999*, 1596–1608.
22. Li, Q.; Zhang, Q.; Sun, Z. The study on biocompatibility of diamond-like carbon coated nickel-titanium shape memory alloy with osteoblasts cultured in vitro. *Chin. J. Repar. Reconstr. Surg.* **2006**, *20*, 5–8.
23. Arciniegas, M.; Pena, J.; Gil, F.J.; Manero, J.M. In vitro response of preosteoblastic MG63 cells on Ni-free Ti shape memory substrates. *J. Biomed. Mater. Res. Part B Appl. Biomater.* **2013**, *101*, 709–720. [CrossRef] [PubMed]
24. Sahu, S.C. *Toxicogenomics: Toxicogenomics*; John Wiley & Sons: Chichester, UK, 2008.
25. Florencio-Silva, R.; Sasso, G.R.; Sasso-Cerri, E.; Simoes, M.J.; Cerri, P.S. Biology of bone tissue: Structure, function, and factors that influence bone cells. *BioMed Res. Int.* **2015**, *2015*, 421746. [CrossRef] [PubMed]
26. Slany, A.; Meshcheryakova, A.; Beer, A.; Ankersmit, H.J.; Paulitschke, V.; Gerner, C. Plasticity of fibroblasts demonstrated by tissue-specific and function-related proteome profiling. *Clin. Proteom.* **2014**, *11*, 41. [CrossRef] [PubMed]
27. Roy, R.K.; Lee, K.-R. Biomedical applications of diamond-like carbon coatings: A review. *J. Biomed. Mater. Res. Part B Appl. Biomater.* **2007**, *83*, 72–84. [CrossRef] [PubMed]
28. Ziegler-Heitbrock, L.; Ancuta, P.; Crowe, S.; Dalod, M.; Grau, V.; Hart, D.N.; Leenen, P.J.; Liu, Y.J.; MacPherson, G.; Randolph, G.J.; et al. Nomenclature of monocytes and dendritic cells in blood. *Blood* **2010**, *116*, 80. [CrossRef] [PubMed]
29. Lochner, K.; Fritsche, A.; Jonitz, A.; Hansmann, D.; Mueller, P.; Mueller-Hilke, B.; Bader, R. The potential role of human osteoblasts for periprosthetic osteolysis following exposure to wear particles. *Int. J. Mol. Med.* **2011**, *28*, 1055–1063. [CrossRef] [PubMed]
30. Li, Y.; Yang, C.; Zhao, H.; Qu, S.; Li, X.; Li, Y. New developments of Ti-based alloys for biomedical applications. *Materials* **2014**, *7*, 1709–1800. [CrossRef]
31. Fili, P.; Lausmaa, J.; Musialek, J.; Mazanec, K. Structure and surface of TiNi human implants. *Biomaterials* **2001**, *22*, 2131–2138. [CrossRef]
32. Es-Souni, M.; Fischer-Brandies, H. Assessing the biocompatibility of NiTi shape memory alloys used for medical applications. *Anal. Bioanal. Chem.* **2005**, *381*, 557–567. [CrossRef] [PubMed]
33. Es-Souni, M.; Fischer-Brandies, H.; Es-Souni, M. Human gingival fibroblast response to electropolished NiTi surfaces. *J. Biomed. Mater. Res. Part A* **2007**, *80*, 159–166. [CrossRef] [PubMed]
34. Cortizo, M.C.; De Mele, M.F.; Cortizo, A.M. Metallic dental material biocompatibility in osteoblastlike cells: Correlation with metal ion release. *Biol. Trace Elem. Res.* **2004**, *100*, 151–168. [CrossRef]
35. Ponsonnet, L.; Tréheux, D.; Lissac, M.; Jaffrezic, N.; Grosgogeat, B. Review of in vitro studies on the biocompatibility of NiTi alloys. *Int. J. Appl. Electromagn. Mech.* **2006**, *23*, 147–151.
36. Huang, H. Ion release from NiTi orthodontic wires in artificial saliva with various acidities. *Biomaterials* **2003**, *24*, 3585–3592. [CrossRef]
37. Hahn, A.; Fuhlrott, J.; Loos, A.; Barcikowski, S. Cytotoxicity and ion release of alloy nanoparticles. *J. Nanoparticle Res. Interdiscip. Forum Nanoscale Sci. Technol.* **2012**, *14*, 1–10. [CrossRef] [PubMed]
38. Hang, R.; Liu, Y.; Liu, S.; Bai, L.; Gao, A.; Zhang, X.; Huang, X.; Tang, B.; Chu, P.K. Size-dependent corrosion behavior and cytocompatibility of Ni–Ti–O nanotubes prepared by anodization of biomedical NiTi alloy. *Corros. Sci.* **2016**, *103*, 173–180. [CrossRef]
39. Li, Q.; Xia, Y.-Y.; Tang, J.-C.; Wang, R.-Y.; Bei, C.-Y.; Zeng, Y. In vitro and in vivo biocompatibility investigation of diamond-like carbon coated nickel-titanium shape memory alloy. *Artif. Cells Blood Substit. Immobil. Biotechnol.* **2011**, *39*, 137–142. [CrossRef] [PubMed]
40. Sun, T.; Wang, L.-P.; Wang, M.; Tong, H.-W.; Lu, W.W. Characteristics and in vitro biological assessment of (Ti, O, N)/Ti composite coating formed on NiTi shape memory alloy. *Thin Solid Films* **2011**, *519*, 4623–4628. [CrossRef]
41. Mikulewicz, M.; Chojnacka, K. Cytocompatibility of medical biomaterials containing nickel by osteoblasts: A systematic literature review. *Biol. Trace Elem. Res.* **2011**, *142*, 865–889. [CrossRef] [PubMed]

42. Michiardi, A.; Engel, E.; Aparicio, C.; Planell, J.A.; Gil, F.J. Oxidized NiTi surfaces enhance differentiation of osteoblast-like cells. *J. Biomed. Mater. Res. Part A* **2008**, *85*, 108–114. [CrossRef] [PubMed]
43. Shabalovskaya, S.; Anderegg, J.; van Humbeeck, J. Critical overview of Nitinol surfaces and their modifications for medical applications. *Acta Biomater.* **2008**, *4*, 447–467. [CrossRef] [PubMed]
44. Kapanen, A.; Kinnunen, A.; Ryhanen, J.; Tuukkanen, J. TGF-beta1 secretion of ROS-17/2.8 cultures on NiTi implant material. *Biomaterials* **2002**, *23*, 3341–3346. [CrossRef]
45. Kapanen, A.; Ilvesaro, J.; Danilov, A.; Ryhanen, J.; Lehenkari, P.; Tuukkanen, J. Behaviour of nitinol in osteoblast-like ROS-17 cell cultures. *Biomaterials* **2002**, *23*, 645–650. [CrossRef]
46. Liu, X.; Wu, S.; Yeung, K.W.K.; Chan, Y.L.; Hu, T.; Xu, Z.; Liu, X.; Chung, J.C.Y.; Cheung, K.M.C.; Chu, P.K. Relationship between osseointegration and superelastic biomechanics in porous NiTi scaffolds. *Biomaterials* **2011**, *32*, 330–338. [CrossRef] [PubMed]
47. Ryhanen, J.; Niemi, E.; Serlo, W.; Niemela, E.; Sandvik, P.; Pernu, H.; Salo, T. Biocompatibility of nickel-titanium shape memory metal and its corrosion behavior in human cell cultures. *J. Biomed. Mater. Res.* **1997**, *35*, 451–457. [CrossRef]
48. Cui, Z.D.; Chen, M.F.; Zhang, L.Y.; Hu, R.X.; Zhu, S.L.; Yang, X.J. Improving the biocompatibility of NiTi alloy by chemical treatments: An in vitro evaluation in 3T3 human fibroblast cell. *Mater. Sci. Eng. C* **2008**, *28*, 1117–1122. [CrossRef]
49. Gotman, I.; Ben-David, D.; Unger, R.E.; Bose, T.; Gutmanas, E.Y.; Kirkpatrick, C.J. Mesenchymal stem cell proliferation and differentiation on load-bearing trabecular Nitinol scaffolds. *Acta Biomater.* **2013**, *9*, 8440–8448. [CrossRef] [PubMed]
50. Fleischmann, L.; Crismani, A.; Falkensammer, F.; Bantleon, H.-P.; Rausch-Fan, X.; Andrukhov, O. Behavior of osteoblasts on TI surface with two different coating designed for orthodontic devices. *J. Mater. Sci. Mater. Med.* **2015**, *26*, 5335. [CrossRef] [PubMed]
51. Kapanen, A.; Ryhanen, J.; Danilov, A.; Tuukkanen, J. Effect of nickel-titanium shape memory metal alloy on bone formation. *Biomaterials* **2001**, *22*, 2475–2480. [CrossRef]
52. Ryhanen, J.; Kallioinen, M.; Tuukkanen, J.; Lehenkari, P.; Junila, J.; Niemela, E.; Sandvik, P.; Serlo, W. Bone modeling and cell-material interface responses induced by nickel-titanium shape memory alloy after periosteal implantation. *Biomaterials* **1999**, *20*, 1309–1317. [CrossRef]
53. McMahon, R.E.; Ma, J.; Verkhoturov, S.V.; Munoz-Pinto, D.; Karaman, I.; Rubitschek, F.; Maier, H.J.; Hahn, M.S. A comparative study of the cytotoxicity and corrosion resistance of nickel-titanium and titanium-niobium shape memory alloys. *Acta Biomater.* **2012**, *8*, 2863–2870. [CrossRef] [PubMed]
54. Ponsonnet, L.; Comte, V.; Othmane, A.; Lagneau, C.; Charbonnier, M.; Lissac, M.; Jaffrezic, N. Effect of surface topography and chemistry on adhesion, orientation and growth of fibroblasts on nickel–titanium substrates. *Mater. Sci. Eng. C* **2002**, *21*, 157–165. [CrossRef]
55. Rongo, R.; Valletta, R.; Bucci, R.; Rivieccio, V.; Galeotti, A.; Michelotti, A.; D'Anto, V. In vitro biocompatibility of nickel-titanium esthetic orthodontic archwires. *Angle Orthod.* **2016**, *86*, 789–795. [CrossRef] [PubMed]
56. Bogdanski, D.; Koller, M.; Bram, M.; Stover, D.; Buchkremer, H.P.; Choi, J.; Epple, M.; Muhr, G. Rapid analysis of biocompatibility with graded test samples exemplified by Ni-NiTi-Ti. *Biomed. Technik. Biomed. Eng.* **2002**, *47*, 500–502. [CrossRef]
57. Man, H.C.; Zhang, S.; Cheng, F.T.; Guo, X. Laser fabrication of porous surface layer on NiTi shape memory alloy. *Mater. Sci. Eng. A* **2005**, *404*, 173–178. [CrossRef]
58. Rocher, P.; El Medawar, L.; Hornez, J.-C.; Traisnel, M.; Breme, J.; Hildebrand, H. Biocorrosion and cytocompatibility assessment of NiTi shape memory alloys. *Scripta Mater.* **2004**, *50*, 255–260. [CrossRef]
59. Armitage, D.A.; Parker, T.L.; Grant, D.M. Biocompatibility and hemocompatibility of surface-modified NiTi alloys. *J. Biomed. Mater. Res. Part A* **2003**, *66*, 129–137. [CrossRef] [PubMed]
60. Waugh, D.G.; Lawrence, J.; Chan, C.W.; Hussain, I.; Man, H.C. Laser melting of NiTi and its effects on in vitro mesenchymal stem cell responses. In *Laser Surface Engineering*; Elsevier: Cambridge, UK, 2015; pp. 653–676.
61. Liu, X.M.; Wu, S.L.; Chan, Y.L.; Chu, P.K.; Chung, C.Y.; Chu, C.L.; Yeung, K.W.K.; Lu, W.W.; Cheung, K.M.C.; Luk, K.D.K. Surface characteristics, biocompatibility, and mechanical properties of nickel-titanium plasma-implanted with nitrogen at different implantation voltages. *J. Biomed. Mater. Res. Part A* **2007**, *82*, 469–478. [CrossRef] [PubMed]

62. Strauss, S.; Neumeister, A.; Barcikowski, S.; Kracht, D.; Kuhbier, J.W.; Radtke, C.; Reimers, K.; Vogt, P.M. Adhesion, vitality and osteogenic differentiation capacity of adipose derived stem cells seeded on nitinol nanoparticle coatings. *PLoS ONE* **2013**, *8*, e53309. [CrossRef] [PubMed]
63. Fini, M.; Giardino, R.; Borsari, V.; Torricelli, P.; Rimondini, L.; Giavaresi, G.; Nicoli Aldini, N. In vitro behaviour of osteoblasts cultured on orthopaedic biomaterials with different surface roughness, uncoated and fluorohydroxyapatite-coated, relative to the in vivo osteointegration rate. *Int. J. Artif. Organs* **2003**, *26*, 520–528. [PubMed]
64. Chrzanowski, W.; Neel, E.A.A.; Armitage, D.A.; Knowles, J.C. Effect of surface treatment on the bioactivity of nickel–titanium. *Acta Biomater.* **2008**, *4*, 1969–1984. [CrossRef] [PubMed]
65. Maleki-Ghaleh, H.; Khalil-Allafi, J.; Sadeghpour-Motlagh, M.; Shakeri, M.S.; Masoudfar, S.; Farrokhi, A.; Beygi Khosrowshahi, Y.; Nadernezhad, A.; Siadati, M.H.; Javidi, M.; et al. Effect of surface modification by nitrogen ion implantation on the electrochemical and cellular behaviors of super-elastic NiTi shape memory alloy. *J. Mater. Sci. Mater. Med.* **2014**, *25*, 2605–2617. [CrossRef] [PubMed]
66. Wirth, C.; Grosgogeat, B.; Lagneau, C.; Jaffrezic-Renault, N.; Ponsonnet, L. Biomaterial surface properties modulate in vitro rat calvaria osteoblasts response: Roughness and or chemistry? *Mater. Sci. Eng. C* **2008**, *28*, 990–1001. [CrossRef]
67. Kunzler, T.P.; Drobek, T.; Schuler, M.; Spencer, N.D. Systematic study of osteoblast and fibroblast response to roughness by means of surface-morphology gradients. *Biomaterials* **2007**, *28*, 2175–2182. [CrossRef] [PubMed]
68. Wirth, C.; Comte, V.; Lagneau, C.; Exbrayat, P.; Lissac, M.; Jaffrezic-Renault, N.; Ponsonnet, L. Nitinol surface roughness modulates in vitro cell response: A comparison between fibroblasts and osteoblasts. *Mater. Sci. Eng. C* **2005**, *25*, 51–60. [CrossRef]
69. Kapanen, A.; Danilov, A.; Lehenkari, P.; Ryhanen, J.; Jamsa, T.; Tuukkanen, J. Effect of metal alloy surface stresses on the viability of ROS-17/2.8 osteoblastic cells. *Biomaterials* **2002**, *23*, 3733–3740. [CrossRef]
70. Lohmann, C.H.; Bonewald, L.F.; Sisk, M.A.; Sylvia, V.L.; Cochran, D.L.; Dean, D.D.; Boyan, B.D.; Schwartz, Z. Maturation state determines the response of osteogenic cells to surface roughness and 1,25-dihydroxyvitamin D3. *J. Bone Miner. Res.* **2000**, *15*, 1169–1180. [CrossRef] [PubMed]
71. Refai, A.K.; Textor, M.; Brunette, D.M.; Waterfield, J.D. Effect of titanium surface topography on macrophage activation and secretion of proinflammatory cytokines and chemokines. *J. Biomed. Mater. Res. Part A* **2004**, *70*, 194–205. [CrossRef] [PubMed]
72. Soskolne, W.A.; Cohen, S.; Shapira, L.; Sennerby, L.; Wennerberg, A. The effect of titanium surface roughness on the adhesion of monocytes and their secretion of TNF-alpha and PGE2. *Clin. Oral. Implants Res.* **2002**, *13*, 86–93. [CrossRef] [PubMed]

Materials Science and Engineering C 73 (2017) 756–766

Contents lists available at ScienceDirect

Materials Science and Engineering C

journal homepage: www.elsevier.com/locate/msec

Influence of different grained powders and pellets made of Niobium and Ti-42Nb on human cell viability

Jana Markhoff [a,*], Markus Weinmann [b], Christian Schulze [a], Rainer Bader [a]

[a] University Medicine Rostock, Department of Orthopedics, Biomechanics and Implant Technology Laboratory, Doberaner Strasse 142, 18057 Rostock, Germany
[b] H.C. Starck Tantalum and Niobium GmbH, Im Schleeke 78-91, 38642 Goslar, Germany

ARTICLE INFO

Article history:
Received 16 August 2016
Received in revised form 15 December 2016
Accepted 20 December 2016
Available online 24 December 2016

Keywords:
Niobium
Ti-42Nb
Ti6Al4V
Human osteoblasts
Human fibroblasts
Powder particles

ABSTRACT

Nowadays, biomaterials can be used to maintain or replace several functions of the human body if necessary. Titanium and its alloys, i.e. Ti6Al4V are the most common materials (70 to 80%) used for structural orthopedic implants due to their unique combination of good mechanical properties, corrosion resistance and biocompatibility. Addition of β-stabilizers, e.g. niobium, can improve the mechanical properties of such titanium alloys further, simultaneously offering excellent biocompatibility. In this in vitro study, human osteoblasts and fibroblasts were cultured on different niobium specimens (Nb Amperit, Nb Ampertec), Nb sheets and Ti-42Nb (sintered and 3D-printed by selective laser melting, SLM) and compared with forged Ti6Al4V specimens. Furthermore, human osteoblasts were incubated with particulates of the Nb and Ti-42Nb specimens in three concentrations over four and seven days to imitate influence of wear debris. Thereby, the specimens with the roughest surfaces, i.e. Ti-42Nb and Nb Ampertec, revealed excellent and similar results for both cell types concerning cell viability and collagen synthesis superior to forged Ti6Al4V. Examinations with particulate debris disclosed a dose-dependent influence of all powders with Nb Ampertec showing the highest decrease of cell viability and collagen synthesis. Furthermore, interleukin synthesis was only slightly increased for all powders. In summary, Nb Ampertec (sintered Nb) and Ti-42Nb materials seem to be promising alternatives for medical applications compared to common materials like forged or melted Ti6Al4V.

1. Introduction

Constraint or loss of functions in the human body can be the result of tumors, fractures, injuries as well as chronic diseases, infections or simply aging [1]. Nowadays, maintenance or replacement of those functions can be achieved through the application of biomaterials mainly consisting of metals, ceramics or polymers [2–4]. Titanium and its alloys are the most common used implant materials in orthopedic surgery with an amount of 70 to 80% [5–7]. Their application ranges from load bearing areas like in orthodontics and orthopedics to gastroenterology as well as cardiovascular and reconstructive aspects. They possess appreciable mechanical properties, good corrosion resistance and biocompatibility [8–12]. The most frequently used titanium-based material is the titanium aluminum vanadium alloy Ti6Al4V (also referred to Ti Grade 5) [13–16]. However, by now the elemental component vanadium is proved to be toxic and aluminum is suspected to cause e.g. Alzheimer disease [7,17–19].

Titanium alloys in general crystallize in a hexagonal close-packed α-phase (stable at 25 °C) which at 882 °C reversibly transforms into a β-phase with body-centered cubic crystal structure. Addition of alloying elements may stabilize this phase or cause crystallization, i.e. stabilization of α + β mixtures [20]. The β–type titanium alloys possess significantly smaller Young's moduli compared with α- or α + β alloys. Some of the even build deformation-induced martensite structure possessing a shape-memory effect [21]. The formation of the β–type structure may avoid a mechanical mismatch in elasticity of bone and implant, causing stress shielding associated with implant loosening. Specific β-stabilizers for titanium alloys further improve the material properties [22–26]. For example, non-toxic and non-allergenic niobium represents a relatively new and promising implantable biomaterial, which is proved for its biocompatibility in vitro and in vivo. It has a corrosion resistance superior to titanium resulting from a self-passivating inert (native) oxide surface layer [27–32]. Furthermore, some niobium alloys offer a shape memory effect (SME) and possess superelastic properties, analogous to selected nickel alloys [7,32,33]. Nickel titanium alloys (NiTi) gained in importance in the last decades [34] being accounted for by its SME up to 8% [35], biocompatibility and mechanical properties (elastic modulus, compressive strength) which are close to bone. Even though NiTi is corrosion and wear resistant [35–38] there are concerns including toxicity, allergenic reactions and carcinogenic potential of dissolved nickel ions [27,39,40].

Niobium and Ti-Nb alloys or niobium oxide (Nb_2O_5) materials represent excellent alternatives for medical applications [31,39,41,42], even

* Correponding author.
E-mail address: markhoffj@gmail.com (J. Markhoff).

http://dx.doi.org/10.1016/j.msec.2016.12.098
0928-4931/

though mechanical properties require for improvement [2]. Moreover, one of the problems of biomaterials used is the surface contamination with residues or particles within the production process and the formation of wear debris due to mechanical strain and friction of articulating implant components [43–45]. Particles and wear debris can accumulate in the periprosthetic tissue being size-dependent phagocytosed and activating or inhibiting the attendant cells. For example, osteoblasts, macrophages and osteoclasts are known to interact in various fashions [43, 45–47]. Those particles cause inflammatory reactions and moreover, lead to increased differentiation of bone resorbing osteoclasts and inhibition of bone forming osteoblasts. Finally, all these factors result in osteolysis and aseptic implant loosening [43,45,47].

The intention of the present study is to demonstrate the superior biocompatibility of Ti/Nb-based alloys compared with conventional metallic implant materials like Ti6Al4V. This includes biomedical issues, i.e. preservation of cell activities (osteoblasts, fibroblasts) and non-toxicity as well as (bio-) mechanical aspects, which are work in progress and will be published subsequently. The focus is not only on intrinsic material properties, but also on their morphologies, also considering 3D-printed bulk materials.

Therefore, in the present in vitro study, human osteoblasts and fibroblasts were cultured on two different niobium specimens (Nb Amperit, Nb Ampertec), Nb sheets as well as Ti-42Nb specimens (sintered and manufactured by SLM), compared with forged Ti6Al4V and referenced to tissue culture polystyrene (TCPS) as growth control. Furthermore, human osteoblasts were incubated with four particulates of the above mentioned groups to imitate influence of wear debris.

2. Materials & methods

Niobium powders and niobium sheet used in this study are commercial products produced and distributed by H.C. Starck Tantalum and Niobium GmbH, Goslar, Germany. Product data sheets can be obtained on request from www.hcstarck.com. Spherical Ti-42Nb powder was obtained by EIGA (Electrode Induction Melting Gas Atomization, EIGA) of Ti-42Nb rods. Appropriate SEM images are displayed in Fig. 1. Chemical analysis, particle size and abbreviations of the different powders used in this study are provided in Table 1. Additionally, chemical analysis of niobium sheet is given.

2.1. Preparation of test specimens

All specimens prepared for cell-biological investigations were cylindrical pellets with dimensions of d × l = 10 mm × 2 mm compounded from the above mentioned powders. Nb Amperit was uniaxially pressed at 25 °C using a lab toggle press applying a load of 65 bars. Nb Ampertec was uniaxially pressed at 25 °C using a lab toggle press applying a load of 65 bars and subsequently sintered in vacuum at 1200 °C for 10 min. Ti-42Nb powders could not successfully be compacted by uniaxial pressing due to their spheroidal shape. Accordingly, powder consolidation was performed pressureless by sintering at 1000 °C for 10 min of a 3 mm powder bed in Al_2O_3 sinter rings on Nb sheets. As-obtained specimens were machined to 2 mm height. Ti-42Nb specimens were obtained by additive manufacturing, i.e. selective laser melting (SLM) of Ti-42Nb (sieve fraction < 63 μm) using a TruPrint 1000 equipment (TRUMPF GmbH + Co. KG, Ditzingen, Germany) operated at Laserzentrum Hannover, Hannover, Germany. The following laser/scan parameters were applied: laser power 50 W, scan speed 400 mm/s, hatch 120 μm, powder bed feed rate 50 μm/layer. Surface roughness of the test specimens (Rz, Ra) was analyzed by means of a tactile measurement method using a Hommel-Etamic T1000 and a sampler (TKU300, probe tip radius 5 μm,) (both: Jenoptik, Jena, Germany). Thereby, a probe tip with defined radius slides across the surface of the test specimen permeating into the surface subject to the probe tip radius. The measuring range was 320 μm and the length of tactile measurement was 8 mm. Three surface points per specimen ($n \geq 3$) were swept (Table 2).

To illustrate surface properties of the several metallic samples field emission scanning electron microscopic (FESEM) images were generated. The sample surface is gold-plated (~25 nm) using a sputter coater (Leica SCD004, Wetzlar, Germany) and figured with a Merlin VPcompact microscope (Carl Zeiss AG, Oberkochen, Germany) with a 50-fold magnification (Fig. 2).

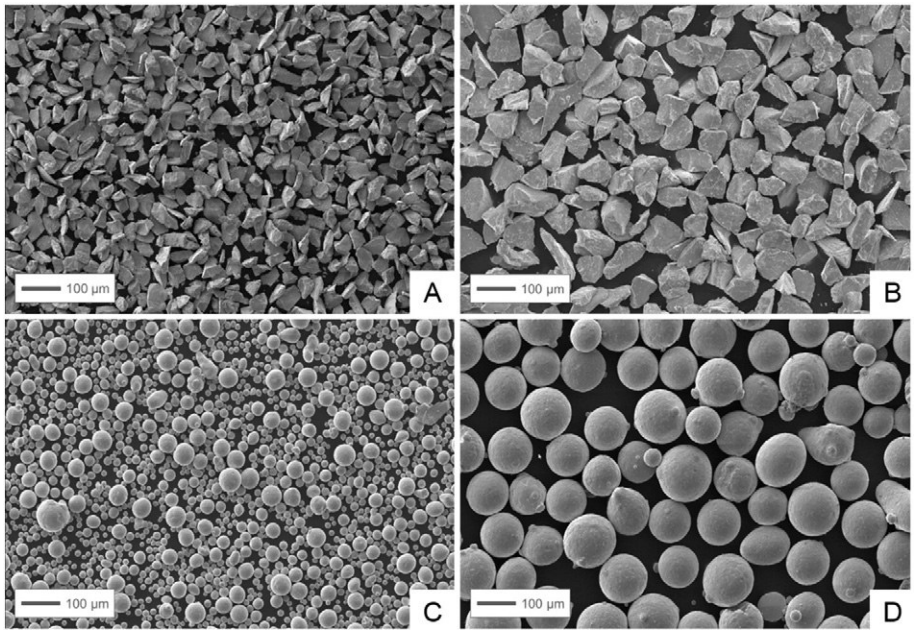

Fig. 1. SEM images of niobium powders recorded at 100× magnification. A: AMPERIT 160 NIOBIUM METAL 14–45 μm, B: AMPERTEC NIOBIUM EB MELTED 45–75 μm, C/D: AMPERTEC MAP Ti-42Nb powders - C: powder fraction <63 μm, D: powder fraction 103 μm - 350 μm.

Table 1
Particle size (PS) and chemical analysis of the powders used in this study. The chemical composition of the niobium sheet is provided for comparison.

	Abbreviation	PS (μm)	Nb (%)	Ti	O (ppm)	C (ppm)	H (ppm)	N (ppm)	Mg (ppm)
AMPERIT 160 NIOBIUM METAL	Nb Amperit	15–45	99.90%	n.d.	<2500	<100	<100	<150	<10
AMPERTEC NIOBIUM EB MELTED	Nb Ampertec	45–75	99.90%	n.d.	750	10	<10	41	<1
AMPERTEC MAP Ti-42Nb[a]	Ti-42Nb	<350	41.47	58.26%	2212	103	<10	51	<10
NIOBIUM SHEET	Nb Sheet	n.a.	>99.99%	20 ppm	90	30	10	24	n.d.

[a] AMPERTEC MAP Ti-42Nb was subsequently fractionized (<63 μm, 63 μm–105 μm, 105 μm–350 μm) by sieving.

Forged Ti6Al4V pellets, which served as bench mark material to compare with niobium (Nb) and Ti-42Nb samples, were provided by DOT GmbH, Rostock, Germany.

2.2. Cell isolation

Cell cultivation was carried out in an incubator (Binder GmbH, Tuttlingen, Germany) at simulated in vivo conditions at 5% CO_2, 21% O_2 and 37 °C with regular medium changes. Human osteoblasts were isolated after patient agreement from the spongiosa of patients undergoing primary total hip replacement as previously described by Lochner et al. [48]. Briefly, the spongiosa was mechanically removed from the femoral head, washed with PBS and enzymatically digested using collagenase A, culture medium without fetal calf serum (FCS) and dispase II. The gained suspension was sown out in cell culture flasks after removing spongiosa fragments. Cultivation was carried out in osteogenic cell culture medium (MEM Dulbecco, Biochrom AG, Berlin, Germany) with 10% FCS, 1% penicillin/streptomycin, 1% amphotericin B, 1% HEPES buffer (all: Gibco®-Invitrogen, Darmstadt, Germany) and additional osteogenic additives (dexamethason (100 nM), L-ascorbic acid (50 μg/ml) and β-glycerophosphate (10 mM) (all from Sigma-Aldrich, Munich, Germany). The osteogenic character of the isolated cells was proved via alkaline phosphatase staining with fuchsin substrate chromogen (DAKO, Hamburg, Germany).

Human fibroblasts were isolated from skin biopsies (breast, eyelid) provided by a local aesthetic clinic. After excision of adipose tissue, the remaining tissue was cut in equal segments (2–3 mm edge length), which were then transferred to 6-well-plates (2–3 per well) with the epidermis upwards. After 20 min of surface drying, skin was overlaid with 3 ml DMEM-medium (with Glutamax, 10% FCS, 1% penicillin/streptomycin, 1% amphotericin B (all: Gibco®-Invitrogen, Darmstadt, Germany)) and cultured for three weeks. Subsequently, cells were transferred to tissue culture flasks and cryo-preserved after further confluence.

The test pellets were seeded with osteoblasts and fibroblasts in a density of 20.000 cells (third and fifth passage) per 48-Well in 500 μl culture medium. Ti-42Nb SLM specimen were tested subsequently and only used for human osteoblast cultivation. Cultivation on the test pellets was carried out for 96 h with an exchange of culture medium after 48 h. The Local Ethical Committee approved the use of the human cells for the experiments. The characteristics of the used human cells are listed in Table 3.

For incubation with niobium powders, the several powders were apportioned in amounts of 5 mg in glass jars and gamma-sterilized with 25 kGy. To produce a stock solution powders were re-suspended in 500 μl of PBS (= 10 mg/ml) and diluted with culture medium to get three working solutions (0.1/0.2/0.5 mg/ml). These concentrations were determined by means of appropriate pre-testings. First trials were performed on the basis of preliminary works of the working group regarding the influence of orthopedic wear particles on human cells [48–50]. Based on these results powder concentrations were adapted. The wide range was used to reveal concentration-dependent differences. Osteoblasts free of powder served as control group. Cultivation was carried out for four and seven days with exchanges of culture medium after 48 h and after 48 h and 96 h, respectively.

2.3. Metabolic cell activity and live/dead staining

Metabolic activity of cells on the test pellets was determined via mitochondrial dehydrogenase activity (WST-1 test) (Roche, Grenzach-Wyhlen, Germany) after 96 h of cultivation. Activity of cells cultured with niobium powders was proven after four and seven days, respectively. The tetrazolium salt WST (water soluble tetrazolium) is transformed to formazan by mitochondrial succinate dehydrogenase from metabolically active cells. Thereby, adsorption is directly proportional to the metabolic cell activity and was measured at 450 nm in a Tecan reader (Infinite F200 Pro, Männedorf, Switzerland). Live/dead staining (Live/Dead Cell Viability Assay, Invitrogen, Darmstadt, Germany) was used to analyze qualitative cell viability. Therefore, adherent cells were simultaneously incubated with two fluorescence dyes after removing the culture medium. Vital cells were visualized green due to calcein AM (494/517 nm), which is embedded in the cell plasma. Dead cells get red by ethidium homodimer-1 (528/617 nm) interacting with the cell nuclei. Microscopic pictures were taken using an inverted microscope (Nikon TS 100, Nikon GmbH, Duesseldorf, Germany) with the appropriate filters for fluorescence images. All images were made using similar magnification and exposure time.

2.4. Enzyme-linked immunosorbent assays

Protein syntheses were quantified by means of enzyme-linked immunosorbent assays (ELISAs). Pro-collagen type I (Metra C1CP EIA Kit, Quidel, Buende, Germany) was chosen for human osteoblasts and fibroblasts. Therefore, protein content in the culture supernatants was determined according to the manufactures instructions after 96 h of cultivation with test pellets. CICP synthesis of osteoblasts cultured with niobium powders was measured after four and seven days, respectively.

Table 2
Dimensions and roughness values[a] of the test pellets.

Test pellet	Dimensions d × l [mm]	Ø Rz [μm]	Ø Ra [μm]
Ti6Al4V	10 × 2	15.71 ± 1.27	2.38 ± 0.15
Nb Amperit	10 × 2	7.04 ± 3.08	1.28 ± 0.88
Nb Ampertec	10 × 2	17.50 ± 8.95	2.49 ± 1.08
Nb sheet	10 × 1	18.14 ± 3.23	4.39 ± 0.38
Ti-42Nb sintered	10 × 2	41.65 ± 28.39	7.38 ± 5.86
Ti-42Nb SLM	10 × 2	46.83 ± 5.70	9.06 ± 1.28

[a] Rz - arithmetical mean deviation of the profile|Ra – average roughness of all individual measured values.

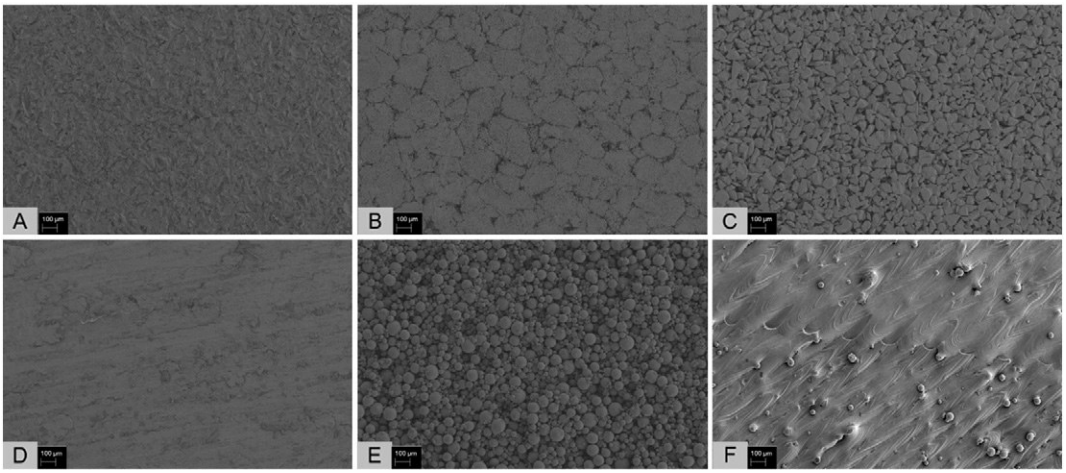

Fig. 2. FESEM images of the tested pellets. A – Ti6Al4V, B – Nb Amperit, C – Nb Ampertec, D – Nb sheet, E – Ti-42Nb sintered; F - Ti-42Nb SLM; magnification: 50×; bar: 100 μm.

2.5. Cytokine analysis

To verify a possible immune-stimulatory effect of the different niobium powders, a cytokine multiplex (interleukin (IL)-6, IL-8, monocyte chemotactic protein (MCP-1)) (Bio-Rad, Munich, Germany) was done according to the manufactures instructions. In brief, a multi-cytokine-detection in the culture supernatants was conducted by means of microsphere beads interlinking several cytokines via specific monoclonal antibodies and fluorescence dyes. The appropriate cytokine concentration was calculated based on a standard curve. Concentration of MCP-1 was mainly out of range.

2.6. Statistical analysis

The statistical significance was calculated with Mann-Whitney-*U* test using IBM® SPSS® Statistics Version 20 (IBM Corp., New York, USA). Data were shown as box plots or mean + SEM. Boxes denote interquartile ranges, horizontal lines within the boxes denote medians, and whiskers denote minimum and maximum values. Values of $p < 0.05$ were set to be significant.

3. Results

Human osteoblasts and fibroblasts were cultured on different niobium pellets for 96 h to verify their biocompatibility. The specimens were compared to Ti6Al4V pellets and referenced to TCPS as growth control. Metabolic activity of human osteoblasts was significantly decreased on Nb Amperit (−52%) and Nb sheet (−80%) (Fig. 3, left). Ti6Al4V (−29%), Nb Ampertec (−15%) and Ti-42Nb SLM (−8%) caused a slightly reduced activity compared with the reference. Against this, cultivation on Ti-42Nb sintered (+17%) significantly increased metabolic activity of human osteoblasts towards control.

Similar results were obtained if cultivating human fibroblasts on those surfaces. While Ti6Al4V (−68%) and Nb Amperit specimen (−52%) as well as Nb sheet (−92%) led to significant loss of metabolic activity, Nb Ampertec (−6%) and Ti-42Nb sintered (−13%) only slightly deviated from the reference. Accordingly, the metabolic activity of human fibroblast on these specimen was much higher than on the other samples (Fig. 3, right). These results are to a certain extend sustained by live/dead staining (Fig. 4). Thereby, results depended on the amount of metabolic cells as well as the specific level of cell activity.

Furthermore, protein synthesis of matrix relevant pro-collagen type 1 (CICP) was determined using ELISA. CICP synthesis was significantly reduced in supernatants of human osteoblasts cultured on the metallic surfaces. Nb Amperit (−92%) and Nb sheet (−78%) resulted in the lowest synthetic activity, followed by Ti6Al4V (−58%), Ti-42Nb sintered (−45%), Ti-42Nb SLM (−39%) and Nb Ampertec (−26%) compared to TCPS (Fig. 5, white). Accordingly, Ti-42Nb sintered as well as Ti-42Nb SLM and Nb Ampertec revealed a significantly higher metabolic activity towards CICP compared with the other metals. Cultivation of human fibroblasts on Ti6Al4V and niobium surfaces, i.e. Nb Amperit (−69%) and Nb sheet (−54%) resulted in a distinct decrease of metabolic activity towards control (Fig. 5, gray). Ti6Al4V (−3%) and control medium displayed a similar performance in the Pro-collagen type I synthesis whereas CICP synthesis was noticeably increased on Nb Ampertec (+12%) and Ti-42Nb sintered (+9%)

In addition, human osteoblasts were cultured in the presence of different Nb powders using three concentrations (0.1/0.2/0.5 mg/ml) over four and seven days. The metabolic activity of the cells was significantly reduced compared with the control in all experiments and mostly concentration-dependent. To receive information of the influence of surface area of the powders on the metabolic activity, two sieve fractions of Ti-42Nb powder namely a fine-grained powder with $x < 63$ μm and a coarse powder with $103\ \mu m < x < 350\ \mu m$ were investigated.

Each experiment indicated a considerable impact of the powders on the cell metabolism, i.e. a decrease of activity after four and seven days of cultivation (Fig. 6). While the cell activity of Nb Amperit powder was reduced from day four to seven there was no time-dependent influence for Nb Ampertec detectable. However, the latter had the strongest impact on the cell metabolism and reduced the cell activity to <40% compared with the reference, for concentrations of 0.2 and 0.5 mg Nb/ml. In contrast, Ti-42Nb powders provoked higher activities after seven days than after four days. Interestingly, the coarse Ti-42Nb powder ($103\ \mu m < x < 350\ \mu m$) caused a slight concentration-dependent increase of metabolic activity at day four, which became significant at day seven. Table 4 depicts the significant differences between all tested powders at day 4 and 7, respectively.

To investigate the cell-powder interaction, light microscopic pictures were recorded using an inverted microscope (Nikon TS 100, Nikon GmbH, Duesseldorf, Germany). Those indicate up-take of small particulates (Fig. 7, right picture) and partially powder agglomeration.

Table 3
Characteristics of the human donors[a] used for the cell experiments.

Test material	Donors	Gender	Average age
Pellets (A-E in Fig. 2)	Osteoblasts ($n = 7$)	5♂/2♀	65.29 ± 14.47
Ti-42Nb SLM	Osteoblasts ($n = 4$)	4♂/-♀	61.25 ± 6.34
Pellets (A-E in Fig. 2)	Fibroblasts ($n = 4$)	-♂/2♀ (2 n/a)	40 ± 7.07 (2 n/a)
Powders (A-D in Fig. 1)	Osteoblasts ($n = 8$)	4♂/4♀	69.25 ± 8.46

[a] n = number of different donors.

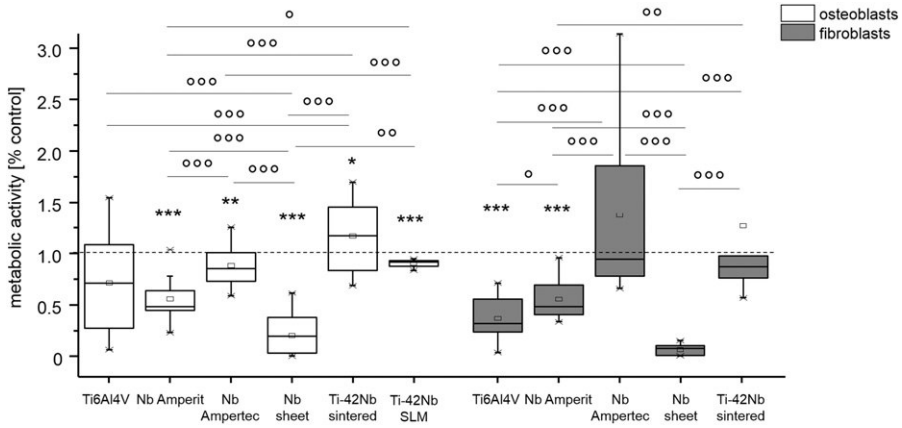

Fig. 3. Metabolic activity of human osteoblasts (left, $n \geq 4$) and human fibroblasts (right, $n = 4$) on different test pellets (Ti6Al4V, Nb Amperit, Nb Ampertec, Nb sheet, Ti-42Nb sintered, Ti-42Nb SLM) after 96 h cultivation. Boxes denote interquartile ranges, horizontal lines within the boxes denote medians, and whiskers denote minimum and maximum values. For statistical analysis Mann-Whitney-*U* test was conducted. Data were compared to the growth control (100%, *p) and against each other (°p). *$p < 0.05$, **$p < 0.01$, ***$p \leq 0.001$.

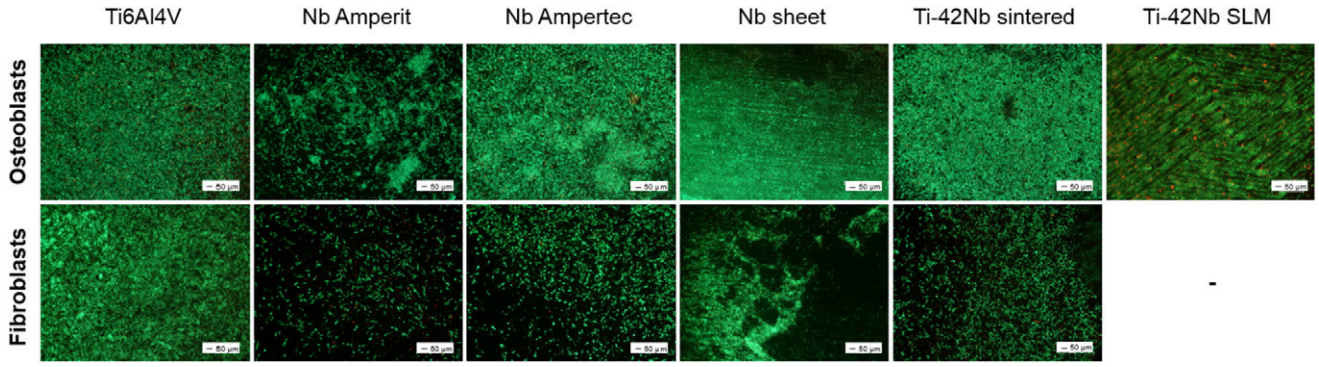

Fig. 4. Live/dead staining of human osteoblasts and fibroblasts on different test pellets (Ti6Al4V, Nb Amperit, Nb Ampertec, Nb sheet, Ti-42Nb sintered, Ti-42Nb SLM) after 96 h cultivation. Living cells are displayed in green, dead ones in red. Magnification: 40×, Scale bar: 50 μm.

After cultivation with several niobium powders live/dead staining was conducted which approved the results of the investigations on the metabolic activity (Fig. 8).

In addition, pro-collagen type I synthesis was analyzed. Data of collagen synthesis were relativized to metabolic activity and referred to powder-free control (Fig. 9). Again, concentration-dependent influence of niobium powders was clearly visible. While Nb Amperit powder resulted in a significant increase of collagen synthesis higher than control at nearly any point, Nb Ampertec and fine-grained Ti-42Nb revealed a decreasing pro-collagen type I synthesis with raising powder concentrations. Ti-42Nb powder (103 μm < x < 350 μm) only led to a negligible decrease of synthesis compared to control. Altogether, the pro-collagen type I syntheses increased with increasing time for either of the substrates in either concentration (Table 5).

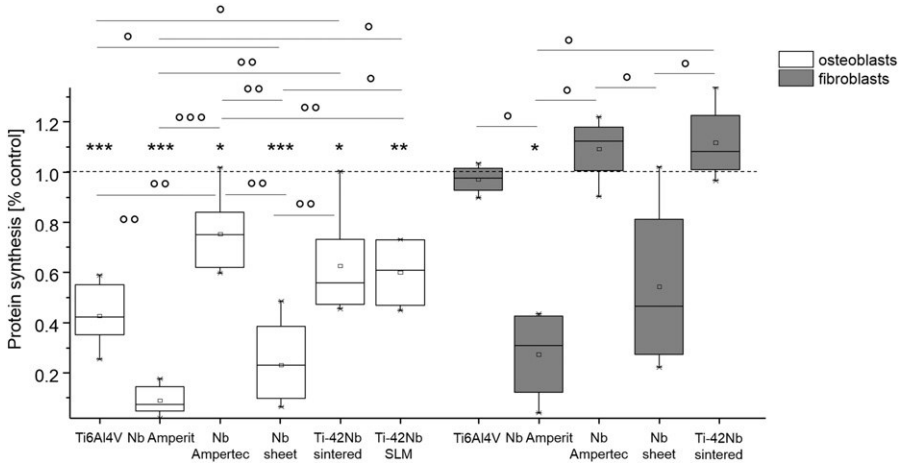

Fig. 5. Pro-collagen type I synthesis of human osteoblasts (white, $n \geq 4$) and human fibroblasts (gray, $n \geq 2$) on different test pellets (Ti6Al4V, Nb Amperit, Nb Ampertec, Nb sheet,Ti-42Nb sintered, Ti-42Nb SLM) after 96 h cultivation. Boxes denote interquartile ranges, horizontal lines within the boxes denote medians, and whiskers denote minimum and maximum values. For statistical analysis Mann-Whitney-*U* test was conducted. Data were compared to the growth control (100%, *p) and against each other (°p). *$p < 0.05$, **$p < 0.01$, ***$p \leq 0.001$.

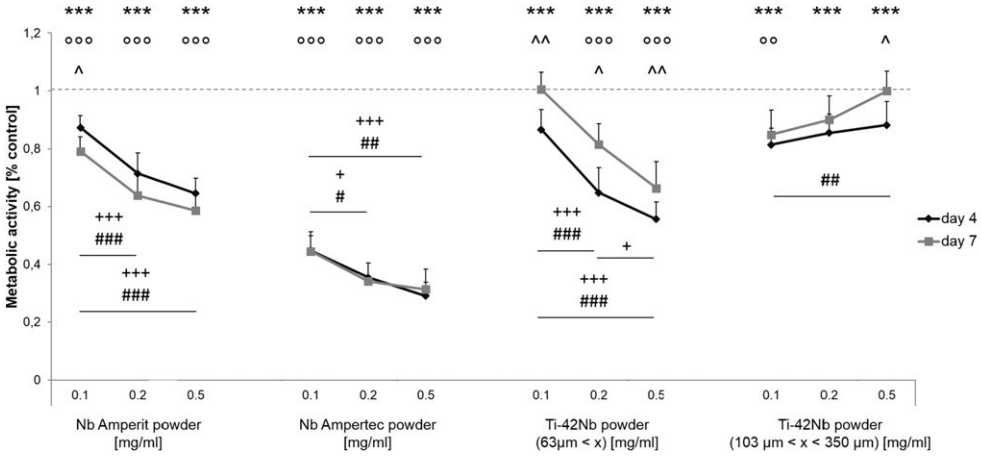

Fig. 6. Metabolic activity of human osteoblasts cultivated with different Nb and Ti-42Nb powders in three concentrations (0.1, 0.2 and 0.5 mg/ml) for four and seven days. Data are mean ± SEM ($n = 8$). For statistical analysis Mann-Whitney-*U* test was conducted. Data were compared to the growth controls (day 4 = *p/day 7 = °p) and between day 4 and day 7 (^p). Comparison of powder concentrations per niobium/Ti-42Nb powder is marked with +p (4 days) and #p (7 days); $^{*}p < 0.05$, $^{**}p < 0.01$, $^{***}p \leq 0.001$.

To evaluate an inflammatory response of human osteoblasts to four different niobium powders, interleukin syntheses were examined. IL-6 production was slightly increased after cultivation with Nb Amperit, Nb Ampertec and fine-grained Ti-42Nb powder at day four compared to control and raised further to day seven (Fig. 10). Dose-dependency is not that consistent between the powders. Coarse-grained Ti-42Nb caused a slight dose-dependent increased IL-6 synthesis being significantly higher than control at day four and decreasing with further cultivation until day seven.

Measurement of IL-8 synthesis revealed similar results compared to IL-6 synthesis for the several niobium powders. However, IL-8 was synthesized in a lower amount and was most widely equal to the control group (Fig. 11). There was no consistent trend perceptible between the several groups concerning dose- and time-dependency.

4. Discussion

In the present in vitro study, the biocompatibility of five different niobium-based metallic samples (Nb Amperit, Nb Ampertec, Nb sheet, Ti-42Nb sintered, Ti-42Nb SLM) towards human osteoblasts and fibroblasts is investigated and compared with Ti6Al4V pellets. In a previous work niobium exhibited better performance than titanium, using cell lines and testing proliferation, metabolic activity and maintenance of cell morphology [51]. Woo et al. [52] also used sintered Ti-42Nb, which was obtained by high energy ball milling, and demonstrated that mechanical properties and biocompatibility were superior to Ti6Al4V. An improved biocompatibility of coated Ti-Nb alloys has also been stated compared with pure Ti [53]. Moreover, shape memory effect and superelasticity are proved for Ti-Nb alloys [25,53]. Park et al.

Table 4
Appropriate significances to Fig. 5 comparing the different test powders. For statistical analysis Mann-Whitney-*U* test was conducted. Values of $p < 0.05$ were set to be significant. Significances for day 4 are above those of day 7, respectively.

	WST-1	Nb Amperit powder			Nb Ampertec powder			Ti-42Nb powder (63µm < x)			Ti-42Nb powder (103 µm < x < 350 µm)		
	[mg/ml]	0.1	0.2	0.5	0.1	0.2	0.5	0.1	0.2	0.5	0.1	0.2	0.5
Nb Amperit powder	0.1	n.s.	≤ 0.001 0.001	≤ 0.001 ≤ 0.001	≤ 0.001 ≤ 0.001	n.s.	n.s.	n.s. ≤ 0.001	n.s.	n.s.	0.040 n.s.	n.s.	n.s.
	0.2	≤ 0.001 0.001	n.s.	0.052 n.s.	n.s.	≤ 0.001 ≤ 0.001	n.s.	n.s.	n.s. 0.001	n.s.	n.s.	0.025 ≤ 0.001	n.s.
	0.5	≤ 0.001 ≤ 0.001	0.052 n.s.	n.s.	n.s.	n.s.	≤ 0.001 ≤ 0.001	n.s.	n.s.	0.012 0.017	n.s.	n.s.	≤ 0.001 ≤ 0.001
Nb Ampertec powder	0.1	≤ 0.001 ≤ 0.001	n.s.	n.s.	n.s.	0.028 0.017	≤ 0.001 0.005	≤ 0.001 ≤ 0.001	n.s.	n.s.	≤ 0.001 ≤ 0.001	n.s.	n.s.
	0.2	n.s.	≤ 0.001 ≤ 0.001	n.s.	0.028 0.017	n.s.	0.076 n.s.	n.s.	≤ 0.001 ≤ 0.001	n.s.	n.s.	≤ 0.001 ≤ 0.001	n.s.
	0.5	n.s.	n.s.	≤ 0.001 ≤ 0.001	≤ 0.001 0.005	0.076 n.s.	n.s.	n.s.	n.s.	≤ 0.001 ≤ 0.001	n.s.	n.s.	≤ 0.001 ≤ 0.001
Ti-42Nb powder (63µm < x)	0.1	n.s. ≤ 0.001	n.s.	n.s.	≤ 0.001 ≤ 0.001	n.s.	n.s.	n.s.	0.001 ≤ 0.001	≤ 0.001 ≤ 0.001	n.s. 0.006	n.s.	n.s.
	0.2	n.s.	n.s. 0.001	n.s.	n.s.	≤ 0.001 ≤ 0.001	n.s.	0.001 ≤ 0.001	n.s.	0.050 0.088	n.s.	≤ 0.001 n.s.	n.s.
	0.5	n.s.	n.s.	0.012 0.017	n.s.	n.s.	≤ 0.001 ≤ 0.001	≤ 0.001 ≤ 0.001	0.050 0.088	n.s.	n.s.	n.s.	≤ 0.001 ≤ 0.001
Ti-42Nb powder (103 < x < 350 µm)	0.1	0.040 n.s.	n.s.	n.s.	≤ 0.001 ≤ 0.001	n.s.	n.s.	n.s. 0.006	n.s.	n.s.	n.s.	n.s.	n.s. 0.010
	0.2	n.s.	0.025 ≤ 0.001	n.s.	n.s.	≤ 0.001 ≤ 0.001	n.s.	n.s.	≤ 0.001 n.s.	n.s.	n.s.	n.s.	n.s. 0.068
	0.5	n.s.	n.s.	≤ 0.001 ≤ 0.001	n.s.	n.s.	≤ 0.001 ≤ 0.001	n.s.	n.s.	≤ 0.001 ≤ 0.001	n.s. 0.010	n.s. 0.068	n.s.

n.s. - not significant.

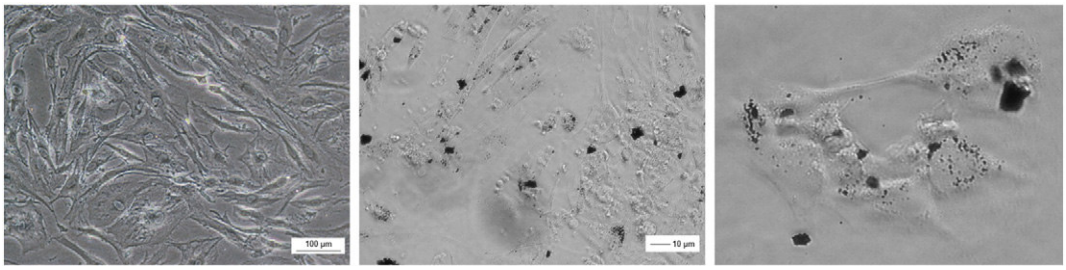

Fig. 7. Light microscopic pictures of control cells without powder (left, scale bar: 100 μm) and incorporation of powder particles by human osteoblasts at day four (Nb Ampertec (0.5 mg/ml), scale bar: 10 μm).

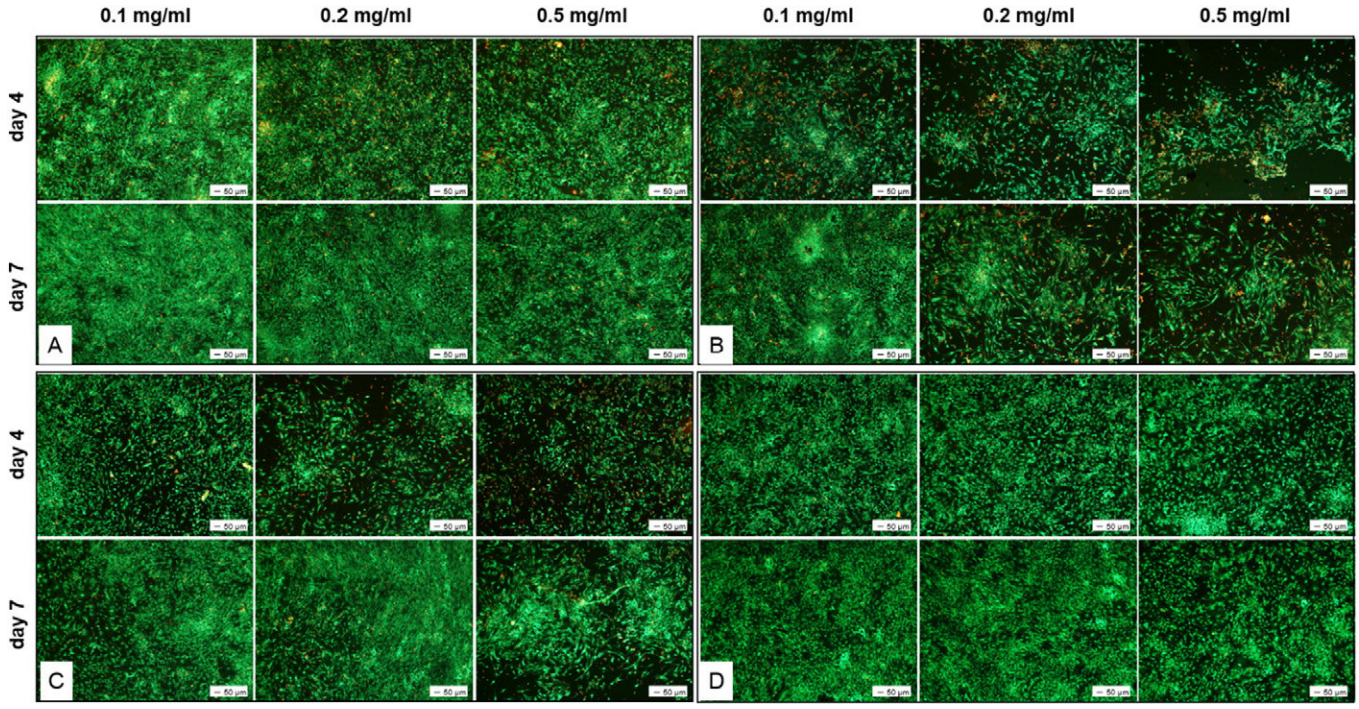

Fig. 8. Live/dead staining of human osteoblasts cultured with different Nb and Ti-42Nb powders in three concentrations (0.1, 0.2 and 0.5 mg/ml) after four and seven days. A – Nb Amperit, B - Nb Ampertec, C – Ti-42Nb powder (63 μm < x), D - Ti-42Nb powder (103 μm < x < 350 μm). Living cells are displayed in green, dead cells are displayed in red. Magnification: 40×, Scale bar: 50 μm.

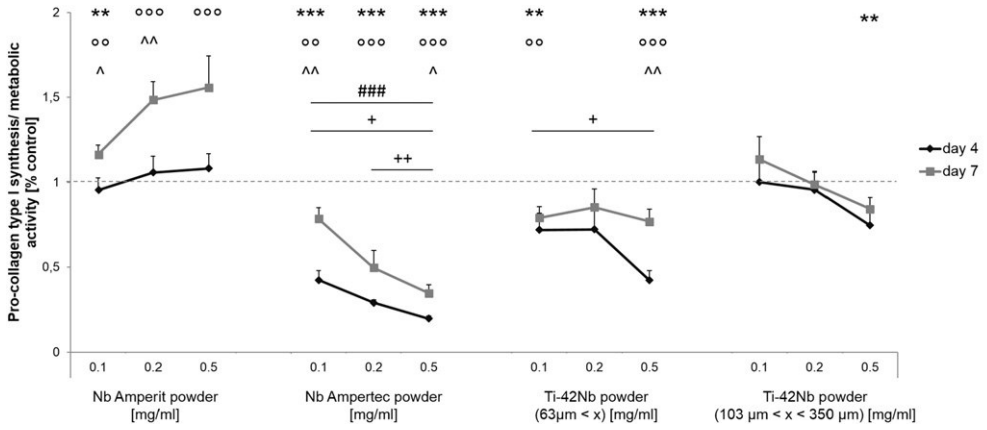

Fig. 9. Pro-collagen type I synthesis of human osteoblasts cultivated with different Nb and Ti-42Nb powders in three concentrations (0.1, 0.2 and 0.5 mg/ml) for four and seven days. Data are mean ± SEM ($n = 8$). For statistical analysis Mann-Whitney-*U* test was conducted. Data were compared to the growth controls (day 4 = *p/day 7 = °p) and day 4 towards day 7 (^p). Comparison of concentrations is marked with + p (4 days) and #p (7 days); $^{*}p < 0.05$, $^{**}p < 0.01$, $^{***}p \leq 0.001$.

Table 5
Appropriate significances to Fig. 8 comparing the several test powders against each other. For statistical analysis Mann-Whitney-*U* test was conducted. Values of $p < 0.05$ were set to be significant. Significances for day 4 are above those of day 7, respectively.

	CICP	Nb Amperit powder			Nb Ampertec powder			Ti-42Nb powder (63µm < x)			Ti-42Nb powder (103 µm < x < 350 µm)		
	[mg/ml]	0.1	0.2	0.5	0.1	0.2	0.5	0.1	0.2	0.5	0.1	0.2	0.5
Nb Amperit powder	0.1	n.s.	n.s. 0.059	n.s.	0.001 0.002	n.s.	n.s.	n.s. 0.002	n.s.	n.s.	n.s.	n.s.	n.s.
	0.2	n.s. 0.059	n.s.	n.s.	n.s.	0.001 0.001	n.s.	n.s.	0.093 0.003	n.s.	n.s.	n.s. 0.005	n.s.
	0.5	n.s.	n.s.	n.s.	n.s.	n.s.	0.001 0.001	n.s.	n.s.	0.001 0.001	n.s.	n.s.	0.021 0.001
Nb Ampertec powder	0.1	0.001 0.002	n.s.	n.s.	n.s.	n.s.	0.021 0.001	0.059 n.s.	n.s.	n.s.	0.001 0.036	n.s.	n.s.
	0.2	n.s.	0.001 0.001	n.s.	n.s.	n.s.	0.003 n.s.	n.s.	0.002 0.046	n.s.	n.s.	0.001 0.006	n.s.
	0.5	n.s.	n.s.	0.001 0.001	0.021 0.001	0.003 n.s.	n.s.	n.s.	n.s.	0.002 0.002	n.s.	n.s.	0.001 0.001
Ti-42Nb powder (63µm < x)	0.1	n.s. 0.002	n.s.	n.s.	0.059 n.s.	n.s.	n.s.	n.s.	n.s.	0.027 n.s.	n.s. 0.036	n.s.	n.s.
	0.2	n.s.	n.s. 0.003	n.s.	n.s.	0.002 0.046	n.s.	n.s.	n.s.	0.093 n.s.	n.s.	n.s.	n.s.
	0.5	n.s.	n.s.	0.001 0.001	n.s.	n.s.	0.002 0.002	0.027 n.s.	0.093 n.s.	n.s.	n.s.	n.s.	0.006 n.s.
Ti-42Nb powder (103 < x < 350 µm)	0.1	n.s.	n.s.	n.s.	0.001 0.036	n.s.	n.s.	n.s. 0.036	n.s.	n.s.	n.s.	n.s.	n.s. 0.093
	0.2	n.s.	n.s. 0.005	n.s.	n.s.	0.001 0.006	n.s.	n.s.	n.s.	n.s.	n.s.	n.s.	n.s.
	0.5	n.s.	n.s.	0.021 0.001	n.s.	n.s.	0.001 0.001	n.s.	n.s.	0.006 n.s.	n.s.	n.s.	n.s.

n.s. - not significant.

[22] cultured fibroblast cell lines on several pure metals and Ti alloys containing e.g. Nb, V or Al. WST-1 test showed good biocompatibility of pure Nb and the highest cell viability for Ti-10Nb. Those results are approved by de Andrade et al. [8] and Cremasco et al. [6] culturing rat osteoblasts and a fibroblast cell line on Ti-35Nb, respectively. Do Prado et al. [23] analyzed expression of relevant genes encoding for cell adhesion, differentiation and matrix synthesis in human osteoblasts. Thereby, Ti-35Nb revealed similar results to titanium. Bai et al. [31] used fibroblast and osteoblast cell lines to examine and prove cell proliferation and differentiation on Ti-45Nb. Biocompatibility of Ti–50Nb, Ti-30Nb, Ti-26Nb as well as Ti-15Nb, Ti-10Nb and Ti-5Nb with osteoblast and fibroblast cell lines was also attested [24,32,54–56]. Hofstetter et al. [57] also used human osteoblasts suggesting that Nb surfaces are more suitable than titanium. Likewise alloys containing Ti, Nb and a further element like e.g. tantalum or aluminum are proved to be suitable for medical applications [7,14,18,58–60]. Besides in vitro biocompatibility, niobium is also verified for in vivo use [27,61,62]. Nevertheless, a cell specific behavior on materials with different surface roughness is also stated. For instance, proliferation and differentiation of osteoblasts is proved to be roughness-dependent [63–66]. It is controversially discussed whether osteoblasts prefer rough surfaces [63,67] [10,68,69]. Our present study strongly supports these thesis, since the specimens with the roughest surfaces (both Ti-42Nb and Nb Ampertec) revealed the best results concerning metabolic activity and collagen synthesis. As described by Lohmann et al. [70], cell response of osteoblasts to surface roughness depends on their maturation state. In

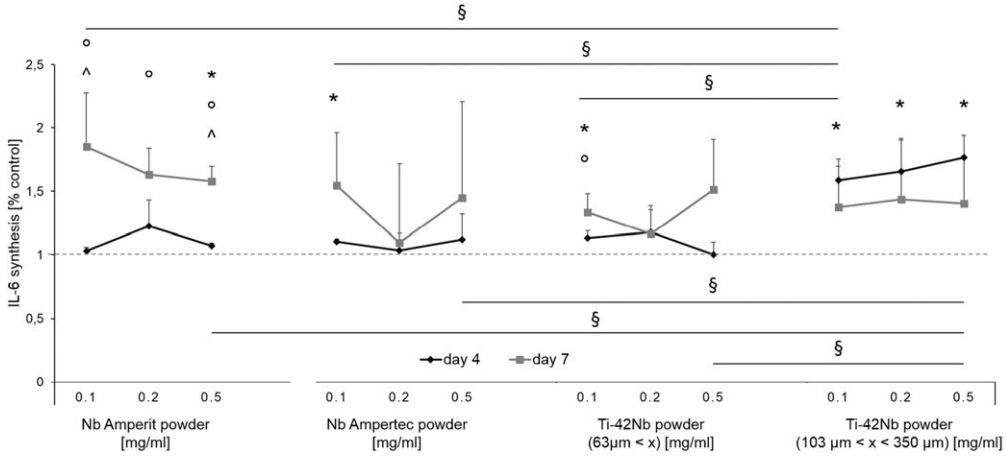

Fig. 10. IL-6 synthesis of human osteoblasts cultivated with different Nb and Ti-42Nb powders in three concentrations (0.1, 0.2 and 0.5 mg/ml) for four and seven days. Data are mean ± SEM ($n = 8$). For statistical analysis Mann-Whitney-*U* test was conducted. Data were compared to the growth controls (day 4 = *p/day 7 = °p) and day 4 towards day 7 (^p).). §p tags difference between the several niobium powders at day 7; $^{*}p < 0.05$, $^{**}p < 0.01$, $^{***}p \leq 0.001$.

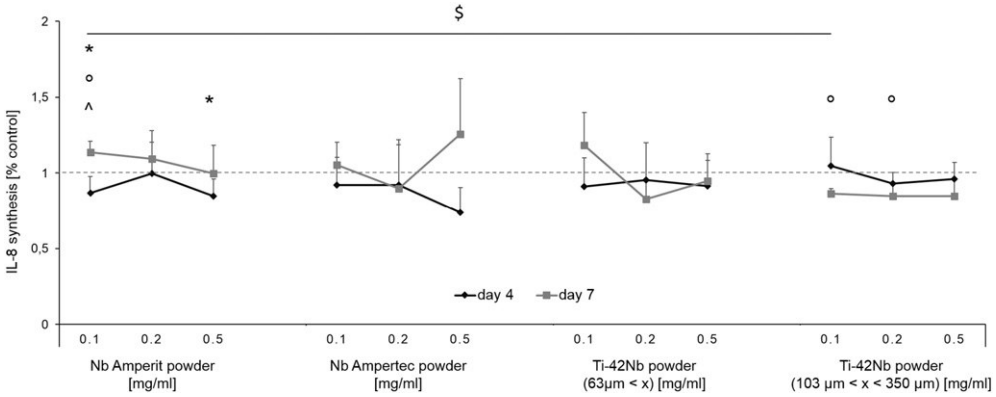

Fig. 11. IL-8 synthesis of human osteoblasts cultivated with different Nb and Ti-42Nb powders in three concentrations (0.1, 0.2 and 0.5 mg/ml) for four and seven days. Data are mean ± SEM ($n = 8$). For statistical analysis Mann-Whitney-*U* test was conducted. Data were compared to the growth controls (day 4 = *p/day 7 = °p) and day 4 towards day 7 (^p). $p tags difference between the several niobium powders at day 7; $^{*}p < 0.05$, $^{**}p < 0.01$, $^{***}p \leq 0.001$.

contrary, preference for smooth surfaces is well displayed for fibroblasts [67,68,71]. The presented data do not endorse these studies since behavior of human osteoblasts and fibroblasts was nearly similar indicating the best results for both Ti-42Nb surfaces and Nb Ampertec. Those surfaces differed strongly in their roughness values. Thus, the results might also be influenced by the surface material. Furthermore, Nb Ampertec and Nb sheet showed nearly identical coefficients of roughness, while Nb Ampertec resulted in great metabolic activity and procollagen type I synthesis for both types of cells. Hence, the adverse results for Nb sheets might be ascribed to production residues since those specimen were only stamped from on big sheet of metal without any further post-processing except ultrasonic bath and sterilization.

Furthermore, niobium powders (Nb Amperit, Nb Ampertec, and spherical Ti-42Nb in two particle sizes) were used for osteoblast exposition to imitate influence of particulate debris on potential osteolysis. The time- and dose-dependent influence of powders on the metabolic activity of human osteoblasts (Fig. 6) is supported by the live/dead fluorescence staining quite well (Fig. 8). A decrease of cell density and increase of dead cells is perceptible mainly for Nb Ampertec and Ti-42Nb powder (63 µm < x) with higher concentrations and cultivation time reflecting the results of metabolic activity. Nb Amperit und Ti-42Nb powder result in a slight decrease of cell density. Nevertheless, human cells are more sensitive than cell lines, but reacting in a donor-specific manner. Accordingly, metabolic activity is not reflected by live/dead staining, generally. For comparison it should be taken into account that pure powders (Amperit, Ampertec) and "alloy powders" (Ti-42Nb) had been used offering different chemical compositions. Apart from that particle size is one of the main factors influencing cell reaction. Particles of Nb Ampertec are larger than Nb Amperit ones, which might be a reason for the decreased metabolic cell activity. Since Ti-42Nb powders revealed an opposite result, here the chemical particle composition might be with higher influence than the particle size. As discernible in Fig. 1, titanium free niobium powders show a different particle morphology compared to Ti-42Nb ones. The particles are more edged than the spherical particles of the Ti-42Nb powders, which is proven to be an important factor for biological response. Dependency of cellular responses on the shape of particles is stated for at least polymer wear debris showing a decreased aggressive potential of spherical particles compared to other morphologies [72,73]. For a more detailed evaluation further investigations on this topic are required. A previous work investigating wear debris of Nb alloys like e.g. Ti-6Al-7Nb compared with common Ti6Al4V indicated a lower inflammatory response of monocytes cultured with Nb-containing particulates [27]. Kuroda et al. [74] examined influence of Nb and Ti wear debris in different concentrations over four and seven days on osteoblast cell lines and proved a dose-dependent influence on cell viability being depressed and lowest with the highest particle concentration. Thereby, viability of cells was still slightly higher using Nb debris. Similar experiments were done by Sakai et al. [46], who approved these results, but suggested that rather particulates wielded a slight effect on cells, but not the extracts. It is still proven that the effects of particulates on cells are caused by the direct contact of particulates with the cell membrane and phagocytosis of particles by cells [46]. Nevertheless, the recovery of viability is possible if the exposure level is below the "threshold particulate concentration value" [46]. Furthermore, it is well known, that cell viability is influenced by particulate size, concentration, composition and dissolved ions. Even contact with body fluid (blood, urine, saliva, serum) or culture medium results in corrosion processes of metals releasing ions to their environment [3,75], while intensity of ion dissolution is depending on medium properties (pH, temperature, chemical composition) [11,75,76] and the dissolution rate and roughness of the metal [77,78]. Caicedo et al. [79] published a comprehensive study concerning metal ion-induced cell effects. Additionally, in our present study random supernatants of the test specimens were analyzed after 72 h via Inductively Coupled Plasma - Atomic Emission Spectroscopy (ICP-AES) for testing purposes using an ICP Optical Emission Spectrometers (Varian/Agilent 715-ES, Waldbronn, Germany). Sample digestion and dilution were done with HNO_3 and with H_2O_2 and H_2O, respectively. Due to technical incidents a high dilution of samples was necessary, so all tested supernatants were under the detectable limit. However, Obata et al. [80] demonstrated a concentration-dependent influence of Nb ions, which induced differentiation and mineralization of osteogenic cells rather than initial cell adhesion and proliferation. Niobium surfaces are well known to exhibit good resistance against corrosion in simulated body fluid and excellent biocompatibility [41].

There are no previous in vitro studies regarding the influence of niobium and Ti-42Nb powders on human cells examining cell viability, collagen and interleukin synthesis. Our results indicate a slight release of IL-6 after particulate exposure, while IL-8 synthesis is nearly unaffected. Therefore, further work concerning inflammatory influence should be done. In addition, gene expression analysis and measurement of other matrix relevant markers should be taken into account. Moreover, comparative analysis in terms of the influence of particle sizes to cell behavior are obligatory.

In summary, there are only few previous studies covering the in vitro biocompatibility of niobium and especially Ti-42Nb. None of them are dealing with spherical Ti-42Nb powders which are required for production of patient-specific implants using 3D-printing, e.g. SLM or EBM. In the present study, those materials show promising results with human osteoblasts and fibroblasts and might be an alternative for medical applications to common metallic implant materials like Ti6Al4V alloys.

5. Conclusions

Specimens and powders based on niobium (Nb Amperit, Nb Ampertec) and spherical Ti-42Nb (sintered, SLM) were determined in cell cultures of human osteoblasts and fibroblasts. Thereby, the roughest surfaces, both Ti-42Nb surfaces and Nb Ampertec specimen, revealed excellent results concerning cell viability and collagen synthesis compared to commonly used implant material Ti6Al4V. Nevertheless, the cell specific preferences for surface roughness known from literature could not be ascertained. Both cell types acted in a similar manner. Examinations with particulate debris disclosed a dose-dependent and partly time-dependent influence of all four powders, thereby Nb Ampertec showed the highest decrease of cell viability and collagen synthesis. Furthermore, interleukin synthesis was only slightly increased for all powders. In summary, Nb Ampertec and Ti-42Nb seem to be promising alternatives for medical applications compared to commonly applied implant materials such as Ti6Al4V.

Conflicts of interest

The authors declare no conflict of interest.

Acknowledgments

The authors thank Dr. Jürgen Weber (Aesthetics clinic Rostock) for allocation of tissues for fibroblast isolation. We would like to thank the electron microscopy center, University Medicine Rostock for enabling FESEM images. We thank DOT GmbH Rostock for providing the Ti6Al4V test pellets. Furthermore Dr. Anika Jonitz-Heincke, Doris Hansmann and Mario Jackszis are gratefully acknowledged for technical support and Ronny Hagemann (Laser Zentrum Hannover e.V., LZH) for selective laser melting (SLM) of the Ti-42Nb test specimens. We thank PD Dr. Wolfgang Baumann (Leibniz Institute for Catalysis, Rostock) for performing ICP-OES measurements.

This research did not receive any specific grant from funding agencies in the public, commercial, or not-for-profit sectors.

References

[1] E.A. Lewallen, S.M. Riester, C.A. Bonin, H.M. Kremers, A. Dudakovic, S. Kakar, R.C. Cohen, J.J. Westendorf, D.G. Lewallen, A.J. van Wijnen, Tissue engineering. Part B, Reviews 21 (2015) 218–230.
[2] J.R. Davis (Ed.), Handbook of Materials for Medical Devices, fourth ed.ASM International, Materials Park, Ohio, 2006.
[3] M. Geetha, A.K. Singh, R. Asokamani, A.K. Gogia, Prog. Mater. Sci. 54 (2009) 397–425.
[4] M. Kulkarni, A. Mazare, P. Schmuki, A. Iglič, Biomaterial surface modification of titanium and titanium alloys for medical applications, A. Seifalian, A. de Mel, D.M. Kalaskar (Eds.), Nanomedicine, One Central Press (OCP) (2014) 111–136.
[5] L.M.R. de Vasconcellos, Y. Rodarte, R.F. do Prado, L.G.O. de Vasconcellos, M.L.D. Alencastro Graa, C.A. Alves Cairo, R. Hudak, Biomedical Engineering - Technical Applications in Medicine, InTech, 2012.
[6] A. Cremasco, A.D. Messias, A.R. Esposito, E.A.d.R. Duek, R. Caram, Mater. Sci. Eng. C 31 (2011) 833–839.
[7] Y. Li, C. Yang, H. Zhao, S. Qu, X. Li, Y. Li, Materials 7 (2014) 1709–1800.
[8] D.P. de Andrade, L.M.R. de Vasconcellos, I.C.S. Carvalho, L.F.d.B.P. Forte, S. de Souza, E. Luzia, R.F.D. Prado, D.R.D. Santos, C.A.A. Cairo, Y.R. Carvalho, Mater. Sci. Eng., C 56 (2015) 538–544.
[9] E. Goyenvalle, E. Aguado, R. Cognet, X. Bourges, G. Daculsi, KEM 361-363 (2008) 1351–1354.
[10] C.W. Chan, I. Hussain, D.G. Waugh, J. Lawrence, H.C. Man, Mater. Sci. Eng. C 42 (2014) 254–263.
[11] S.W. Fage, J. Muris, S.S. Jakobsen, J.P. Thyssen, Contact Dermatitis 74 (2016) 323–345.
[12] T.A. Tabish, M.T. Butt, M. Ali, Journal of Faculty of Engineering & Technology 19 (2006).
[13] L.M. da Silva, A.P.R.A. Claro, T.A.G. Donato, V.E. Arana-Chavez, J.C.S. Moraes, M.A.R. Buzalaf, C.R. Grandini, Artif. Organs 35 (2011) 516–521.
[14] A. Cimpean, V. Mitran, C.M. Ciofrangeanu, B. Galateanu, E. Bertrand, D.-M. Gordin, D. Iordachescu, T. Gloriant, Mater. Sci. Eng., C 32 (2012) 1554–1563.
[15] P.F. Gostin, A. Helth, A. Voss, R. Sueptitz, M. Calin, J. Eckert, A. Gebert, J. Biomed. Mater. Res. B Appl. Biomater. 101 (2013) 269–278.
[16] M. MetikošHuković, A. Kwokal, J. Piljac, Biomaterials 24 (2003) 3765–3775.
[17] R. Medda, A. Helth, P. Herre, D. Pohl, B. Rellinghaus, N. Perschmann, S. Neubauer, H. Kessler, S. Oswald, J. Eckert, J.P. Spatz, A. Gebert, E.A. Cavalcanti-Adam, Interface Focus 4 (2014) 20130046.
[18] T. Osathanon, K. Bespinyowong, M. Arksornnukit, H. Takahashi, P. Pavasant, J. Mater. Sci. Mater. Med. 17 (2006) 619–625.
[19] S. Sista, C. Wen, P.D. Hodgson, G. Pande, J. Biomed. Mater. Res. A 97 (2011) 27–36.
[20] M. Niinomi, M. Nakai, J. Hieda, Acta Biomater. 8 (2012) 3888–3903.
[21] T. Grosdidier, M.J. Philippe, Mater. Sci. Eng. A 291 (2000) 218–223.
[22] Y.-J. Park, Y.-H. Song, J.-H. An, H.-J. Song, K.J. Anusavice, J. Dent. 41 (2013) 1251–1258.
[23] R.F. do Prado, S.B. Rabelo, D.P. de Andrade, R.D. Nascimento, V.A.R. Henriques, Y.R. Carvalho, C.A.A. Cairo, de Vasconcellos, Luana Marotta Reis, J. Mater. Sci. Mater. Med. 26 (2015) 259.
[24] I. Jirka, M. Vandrovcova, O. Frank, Z. Tolde, J. Plsek, T. Luxbacher, L. Bacakova, V. Stary, Mater. Sci. Eng., C 33 (2013) 1636–1645.
[25] Y. Guo, K. Georgarakis, Y. Yokoyama, A.R. Yavari, J. Alloys Compd. 571 (2013) 25–30.
[26] J. Xu, X.-J. Weng, X. Wang, J.-Z. Huang, C. Zhang, H. Muhammad, X. Ma, Q.-D. Liao, PLoS One 8 (2013), e79289. .
[27] M. Niinomi, T. Narushima, M. Nakai (Eds.), Advances in Metallic Biomaterials: Tissues, Materials and Biological Reactions, Springer Berlin Heidelberg, Berlin Heidelberg, 2015.
[28] R. Olivares-Navarrete, J.J. Olaya, C. Ramírez, S.E. Rodil, Coatings 1 (2011) 72–87.
[29] K. Mediaswanti, C. Wen, E. P., C.C. Berndt, J. Wang, in: J. Sieniawski (Ed.), Titanium Alloys - Advances in Properties Control, InTech, 2013.
[30] M. Vandrovcova, I. Jirka, K. Novotna, V. Lisa, O. Frank, Z. Kolska, V. Stary, L. Bacakova, PLoS One 9 (2014), e100475. .
[31] Y. Bai, Y. Deng, Y. Zheng, Y. Li, R. Zhang, Y. Lv, Q. Zhao, S. Wei, Mater. Sci. Eng., C 59 (2016) 565–576.
[32] R.E. McMahon, J. Ma, S.V. Verkhoturov, D. Munoz-Pinto, I. Karaman, F. Rubitschek, H.J. Maier, M.S. Hahn, Acta Biomater. 8 (2012) 2863–2870.
[33] C.E. Wen, J.Y. Xiong, Y.C. Li, P.D. Hodgson, Phys. Scr. T139 (2010) 14070.
[34] S.A. Bernard, V.K. Balla, N.M. Davies, S. Bose, A. Bandyopadhyay, Acta Biomater. 7 (2011) 1902–1912.
[35] M.H. Elahinia, M. Hashemi, M. Tabesh, S.B. Bhaduri, Prog. Mater. Sci. 57 (2012) 911–946.
[36] K. Alvarez, H. Nakajima, Materials 2 (2009) 790–832.
[37] A. Bansiddhi, T.D. Sargeant, S.I. Stupp, D.C. Dunand, Acta Biomater. 4 (2008) 773–782.
[38] C. Chu, C. Chung, P. Lin, S. Wang, Mater. Sci. Eng. A 366 (2004) 114–119.
[39] D. Pradhan, A.W. Wren, S.T. Misture, N.P. Mellott, Mater. Sci. Eng., C 58 (2016) 918–926.
[40] A. Biesiekierski, J. Wang, M. Abdel-Hady Gepreel, C. Wen, Acta Biomater. 8 (2012) 1661–1669.
[41] P. Neacsu, D.-M. Gordin, V. Mitran, T. Gloriant, M. Costache, A. Cimpean, Mater. Sci. Eng., C 47 (2015) 105–113.
[42] S. Zhang, X. Cheng, Y. Yao, Y. Wei, C. Han, Y. Shi, Q. Wei, Z. Zhang, Mater. Sci. Eng., C 53 (2015) 50–59.
[43] Y. Abu-Amer, I. Darwech, J.C. Clohisy, Arthritis Res. Ther. 9 (Suppl. 1) (2007) S6.
[44] G.M. Keegan, I.D. Learmonth, C.P. Case, J. Bone Joint Surg. Br. Vol. 89 (2007) 567–573.
[45] Y. Jiang, T. Jia, P.H. Wooley, S.Y. Yang, Acta Orthop. Belg. 79 (2013) 1–9.
[46] T. Sakai, S. Takeda, M. Nakamura, Dent. Mater. J. 21 (2002) 133–146.
[47] D. Bitar, J. Parvizi, World J. Orthod. 6 (2015) 172–189.
[48] K. Lochner, A. Fritsche, A. Jonitz, D. Hansmann, P. Mueller, B. Mueller-Hilke, R. Bader, Int. J. Mol. Med. 28 (2011) 1055–1063.
[49] A. Jonitz-Heincke, K. Lochner, C. Schulze, D. Pohle, W. Pustlauk, D. Hansmann, R. Bader, Mol. Med. Rep. 14 (2016) 1491–1500.
[50] C. Schulze, K. Lochner, A. Jonitz, R. Lenz, O. Duettmann, D. Hansmann, R. Bader, Int. J. Mol. Med. 32 (2013) 227–234.
[51] B. O'Brien, in: M. Niinomi, T. Narushima, M. Nakai (Eds.), Advances in Metallic Biomaterials: Tissues, Materials and Biological Reactions, Springer Berlin Heidelberg, Berlin Heidelberg, 2015.
[52] K.D. Woo, Met. Mater. Int. 14 (2008) 327–333.
[53] J. Xiong, Y. Li, P.D. Hodgson, C. Wen, J. Biomed. Mater. Res. A 95 (2010) 766–773.
[54] S. Sista, C. Wen, P.D. Hodgson, G. Pande, Mater. Sci. Eng., C 33 (2013) 1573–1582.
[55] S.E. Kim, H.W. Jeong, Y.T. Hyun, Y.T. Lee, C.H. Jung, S.K. Kim, J.S. Song, J.H. Lee, Met. Mater. Int. 13 (2007) 145–149.
[56] Y. Li, C. Wong, J. Xiong, P. Hodgson, C. Wen, J. Dent. Res. 89 (2010) 493–497.
[57] W. Hofstetter, H. Sehr, M. de Wild, J. Portenier, J. Gobrecht, E.B. Hunziker, J. Biomed. Mater. Res. A 101 (2013) 2355–2364.
[58] V.S.A. Challa, S. Mali, R.D.K. Misra, J. Biomed. Mater. Res. A 101 (2013) 2083–2089.
[59] L. Shapira, A. Klinger, A. Tadir, A. Wilensky, A. Halabi, Clin. Oral Implants Res. (2009).
[60] C. Treves, M. Martinesi, M. Stio, A. Gutierrez, J.A. Jimenez, M.F. Lopez, J. Biomed. Mater. Res. A 92 (2010) 1623–1634.
[61] M. Bruschi, D. Steinmüller-Nethl, W. Goriwoda, M. Rasse, Journal of Oral Implants 2015 (2015) 1–14.
[62] H. Matsuno, A. Yokoyama, F. Watari, M. Uo, T. Kawasaki, Biomaterials 22 (2001) 1253–1262.
[63] A.F. Mavrogenis, R. Dimitriou, J. Parvizi, G.C. Babis, J. Musculoskelet. Nueronal Interact. 9 (2009) 61–71.
[64] E. Eisenbarth, D. Velten, M. Muller, R. Thull, J. Breme, J. Biomed. Mater. Res. A 79 (2006) 166–175.
[65] C. Wirth, B. Grosgogeat, C. Lagneau, N. Jaffrezic-Renault, L. Ponsonnet, Mater. Sci. Eng. C 28 (2008) 990–1001.
[66] H. Zhang, J. Han, Y. Sun, Y. Huang, M. Zhou, Mater. Sci. Eng., C 56 (2015) 22–29.
[67] T.P. Kunzler, T. Drobek, M. Schuler, N.D. Spencer, Biomaterials 28 (2007) 2175–2182.
[68] C. Wirth, V. Comte, C. Lagneau, P. Exbrayat, M. Lissac, N. Jaffrezic-Renault, L. Ponsonnet, Mater. Sci. Eng. C 25 (2005) 51–60.

[69] W. Chrzanowski, E.A.A. Neel, D.A. Armitage, X. Zhao, J.C. Knowles, V. Salih, J. Biomed, Mater. Res. 9999A (2009) NA-NA.
[70] C.H. Lohmann, L.F. Bonewald, M.A. Sisk, V.L. Sylvia, D.L. Cochran, D.D. Dean, B.D. Boyan, Z. Schwartz, J. Bone Miner. Res. Off. J. Am. Soc. Bone Miner. Res. 15 (2000) 1169–1180.
[71] D.G. Waugh, J. Lawrence, C.W. Chan, I. Hussain, H.C. Man, Laser Surface Engineering, Elsevier, 2015 653–676.
[72] S.-Y. Yang, W. Ren, Y. Park, A. Sieving, S. Hsu, S. Nasser, P.H. Wooley, Biomaterials 23 (2002) 3535–3543.
[73] W. Ren, S.-Y. Yang, H.-W. Fang, S. Hsu, P.H. Wooley, Biomaterials 24 (2003) 4819–4826.
[74] S. Kuroda, S. Takeda, M. Nakamura, Dent. Mater. J. 22 (2003) 507–520.
[75] M. Es-Souni, H. Fischer-Brandies, Anal. Bioanal. Chem. 381 (2005) 557–567.
[76] P. Fili, J. Lausmaa, J. Musialek, K. Mazanec, Biomaterials 22 (2001) 2131–2138.
[77] M.C. Cortizo, M.F.L. De Mele, A.M. Cortizo, Biol. Trace Elem. Res. 100 (2004) 151–168.
[78] H. Huang, Biomaterials 24 (2003) 3585–3592.
[79] M. Caicedo, J.J. Jacobs, A. Reddy, N.J. Hallab, J. Biomed. Mater. Res. 86A (2008) 905–913.
[80] A. Obata, Y. Takahashi, T. Miyajima, K. Ueda, T. Narushima, T. Kasuga, ACS Appl. Mater. Interfaces 4 (2012) 5684–5690.

Society For Biomaterials

Direct influence of titanium and zirconia particles on the morphology and functionality of mature human osteoclasts

Juliane Pasold, Jana Markhoff, Jenny Tillmann, Martin Krogull, Phillip Pisowocki, Rainer Bader

Department of Orthopaedics, Biomechanics and Implant Technology Laboratory, University Medicine Rostock, Doberaner Strasse 142, Rostock, 18057, Germany

Received 8 September 2016; revised 10 April 2017; accepted 12 May 2017
Published online 21 June 2017 in Wiley Online Library (wileyonlinelibrary.com). DOI: 10.1002/jbm.a.36114

Abstract: Within the last ten years of biomedical implants, the focus is increasingly on bioceramics, specifically on zirconia (ZrO_2). Hence, we analyzed the impact of ZrO_2 particles in comparison to titanium particles on mature human osteoclasts (OCs) as little is known about the direct effect of wear particles on mature OCs and their role in the osteolytic process during aseptic endoprosthesis loosening. Changes in cell morphology and functionality of OCs incubated with particles in different concentrations were investigated *in vitro*. OCs tend to be enlarged after three days of cultivation with both types of particles, especially with high concentrations of ZrO_2, suggesting increased cell fusion. Further, we identified significantly increased expression of OC specific and bone matrix related genes: *VNR*, *RANK*, *TRAP,* and *CTSK* pointing on a direct stimulatory particle effect on the functionality of mature OCs. In completion, we quantified the bone resorption activity of particle treated mature OCs but could not detect a significant difference in bone resorption compared to OCs cultivated without particles. However, we could identify significantly higher gene expression of *MMP-1* in particle treated OCs compared to untreated control OCs after three days of incubation. We also detected an impaired production of the tissue inhibitor of metalloproteinase, especially for OCs treated with high ZrO_2 concentrations. In conclusion, our *in vitro* data show that abrasion particles could have a direct influence on mature OCs and therefore could promote increased OC-mediated bone resorption during aseptic loosening of total joint replacements. J Biomed Mater Res Part A: 105A: 2608–2615, 2017.

Key Words: mature osteoclasts, wear particle, morphology, functionality, bone resorption

How to cite this article: Pasold J, Markhoff J, Tillmann J, Krogull M, Pisowocki P, Bader R. 2017. Direct influence of titanium and zirconia particles on the morphology and functionality of mature human osteoclasts. J Biomed Mater Res Part A 2017:105A:2608–2615.

INTRODUCTION

Over the past two decades, metal alloys have evolved into the most widely used material for total knee and hip endoprostheses due to their high mechanical resistance, excellent molding characteristics, and biological compatibility.[1] Within the last 10 years, however, the focus is increasingly on ceramic implant materials, especially on zirconium oxide (ZrO_2) and alumina (Al_2O_3) for load-bearing implants.[2,3]

Although implantation of endoprostheses provides positive results in terms of pain relief and recovery of joint mobility, there is still a high failure rate, resulting in the need for revision surgery. The most common mode of failure after total joint arthroplasty is aseptic implant loosening due to wear debris, which is mechanically generated and accumulated in articulating surfaces.[4] As a result, inflammatory reactions may occur in the periprosthetic tissue initiating osteolysis and consequent loosening of the implant. For instance, in Germany, which is among the countries with the highest number of joint replacement surgeries, 160.848 primary total hip replacements and 26.702 revision surgeries were performed in 2014. The time between initial implantation and endoprosthetic exchange ranged from 7 to 142 months for varying reasons.[5] Compared with metallic implants, there is significantly less data for ceramics, especially long-term studies, due to the shorter research periods.

Monocytes/macrophages belong to the major cell type involved in the process of aseptic osteolysis related to wear particles. It is known that macrophages become activated through particle contact, which then initiates a complex biological cascade leading to increased osteolytic processes.[4] Macrophages indirectly cause osteolysis by releasing numerous chemotactic inflammatory mediators but also directly through the resorption of bone.[6] It is known that macrophages become activated through phagocytosis of wear particles and start producing proinflammatory cytokines, which then stimulate bone-resorbing cells (osteoclasts, OCs).[7,8] It was found that abrasive ZrO_2 wear particles caused the smallest altered reactions in the metabolism of osteoblasts compared with other particle types.[9] Fibroblasts, osteoblasts, OCs and mesenchymal stem cells are also known to play a

Correspondence to: Dr. J. Pasold, Fraunhofer Institute of ceramic technologies and systems (IKTS), Perlickstr. 1, 04103 Leipzig, Germany; e-mail: juliane.pasold@ikts.fraunhofer.de
Contract grant sponsor: Medical faculty of the University Rostock (FORUN)

critical role during the hostile inflammatory process in the periprosthetic tissue.[10–13] They influence each other by secreting enzymes [e.g., matrix metalloproteinases (MMPs) and tissue inhibitor of metalloproteinase (TIMPs)], growth factors [e.g., macrophage colony-stimulating factor (M-CSF)] and proinflammatory cytokines (e.g., interleukins, tumor necrosis factors).[14] Most studies dealing with aseptic loosening concentrated on macrophages, osteoblasts, and on the recruitment and activation of OCs. OCs develop by fusion of mononuclear precursors of the monocyte/macrophage lineage.

MMP-1 degrades different types of collagen and is expressed by OCs sitting at resorption sites.[15] TIMP-1, important for bone developmental processes, was shown to be highly expressed in neonatal bone OCs.[16] TIMPs interact with MMPs by blocking their activity.[17] Particles and metallic ions have been shown to stimulate osteoblasts to produce proinflammatory mediators *in vitro*[18] and regulate OC differentiation and activation by releasing M-CSF and Receptor Activator of NF-κB Ligand (RANKL). Currently, we found that titanium and zirconia (ZrO_2) particles stimulate the osteoclastic differentiation and upregulate OC activation (manuscript in preparation, Markhoff et al.).

In this *in vitro* study, we focused on the impact of titanium and ZrO_2 particles on mature human OCs, because until now little is known concerning the direct effect of wear particles on mature OCs and their role during the osteolytic process. Hence, we analyzed changes in cell morphology and functionality of OCs. Furthermore, we analyzed OC specific genes encoding for (1) vitronectin receptor (*VNR*) important for bone adhesion, (2) Receptor Activator of NF-κB (*RANK*), expressed by OCs regulating migration, proliferation and activation, (3) tartrate-resistant acid phosphatase (*TRAP*), and (4) cathepsin K (*CTSK*), both involved in bone matrix resorption. Additionally, we have quantified the bone resorption activity of particle treated OCs and hereby focused on MMP-1 and TIMP-1.

MATERIALS AND METHODS

Buffy coat isolation and OC differentiation

Human peripheral blood mononuclear cells (PBMCs) were isolated with density gradient centrifugation (Ficoll Hypaque method) from buffy coats (anonymous donors, $n = 6$). Patient agreements as well as the approval of the Local Ethics Committee (registration number: A2011–140) were obtained. Buffy coats were diluted with Phosphate buffered saline (PBS 1×, Biochrom GmbH, Berlin, Germany) and carefully layered on lymphocyte separation medium (Histopaque®-1077, Sigma-Aldrich, Hamburg, Germany) followed by a centrifugation step at 2500 rpm for 20 min at room temperature (RT). The resulting interfaces containing the PBMC-like lymphocytes and monocytes (density: 1.07 g/mL) were extracted with a sterile Pasteur pipette. These cells were washed with PBS via multiple centrifugation steps and were layered on lymphocyte separation medium and washed again as necessary. Afterwards, cells were resuspended in RPMI1640 medium (Biochrom, Berlin, Germany) containing 2% fetal calf serum (FCS), 1% Penicillin/Streptomycin (P/S, all from Gibco®-Invitrogen, Darmstadt, Germany) and 2% L-Glutamin (PAA Laboratories GmbH, Coelbe, Germany). The cells were cultured in a 6-well suspension culture plate (Cellstar® Cell-Repellent surface, Greiner Bio-One, Frickenhausen, Germany) at a density of 1×10^7 cells per well for seven days for increased accumulation of monocytes. Then, suspension cells were transferred to a 48-well standard cell culture plate for osteoclastic differentiation. Cells were cultivated at a density of 4×10^4 cells/well with α-MEM Dulbecco (MEM Alpha-Medium (1×), Life Technologies GmbH, Darmstadt, Germany) containing 10% FCS, 2% P/S, monocyte-colony stimulating factor (M-CSF, 25 ng/mL) and Receptor Activator of NF-κB Ligand (RANKL, 50 ng/mL; both: PeproTech, Hamburg, Germany) at 37°C and 5% CO_2 for seven days. Undifferentiated control cells were cultivated in the absence of RANKL.

In vitro *particle exposure.* During particle experiments, pure polycrystalline zirconium dioxide (ZrO_2) particles (mean size of 1.75 ± 4.66 μm; Selectipur, Heraeus Kulzer, Wehrheim, Germany) and commercially pure titanium oxide (cpTi) particles (Grade E, dry, diameter mean size of 3 μm; Chemetall, Frankfurt, Germany) were used. The several particles were apportioned in amounts of 5 mg in glass jars and gamma-sterilized with 25 kGy. The endotoxin load was checked with a Limulus amebocyte lysate (LAL) test (range of sensitivity 0.015–0.0001 EU/mL), which was negative. To produce a stock solution powders were re-suspended in 500 μL of PBS (=10 mg/mL) and diluted with culture medium to get two working solutions (0.01/0.1 mg/mL). These concentrations were determined by means of appropriate pretesting. First trials were performed based on preliminary works of the working group regarding the influence of orthopedic wear particles on human cells.[9,19]

Particles were added in two different concentrations (0.01/0.1 mg/mL) to human OCs after seven days of differentiation and incubated for an additional seven days (Fig. 1). After three days (day 10), medium was changed to remove all particles which had not been phagocytosed.

Cell biological analysis

TRAP staining and quantification of cell sizes. The osteoclastic cell type was confirmed by staining for tartrate-resistant acid phosphatase 5 b (TRAP5b) using an Acid Phosphatase, Leukocyte (TRAP) Kit (Sigma-Aldrich, Hamburg, Germany) according to the manufacturer's instructions. Briefly, OCs were fixed with a mixed citrate solution, acetone (VWR International, Darmstadt, Germany) and formaldehyde (37%), for 30 s (300 μl per 24-well) after removing the cell culture medium. Wells were rinsed twice with preheated (37°C) deionized water before a mixture of fast garnet GBC standard and sodium nitrite solution was added. For TRAP staining deionized water, the previously mixed solution, naphtol AS-Bi phosphate solution and acetate solution were added together as well as a tartrate solution. Control cells were stained without tartrate solution. After two washing steps the cells were stained for 1 h in the appropriate solution (300 μl, 37°C) followed by two additional washing steps. The cells were counterstained with hematoxylin (30 s, 300 μl per 24-well). Finally, we rinsed the wells for 10 min with tap water and let

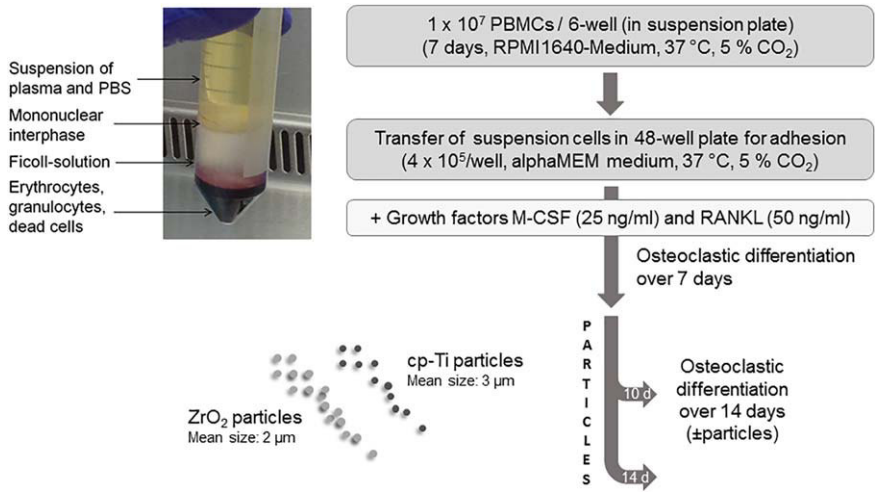

FIGURE 1. Flow chart for *in vitro* particle experiments with human mature OCs.

them dry. Violet/dark red granules were visible in the cell plasma indicating the presence of tartrate resistant acid phosphatase. Furthermore, cells with more than three cell nuclei were identified as OCs.

For quantitative analysis of cell size distribution we selected five microscopic field images (100 x magnification) per sample ($n = 3$) randomly with a light microscope plus integrated camera (Nikon Type 120 and NIS-Elements software, Nikon Corporation, Tokyo, Japan). Blinded cell images were analyzed using ImageJ software (Java 1.8.0). We calculated minimum, maximum and mean cell size per field and averaged the data for each sample.

Metabolic cell activity. We used the Water-Soluble-Tetrazolium salt (WST-1) assay (Roche, Grenzach-Wyhlen, Germany) to determine the mitochondrial dehydrogenase activity of OCs after three and seven days of exposure to particles as described before. In metabolically active cells the tetrazolium salt WST is transformed to formazan by mitochondrial succinate dehydrogenase. The resulting color change in the cell supernatant was measured at 450 nm in a Tecan reader (Infinite F200 Pro, Männedorf, Switzerland).

Gene expression analyses. Total RNA from OCs was isolated by using TRIzol reagent (Invitrogen, Darmstadt, Germany) and the Direct-zol RNA kit (Zymo Research, Freiburg, Germany) according to the manufactures instructions including optional DNAse digestion. RNA purity and concentration was determined with the Tecan reader (Infinite F200 Pro, Männedorf, Switzerland) by using Tecań's NanoQuant plate.

Total RNA was transcribed to cDNA using the High Capacity cDNA Reverse Transcription Kit (Applied Biosystems, Darmstadt, Germany) with 10x RT buffer, 25x dNTP Mix (100 mM), RT random primers, MultiScribe® Reverse Transcriptase (50 U/µL) and DEPC water in a final volume of 20 µL. The transcription program consisted of 10 min at 25°C, 120 min at 37°C and a final step of 15 s at 85°C done in a thermocycler (Personal Thermocycler, Biometra, Göttingen, Germany). In the following quantitative Real-Time PCR, cDNA was incubated with innuMIX qPCR MasterMix SyGreen (Analytik Jena, Jena, Germany) including high specific Taq DNA Polymerase, high quality dNTP's and intercalating dye. DEPC water, each forward and reverse primer (Sigma-Aldrich, Hamburg, Germany) was added in a final reaction volume of 20 µL. The primer used are listed in Table I. The q RT-PCR reaction, consisting of 40 cycles (95°C for 3 min, 95°C for 5 s and 60°C for 30 s), was done in the qTower 2.0 (Analytik Jena, Jena, Germany). OC specific markers (*Vitronectin* (*VNR*), *RANK*, *TRAP5b*, *cathepsin K* (*CTSK*), *MMP-1*, *TIMP-1*) were examined and *β-Actin* was chosen as a housekeeping gene.

Protein expression. Specific enzyme-linked immunosorbent assays (ELISAs) were used to verify protein syntheses by the *in vitro* cultured human OCs. We analyzed matrix metalloproteinase 1 (Human MMP-1 ELISA, RayBiotech, Köln, Germany), which is involved in cleavage of type I collagen, the main component of the bone matrix, and the TIMP 1 (Human TIMP-1 ELISA, RayBiotech, Köln, Germany). Both ELISAs were conducted according to the manufacturer's instructions.

TABLE I. Primers and Primer Sequences used for Gene Expression Analysis

Primer ID	Primer Sequence
VNR	Forward primer: 5′-TCACCAACTCCACATTGGTT-3′
	Reverse primer: 5′-CCATTTTCATGAGGTTGAAGC-3′
RANK	Forward primer: 5′-AGAAAACCACCAAATGAACCCC-3′
	Reverse primer: 5′-GCCACAAGCCTCATTGATCC-3′
TRAP5b	Forward primer: 5′-GGGAGATCTGTGAGCCAGTG-3′
	Reverse primer: 5′-GTCCACATGTCCATCCAGGG-3′
CTSK	Forward primer: 5′-GGCCAACTCAAGAAGAAAAC-3′
	Reverse primer: 5′-GTGCTTGTTTCCCTTCTGG-3′
MMP-1	Forward primer: 5′-AGAGCAGATGTGGACCATGC-3′
	Reverse primer 5′-TCCCGATGATCTCCCCTGAC-3′
TIMP-1	Forward primer: 5′-ATTGCTGGAAAACTGCAGGATG-3′
	Reverse primer 5′-GTCCACAAGCAATGAGTGCC-3′
β-Actin	Forward primer: 5′-CTTCCTGGGCATGGAGTC-3′
	Reverse primer: 5′-AGCACTGTGTTGGCGTACAG-3′

Bone resorption assay. OCs (after seven days of differentiation as described before) were seeded into OsteoLyse™ Cell Culture 8-Well-Stripes (96-well format; OsteoLyse™ Assay Kit "Human Collagen", Lonza, Basel, Switzerland) at a density of 2 x 10^4 cells per well. The medium was changed every three days. A supernatant sample of 50 µl was collected from every well for a fluorescence measurement after three, seven, 10 and 14 days, respectively.

For the fluorescence measurement 200 µl of the Fluorophore Releasing Reagent (RT) was placed per well of a black 96-well assay plate (measure plate). Then, 10 µl of each sample (cell supernatant taken at various time points) was added to the corresponding well. The assay plate was briefly shaken and measured using the Tecan reader. We performed a time resolved fluorescence analysis at 340 nm for 400 µs after an initial delay of 400 µs.

Statistical analysis

The nonparametric two-tailed Mann-Whitney-*U* test was conducted and the statistical significance of the data was evaluated by using IBM® SPSS® Statistics Version 20 (IBM Corp., New York, USA). We also used, as indicated, ANOVA *post hoc*-Least Significant Difference (LSD) test. A p value < 0.05 was considered statistically significant for both statistical tests.

RESULTS

Metabolic cell activity and OC morphology

In our *in vitro* studies, we were looking for a possible dose- and time-dependent impact of titanium (cpTi) and ZrO_2 particles on mature OCs. Therefore, we first led the monocytes to differentiate into mature OCs over seven days. We then incubated them with metallic and ceramic particles at two different concentrations (0.01 and 0.1 mg/mL) and cultivated the cells for another three and seven days (Fig. 2). We confirmed the initial up-take of supplemented particles by the cells via light microscopy (LM) [Fig. 2(A), upper panel] and the osteoclastic cell type through TRAP5b staining [Fig. 2(A), lower panels].

Within the cultivation period of four days (from day 10 to day 14) the mean cell size significantly increased in all approaches, regardless of what particle type and dose was used [Fig. 2(B), middle boxes]. Notably, we found significantly larger cell sizes at day 10 when OCs were stimulated with high concentrations of ZrO_2 (0.1 mg/mL) compared to low ZrO_2 (0.01 mg/mL) concentrations [Fig. 2(B), upper boxes]. Related to this, the control cell sizes were smaller at day 10 in comparison to the size range of cells stimulated with both types and doses of particles. At day 14, however, the smallest cell sizes were found after stimulation with cpTi (0.1 mg/mL) and ZrO_2 (0.01 and 0.1 mg/mL).

OCs exposed to cpTi particles over three days (day 10) showed a significantly reduced metabolic activity compared with control OCs cultivated without particles. Additionally, this particle effect was dose-dependent [Fig. 2(C)]. OCs treated with ZrO_2 particles, however, showed a comparable activity to the untreated control cells after three days (day 10), but a significantly reduced activity after seven days (day 14) of exposure to 0.1 mg/mL of ZrO_2 particles [Fig. 2(C), right]. The OC number per well was comparable between the control and the particle treated approaches (data not shown).

Expression of specific osteoclastic markers

Vitronectin, *VNR,* plays an important role in bone adhesion and was found to be significantly higher expressed by OCs treated with both concentrations of cpTi and ZrO_2 particles over three days compared with untreated OCs. Seven days after the initial exposure to particles, only the OCs treated with higher concentrations of both types of particles still expressed *VNR* at significantly higher levels compared to the control (Fig. 3, upper left chart).

The osteoclastic genes, *TRAP* and *RANK,* are important key factors in the regulation of OC migration, differentiation, proliferation, and activation. TRAP was dose-dependently upregulated in OCs (day 14) exposed to cpTi particles (0.1 mg/mL) and in OCs (day 10 and day 14) exposed to low and high concentrations of ZrO_2 particles compared to the control (Fig. 3, upper right chart). *RANK* expression was not affected by the addition of titanium particles after three days. ZrO_2 particles, however, led to a significant up-regulation within three days of exposure to both concentrations. At day 14, we found significantly higher *RANK* expression for OCs treated with 0.01 mg/mL cpTi particles and with 0.1 mg/mL ZrO_2 particles compared to control cells (Fig. 3, bottom left chart).

We also quantified the TRAP5b release into the supernatant via ELISA, which clearly marked an increased protein production over time, but did not reveal significant differences between control cells and cells stimulated with the two types and doses of particles (data not shown).

Cathepsin K encodes for a lysosomal cysteine protease, which plays an important role in bone resorption. Significantly up-regulated gene expression was found within the first three days of exposure for both types and concentrations of particles in comparison to the untreated control (Fig. 3, bottom right chart).

Expression of matrix associated genes

In the next step, we wanted to investigate the impact of cpTi and ZrO_2 particles on matrix remodeling and bone resorption by analyzing the gene expression level of the matrix degrading protein, matrix metalloproteinase-1 (*MMP-1*) and of the *TIMP-1*, (Fig. 4, upper panels).

OCs treated with low or high doses of both particle types for three days showed a significantly higher expression of *MMP-1* compared to untreated control OCs. During further cultivation, the expression of *MMP-1* declined dose-dependently to below the expression level of *MMP-1* of control OCs but did not reach significant differences. Additionally, *TIMP-1* expression by OCs treated with particles dropped during the cultivation period and was lowest in OCs with 0.1 mg/mL cpTi particles. Interestingly, we only found significantly higher gene expression values in OCs exposed to cpTi particles (0.01 mg/mL) and to ZrO_2 particles (0.1 mg/mL) compared to control OCs at day 10.

The amount of MMP-1 released by OCs treated with particles remained at an equal level compared with the control during cultivation time (Fig. 4, left lower panel). After 14

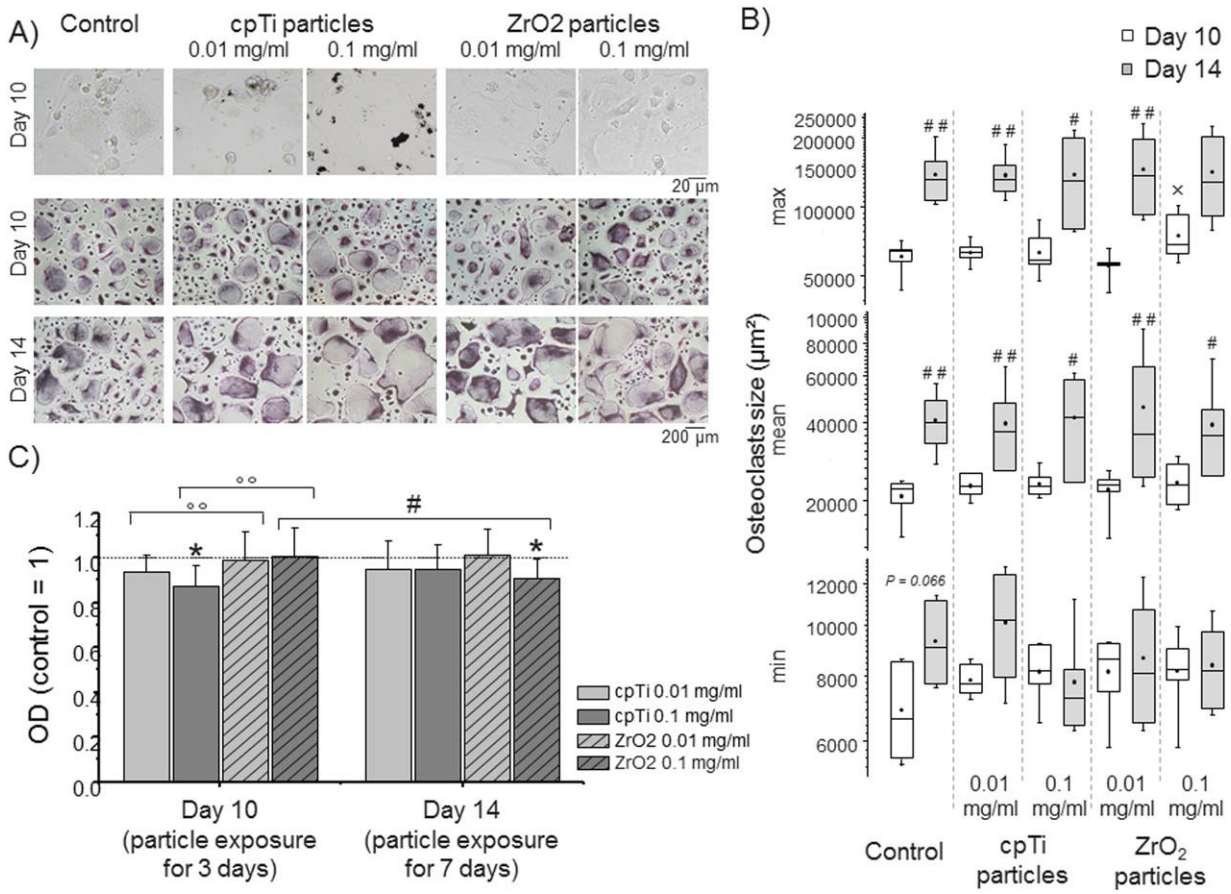

FIGURE 2. Impact of cpTi and ZrO_2 particles on the morphology, size, and metabolic activity of human mature OCs. Monocytes were isolated from human buffy coats ($n = 6$) and seeded (4×10^4 cells/cm^2) in 48-well cell culture plates. Cells were stimulated with M-CSF (25 ng/mL) and RANKL (50 ng/mL) over 7 days before cpTi and ZrO2 particles were added in two different concentrations (0.01 and 0.1 mg/mL). Control cells were cultured without particles. A: After 10 days and 14 days of cultivation the cells were stained for TRAP (upper panel: representative LM pictures of unstained OCs, lower panels: representative LM pictures of TRAP-positive OCs) and (B) size distribution (maximum, mean and minimum) of OCs, with at least three nuclei, was measured using ImageJ. Boxes denote interquartile ranges, horizontal lines within the boxes denote medians, and whiskers denote minimum and maximum values. For statistical analysis Mann-Whitney-U test was conducted. $p^{\#} < 0.05$, $p^{\#\#} < 0.01$ compared with day 10. $p^{x} < 0.05$ compared between different particle concentrations. Metabolic activity was analyzed via WST-1 assay (C). Data are means + SD. For statistical analysis, ANOVA *post hoc*-LSD was conducted. $p^{*} < 0.05$ versus the control. $p^{\#} < 0.05$ compared with the same particle type and concentration at different time points; $p^{\circ\circ} < 0.01$ compared between the two particle types (same concentrations).

days of cultivation, however, OCs treated with high concentrations (0.1 mg/mL) of ZrO_2 particles released significantly lower amounts of TIMP-1 protein in the supernatant in comparison to control or titanium particle (0.1 mg/mL) treated cells and compared with OCs which were exposed to the low ZrO_2 concentration (0.01 mg/mL).

As expected, bone resorption activity was lowest in the negative control (without RANKL) while, in general, the highest values in all approaches were found after 14 days of cultivation (Fig. 5). However, we could not detect a significant effect on the resorptive activity of the OCs treated with the two different types of particles in low and high concentrations compared to OCs cultivated without particles.

DISCUSSION

The aim of this *in vitro* study was to evaluate the direct impact of titanium and ZrO_2 particles on the morphology and functionality of mature human OCs to analyze how this specific cell type is influenced by wear debris leading to aseptic endoprosthesis loosening. The osteolytic process is based on complex cell signaling pathways involving macrophages, fibroblasts, mesenchymal stem cells, osteoblasts, and OCs, which interact with each other through the release of cytokines, chemokines, and growth factors and finally result in increased bone resorption.[6]

Before starting the particle experiments, the monocytes were allowed to differentiate into mature OCs which we then incubated with metallic and ceramic particles in two different concentrations (0.01 and 0.1 mg/mL). We could confirm an up-take of particles by the cells as shown for differentiating OCs and mature OCs before[20,21] indicating that particles can directly impact the cells during osteoclastic differentiation and bone resorption.[21–23] Moreover, we found an initially increased cell size range for mature OCs stimulated with both types of particles, especially with high concentrations of ZrO_2. This is indicative of higher levels of cell fusion, also recognizable by an increased number of nuclei. This direct relation between the number of nuclei

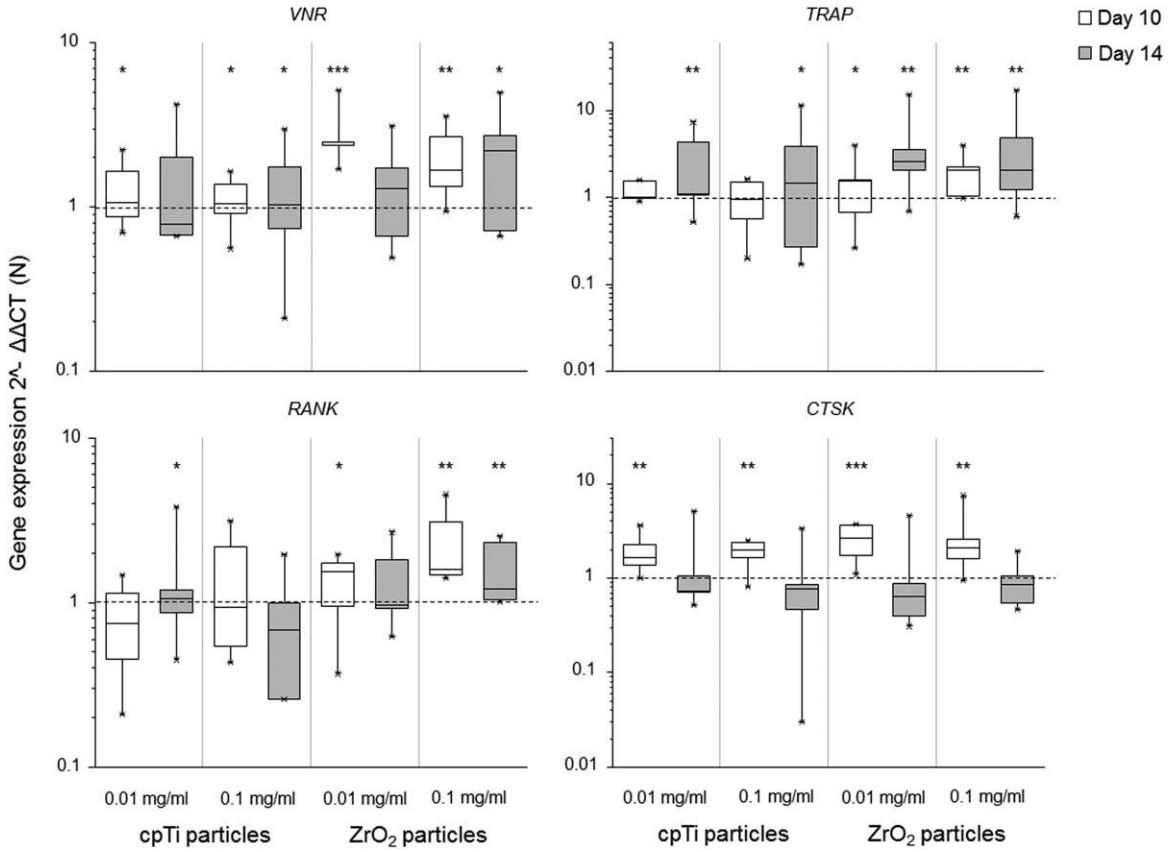

FIGURE 3. Impact of titanium and ZrO_2 particles on the expression of OC specific marker genes (VNR, TRAP, RANK, and CTSK). Monocytes, isolated from human blood samples (buffy coats; $n = 6$), were seeded (4×10^4 cells/cm^2) in 48-well cell culture plates. Cells were stimulated with M-CSF (25 ng/mL) and RANKL (50 ng/mL) over seven days before cpTi and ZrO2 particles were added in two different concentrations (0.01 and 0.1 mg/mL). After 10 days (including three days with particles) and 14 days (including seven days with particles) RNA was isolated for qRT-PCR. Data were normalized to control cells (without particles) indicated by the dotted line (=100%). Boxes denote interquartile ranges, horizontal lines within the boxes denote medians, and whiskers denote minimum and maximum values. For statistical analysis the nonparametric two-tailed Mann-Whitney *U* test was conducted. *$p < 0.05$, ** $p < 0.01$, *** $p < 0.001$ versus the control.

per OC and their bone resorption activity has been shown before.[24] We also counted the number of nuclei per OC in this study (data not shown) but could not identify a direct effect of particle exposure on the amount of nuclei found in mature OCs. Since the cells we used, mature OCs, had already fused before the particles were added, we did not expect any differences. However, at the later time point during cultivation, we identified a higher proportion of smaller OCs after treatment with cpTi and ZrO_2 particles. A previous study elucidated a stimulating effect of metallic particles on size and number of developing OCs, however, only in combination with bone morphogenetic protein-2.[25] Greenfield et al. described only a slight particle impact on the activation and survival of OCs, but a more likely impact on recruitment and osteoclastic differentiation.[23] In addition, we found that the metabolic cell activity remained at an equal or even decreased level compared to the control cells after three and seven days of incubation with both particle types. The reason for this might be due to a reduced mitochondrial dynamic measurable in the supernatant of the OCs during phagocytosis of particles and increased cell fusion.[26] We did not find significant differences in cell number, however, in a previous study it was shown that the number of OCs was increased by abrasive wear particles *in vivo*.[23] This confirms that particles and additional factors, like growth factors and signaling proteins, synergistically contribute to OC proliferation.[25]

Looking at OC specific and bone matrix related genes, we found significant differences between mature OCs stimulated with metallic and ceramic particles compared with untreated control OCs. These results point on the direct involvement of mature OCs in bone resorption during endoprosthetic loosening induced by wear particles. There was an initial dose-dependent effect of both types of particles on the expression of *VNR*, which is important for cell adhesion to the bone matrix initiating the degradation process. *VNR* showed significantly higher expression in OCs exposed to ZrO_2 particles. Two other crucial key factors, *TRAP5b* and *RANK,* involved in the regulation of OC migration, differentiation, proliferation, and activation, were found to be upregulated in particle treated OCs. We also found increased TRAP5b protein secretion by analyzing the supernatant in an ELISA but could not detect significant differences compared with untreated control cells (data not shown). There was also a dose- and time-dependent up-regulation of *RANK* after exposure to ZrO_2 particles. Furthermore, we detected a

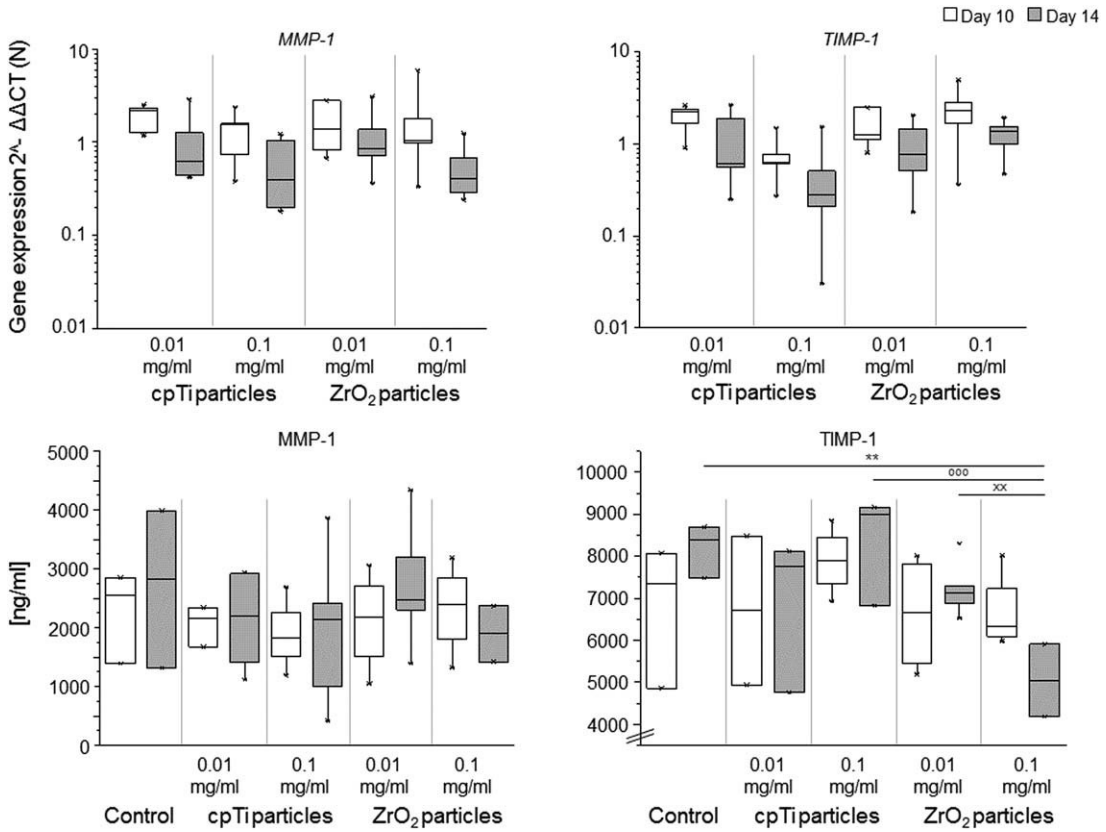

FIGURE 4. Impact of titanium and ZrO_2 particles on matrix degradation. Analysis of the protein expression of MMP-1 and TIMP-1 by human OCs. Monocytes were stimulated with M-CSF and RANKL over seven days before cpTi and ZrO2 particles were added in two different concentrations (0.01 and 0.1 mg/mL). After 10 and 14 days, RNA was isolated for qRT-PCR. Data were normalized to control cells (without particles) indicated by the dotted line (=100%). Additionally, supernatants were collected and analyzed using a plate reader (fluorescence intensity). Positive control (without particles). Boxes denote interquartile ranges, horizontal lines within the boxes denote medians, and whiskers denote minimum and maximum values. Statistical analysis with nonparametric two-tailed Mann-Whitney *U* test (gene expression) and ANOVA *post hoc*-LSD (protein expression), respectively. $p^* < 0.05$, $p^{**} < 0.01$ versus the control. $p^{ooo} < 0.001$ compared between the two particle types (same concentrations). $p^{xx} < 0.01$ compared between different particle concentrations.

significantly higher *RANK* expression in OCs treated with cpTi particles after seven days of incubation. Additionally, our results revealed an initial significant up-regulation of *CTSK* expression in general, which is also important in bone resorption. Overall, we found evidence for a particle-induced activity of OCs including bone resorption consistent with literature data.[21] However, we could not measure a significantly higher bone resorption at the protein level as described in the literature, for example, of OCs treated with polymethylmethacrylate-particles.[4,21] We therefore also investigated the expression of MMP-1, encoding for an ECM degrading enzyme, and its antagonist TIMP-1 at the RNA and protein level. Interestingly, mature OCs treated with low or high doses of both particle types showed a significantly higher gene expression of *MMP-1* compared with untreated control OCs. However, this only applied to the early stage (after three days of incubation), while during further cultivation the values between particles treated OCs and the control arrived at the same level. It is known that MMP-1 production is influenced by IL-1, a cytokine promoting bone resorption.[27] This would explain why we only measured a slightly increased bone resorption activity under the influence of particles. In an *in vivo* study by Liu et al.[28] a direct and significant correlation between an increased *MMP-1* and *-13* expression and a higher OC number and resorption activity was stated. Consistent with that finding, we found that *TIMP-1* (tissue inhibitor of MMPs) expression by OCs treated with particles dropped during the cultivation period. This was also true for the expression on the protein level, especially for OCs treated with high concentrations of ZrO_2 particles. From this we can conclude, that ZrO_2-based wear particles influence bone resorption activity of OCs by impairing TIMP-1 production, which has not been previously described. Research studies focused on TIMP-1 expression by osteoblasts have found that an overexpression of TIMP-1 by osteoblasts led to reduced osteoclastic bone resorption *in vitro* and *in vivo*.[29,30] Moreover, it was found that ZrO_2 abrasive wear particles caused the smallest altered reactions in the metabolism of osteoblasts compared to a range of other particle types.[9] One should also keep in mind, that the bioreactivity, including cytotoxicity, of abrasive wear particles depends both on particle amount and characteristics (type of material, size, morphology, concentration, etc.) and on susceptibility of the endoprosthetic

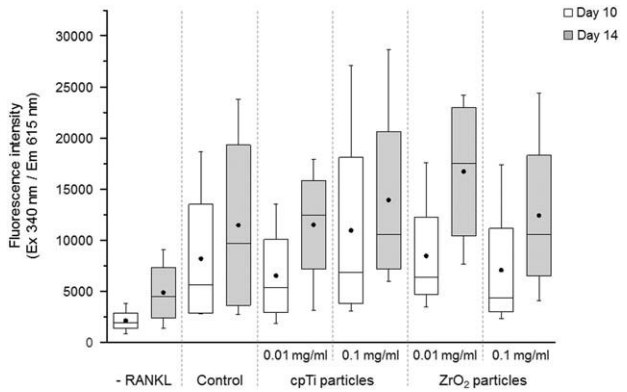

FIGURE 5. Impact of titanium and ZrO_2 particles on the resorption activity of human OCs. Monocytes, isolated from human blood samples (buffy coats; $n = 4$), were seeded (4×10^4 cells/cm^2) in 96-well cell culture plates coated with europium-labeled human collagen. Cells were stimulated with M-CSF and RANKL over seven days before cpTi and ZrO2 particles were added in two different concentrations (0.01 and 0.1 mg/mL). After 10 days (including three days with particles) and 14 days (including seven days with particles) supernatants were collected and analyzed using a plate reader (fluorescence intensity). Two control groups (without particles): (1) Negative control without RANKL (-RANKL); (2) Positive control (with M-CSF and RANKL). Boxes denote interquartile ranges, horizontal lines within the boxes denote medians, and whiskers denote minimum and maximum values. For statistical analysis, the nonparametric two-tailed Mann-Whitney *U* test was conducted showing no significant differences.

patient.[6,31] In summary, both particle types, titanium and ZrO_2 particles, may have direct impact on OC-mediated bone resorption during aseptic loosening of total joint replacements.

ACKNOWLEDGMENTS

The authors would like to thank Doris Hansmann and Anika Witt for technical support.

CONFLICTS OF INTEREST

The authors declare no conflict of interest.

REFERENCES

1. Knight SR, Aujla R, Biswas SP. Total Hip Arthroplasty - over 100 years of operative history. Orthop Rev (Pavia) 2011;3:e16.
2. Kosyfaki P, Swain MV. Adhesion determination of dental porcelain to zirconia using the Schwickerath test: Strength vs. fracture energy approach. Acta Biomater 2014;10:4861–4869.
3. Li RW, Chow TW, Matinlinna JP. Ceramic dental biomaterials and CAD/CAM technology: State of the art. J Prosthodont Res 2014; 58:208–216.
4. Ollivere B, Wimhurst JA, Clark IM, Donell ST. Current concepts in osteolysis. J Bone Joint Surg Br 2012;94:10–15.
5. AQUA-Institut GmbH 2014. Qualitätsreport 2015:1–220.
6. Bitar D, Parvizi J. Biological response to prosthetic debris. World J Orthop 2015;6:172–189.
7. Xia Z, Triffitt JT. A review on macrophage responses to biomaterials. Biomed Mater 2006;1:R1–R9.
8. Ingham E, Fisher J. The role of macrophages in osteolysis of total joint replacement. Biomaterials 2005;26:1271–1286.
9. Lochner K, Fritsche A, Jonitz A, Hansmann D, Mueller P, Mueller-Hilke B, Bader R. The potential role of human osteoblasts for periprosthetic osteolysis following exposure to wear particles. Int J Mol Med 2011;28:1055–1063.
10. Jacobs JJ, Roebuck KA, Archibeck M, Hallab NJ, Glant TT. Osteolysis: Basic science. Clin Orthop Relat Res 2001;71–77.
11. Goodman SB, Gibon E, Yao Z. The basic science of periprosthetic osteolysis. Instr Course Lect 2013;62:201–206.
12. Trindade MC, Lind M, Sun D, Schurman DJ, Goodman SB, Smith RL. In vitro reaction to orthopaedic biomaterials by macrophages and lymphocytes isolated from patients undergoing revision surgery. Biomaterials 2001;22:253–259.
13. Tuan RS, Lee FY, Konttinen Y, Wilkinson JM, Smith RL. What are the local and systemic biologic reactions and mediators to wear debris, and what host factors determine or modulate the biologic response to wear particles? J Am Acad Orthop Surg 2008;16 Suppl 1:8.
14. Gallo J, Goodman SB, Konttinen YT, Wimmer MA, Holinka M. Osteolysis around total knee arthroplasty: A review of pathogenetic mechanisms. Acta Biomater 2013;9:8046–8058.
15. Bord S, Horner A, Hembry RM, Reynolds JJ, Compston JE. Distribution of matrix metalloproteinases and their inhibitor, TIMP-1, in developing human osteophytic bone. J Anat 1997;191:39–48.
16. Bord S, Horner C, Beeton CA, Hembry RM, Compston JE. Tissue Inhibitor of Matrix Metalloproteinase-1 (TIMP-1) Distribution in Normal and Pathological Human Bone. Bone 1999;229–235.
17. Gomis-Rüth F-X, Maskos K, Betz M, Bergner A, Huber R, Suzuki K, Yoshida N, Nagase H, Brew K, Bourenkov GP, Bartunik H, Bode W. Mechanismof inhibition of the humanmatrix metalloproteinase stromelysin-1byTIMP-1. Nature 1997;77–81.
18. O'Neill SC, Queally JM, Devitt BM, Doran PP, O'Byrne JM. The role of osteoblasts in peri-prosthetic osteolysis. Bone Joint J 2013;95-B:1022–1026.
19. Schulze C, Lochner K, Jonitz A, Lenz R, Duettmann O, Hansmann D, Bader R. Cell viability, collagen synthesis and cytokine expression in human osteoblasts following incubation with generated wear particles using different bone cements. Int J Mol Med 2013; 32:227–234.
20. Neale SD, Haynes DR, Howie DW, Murray DW, Athanasou NA. The effect of particle phagocytosis and metallic wear particles on osteoclast formation and bone resorption in vitro. J Arthroplasty 2000;15:654–662.
21. Zhang H, Ricciardi BF, Yang X, Shi Y, Camacho NP, Bostrom MG. Polymethylmethacrylate particles stimulate bone resorption of mature osteoclasts in vitro. Acta Orthop 2008;79:281–288.
22. Bi Y, van de Motter RR, Ragab AA, Goldberg VM, Anderson JM, Greenfield EM. Titanium particles stimulate bone resorption by inducing differentiation of murine osteoclasts. J Bone Joint Surg Am 2001;83-A:501–508.
23. Greenfield EM, Bi Y, Ragab AA, Goldberg VM, van de Motter RR. The role of osteoclast differentiation in aseptic loosening. J Orthop Res 2002;20:1–8.
24. Oursler MJ. Recent advances in understanding the mechanisms of osteoclast precursor fusion. J Cell Biochem 2010;110:1058–1062.
25. Sun SX, Guo HH, Zhang J, Yu B, Sun KN, Jin QH. BMP-2 and titanium particles synergistically activate osteoclast formation. Braz J Med Biol Res 2014;47:461–469.
26. Otera H, Mihara K. Molecular mechanisms and physiologic functions of mitochondrial dynamics. J Biochem 2011;149:241–251.
27. Hill PA, Murphy G, Docherty AJP, Hembry RM, Millican A, Reynolds JJ, Meikle MC. The effects of selective inhibitors of matrix metalloproteinases (MMPs) on bone resorption and the identification of MMPs and TIMP-1 in isolated osteoclasts. J Cell Sci 1994;3055–3064.
28. Liu Y, Song F, Sun J, Yu H, Liu SS-Y. Suture compression induced bone resorption with intensified MMP-1 and 13 expressions. Bone 2012;51:695–703.
29. Geoffroy V, Marty-Morieux C, Le Goupil N, Clement-Lacroix P, Terraz C, Frain M, Roux S, Rossert J, de Vernejoul MC. In vivo inhibition of osteoblastic metalloproteinases leads to increased trabecular bone mass. J Bone Miner Res 2004;19:811–822.
30. Schiltz C, Prouillet C, Marty C, Merciris D, Collet C, Vernejoul MC. d, Geoffroy V. Bone loss induced by Runx2 over-expression in mice is blunted by osteoblastic over-expression of TIMP-1. J Cell Physiol 2010;222:219–229.
31. Jiang Y, Jia T, Gong W, Wooley PH, Yang SY. Effects of Ti, PMMA, UHMWPE, and Co-Cr wear particles on differentiation and functions of bone marrow stromal cells. J Biomed Mater Res A 2013;101:2817–2825.